Titre: Title:	Thin Film-Based Optically Variable Security Devices : From Passive to Active
Auteur: Author:	Bill Baloukas
Date:	2012
Type:	Mémoire ou thèse / Dissertation or Thesis
Référence: Citation:	Baloukas, B. (2012). Thin Film-Based Optically Variable Security Devices : From Passive to Active [Ph.D. thesis, École Polytechnique de Montréal]. PolyPublie. https://publications.polymtl.ca/919/

URL de PolyPublie: PolyPublie URL:	https://publications.polymtl.ca/919/
Directeurs de recherche: Advisors:	Ludvik Martinu
Programme: Program:	Génie physique

UNIVERSITÉ DE MONTRÉAL

THIN FILM-BASED OPTICALLY VARIABLE SECURITY DEVICES: FROM PASSIVE TO ACTIVE

BILL BALOUKAS
DÉPARTEMENT DE GÉNIE PHYSIQUE
ÉCOLE POLYTECHNIQUE DE MONTRÉAL

THÈSE PRÉSENTÉE EN VUE DE L'OBTENTION
DU DIPLÔME DE PHILOSOPHIÆ DOCTOR
(GÉNIE PHYSIQUE)
AOÛT 2012

UNIVERSITÉ DE MONTRÉAL

ÉCOLE POLYTECHNIQUE DE MONTRÉAL

Cette thèse intitulée :

THIN FILM-BASED OPTICALLY VARIABLE SECURITY DEVICES: FROM PASSIVE TO ACTIVE

présentée par : BALOUKAS Bill
en vue de l'obtention du diplôme de : Philosophiæ Doctor
a été dûment acceptée par le jury d'examen constitué de :

M. PETER Yves-Alain, Dr. Sc., président
M. MARTINU Ludvik, Ph.D., membre et directeur de recherche
Mme. SANTATO Clara, Ph.D., membre
M. GRANQVIST Claes-Göran S., Ph.D., membre

To Ellie...

ACKNOWLEDGMENTS

It goes without saying that in the course of my studies, I have had the pleasure of meeting quite a few people. I would thus begin by thanking you all for simply being there ; I have become what I am today in part because of you !

There are obviously a few people whom I wish to thank personally. First and foremost, I would like to thank my director Ludvik Martinu who, more than a decade ago, accepted me as a summer student in his laboratory, Functional Coating and Surface Engineering Laboratory (FCSEL). Since then, he has shown a confidence in me which has allowed me to grow as a scientist, but also as an individual. Being at his side has offered me the chance of participating in many enriching activities which I believe are essential for any future researcher. I look forward to our continued collaboration within the Natural Sciences and Engineering Research Council of Canada (NSERC) Multisectorial Industrial Research Chair in Coatings and Surface Engineering (MIC-CSE).

I would also like to thank professor Jolanta Klemberg-Sapieha for her kindness, positive comments and encouragements.

A special thank you goes out to Oleg Zabeida who's keen mind has found solutions to my problems on so many occasions. Throughout the years he has become a good friend and his humour is always welcome during our weekly meetings.

Thank you to both my « mentors » in my initial years, Aram Amassian and Stéphane Larouche. Aram took me under his wing and through his enthusiasm encouraged me to continue in the field of thin films. As for Stéphane, no matter how busy, he always found the time to help me and his suggestions were always welcome.

Thank you to my friend Jean-Michel Lamarre, whose astute critical nature has been missed since his departure from our laboratory. Our collaboration and discussions have allowed me to refine my work and see the world differently. Thank you also for finding time to read my thesis.

Let's not forget my colleagues and ex-colleagues who have very often become good friends and with whom I've had the chance of sharing all these years : Moushab Benkahoul, Samih Beskri, Etienne Bousser, Jiri Čapek, Eda Çetinörgü-Goldenberg, Marie-Maude de Denus Baillargeon, Mariusz-Andrzej Dudek, Jean-Philippe Fortier, Srinivasan Guruvenket, Matěj Hála, Salim Hassani, Christophe Hecquet, Paweł Jędrzejowski, Duanji Li, Simon Loquai, Jean-Philippe Masse, Matjaz Panjan , Thomas Poirié, Alexis Ragusich, Richard Vernhes, and Nicolas Viau. I will not forget how our daily discussions were a great source of inspiration for advancing my project as well as a great way of simply talking of everyday life.

Speaking of advancing my project, a big thank you goes out to Sébastien Chenard, Yves Drolet and Francis Turcot for their technical help without which not much would still be functioning in our laboratory.

I particularly want to mention Alexandre Dupuis and Christian Lacroix with whom I started my studies and who, to this day, remain good friends. A particular mention goes to my friend Jerôme Poulin who's energy and motivation never cease to amaze me and which are an example for all. Lastly, thank you to my kung fu teacher Franklin Eyelom who tought me to have confidence in myself and whose teachings have helped me to become a stronger individual.

A special mention goes to professor Thomas Gervais who offered me the opportunity of presenting my work on the *Code Chastenay* show on TéléQuébec. Such an experience is not given to all and was highly enriching and motivating ; thank you !

I must also thank Univalor for supporting our patents and Thomas Martinuzzo for representing us. In this same context, thank you to the Bank of Canada for their interest, suggestions and support.

I would like to thank the members of the jury who have graciously accepted to evaluate my thesis as well as the Fonds de recherche du Québec - Nature et technologies (FQRNT), the Greek Hellenic Foundation and the Fondation de Polytechnique for their support through scholarships. Finally, thank you to the Université de Montréal and the NSERC who have supported our research through various strategic grants (VINCI program, Idea to Innovations, etc.).

Last but not least, I wish to sincerely thank my parents Diane and Jimmy who have sacrificed so much so that I could have access to the best education possible and who have believed in me and supported me over the past 30 years. My heart also goes out to my wife Ève, whose daily support and love has helped me get through life's ups and downs. Finally, although she is still too young to know how much she is important to me, thank you to my daughter Ellie whose smile lights up my day every morning.

RÉSUMÉ

La contrefaçon coûte des milliards de dollars à l'économie mondiale chaque année. Mis à part ces pertes financières, la contrefaçon constitue également une grande menace pour la sécurité du public, entre autre à travers l'existence de faux passeports (terrorisme), de produits pharmaceutiques d'origines incertaines (risques pour la santé) et même de pièces d'avion contrefaites (fiabilité). Les dispositifs de sécurité optiques jouent ainsi un rôle crucial dans la lutte contre la contrefaçon. Les dispositifs optiques tels que ceux basés sur l'interférence de la lumière, introduits dans les années 1980, ont depuis longtemps démontré leur efficacité ; efficacité qui est le résultat de la facilité avec laquelle peut être observé leur changement de couleur angulaire ainsi que le coût relativement élevé de l'équipement nécessaire à leur production. Malheureusement, de nos jours, en raison de l'apparition de produits de consommation iridescents, tel le papier d'emballage à base de polymères coextrudés, les dispositifs basés sur l'interférence devront être mis à jour. Le but de la présente thèse est donc de démontrer que, grâce à l'utilisation du métamérisme et de matériaux électrochromiques, de nouveaux types de dispositifs de sécurité actifs présentant des caractéristiques intéressantes peuvent être créés ; en effet, la plupart des dispositifs actuels sont de nature passive. Il est également important d'ajouter que, bien que ces dispositifs soient plus complexes à fabriquer et donc difficiles à contrefaire, ceux-ci restent simples à authentifier.

Je démontre tout d'abord, que l'ajout du métamérisme dans la conception de filtres interférentiels permet de générer des dispositifs possédant de nouvelles fonctionnalités. Plusieurs structures différentes, qui peuvent être utilisées soit en transmission ou en réflexion, sont ainsi conçues, fabriquées, et évaluées. La première structure qui est présentée est basée sur la combinaison de deux filtres interférentiels métamériques. Possédant des spectres de transmission très différents, ces deux filtres possèdent également différents parcours colorimétriques en fonction de l'angle d'observation, ce qui, par conséquent, rend possible la création d'un effet d'image cachée. En dépit de leurs propriétés intéressantes, ces dispositifs métamériques sont révélés comme étant très sensibles aux changements d'illuminants et d'observateurs ; i.e. que le pairage de couleur est perdu dans la plupart des conditions d'observation. Ces problèmes sont résolus par l'implémentation d'une structure plus simple basée sur la juxtaposition d'un filtre interférentiel et d'un matériau coloré non-iridescent. Dans ce cas particulier, en concevant un filtre reproduisant fidèlement le spectre du matériau non-iridescent, la sensibilité du dispositif aux changements de sources de lumière et d'observateurs est minimisée. Puisque seulement le filtre interférentiel change de couleur en fonction de l'angle d'observation, un effet d'image cachée est encore une fois possible. La présence d'un effet d'image cachée ainsi

que du matériau non-iridescent, qui sert de référence de couleur, facilite le processus d'authentification ainsi que la détection automatisée en utilisant un laser à un angle d'incidence spécifique. Tout au long de cette étude, je présente la démarche de conception, j'analyse la sensibilité des filtres aux erreurs de dépôt, et j'évalue la performance de dispositifs prototypes préparés par pulvérisation double faisceaux d'ions.

Suite à mes travaux sur les dispositifs métamériques passifs, je propose d'aller encore plus loin en implémentant une composante active à base d'un matériau électrochromique. Ce nouveau dispositif, qui est basé sur l'utilisation conjointe d'un filtre métamérique et d'un matériau électrochromique, offre la possibilité de créer différents effets optiques. Un tel système est d'autant plus difficile à contrefaire en raison de sa complexité, mais ajoute également un deuxième niveau d'authentification accessible à un personnel spécialisé. En concevant un filtre métamérique qui reproduit soit l'état blanchi ou coloré d'un dispositif électrochromique, je montre qu'il est possible de générer deux effets d'images cachées : l'une qui apparaît lorsque la structure est inclinée, et l'autre qui disparaît lorsque le matériau électrochromique est coloré suite à l'application d'un potentiel. Plus particulièrement, cette étude présente un exemple de filtre interférentiel qui est métamérique avec l'état coloré d'un dispositif électrochromique, de type Deb, à base d'oxyde de tungstène. Il est également démontré que le changement de couleur dynamique permet une plus grande flexibilité lorsqu'il s'agit de fabriquer le filtre métamérique. Enfin, la méthodologie développée permettant de concevoir des filtres métamériques plus performants est présentée. Cette nouvelle approche, basée sur la courbe d'efficacité lumineuse de l'œil humain, résulte en des filtres qui possèdent un nombre plus faible de couches et donc un coût de fabrication inférieur, sans compromettre leur performance sous différentes sources lumineuses et pour des observateurs non-standards.

Un dispositif hybride tel que présenté dans l'étude précédente est clairement intéressant d'un point de vue prototype. Malheureusement, ayant à concevoir et à fabriquer deux composantes individuelles résulterait en un agencement très coûteux. Par conséquent, mon objectif était de combiner à la fois le changement de couleur angulaire et le changement de couleur électrochromique dans une structure unique. L'étude qui suit démontre ainsi que, par la conception et la fabrication d'un filtre interférentiel basé sur l'utilisation de WO_3 dense et poreux, cet objectif peut être atteint. Avant d'entrer dans le cas complexe d'un filtre, j'ai d'abord étudié l'effet de la porosité sur les propriétés physiques et électrochromiques de divers couches minces de WO_3 préparées par pulvérisation magnétron. Succinctement, les couches denses offrent une faible variation de transmission et une dynamique très lente, tandis que les couches poreuses quant à elle, offrent une variation de transmission plus grande et une dynamique plus rapide. Il est ensuite dévoilé qu'un revêtement dense n'inhibe pas la coloration d'un revêtement poreux sous-jacent. Suite à ces observations, un filtre de 27

couches quart d'onde, offrant une transmission attrayante et donc un changement de couleur angulaire intéressant, est fabriqué et cyclé entre un état blanchi et coloré. La dernière partie de cette étude démontre que les filtres interférentiels développés pourraient également être utiles pour d'autres applications telles que les fenêtres intelligentes. En effet, en remplaçant l'unique couche de WO_3 d'une fenêtre électrochromique par un filtre WO_3 poreux|WO_3 dense, la transmission lumineuse de celle-ci dans son état décoloré peut être accrue en limitant les pertes en réflexion. Une telle stratégie pourrait également donner lieu à une fenêtre d'une couleur spécifique ou aider à neutraliser sa couleur.

Enfin, je propose une deuxième méthode de fabrication qui entraîne une diminution significative du nombre total de couches des filtres interférentiels actifs. En remplaçant les couches poreuses de WO_3 par un composite WO_3/SiO_2, dont l'indice de réfraction peut être beaucoup plus bas, il est possible d'obtenir un contraste d'indice de réfraction encore plus grand (0,61 contre 0,22 dans l'étude précédente). Cette étude explore tout d'abord les propriétés physiques et électrochromiques de mélanges de WO_3/SiO_2 . Par la suite, des couches de bas et haut indice de réfraction sont combinées afin d'observer leur dynamique de blanchiment/coloration. Afin d'expliquer la mauvaise performance de la configuration ITO|Composite|WO_3, je présente également une explication basée sur la grande différence de coefficients de diffusion des électrons des couches concernées. Je conclus cette étude avec la démonstration d'un filtre électrochromique de 11 couches, affichant un changement de couleur angulaire attrayant du bleu au pourpre, conçu par l'alternance de couches de WO_3 pures et de couche composites $(WO_3)_{0,17}(SiO_2)_{0,83}$. Une brève discussion sur des solutions possibles pour les limitations observées s'ensuit.

ABSTRACT

Counterfeiting costs the world economy billions of dollars every year. Aside from financial losses, counterfeiting also poses a great threat to the public's safety, for example through the existence of counterfeit passports (terrorism), pharmaceutical products (health hazards) and even airplane parts (safety issues). Optical security devices (OSDs) have therefore played a critical role in the fight against counterfeiting. OSDs, such as those based on interference introduced in the 1980s, have clearly proven their efficiency; this high efficiency being the result of the facility with which the color shift can be observed as a function of the observation angle as well as the relatively high cost of the production equipment. On the other hand, nowadays, due to the appearance of iridescent consumer products such as coextruded polymer "wrapping paper", interference-based devices will need to be "upgraded". It is the aim of the present thesis to show that through the use of metamerism and electrochromic materials, new types of active security devices with interesting features can be created; indeed, most present-day devices are passive in nature. It is also important to add, that although these devices are more complex to fabricate and therefore difficult to counterfeit, they do remain simple to authenticate for the man on the street.

I first demonstrate that the addition of metamerism in the design of interference filters can result in innovative features. Different structures which can be used in transmission and/or in reflection are designed, fabricated, and evaluated. The first structures which are presented here are based on a combination of two different metameric interference filters. Possessing widely different transmission spectra, these filters also offer different angular color shifts and, as a result, offer an opportunity of creating hidden image effects. Despite their interesting properties, such metameric devices are shown to be highly illuminant and observer sensitive; that is the color match is lost under most observation conditions. These issues are solved by a simpler structure based on the juxtaposition of an interference filter and a non-iridescent colored material. In this case, by closely matching the transmission or reflection spectra of both elements, the sensitivity of the device to changes in light sources and observers is minimized. Since only the interference filter will change color as a function of the observation angle, a hidden image effect is yet again possible. The presence of the hidden image, as well as of the non-iridescent material, which serves as a color reference, facilitates the user's authentication process as well as automated detection by using a laser at a specific angle. Throughout this study, I present the design approach, analyze the filters' sensitivity to deposition errors, and evaluate the performance of prototype devices prepared by dual ion beam sputtering.

Following my work on passive metameric systems, I then propose to go one step further by implementing an active component using an electrochromic material. This novel concept, which is based on the joint use of a metameric filter and electrochromic device, offers the possibility of creating various surprising optical effects. Such a system is obviously more challenging to duplicate due to its complexity, but also adds a second level of authentication accessible to specialized personnel. By designing a metameric filter which matches either the bleached or colored state of an electrochromic device, I show that one can generate two hidden image effects: one which appears when the structure is tilted, and the other one which disappears when the electrochromic material is colored under an applied potential. In this specific study, I present an example of a filter that is metameric with the colored state of a tungsten-oxide-based Deb-type electrochromic device. I also demonstrate how the dynamic voltage-driven color change allows for more fabrication flexibility in terms of the metameric filter. I finally describe the design methodology of metameric filters which is based on the luminous efficiency curve of the human eye. This new approach results in filters which possess a lower number of layers and hence lower fabrication cost, but does not compromise their performance under various light sources and for non-standard observers.

A hybrid device such as presented in the previous study is clearly interesting from a prototype point of view. Unfortunately, having to design and fabricate two individual components would make such a security feature very expensive. Consequently, my goal was to combine both the color shift and electrochromic color change into a single structure. The following study thus demonstrates, that by designing and fabricating an interference filter based on dense and porous WO_3, this goal can be achieved. Before getting into the complex case of an interference filter, I first study the effect of porosity on the physical and electrochromic properties of WO_3 films prepared by radiofrequency magnetron sputtering. In short, dense films show poor transmission variation and slow dynamics, whereas porous films show large transmission variations and faster dynamics. I then demonstrate that an overlying dense coating does not inhibit the coloration of an underlying porous film. Following these observations, a 27 layer quarter-wave interference filter is fabricated and shown to cycle between bleached and colored states, while providing an attractive transmission and therefore interesting color shift. The final part of this study also demonstrates that electrochromic interference filters could also be useful for other applications such as in smart windows. Indeed, replacing the single WO_3 film in a smart window by a porous|dense WO_3 filter can increase the luminous transmittance of the window in its bleached state by decreasing the losses in reflection. Such a strategy could also give a window a specific color or help in neutralizing its color.

Finally, a second method of fabricating electrochromic interference filters is proposed which results in a significant decrease in the total numbers of layers of the filters. Replacing

the porous WO_3 films by a WO_3/SiO_2 composite allows for much lower refractive indices to be obtained thus resulting in a larger index contrast (0.61 versus 0.22 in the previous study). In this study, I first explore the physical and electrochromic properties of WO_3/SiO_2 mixtures. I then combine high and low index films in tandem configurations to observe the bleaching/coloration dynamics. To account for the poor performance of the ITO|Composite|WO_3 film configuration, I also present an explanation based on the differences in electron diffusion coefficients of the films. I conclude this study with the demonstration of an 11 layer electrochromic interference filter based on the alternation of pure WO_3 and $(WO_3)_{0.17}(SiO_2)_{0.83}$ films (with a blue to purple angular color shift) as well as a short discussion on some possible solutions for the observed limitations.

TABLE OF CONTENTS

LIST OF TABLES

LIST OF FIGURES

LIST OF ACRONYMS AND SYMBOLS

Acronyms

3D	Three dimensional
AFM	Atomic force microscopy
AR	Antireflective
BASCAP	Business Action to Stop Counterfeiting and Piracy
CCD	Charge-coupled device
CE	Coloration efficiency
CIE	Commission Internationale de l'Éclairage
CIE94	CIE 1994 color difference formula
CIEDE2000	CIE 2000 color difference formula
CIELAB	CIE 1976 $L^\star a^\star b^\star$ color space
CR	Contrast ratio
CV	Cyclic voltammetry
CVD	Chemical vapor deposition
DC	Direct current
DIBS	Dual ion beam sputtering
DOVID	Diffractive optical variable image device
E.T.	Equal tolerances
EC	Electrochromic
ECD	Electrochromic device
EDX	Energy-dispersive X-ray spectroscopy
EIF	Electrochromic interference filter
EMA	Effective medium approximation
EMF	Electromotive force
ERD	Elastic recoil detection
FAA	Federal Aviation Administration
FCSEL	Functional Coating and Surface Engineering Laboratory
FEG	Field emission gun
FQRNT	Fonds de recherche du Québec - Nature et technologies
GLAD	Glancing angle deposition
HeNe	Helium-neon laser
IR	Infrared
I.P.T.	Inversely proportional tolerances

ID	Identification
ISIS	Interference security image structure
ISO	International Organization for Standardization
ITO	Indium tin oxide
MIC-CSE	Multisectorial Industrial Research Chair in Coatings and Surface Engineering
NIM	Non-iridescent material
NRC	National Research Council
NSERC	Natural Sciences and Engineering Research Council of Canada
OD	Optical density
OVD	Optically variable device
OVI	Optically variable ink
OVP	Optically variable pigment
PECVD	Plasma enhanced chemical vapor deposition
PEN	Polyethylene naphtalate
PET	Polyethylene terephthalate
PMMA	Poly(methyl methacrylate)
PVD	Physical vapor deposition
QW	Quarter-wave
RAE	Rotating analyzer ellipsometer
RCE	Rotating compensator ellipsometer
RBS	Rutherford backscattering spectrometry
RF	Radio frequency
RFID	Radio frequency identification
RMS	Root mean square
SAD	Surface area difference
SCE	Saturated calomel electrode
SEM	Scanning electron microscopy
STPGP	Strategic Project Grant Program
TCO	Transparent conductive oxide
UV	Ultraviolet
VASE	Variable angle spectroscopic ellipsometry
VINCI	Valorisation de l'innovation et du capital intellectuel
WDX	Wavelength-dispersive X-ray spectroscopy
WHO	World Health Organization
XRD	X-ray diffraction

ZOD	Zero-order diffraction

Symbols

$a^\star$	Green-red axis in CIELAB color space
A	Standard illuminant CIE A
A	Area
$A(\lambda)$	Absorption as a function of wavelength
$b^\star$	Yellow-blue axis in CIELAB color space
$\vec{B}$	Blue primary color
B_Q	Blue trichromatic value
c	Speed of light in vacuum
c_s	Solution concentration
$C^\star_{\mathrm{ab}}$	Chroma in the $L^\star a^\star b^\star$ color space
CE	Coloration efficiency
CR	Contrast ratio
d	Thickness of a thin film
D	Diffusion coefficient
D_e	Electron diffusion coefficient
D_i	Ionic diffusion coefficient
D65	Standard illuminant CIE D65
e	Electronic charge
$\mathrm{e^-}$	Electron
$\vec{E}$	Additive color mixture vector
E	Energy
E_g	Bandgap energy
f	Relative concentration
F	Faraday constant
F1	Standard illuminant CIE F1
$\vec{G}$	Green primary color
G_Q	Green trichromatic value
h	Planck constant
$h^\star_{\mathrm{ab}}$	Hue in the $L^\star a^\star b^\star$ color space
H	Quarter-wave optical film of high refractive index
I	Illuminant
i_0	Exchange current
i_b	Bleaching current

i_c	Coloration current
i_p	Anodic peak current
k	Extinction coefficient
k_{B}	Boltzmann constant
k_{N}	Normalizing constant
K	Empirical parameter in theoretical Deb model
l	Spacing between grooves
L	Quarter-wave optical film of low refractive index
L	Long wavelength sensitive cone
$L^\star$	Luminance axis in CIELAB color space
m	Diffraction order
M	Medium wavelength sensitive cone
M	Molar mass
M^+	Cation
n	Index of refraction
$\bar{n}$	Average index of refraction
$n_{550\ \mathrm{nm}}$	Index of refraction at 550 nm
n_b	Index of refraction of bulk material
n_e	Number of electrons participating in a reaction
n_f	Index of refraction of film
n_{H}	Refractive index of a high index quarter-wave optical film
n_{L}	Refractive index of a low index quarter-wave optical film
n_x	Index of refraction of medium x, for $x = 0, 1 \cdots$
N	Complex index of refraction
N_A	Avogadro constant
N_x	Complex index of refraction of medium x
N_0	Concentration of water in ambient
N_{B}	Concentration of tungsten bronze in WO_3
N_{H}	Concentration of protons in electrolyte
$N_{\mathrm{H_2O}}$	Concentration of water in electrolyte
N_{W}	Concentration of protons in WO_3
OD	Optical density
p	Polarization of light parallel to the plane of incidence
p_H	Volume charge density of protons
P	Packing density
q	Density of charge

Q	Inserted charge
$\vec{Q}$	Color vector
$\bar{r}\bar{g}\bar{b}$	Color matching functions
r_c	Radius of colored circle
r_p	Fresnel reflection coefficient for p polarized light
r_s	Fresnel reflection coefficient for s polarized light
$R(\lambda)$	Reflectivity as a function of wavelength
R	Universal gas constant
$\vec{R}$	Red primary color
R_b	Reflection in bleached state
R_c	Reflection in colored state
R_Q	Red trichromatic value
rgb	Color coordinates in Maxwell's color triangle
s	Polarization of light perpendicular to the plane of incidence
S	Short wavelength sensitive cone
$S(\lambda)$ or S_λ	Illuminant spectral distribution
t	Time
t_b	Bleaching time
t_D	Diffusion time
T	Temperature
$T(\lambda)$ or T_λ	Transmission as a function of wavelength
T_b	Transmission in the bleached state
$T_{\text{E.T.}}$	Transmission targets with equal tolerances
$T_{\text{I.P.T.}}$	Transmission targets with tolerances inversely proportional to the luminous efficiency curve of the human eye
T_m	Melting point temperature of a material
T_{c}	Transmission in the colored state
T_{C}	Correlated temperature
U	Radiate energy
v	Scan rate
V_{a}	Applied voltage
V_{eff}	Effective voltage
V_{emf}	Back potential - back electromotive force
x	Intercalation level
x_C	Correlated color temperature, x color coordinate
xyz	CIE trichromatic color coordinates

xyY	CIE 1931 color space
$\bar{x}\bar{y}\bar{z}$	CIE 1931 2° color matching functions
$\bar{x}_{10}\bar{y}_{10}\bar{z}_{10}$	CIE 1964 10° color matching functions
XYZ	CIE 1931 tristimulus values
$X_nY_nZ_n$	Reference white tristimulus values
$\bar{y}_\lambda$	CIE 1931 2° standard observer color-matching function
y_C	Correlated color temperature, y color coordinate
Y_T	Luminous transmittance

Greek symbols

α	Absorption coefficient
β	Angle of diffraction
Δ	Ellipsometric parameter related to the phase difference between r_p and r_s
ΔE	Color difference
$\Delta E^\star_{00}$	CIE 2000 color difference formula
$\Delta E^\star_{94}$	CIE 1994 color difference formula
$\Delta E^\star_{\text{ab, I}}$	Color difference in the $L^\star a^\star b^\star$ color space under illuminant I
Δ(OD)	Change in optical density
Δ(OP)	Optical path difference
ΔT	Maximum transmission variation
ϵ	Dielectric permittivity
ϵ_0	Vacuum permittivity
$\epsilon(\lambda)$	Emissivity as a function of wavelength
λ	Wavelength of light
λ_1	Empirical parameter in theoretical Deb model
λ_2	Empirical parameter in theoretical Deb model
λ_{max}	Black body maximum emission wavelength
μ_H	Chemical potential
μ_{H^+}	Ionic mobility
ν	Frequency of light
ρ	Ratio of $-r_p/r_s$
ρ_M	Density of a material
ρ_W	Density of W atoms
τ_0	Constant equal to $\rho_W de/2i_0$
ϕ	Angle of incidence

$\phi(\lambda)$	Stimulus as a function of wavelength
Ψ	Ellipsometric parameter related to the amplitude ratio between r_p and r_s

CHAPTER 1

INTRODUCTION

Since the tragic events of September 11 2001, security has become a major issue and concern for our society. Protection of key documents such as passports and identity cards is therefore a priority. Obviously, there are many levels of security when it comes to these documents, but the most basic one is their robustness against counterfeiting. As a result, governments and institutions have applied security devices to them. In our fast-paced, technology-driven world, it has become critical to incorporate the latest technological advancements into anticounterfeiting devices in an effort to constantly stay ahead of counterfeiters. For example, banks in the past would typically change their banknotes every 10 to 15 years, while nowadays, the tendency is to change them every 5 to 10 years.

Before going any further, it is important to add that counterfeiting does not only affect banks and governments, but it also costs the world economy hundreds of billions of dollars a year. These losses are mainly due to counterfeiting of consumer products such as luxury items (clothing, watches, etc.), DVDs, pharmaceutical products and even airplane parts. Other than direct financial losses through decreased sales, an indirect and difficult to quantify effect is its impact on a companie's image. Indeed, since counterfeited products are rarely subjected to strict quality control, they rarely fulfil the expected durability and safety requirements. This brings us to the second and most severe impact of counterfeiting, that is, its effect on the public's safety. One can easily imagine what could happen in the case of a faulty airplane part or from taking a pharmaceutical product of unknown origin.

Although counterfeiting practically affects everything that surrounds us, the "product" which has most often benefited from the most advanced security devices has been without exception the banknote. Although there are many ways to protect a banknote, it has now become obvious that the most effective ways to limit counterfeiting is to catch it at the source by having the user, that is the man on the street, authenticate the banknote. Such devices are termed overt, versus their covert counterparts which require special equipment to detect, e.g., chemical taggents. Therefore, banknotes are frequently outfitted with several overt security devices each with their respective strengths and weaknesses. For example, on the Canadian Journey series of the Bank of Canada, one can find six elements of protection :

- Tactile raised ink resulting from intaglio printing which is practically impossible to obtain using inkjet printing (currently one of the most popular means of counterfeiting).
- An element, partly printed on both sides of the banknote which becomes complete when

looking through the banknote allows to verify that both sides of the bill are in register.
- A watermark, the oldest optical security device obtained by varying the thickness of the paper, reproducing the portrait printed on the banknote (humans are very sensitive to changes in human features).
- Fluorescent inks which can be easily observed using an ultraviolet (UV) light.
- A metallic foil consisting in a hologram displaying rainbow-like color changes when tilted (diffraction-based).
- Finally, a thread woven through the bill displaying a gold to green color shift when tilted (interference-based).

These last two elements are the most eye catching and attractive features. It also turns out, that they are a very effective means against counterfeiting due to their color shifting properties as a function of the observation angle, that is their iridescence. In fact, to display iridescence, matter must be organized at the nanometer scale in order to generate diffraction or interference effects with visible light. As a result, these types of features are excellent barriers to standard reprographic techniques (printing, photocopying, etc.) which do not possess any iridescence due to the disorganized nature of the inks which are used.

It is for this main reason, that holograms, which are based on diffractive gratings, have been a very popular optical security feature (diffractive optical variable image device (DOVID)). Unfortunately, there now exist many laboratories around the world which can fabricate holograms and as a result, the effectiveness of holograms has been seriously compromised [1]. Interference-based features form another family of popular iridescent devices termed interference security image structures (ISISs). Commonly displaying a simple to authenticate color shift between two colors, ISISs have been shown to be a very effective optical feature as well as being appreciated by the general public [2]. Their effectiveness does not only derive from the ease with which they can be authenticated, but also by the fact that the equipment and know-how required to fabricate them economically in large quantities is only available to a few.

The concept of using interference filters as a security feature was first introduced by J.A. Dobrowolski, working at the National Research Council (NRC) Canada, and described in a paper published in 1975 ; although work on the subject had already begun in the late 1960s [3]. Apart from a commemorative banknote issued in Thailand presenting an ISIS in 1987 (optically variable ink-based), the Bank of Canada was the first bank to officially apply ISISs to a banknote series starting with the 50 dollar Birds of Canada banknote in 1989 (it was then applied to the 20, 100 and 1000 dollar bills). Since then, two main technologies have been in circulation, the one formally developed by the Bank of Canada, now by Fortress Optical Features, and the other developed by Flex Products, a subsidiary of JDSU. While the former

device consists of a multilayer filter which is integrally transferred to the document to protect, the latter one is based on a filter which is ground into pigments and incorporated into an ink (known as optically variable ink (OVI)). Even if OVI's colors are more subdued, due to the diffused reflection caused by the pigments, the fact that one can create complex images by simply using printing has made it the most popular and widely used ISIS technology.

Fairly recently, iridescent interference-based consumer products have also become available (coextruded polymer filters for gift wrapping, iridescent pigments sold by JDSU, etc.) and they could eventually be used to mimic, albeit not as convincingly, present-day ISISs. As a consequence, it has become essential to implement new security elements to ISISs. This requirement for innovation obviously provided the main motivation for the research presented in this thesis.

In this chapter, I will first explain the context of this work as well as the objectives of my Ph.D. This will be followed by the list of publications resulting from this work and finally concluded by presenting the general outline of this thesis.

1.1 Context

I joined the FCSEL during the second year of my bachelor's degree in 2001 in the context of a summer project. At the time, I had told professor Martinu that I obviously had a strong interest for science and engineering but also for art. Having mentioned my interests, he then proposed two subjects to me : the study of iridescence in birds and insects or the study of colorimetry and its application to interference filters. My knowledge of interference filters being limited at the time, I wasn't immediately attracted to the study of iridescent structures developed by nature and therefore chose the second subject. I then spent the summer under the co-supervision of Aram Amassian and Stéphane Larouche, developing my own interference filter simulation software as well as depositing filters using plasma enhanced chemical vapor deposition (PECVD), all the while learning about colorimetry. Having enjoyed my experience and explored other avenues during the summer of 2002 (ultrasound cartography of articular cartilage under the supervision of professor Michael Buschmann), I came back to the FCSEL in 2003 for another summer project and eventually a master's degree. Having gained experience in optical filter design and colorimetry, it was decided that my project would be on interference-based optical security devices.

It is interesting to note that the choice of this particular subject, not taking into account my personal interests, was highly motivated by two majors events which happened in 2001 : the *telecom crash* as well as *911*. Indeed, before the *telecom crash*, the FCSEL was mostly interested in interference filters for telecommunication applications and as a result lost most

of its funding following 2001. Professor Martinu therefore chose to explore new applications where interference filters could be of interest, such as in security, astronomy, sensors, etc. Also, as is often the case after tragic events, *911* propelled security and all related subject matter to the forefront. Hence, the timing could not have been better to begin our work on security devices.

It is after having spent some time familiarizing myself with the domain of security and after following a course on the psychophysics of human vision, that the idea of developing metameric devices appeared to me as a means of augmenting the security offered by ISISs. Incidentally, in the mean time, I also discovered another effect based on the use of very thin metallic films resulting in an interesting triple-color-shift device. Note, that all of these aspects will be covered in more detail further on. Having presented this work to J.A. Dobrowolski during my master's project presentation, and confirmed its innovative aspects, it was decided that this work would be patented. To our disarray, as is often the case, it was latter discovered that the concept of metameric OVIs had been patented in the year 2000. In the mean time, during the initial stages of my Ph.D., professor Martinu and I applied for various grants to further develop the concept of metameric ISISs and were fortunate enough to be awarded a "Valorisation de l'innovation et du capital intellectuel (VINCI)" grant from the University of Montreal and an Idea to Innovation grant from NSERC. In the context of these grants, we were able to develop transmission-based metameric devices displaying a good performance under multiple illuminants. This work led to my first publication in the context of optical security devices and was presented at the Optical Security Devices conference in 2008 where to my distress, the inventor of the previous patent, R.W. Phillips was the moderator for the session during which I would be presenting. To my surprise, during the question period, he clearly mentioned, that although metameric devices already existed, I had brought the field to a new level. This was a key moment in my studies since it encouraged me to pursue my work on security devices. It turns out R.W. Phillips was not wrong since our patent was awarded on November 22nd 2011 by the U.S. patent office despite the existence of the previous patent. Since then, we have had multiple discussions with various companies and institutions which have further led to the fabrication of prototype devices.

At the same time, we had also begun a collaboration with the Optical Security Material team responsible for the production of ISISs at the Bank of Canada. It is through our discussions with them, that the idea of exploring active materials was brought about. In fact, most present day devices are passive in nature, that is they do not change their appearance following the application of an external source of energy. Part of the future generation of security devices will therefore be active. For reasons which are explained in Chapter 4, I chose to explore electrochromic (EC) materials and their integration in optical security devices during

my Ph.D. As a matter of fact, as will be shown, EC materials can play an important role in the creation of innovative systems presenting two levels of authentication, an angle-depended color shift as well as a voltage-driven color change.

1.2 Objectives

Having begun my work on optical security devices during my master's, the main objective of my Ph.D. project were oriented in a similar direction, namely :

1. To develop new thin-film-based optical security devices.

Specifically, the objective was to add a higher level of complexity from a technological point of view, without compromising the simplicity of use of the device (ease of authentication). In the case of ISISs we accomplished this objective by the addition of the two previously mentioned effects (metamerism and triple-color-shift).

In the context of my Ph.D. whose goal was to focus on the exploration of EC-based active devices, additional objectives were defined :

2. Understand the basic principles behind the performance of electrochromic materials.
3. Characterize their properties and optimize their performance for their integration into an optical security device.
4. Integrate the most interesting materials into active prototype optical security devices.

It is also important to add, that although EC materials have been extensively studied, most of the research has been oriented towards their integration into smart windows and display applications.

1.3 Publications

Following the previously mentioned objectives, the work performed during my Ph.D. has led to the publication of four articles in reviewed journals, three conference proceedings and two patent applications, one of which has been awarded. All of these items are presented in Table 1.1. Note, that this being a thesis by article, Chapters 6 to 9 each represent one of the four published articles.

Also note that my collaboration on various projects during the past six years has also resulted in the publication of three other articles in international journals (see Table 1.2) and multiple conference proceedings (not listed here).

1.4 Outline of the thesis

The following three chapters, contain a short, but I believe complete, overview of all the necessary elements required to clearly comprehend the work presented in this thesis. More precisely, Chapter 2 presents an overview of the field of colorimetry and all necessary definitions and equations. In Chapter 3, I cover the field of optical security devices based on interference filters, first by presenting their basic principles and then, by discussing the latest developments in this field ; for example, through the addition of metamerism, the incorporation of magnetic and active materials, etc. In the third and final part of the literature review, Chapter 4, I first explain why I chose EC materials as the most potential candidates for future optical security devices. I then present an outline of the basic principles behind EC materials, discuss their implementation into electrochromic devices (ECDs) and conclude with a list of the most promising applications based on these materials.

The subsequent chapter, Chapter 5, presents the methodology which was employed to deposit and characterize the films presented in this thesis. Specifically, I present a short overview of radio frequency magnetron sputtering. This is followed by a resumé of the main characterization methods, mainly, spectrophotometry, spectroscopic ellipsometry, atomic force microscopy (AFM), Rutherford backscattering spectrometry (RBS), scanning electron microscopy (SEM), X-ray diffraction (XRD) and finally, cyclic voltammetry combined with *in situ* transmission measurements.

Chapter 6, which is an integral copy of my first published article "Metameric interference security image structures", pertains to metameric interference filters ; two objects being termed metameric when they display the same color when viewed under a specific light source, but yet possess different transmission or reflection spectra. It is shown that it is possible to design interference filters which possess very different spectral characteristics, but essentially identical colorimetric properties at specific angles of incidence. More precisely, two filters which are shown to match under normal daylight and at normal incidence, but which possess different colors at oblique incidence, are designed and fabricated. Thus, by displaying different colors at oblique incidence, these filters allow for the creation of a hidden image when patterned and placed side-by-side. On the other hand, such a device suffers from multiple drawbacks such as a high sensitivity to changes in light sources and observers as well as to deposition errors (thickness variation of the layers). It will also be shown, that replacing one of the filters by a non-iridescent material (NIM), which can be either transparent (colored transparent ink) or reflective (metallic-like), helps solve these issues.

The next chapter, Chapter 7, which consists of the second published article "Active metameric security devices using an electrochromic material", continues on the subject of meta-

meric devices. However, in this case, the color match is made between an interference filter and an ECD. This innovative combination results in a device which offers new possibilities in terms of visual effects, is obviously harder to duplicate and also adds an additional level of authentication. The ECD, based on a Deb-type design (see Chapter 4 for more details), is first presented and characterized. Having measured the colorimetric properties of the device then permitted the design of a metameric filter with an intermediate colored state. Doing so results in a disappearing image effect when the ECD is colored. It is then demonstrated that the dynamic nature of the device provides a higher flexibility when depositing the metameric filter. Finally, this same chapter also discusses the design methodology of the filters, based on the luminance efficiency curve of the human eye, employed in order to design metameric filters with a lower number of layers without compromising their performance.

The following chapter, Chapter 8, is composed of the third article "Electrochromic interference filters fabricated from dense and porous tungsten oxide films". This article deals with an innovative solution which allows to decrease the complexity of the previously presented metameric filter/active device combination by implementing a "single material" concept : the fabrication of an EC interference filter based on the use of porous and dense WO_3 films. The effect of porosity on the EC performance of radio frequency magnetron deposited WO_3 films is first discussed. Tandem film configurations are then tested. A 27-layer quarter-wave filter displaying both an angular color shift as well as EC properties is then deposited and characterized. The last section of the chapter also discusses the possibility of replacing the single WO_3 layer of a smart window by a multilayer porous|dense filter in order to increase its bleached state transmittance by decreasing the inherent reflectivity of the WO_3 film.

Chapter 9, featuring the fourth article "WO_3/SiO_2 composite optical films for the fabrication of electrochromic interference filters", offers a solution to the low index contrast of the previous porous|dense filters presented in the previous chapter. By adding SiO_2 to WO_3 the index of refraction can be significantly lowered. The principal question which is asked and explored in this chapter, is how does the addition of SiO_2 affect the intrinsic EC properties of pure WO_3 films. As in the preceding chapter, tandem film configurations are also analyzed. Finally, an 11 layer filter possessing a significant color shift as well as a voltage-driven color change is demonstrated. Possible solutions for the observed drawbacks of using WO_3/SiO_2 composite films are also discussed.

In the final chapter, Chapter 10, I first present a summary of the main results presented in the thesis. This is followed by a general discussion and a summary of the main conclusions. I complete this chapter with what I believe are some interesting research avenues which could be explored in the near future in order to bring the concept of active EC-based optical security devices to fruition.

Table 1.1 List of publications resulting from this Ph.D.

Articles published in reviewed journals
B. Baloukas and L. Martinu, "Metameric interference security image structures", *Applied Optics*, vol. 47, no. 10, pp. 1585-1593, 2008.
B. Baloukas, J.-M. Lamarre and L. Martinu, "Active metameric security devices using an electrochromic material", *Applied Optics*, vol. 50, no. 9, pp. C41-C49, 2011.
B. Baloukas, J.-M. Lamarre and L. Martinu, "Electrochromic interference filters fabricated from dense and porous tungsten oxide films", *Solar Energy Materials & Solar Cells*, vol. 95, no. 9, pp. 807-815, 2011.
B. Baloukas and L. Martinu, "WO_3/SiO_2 composite optical films for the fabrication of electrochromic interference filters", *Applied Optics*, vol. 51, no. 16, pp. 3346-3356, 2012.
Articles published in conference proceedings
B. Baloukas and L. Martinu, "Advances in metameric security image structures", in *Optical Document Security I, San Francisco, California, USA*, Reconnaissance International, 2008.
B. Baloukas, J.-M. Lamarre, L. Martinu, "From Passive to Active : Future Optical Security Devices", in *Optical Interference Coatings, Tucson, Arizona, USA*, Optical Society of America, 2010.
B. Baloukas and L. Martinu, "Electrochromic interference filters based on WO_3 and composite SiO_2/WO_3 films, in *55^{th} Annual Technical Conference. of the Society of Vacuum Coaters, Santa Clara, California, USA*, Society of Vacuum Coaters, 2012.
Granted and submitted patents
B. Baloukas and L. Martinu, "Interference security image structure", *U.S. Patent*, US 8 064 632 2011.
B. Baloukas and L. Martinu, "Metameric Security Devices Using An Active Material", Deposited on June 3rd 2010, WO 2011/150523.

Table 1.2 List of publications resulting from collaborations during this Ph.D.

Articles published in reviewed journals
E. Çetinörgü, B. Baloukas, O. Zabeida, J. E. Klemberg-Sapieha, and L. Martinu, "Mechanical and thermoelastic characteristics of optical thin films deposited by dual ion beam sputtering", *Applied Optics*, vol. 48, no. 23, pp. 4536-4544, 2009.
M. Hála, O. Zabeida, B. Baloukas, J.E. Klemberg-Sapieha and L. Martinu, "Time- and species-resolved plasma imaging as a new diagnostic approach for HiPIMS discharge characterization", *IEEE Transactions on Plasma Science*, vol. 38, no. 11, pp. 3035-3039, 2010.
E. Çetinörgü-Goldenberg, B. Baloukas, O. Zabeida, J.E. Klemberg-Sapieha, and L. Martinu, "Optical and tribomechanical stability of optically variable interference security devices prepared by dual ion beam sputtering", *Applied Optics*, vol. 50, no. 19, pp. 3351-3359, 2011.

CHAPTER 2

COLORIMETRY

2.1 Foreword

Whether it is to calculate the color variation as a function of the observation angle of an interference-based device or simply calculating the color difference between two samples, understanding how colors are perceived is obviously a great asset. Consequently, in order to design optical security devices, one needs to have a solid background in colorimetry, the science of color measurement.

This chapter therefore contains the basic elements which I believe are required to understand colorimetry. For the novice reader who desires to deepen his understanding of colorimetry, I suggest the excellent introductory book *Billmeyer and Saltzman's Principles of Color Technology* by R. S. Berns [4]. For more advanced readers seeking a complete review of colorimetry and the mathematical models which it is based on, the reference and voluminous book *Color science - Concepts and Methods, Quantitative Data and Formulae* by G. Wyszecki [5] is an excellent start. For more up-to-date information on color systems and the recent developments of the Commission Internationale de l'Éclairage (CIE), the reader may consult the book *Colorimetry - Understanding the CIE system* by J. Schanda [6]. Finally, for those seeking information on the basic principles behind the generation of color, the book *The physics and chemistry of color - The fifteen causes of color* by K. Nassau [7] is a must read.

2.2 Introduction

Contrary to popular belief, color is not only an object-dependent characteristic. In fact, color also depends on the illuminating light source and the observer, without which, the concept of color would simply have no meaning. It is the interaction between these three elements which results in the world we perceive around us. Nowadays, our physical understanding of light and light-matter interactions has reached levels which, for most purposes, is sufficient for color calculations. Research in colorimetry is therefore very often focused on refining our understanding of the third component, human perception. Although a human eye may be considered as a complex detector and as a result modeled using physical concepts, things get much more complicated once the detected information is processed by the brain. This is the reason why colorimetry is part of a branch of science termed psychophysics : the

science of how stimuli are perceived. Although this aspect of colorimetry is very interesting, a complete understanding of the psychological component of color perception is not a prerequisite in order to perform color calculations. This chapter will therefore mostly focus on the physical understanding of colorimetry whereas the perceptual part will be implicitly taken into account when discussing the development of the color matching functions and the CIE xyY color space.

In the following chapter, we will first discuss light and its interaction with matter. This short overview will then be followed by a section on the development of the CIE xyY color space and the main light sources which are used in color calculations. We conclude this chapter with a discussion on metamerism, a concept which is essential for anyone having to deal with color.

2.3 Light and color

Light, as described by Maxwell in 1864, is an electromagnetic wave. The electromagnetic spectrum can be separated into different regions depending on the wavelength or energy, given by the Planck equation ($E = h\nu = hc/\lambda$, with h Planck's constant, c the speed of light, and ν and λ the frequency and the wavelength, respectively, of the incident light). In order of decreasing energy, these regions are usually named as follows : gamma rays, x-rays, ultraviolet (UV), visible, infrared (IR), microwave and radio. The visible spectrum, which is the region which our eyes are sensitive to, extends from 380 to 780 nm or, in terms of frequency, from approximately 7.9 x 10^{14} to 3.8 x 10^{14} Hz. This range of wavelengths actually corresponds to average values since some individuals have shown sensitivity to wavelengths down to 360 nm in the near UV and up to 850 nm in the near-IR. This limited range of wavelengths is not shared by all living creatures on Earth ; for example, animals such as some snakes, fish and mosquitoes can also see in the infrared giving them an advantage over their preys. Table 2.1 presents the hues (red, orange, yellow, etc.) which are associated to specific regions of the visible spectrum. Notice that purple is not part of the list since it consists of a mixture of red and blue.

2.4 Light and matter

When light arrives on a surface, it can undergo one or more of the following main optical phenomena : reflection, transmission, absorption, and/or scattering. Figure 2.1a) shows how these phenomena interplay while 2.1b) shows a simplified schematic representation of what can happen when light arrives at an interface. One can see that scattering and absorption are complementary as well as transmission and reflection.

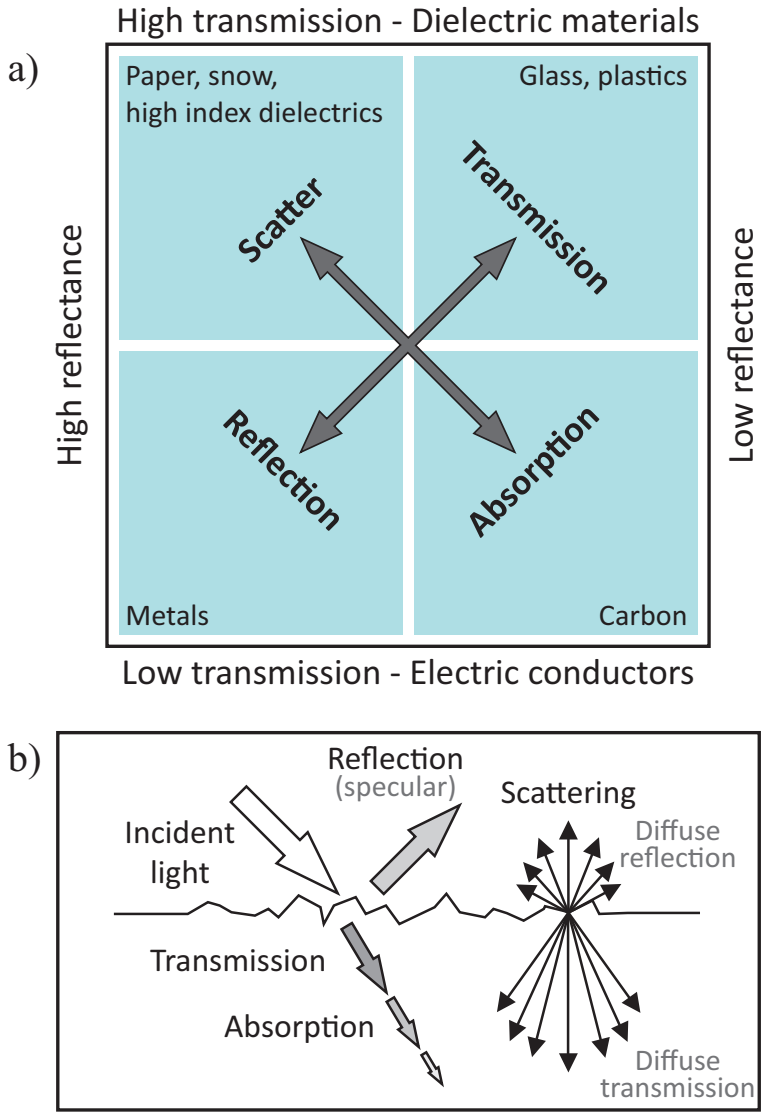

Figure 2.1 a) The four principal optical phenomena light can undergo when interacting with matter. Note that samples with a low transmission are identified as good electric conductors ; indeed dielectrics which have low conductivity have low absorption and vice versa for metals. This figure was inspired by [8]. b) A simplified schematic representation showing what can happen when light interacts with an interface.

Table 2.1 Visible spectrum and the colors that compose it.

Wavelength [nm]	**Color** [Hue]
380-400	Violet
400-410	Indigo
410-440	Blue
440-485	Greenish blue
485-495	Blue-green
495-535	Bluish green
535-555	Green
555-565	Yellowish green
565-575	Greenish yellow
575-580	Yellow
580-585	Orange
585-600	Reddish orange
600-780	Red

Most of the objects that surround us present a highly disorganized structure (rugged surface, disordered microstructure, particle inclusions, defects, porosity or any other element causing light to deviate from its path). This randomness, which is the natural state of matter, leads to a high degree of scattering and thus diffuse reflection. In the particular case where an object is partially transparent as well as diffusive the material is termed translucent. Scattering itself is highly affected by the size of the scattering center. When the scattering center is smaller than the wavelength of the incident light one speaks of Rayleigh scattering. This type of scattering is wavelength dependent ($\propto 1/\lambda^4$) and explains why the sky is blue; shorter blue wavelengths are more scattered than longer red wavelengths. When the scatterers and wavelength of light are approximately of the same dimension, the effect becomes wavelength independent (Mie scattering). Mie scattering is responsible for the white appearance of snow, clouds and milk. Optical diffusers used in integrating spheres (often based on barium sulfate - $BaSO_4$) are an example of objects which display practically no absorption and therefore almost 100% reflection in the visible. Thus, scattering explains why most objects that surround us are matt and show very little specular reflection and color variation as a function of the observation angle (no iridescence). Finally, objects which present very little scattering (low reflectance) as well as no transmission will typically have a high absorption and will usually be black (e.g. : black ink, carbon, carbon nanotubes [9], etc.).

In the case where scattering is negligible, one can easily calculate how light will be divided between the three remaining components by using the well known Fresnel equations [10]. The

absence of scattering also results in a purely specular reflection such as can be observed in a classic aluminium mirror or glass substrate. For example, optical thin films are usually considered (and desired) as having negligible scattering due to their very low surface roughness, amorphous nature and high quality. In the specific case of all-dielectric filters, the absorption in the visible spectrum will also be considered as negligible so that reflection and transmission are complementary. Although less frequent, some materials can also present fluorescence and/or phosphorescence, that is, they will re-emit light when shined upon (fluorescence) and for a prolonged period of time after being illuminated in the case of phosphorescence.

Now, in the case of optical security, as mentioned by Renesse in [8], it is the randomness of nature which makes colored inks and therefore counterfeiting of documents so simple. Therefore, to make things harder to reproduce, one needs to reduce randomness and organize matter in the range of the nanometer (visible light's wavelength) by using, for example, thin film deposition techniques. Doing so results in interesting optical effects such as diffraction and interference. Objects which present interference, such as ISISs, present an angle-dependant color variation which is highly beneficial for security applications. This subject will be covered in more detail in Chapter 3.

2.5 The human eye

The human eye is a fairly complex structure to the point where Darwin himself acknowledged that he had a hard time imagining how such a structure could have evolved. This aspect is outside the scope of the present thesis but let us now look at the main components of the human eye.

The eye can be considered as a sphere of approximately 12 mm in radius. The first element composing the eye is the protective cornea. Having passed through the cornea light then passes through the iris which acts as a diaphragm controlling the amount of light entering the eye. This light is then focused onto the retina by the lens. Problems with the lens result in blurry and distorted images and can be corrected by wearing glasses. The retina itself covers a surface of 11 cm^2, has an average thickness of 250 µm and contains approximately 200 million nerve cells [5]. Most importantly, the retina contains a zone where visual acuity is at its maximum, the fovea. Actually, it is on this part of the retina that light is sent onto when we focus our eyes on an object. The fovea also contains the highest concentration of cones (between 100 000 and 150 000 cones), the photoreceptors responsible for photopic color vision (luminance levels between 1 and 10^6 cd/m^2). All of these elements are in contact with the aqueous humour and vitreous body ; these liquids maintain the structural integrity of the eye.

Other than the cones, the retina also contains rods. Rods are responsible for scotopic monochromatic vision, that is low-light ambient conditions corresponding to luminance levels between 10^{-2} and 10^{-6} cd/m^2. Their larger size when compared to cones also results in a lower spatial resolution. When ambient lighting is increased over a certain threshold, the rods cease functioning. Since there are no rods in the fovea, focusing on a bright object at night will decrease its intensity ; this is easily observed when stargazing.

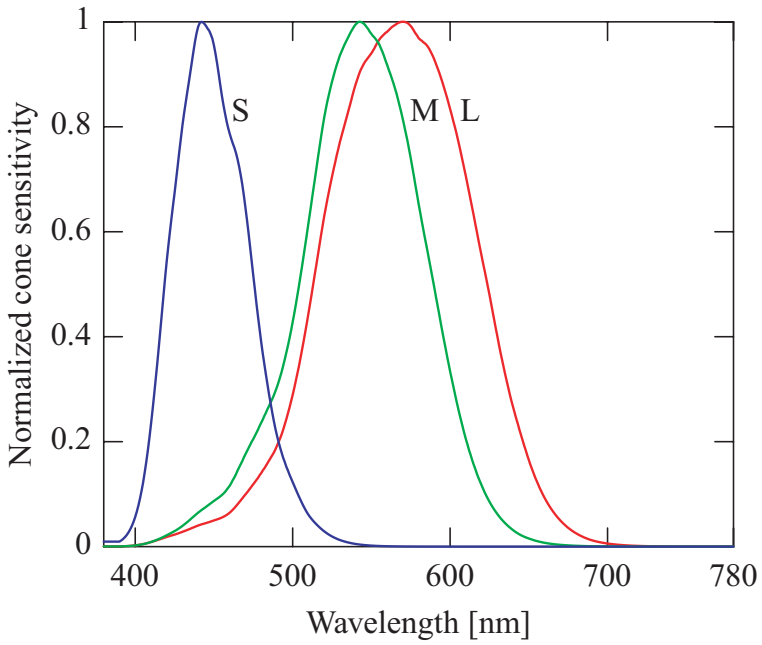

Figure 2.2 Normalized spectral sensitivity of the three types of cones in the human retina. S stands for short, M for medium and L for long [11].

Daytime vision, that is photopic vision (well-lit conditions), as previously mentioned is insured by the cones. There exists three types of cones, each sensitive to a specific region of the visual spectrum, more precisely, the blue, green and red regions. These three cones are also very often identified by short (S), medium (M) and long (L) for the wavelength regions they each are sensitive to. Although higher levels of light are required to switch on the cones, their smaller size results in a greater spatial resolution. The sensitivity curves of the cones are shown in Figure 2.2 [11]. It can be seen that the absorption curves of cones highly overlap ; without this overlap we would only see limited hues (some wavelengths would not be detected).

2.6 Development of the CIE *xyY* color space

Colorimetry owes its foundations to many well known scientists such as Helmholtz, Maxwell, Newton and Young just to name a few. Although by the 19$^{\text{th}}$ century the basic principles of colorimetry were understood, for technological reasons, it is only in 1931 that the first color model based on a standard observer, that is an average human eye, was adopted [i].

Since colorimetry is based on additive color mixing experiments it is first important to note Grassman's laws of additive color matching enunciated by Grassman in 1853 :

1. All colors can be defined by three independent variables (trichromaticity).
2. For all color mixtures, only their trichromatic values are revealing, not their spectral composition (metamerism).
3. In an additive color mixture, if one component of the mixture is gradually changed, the trichromatic values will also gradually change (proportionality).

The first law indicates that it is possible to recreate a color using three primary colors. A primary color is therefore a color which is not obtainable by mixing the other two primary colors (linearly independent vectors). The second law has to do with metamerism as we will soon see below. These three laws actually indicate that color can be treated algebraically. As a result, following these simple rules, a color stimulus $\vec{Q}$ can be defined in vector notation by :

$$\vec{Q} = R_Q\vec{R} + G_Q\vec{G} + B_Q\vec{B}, \tag{2.1}$$

where R_Q, G_Q and B_Q are scalars which allow us to adjust the intensity of the three primary colors $\vec{R}$, $\vec{G}$ and $\vec{B}$.

Figure 2.3 shows an example of a color represented by the vector $\vec{Q}$ which is composed of the three primary vectors $\vec{R}$, $\vec{G}$ and $\vec{B}$. The R_Q, G_Q and B_Q are defined as the trichromatic values. In order to simplify the visualization of the trichromatic color space it is useful to use a two-dimensional space, for example, the plane $R_Q + G_Q + B_Q = 1$ (green surface in Figure 2.3). All colors are then projected onto this plane such as the intersection point I of vector $\vec{Q}$. This projection obviously results in a loss of information, in this case the intensity of vector $\vec{Q}$. The intersection point of vector $\vec{Q}$ with the plane, whose coordinates are noted as rgb, are given by the following equations :

$$r = R_Q/(R_Q+G_Q+B_Q), \quad g = G_Q/(R_Q+G_Q+B_Q), \text{ and } \quad b = B_Q/(R_Q+G_Q+B_Q). \tag{2.2}$$

i. For a more detailed description of the development of colorimetry at the beginning of the 20$^{\text{th}}$ century see the book by Schanda [6].

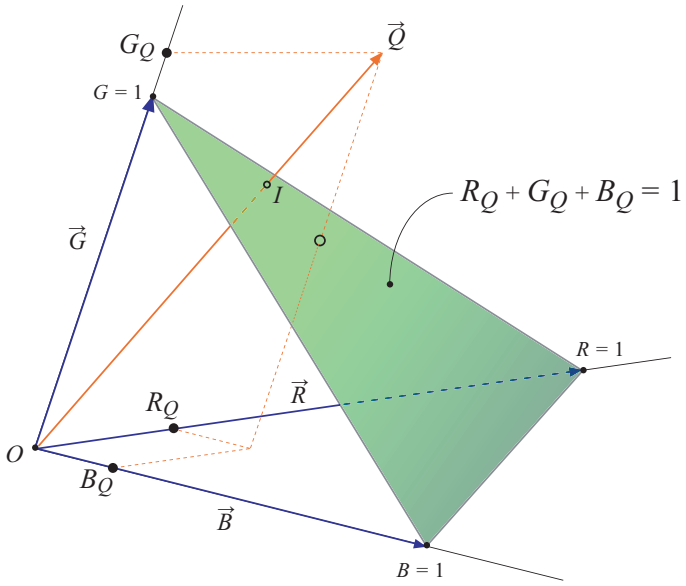

Figure 2.3 Color $\vec{Q}$ composed of three primaries : $\vec{R}$, $\vec{G}$ and $\vec{B}$.

As a result, $r + g + b = 1$. This triangle is named the Maxwell color triangle due to Maxwell's contributions to additive color theory.

Let us now consider the case of a human observer. As was presented in section 2.5, the human retina contains three types of cones, each with their own absorption curves (see Figure 2.2). Ideally, one would want to be able to stimulate each cone individually, but unfortunately, the fact that the absorption curves highly overlap forces us to make the best compromise. As a result, the CIE model is based on a color matching experiment where the following three monochromatic sources were used : one in the red at 700 nm which essentially only stimulates the L cones, one at 546.1 nm which stimulates the L and M cones and one at 435.8 nm. The last two wavelengths are actually emission lines of a mercury lamp. Using a bipartite field of view, a monochromatic light of constant power and of a chosen wavelength was sent on one side of the field while on the other side the three primary colors formed an additive mixture. The test subject then had to adjust the intensity of each of the primaries in order to reproduce the monochromatic reference light. Figure 2.4 shows the results of this experiment which are termed the color-matching functions $\bar{r}\bar{g}\bar{b}$ where the bar indicates that these values are the result of measurements made on many individuals.

This configuration allows us to pose that the additive color mixture is given by :

$$\vec{E}(\lambda) = \bar{r}(\lambda)\vec{R} + \bar{g}(\lambda)\vec{G} + \bar{b}(\lambda)\vec{B}, \tag{2.3}$$

with $\bar{r}$,$\bar{g}$ and $\bar{b}$ the color matching functions, that is the proportion of the three primaries

$\vec{R}$,$\vec{G}$ and $\vec{B}$ required in order to re-create a particular monochromatic light.

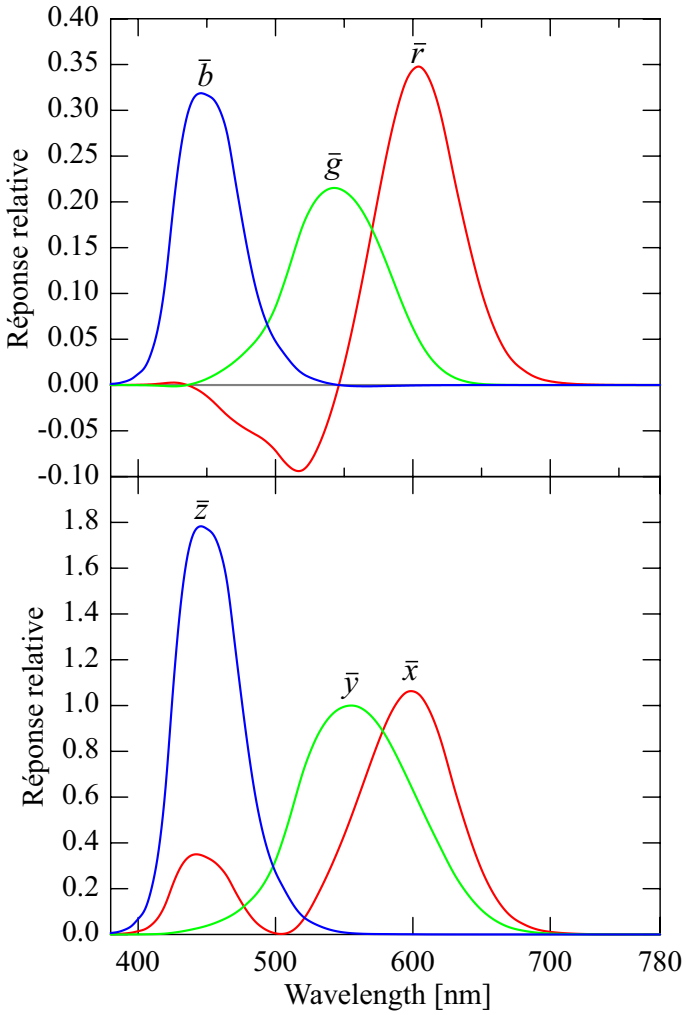

Figure 2.4 Color matching functions for a 2 degree angle of vision before ($\bar{r}\bar{g}\bar{b}$) and after conversion ($\bar{x}\bar{y}\bar{z}$). This angle of vision is sufficiently small to contain the stimulus in the macula lutea where the concentration of cones is at its maximum and fairly uniform.

We first can note that the quantity of green is lower than the other two light sources. This is explained by the higher sensitivity of the human eye to green light, more precisely light at 550 nm. Also note that the color matching functions possess negative values. These negatives values indicate that it was necessary to illuminate the reference color with a primary color in order to reach a color match. Other than the fact that using negative color matching functions was counterintuitive, at the time, taking into account negative values also made for more costly electronics. As a result, after a strong incentive from the American industry, the color matching functions were transformed in order to eliminate negative values. This

transformation was done using the following matrix :

$$\begin{bmatrix} \bar{x} \\ \bar{y} \\ \bar{z} \end{bmatrix} = \begin{bmatrix} 2.768\ 892 & 1.751\ 748 & 1.130\ 160 \\ 1.000\ 000 & 4.590\ 700 & 0.060\ 100 \\ 0 & 0.056\ 508 & 5.594\ 292 \end{bmatrix} \begin{bmatrix} \bar{r} \\ \bar{g} \\ \bar{b} \end{bmatrix} \tag{2.4}$$

This transformation leads to the well known $\bar{x}\bar{y}\bar{z}$ color matching functions for a two degree angle of vision (inside the fovea). It is important to note that other than eliminating negative values the matrix transformation also resulted in the transformation of $\bar{g}$ into the photopic sensitivity curve of the human eye. The fact that these modified color matching functions are the result of a mathematical transformation explains why they are often described as imaginary ; no real primaries could result in these color matching functions. In 1964, a new series of color matching functions were defined with a 10 degree angle of vision $\bar{x}_{10}\bar{y}_{10}\bar{z}_{10}$ which implicates cones which are outside the fovea.

Therefore, to calculate the color of an object with a known reflection or transmission spectrum, one needs to sum all the stimuli arriving into the eye in the visible spectrum $(\vec{E}(\lambda))$:

$$X = k_{\mathrm{N}} \int_{380\ \mathrm{nm}}^{780\ \mathrm{nm}} \phi(\lambda)\bar{x}d\lambda, \quad Y = k_{\mathrm{N}} \int_{380\ \mathrm{nm}}^{780\ \mathrm{nm}} \phi(\lambda)\bar{y}d\lambda, \text{ and } \quad Z = k_{\mathrm{N}} \int_{380\ \mathrm{nm}}^{780\ \mathrm{nm}} \phi(\lambda)\bar{z}d\lambda, \tag{2.5}$$

with k_{N} a normalizing constant and $\phi(\lambda)$ the stimuli. These stimuli are in fact the product of the illuminating light source's energy distribution and the spectral characteristics of the object :

$$\phi(\lambda) = \begin{cases} T(\lambda)S(\lambda) & \text{with } T(\lambda) \text{ the transmission as a function of wavelength} \\ R(\lambda)S(\lambda) & \text{with } R(\lambda) \text{ the reflection as a function of wavelength} \end{cases} \tag{2.6}$$

where $S(\lambda)$ corresponds to the light source's spectral distribution. In order to normalize the Y values between 0 and 100, the k_{N} constant is given by :

$$k_{\mathrm{N}} = \int_{380\ \mathrm{nm}}^{780\ \mathrm{nm}} \frac{100}{S(\lambda)\bar{y}d\lambda}. \tag{2.7}$$

Finally, the CIE xyz trichromatic color coordinates are given by :

$$x = \frac{x}{X+Y+Z}, \quad y = \frac{Y}{X+Y+Z}, \text{ and } \quad z = \frac{Z}{X+Y+Z}. \tag{2.8}$$

Thus, $x + y + z = 1$. This is the reason why the color coordinates are usually presented with

only the xy coordinates followed by the luminance value Y ; these three values form the well known CIE 1931 2° xyY color space.

Using equations 2.5, it is possible to generate the spectral locus, also known as the horseshoe diagram, that is the color space in which all possible colors are represented. This curve can be obtained by calculating the color coordinates using a monochromatic light source varying from 380 to 780 nm. The spectral locus shown in Figure 2.5 therefore corresponds to a luminance value of 0. Hence, each wavelength around the locus represents a specific hue (red, orange, yellow, etc.). The green dot in this same figure represents the perfect white, that is the xy color coordinates (0.33, 0.33) for a light source which would emit uniformly in the whole visible spectrum. At this point, the saturation of a color is equal to zero. As a result the closer a color is to the spectral locus curve the higher is its saturation. For example, lowering the saturation of a pure red would lead to a pinkish color and finally to pure white (see Figure 2.5). Note that the bottom line connecting the 380 nm point with the 780 nm point is called the purple line for the obvious reason that mixing red with blue-violet results in purple. The third dimension, which is not shown in Figure 2.5, is the luminance Y. Most importantly, at higher luminance values, the size of the locus decreases to a point where it becomes only a line at a luminance value of 100. The blue triangle shown in Figure 2.5

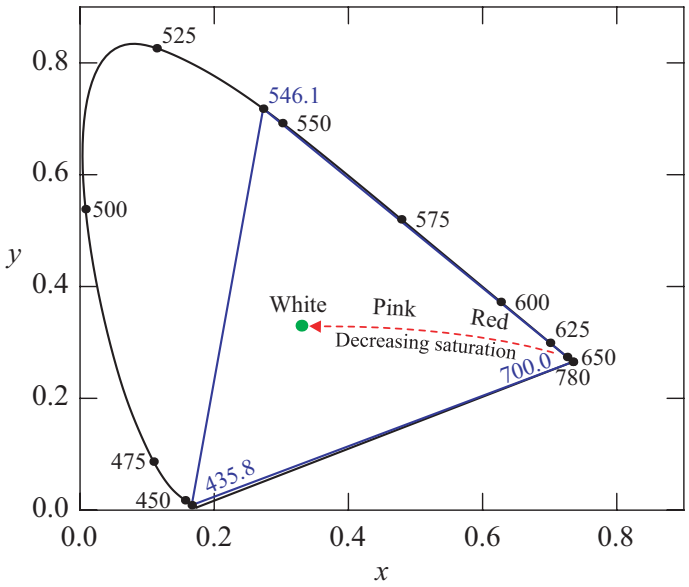

Figure 2.5 The CIE 1931 spectral locus in the xy color space. The blue triangle is formed by the three primaries used to define the color matching functions. The green dot represents a perfect white resulting from a light source emitting equally throughout the visible.

is formed by the three primaries used by the CIE to define the previously presented color matching functions. Therefore, everything outside this triangle represents colors for which

the color matching functions were negative. The space inside the triangle is called the gamut, that is all the colors which can be generated by the three primaries. This concept of gamut is important to consider when one is working with projectors, displays and printers, each of them with their own primary colors. As a result, some colors may be available when looking at a picture on a computer screen but simply not available once printed and vice versa. To obtain a larger gamut, high quality printers are often based on more than three primary colors and some new generation television screens are based on four primary colors (so called quadpixel technology).

Using the spectral locus also allows one to define a dominant wavelength for each color in order to clearly identify its hue. This can be done by simply tracing a line between a particular color and the reference white (illuminant color coordinates) and prolonging this line toward the spectral locus curve ; the intersection between this line and the spectral locus indicates the dominant wavelength. The extension of this line in the other directions indicates the complementary color. Figure 2.6 shows various examples of complementary colors ; mixing them consequently results in white. In the case of colors on the purple line one does not speak of complementary colors since purple is already based on a mixture of colors. Let's take for example color C1 in Figure 2.6. This particular color's dominant wavelength is 479.5 nm (blue-green) and complementary wavelength 580 nm (yellow). It is therefore possible to generate C1 by mixing its dominant wavelength with white light, its dominant wavelength with its complementary wavelength or even by using three primaries. The possibility to recreate a particular color by using different colors is what is called metamerism.

A color can thus be defined by its hue, saturation and brightness. The previously presented Table 2.1 gave examples of hues across the visible spectrum. Thus, saturation denotes the concentration of a hue ; for example, pink is less saturated than red. Finally, brightness is related to the perceived luminance of a color, for example, the difference between a low brightness dark red and a very bright fireman red.

2.6.1 Additive and subtractive color mixing

Having defined the concept of complementary colors, it is also important to clearly define the difference between additive and subtractive color mixing. Additive color mixing arises when different light sources are combined such as in screen projectors which are based on three colored light sources (red, green and blue-violet). The addition of these three colors generates white light. These three colors are most often termed primary colors since any combination of two of them cannot match the third [12]. This situation is illustrated in Figure 2.7, where the colors between the primaries, the secondary colors, result from mixing both the primaries adjacent to it. As a result, mixing red and green results in yellow, green

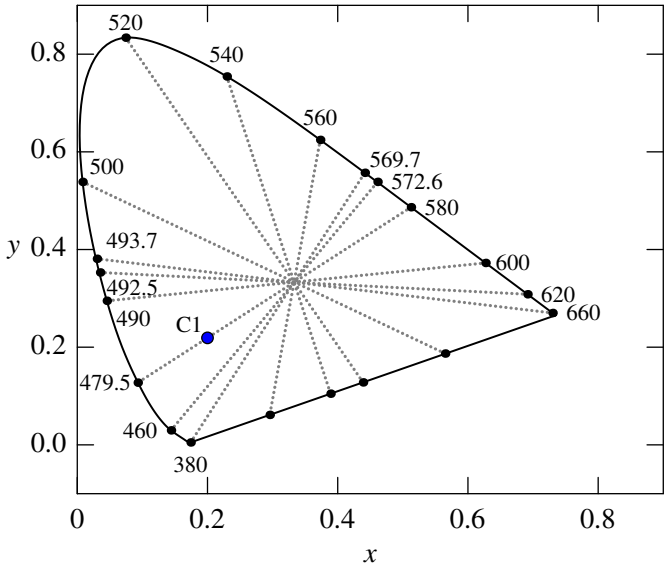

Figure 2.6 Dominant and complementary wavelengths.

and blue-violet in cyan and blue-violet and red in magenta.

In the case of subtractive color mixing, part of the visible spectrum is subtracted from the incident light. This is the case of inkjet printing where each ink absorbs part of the visible spectrum and reflects the rest. The three primary colors, which correspond to the secondary colors of additive color mixing, are cyan, magenta and yellow, and when mixed together these inks generate a brownish color. Since inks are not perfect absorbers, the addition of a black ink is customary in printing in order to be able to remedy the absence of pure black.

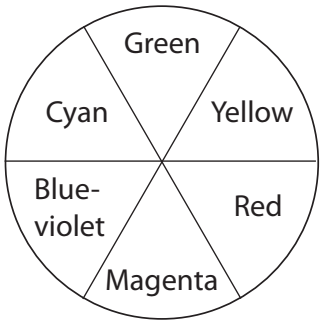

Figure 2.7 Goethe color circle showing the three *RGB* primary colors as well as their three complementary colors also known as subtractive primary colors. Thus red + cyan, blue + yellow and green + magenta all result in white light.

2.7 Light sources

We all know how the color of an object can be affected by the light source under which it is observed. Faced with our home's often insufficient lighting, haven't we all one day or another had the reflex of going towards a window in order to clearly perceive a color or distinguish color differences ? Sunlight, which comes from our Sun, is therefore the Earth's main source of energy, but also our main source of light. Note, that in the case of familiar objects, a psychophysical phenomenon known as color constancy may often occur. Objects will thus retain their color no matter what light source is used. For example, a red apple will remain red even under widely different light sources.

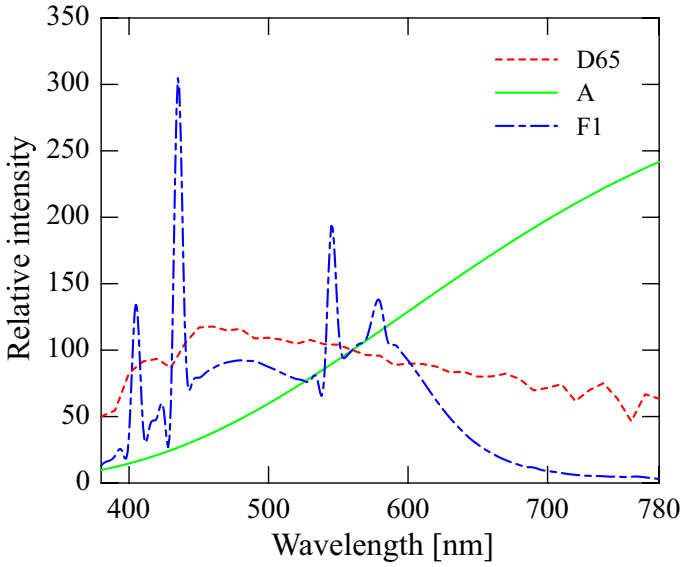

Figure 2.8 Relative intensities of three CIE illuminants (D65, A and F1). Note that they are all normalized by their intensity at 560 nm.

Since light sources are such an important component in color perception, the CIE has developed standard illumination sources which are termed illuminants. For example, illuminant A corresponds to an incandescent light source based on a tungsten filament. The CIE has also adopted a series of illuminants which represent natural daylight (the D series) : D50, D55, D65, D75. The number following the D letter is representative of the correlated temperature of the illuminant ; this concept will be defined below. These temperatures, which vary between 5503 and 7504 K, are given in Table 2.2. Since fluorescent lighting is also common in our everyday life (excited mercury vapour surrounded by phosphor), the CIE has also developed a F series of illuminants (see Table 2.2). Figure 2.8 presents the relative intensity distribution of illuminants D65, A and F1. Note that all these illuminants are normalized by their intensity at 560 nm.

Table 2.2 Illuminants defined by the CIE.

Illuminant	***xy* coordinates**	T_c **[K]**	**Description**
A	(0.44758, 0.40745)	2856	Incandescent lamp based on a tungsten filament. Emission corresponds to a black body at 2856 K.
D50	(0.34567, 0.35850)	5003	Sky with a correlated temperature of approximately 5000 K. When the sun is closest to the horizon.
D55	(0.33243, 0.34744)	5503	Sky with a correlated temperature of approximately 5550 K.
D65	(0.31272, 0.32903)	6504	Sky with a correlated temperature of approximately 6500 K.
D75	(0.29903, 0.31480)	7504	Sky with a correlated temperature of approximately 7500 K. For a cloudy sky.
E	(0.33333, 0.33333)	5454	Source with a uniform spectral emission.
	Fluorescent series		**Common name**
F1	(0.3131, 0.3371)	6430	Daylight
F2	(0.3721, 0.3751)	4230	Cool white
F3	(0.4091, 0.3941)	3450	White
F4	(0.4402, 0.4031)	2940	Warm white
F5	(0.3138, 0.3452)	6350	Daylight
F6	(0.3779, 0.3882)	4150	Lite white
F7	(0.3129, 0.3292)	6500	D65 Daylight
F8	(0.3458, 0.3586)	5000	D50, Sylvania F40 design 50
F9	(0.3741, 0.3727)	4150	Cool white deluxe
F10	(0.3458, 0.3588)	5000	TL85, Ultralume 50
F11	(0.3805, 0.3769)	4000	TL84, SP41, Ultralume 40
F12	(0.4370, 0.4042)	3000	TL83, Ultralume 30

Other light sources which have not been defined by the CIE also include : tungsten-halogen light sources, mercury lamps, xenon lamps, diodes, lasers, etc. For example, the lighting where the FCSEL dual ion beam sputtering (DIBS) system is installed is based on low pressure sodium lamps which are notorious for their very low color rendition index (poor color reproduction) ; as a result, the colors of my deposited filters were always surprisingly different when looked at under these lights.

By looking closely at illuminant A's emission curve in Figure 2.8, one notices how closely it matches that of a black body ; a body which absorbs all incoming electromagnetic radiation and reemits it in the form of heat. More precisely, this particular illuminant is modeled by a black body curve at 2856 K. The Planck equation can be used to calculate the power per surface per unit wavelength for a black body at a specific temperature :

$$U = \frac{2hc^2}{\lambda^5(e^{hc/k_B\lambda T} - 1)} \quad [\mathrm{W/m^3}], \tag{2.9}$$

with k_b the Boltzmann constant and T the temperature. The wavelength at which the emission intensity is the highest is easily calculated using Wien's law :

$$\lambda_{max} = \frac{hc}{4.965k_BT} \quad [\mu\mathrm{m}]. \tag{2.10}$$

Figure 2.9 presents the emission curves for a black body at temperatures varying between 2000 and 4500 K. Just as a stove's heating element glows red when heated, we can see in Figure 2.9 that the peak in emission is shifted towards shorter wavelengths as the temperature increases. It is this shift which explains why the emission becomes visible at higher temperatures. Hence, the temperature of an incandescent body can be approximated by looking at its emission spectrum or even its color. For example, the sun, which to all extent can be approximated as a perfect black body radiator, possesses an effective surface temperature of 5780 K. Using Wien's law (see equation 2.10) results in a maximum emission wavelength of 500 nm. It is interesting to note that our eyes' maximum sensitivity is not at 500 nm, but rather at 550 nm. An explanation for this difference, based on the total energy of a Planckian radiator, can be found in [13].

Most objects that surround us are not perfect black body emitters. These objects, which are termed gray bodies, possess an emission spectrum which can be calculated by multiplying the perfect black body's emission spectrum by a factor between 0 and 1. It is this proportionality factor which is called emissivity. For example, a perfect mirror possesses an emissivity of 0 whereas a perfect black body a value of 1. For an opaque object, the emissivity ϵ and

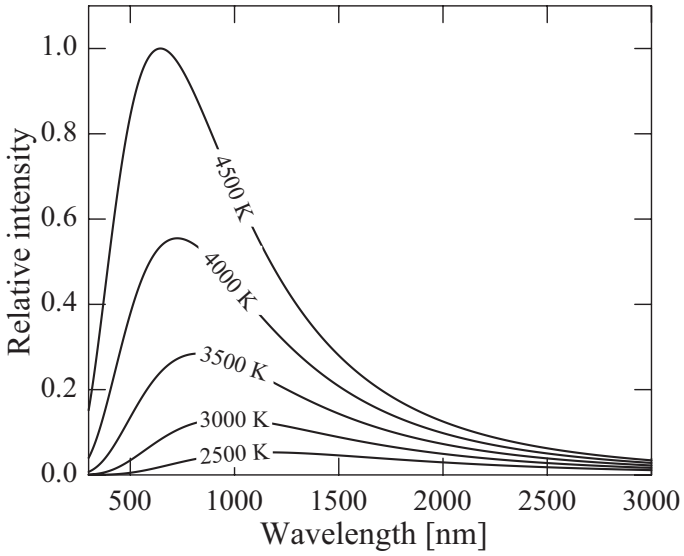

Figure 2.9 Emission intensity of a black body at various temperatures.

reflectivity are related by the following equation :

$$R(\lambda) = 1 - A(\lambda) = 1 - \epsilon(\lambda). \tag{2.11}$$

Therefore, the emissivity is equal to the absorption coefficient. Figure 2.10 presents the xy color coordinates of a black body for temperatures varying between 2000 K and an infinite temperature. Also indicated are the color coordinates of illuminants A, D65 and F1. The correlated temperature T_C of a light source is then determined by finding the xy color coordinates of the Planckian locus which are closest.

The following equations allow one to calculate the xy color coordinates of a black body for temperatures between 4000 K and 7000 K :

$$x_C = \frac{-4.6070 \times 10^9}{T_C^3} + \frac{2.9678 \times 10^6}{T_C^2} + \frac{0.09911 \times 10^3}{T_C} + 0.244063, \tag{2.12}$$

For temperatures between 7000 K and 25 000K :

$$x_C = \frac{-2.0064 \times 10^9}{T_C^3} + \frac{1.9018 \times 10^6}{T_C^2} + \frac{0.24748 \times 10^3}{T_C} + 0.237040. \tag{2.13}$$

The y_C coordinate is given by :

$$y_C = -3.000{x_C}^2 + 2.870x_C - 0.275. \tag{2.14}$$

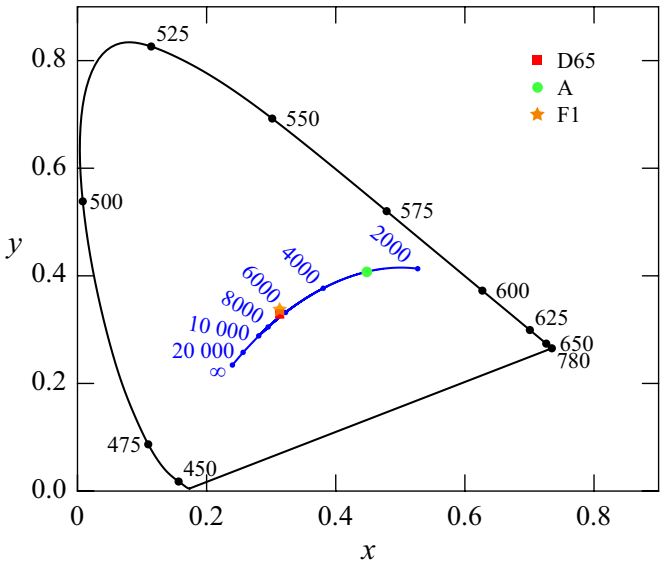

Figure 2.10 Spectra locus showing the color variation of a black body at temperatures varying between 2000 K and infinity. The color coordinates of illuminants A, D65 and F1 are also shown.

Finally, it is interesting to note that the color coordinates of daylight still follow fairly closely those of a black body emitting at various temperatures even though the sun's light is affected by many factors : the Earth's atmosphere, the presence of clouds, the time of day as well as the weather.

2.8 Metamerism

As previously presented, Grassman's second law mentions that the spectral composition of a color mixture is not revealing, but only its trichromatic color coordinates. In other words, different spectral compositions can lead to the same observed color under a specific light source and for a specific observer. This phenomenon is defined as metamerism. It is metamerism that allows an artist to reproduce a scenery using paints and, unfortunately, a counterfeiter to reproduce false documents using printing.

In order to quantify the degree of color matching between two objects, one must calculate a color difference ΔE. This can be done fairly simply by calculating the distance between two sets of color coordinates, for example in the xyY color space. This situation is somehow complicated by the fact that in the case of the xyY color space, the distances between colors are highly non-linear. As a matter of fact, the green region is seen to occupy a much larger area of the spectral locus when compared to other hues. Thus, two different greens may present a large ΔE even though visually two different reds with a lower ΔE present a similar

color disparity. This was measured by MacAdam in 1942 for different colors and is presented in Figure 2.11 where the ellipses represent regions of just noticeable color differences.

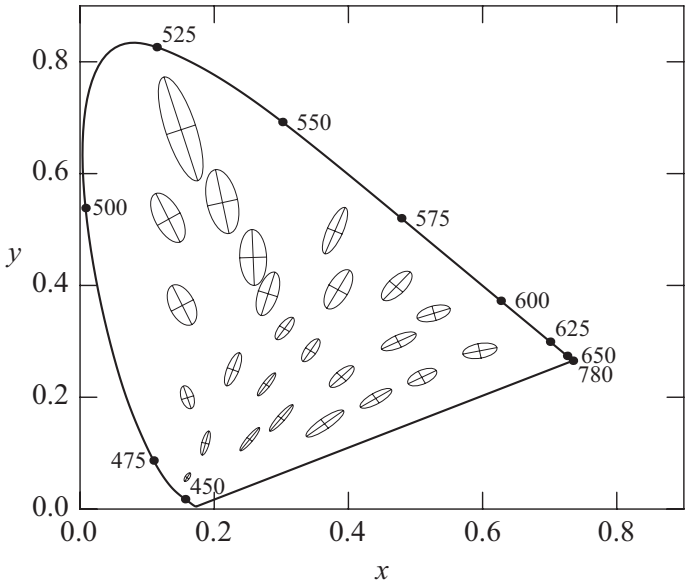

Figure 2.11 xy color space with MacAdam ellipses of just noticeable color differences. Notice how the ellipses are much larger in the green region. Note that the ellipses have been enlarged 10 times for higher clarity.

To solve this issue, color theorists have developed other more linear color spaces (correlating color perception with visual spacing). This is the case of the CIE 1976 $L^\star a^\star b^\star$ color space (CIELAB)) based on the color opponent theory ; the signals generated by the cones are compared and subtracted. In fact, it can be shown that contrary to addition, subtraction leads to differentiation between light intensity and wavelength [14]. In the color opponent theory, which has been experimentally verified by Jameson in 1955 and DeValois in 1958 [4], the interactions between the cones' signals are defined as follows :

- The luminance perception results from L + M [ii].
- The red-green channel results from L - M.
- The yellow-blue channel results from L + M - S.

A simple way of confirming this model is that it is impossible to imagine a reddish-green or bluish-yellow. The $L^\star a^\star b^\star$ color space is therefore defined by the following equations :

$$L^\star = 116\left(\frac{Y}{Y_n}\right)^{1/3} - 16, \tag{2.15}$$

ii. L stands for long wavelength (red sensitive cones), M for medium (green sensitive cones) and S for short (blue sensitive cones).

$$a^\star = 500\left[\left(\frac{X}{X_n}\right)^{1/3} - \left(\frac{Y}{Y_n}\right)^{1/3}\right] \text{ and,} \tag{2.16}$$

$$L^\star = 200\left[\left(\frac{Y}{Y_n}\right)^{1/3} - \left(\frac{Z}{Z_n}\right)^{1/3}\right], \tag{2.17}$$

with X/X_n, Y/Y_n and $Z/Z_n > 0.008856$, where X_n, Y_n and Z_n are the tristimulus values of the reference white (illuminant). $L^\star$ corresponds to the luminance whereas $a^\star$ and $b^\star$ represent the green-red and the blue-yellow channels, respectively. From these values are often calculated two other parameters : the chroma $C^\star_{\text{ab}}$ and hue $h^\star_{\text{ab}}$:

$$C^\star_{\text{ab}} = \sqrt{a^{\star 2} + b^{\star 2}}, \tag{2.18}$$

$$h^\star_{\text{ab}} = \arctan\left(\frac{b^\star}{a^\star}\right). \tag{2.19}$$

Having defined a more perceptually-linear color space, it is now possible to calculate color differences. In this particular case, the difference is given by :

$$\Delta E^\star_{\text{ab}} = \left[(L^\star_1 - L^\star_2)^2 + (a^\star_1 - a^\star_2)^2 + (b^\star_1 - b^\star_2)^2\right]^{1/2}, \tag{2.20}$$

where 1 and 2 represent two different objects (2 is usually set as the standard). Since color differences are regularly calculated under various light sources, we will often indicate the chosen illuminant I in the following fashion $\Delta E^\star_{\text{ab, I}}$. The CIE recommends the use of illuminant D65 as a reference and illuminants A and F1 as test sources. In the case where the color difference remains low under all three illuminants, the degree of metamerism is said to be low. It is accepted that no color difference can be distinguished by the human eye for $\Delta E^\star_{\text{ab}} < 1$ [15]. A value of 2.3 is considered to generate a just noticeable color difference [16, 17].

Since the development of the CIELAB color space, there have been continuous attempts at developing more advanced color difference equations (CIE94 ($\Delta E^\star_{94}$) [4] and CIEDE2000 ($\Delta E^\star_{00}$) [18]). Unfortunately, their metamerism threshold is often not clearly defined and for reasons I will explain in chapter 6, $\Delta E^\star_{\text{ab}}$ was sufficient for the needs of this work.

CHAPTER 3

OPTICAL COATINGS FOR SECURITY APPLICATIONS

3.1 Foreword

At first glance, it may seem that describing the technology behind anti-counterfeiting devices is counterproductive. Indeed, shouldn't this type of information be kept secret ? As it turns out, the security provided by an optically variable device (OVD), is largely based on know-how and skill as well on the high cost of the production equipment rather than by the fabrication recipe itself.

In this chapter, we first give a brief overview of the main reasons why optical security devices are paramount in today's technology-driven world as well as a quick historical overview of their evolution. We then present the basic principles behind interference-based security devices as well as the various possibilities they offer. Additionally, we present features which have been added to increase their simplicity of use as well as ensure the continued efficiency of interference security image structures (ISISs) ; in particular through the addition of metamerism, the incorporation of magnetic materials, the combination of diffraction and interference and finally, the use of photonic color technology and active materials.

3.2 Introduction

Counterfeiting is unfortunately here to stay. Often focused on security documents such as passports and identity cards as well as valuable documents such as banknotes and credit cards, counterfeiting also affects everyday consumer products from golf clubs to airplane parts. In fact, the Federal Aviation Administration (FAA) estimates that some 520 000 counterfeit parts are installed in planes each year [19]. Other than significant financial consequences, economic losses are estimated to reach up to 1.8 trillion dollars in 2015 [20], it is the public's safety that is most at risk. Indeed, copied products made without any regulation and supervision rarely fulfil quality and safety requirements. A perfect example of this being counterfeit pharmaceutical products that according to the World Health Organization (WHO) represent 25% of the available medicine in developing countries [21]. It is therefore no surprise that governments and institutions have always wielded technology to their advantage in order to protect their documents and products.

Historically, currency has always benefited from the most advanced security devices. Before the advent of such devices, one of the most popular methods of anti-counterfeiting was

the death penalty [22]. Although this may have been an effective means of discouragement it was abandoned as human right issues made headway. As a result, emphasis was put on printing bank notes with intricate and complex images, distinctive typefaces, exclusive colored inks, watermarks, microprinting and unique serial numbers. These features were sufficient until the arrival of accurate color copiers and more recently scanners and high-resolution printers (so-called digifeiting). Incidentally, color was introduced on banknotes following the appearance of black and white photography. To counteract these potentially serious threats, optically variable devices (OVDs) based on diffraction (DOVIDs : holograms, stereograms, kinegrams, etc.) and interference (ISIS) were introduced ; the iridescence presented by these devices inhibiting the use of standard reprographic technologies. It is important to note that no device is infallible and for this reason modern banknotes benefit from the use of multiple features each with their specific purpose [23].

Although all of these features have contributed in some way in the fight against counterfeiting, one must never forget that even the best features are rendered useless without the general public's participation. It is now recognized that the public's awareness and understanding, provided through education, is crucial in increasing counterfeit detection [24]. As a result, security features should always remain simple to use and the effects they present easy to remember. Indeed, despite the presence of multiple devices, studies have shown that on average the public remembers a fairly low number of them (1.7 currency features in The Netherlands in 1999 [25]). In another remarkable example, it was shown that the awareness level in the U.S. for the black to green color shifting feature on American banknotes was of only 17% in 2004 [2].

3.2.1 The emergence of interference security image structures

In 1968, the Bank of Canada approached the NRC for ideas of novel security devices. The NRC, spearheaded by J.A. Dobrowolski proposed optical interference coatings as potential candidates [3, 26]. Although a feature often considered as undesirable in the field of optical filters, the observed angular color change was not only judged as an excellent counterfeiting deterrent, but also an efficient and simple means of authentication for the general public. These structures also had the added advantage of being machine readable [27, 28].

In December 1987, the Bank of Thailand introduced a commemorative banknote protected with optically variable ink (OVI) produced by OCLI. A few months later, in April 1988, British Columbia introduced driver's licenses displaying a transparent to red color shifting five-layer ISIS (made by Identicard and NRC). In December 1989, following extensive work at the NRC in collaboration with Vadeko International, an engineering firm, the Bank of Canada introduced its first 50 dollar bill with a gold to green color shifting ISIS. Since then,

ISIS have demonstrated excellent efficiency [29] and are highly appreciated by the general public [2] ; for example, more than 40 metric tons of optically variable pigments (OVPs) are produced yearly [30] and OVI is used on the currencies of more than 100 countries [31].

3.3 Basic principles and structures currently in use

Let us now consider the basic principles behind the use of optical coatings for security purposes. As previously mentioned, it is the intrinsic color shift observed as a function of the observation angle which is the key feature of ISIS. The color change is due to a shift in the spectral characteristics of the filter towards shorter wavelengths at higher angles of incidence. This can be demonstrated by considering the case of a single thin-film of index n_2 and thickness d (see Figure 3.1). The difference in optical paths Δ(OP) between the beam which travels inside the film (ABC) and the incident beam which was simply reflected at point A (AD) is given by (ABC)n_2 - (AD)n_1. One can show following simple trigonometry that :

$$\Delta(\mathrm{OP}) = 2d\sqrt{n_2^2 - \sin\phi_0^2} \quad \text{if} \;\; n_1 = 1, \tag{3.1}$$

where ϕ_0 is the angle of incidence of the beam. As ϕ_0 is increased, Δ is seen to decrease and therefore, if one has constructive interference at λ_0 at normal incidence, meaning that Δ(OP) contains an integer number of wavelengths λ_0, this same constructive interference will occur at a $\lambda < \lambda_0$ at higher ϕ_0. Consequently, all interference-based devices will shift towards shorter wavelengths as a function of the observation angle. A device having a gold color at normal incidence will thus shift towards green and eventually blue when observed at a more inclined angle.

Note that the final optical path difference also depends on the presence of soft (when going from a high to low refractive index) and/or hard (when going from a low to high refractive index) reflections at points A and B. In the case where the incident medium is air, point A will typically present a hard reflection and thus a $\lambda/2$ phase shift. For example, if the thickness of a film is equal to a quarter-wave ($d = \lambda/4n$) then equation 3.1 results in a path difference of $\lambda/2$ at normal incidence. Now, if the index of this quarter-wave film is higher than the substrate's, a hard reflection will only be present at point A. The total path difference will thus be equal to zero and constructive interference will take place between both beams (increased reflectance). If, on the contrary, the index of the film is lower than the substrate's, hard reflections will be present at both points A and B and as a result the final path difference will be $\lambda/2$, therefore destructive interference will ensue (decreased reflectance i.e. antireflection). Correspondingly, these conditions will be inverted for a film of half-wave ($d = \lambda/2n$) thickness. Both these specific thicknesses are very often the basis of many classic

filter designs. For example, one can construct a reflector by alternating high (H) and low (L) index of refraction quarter-wave thick materials ($[HL]^x H$ where x is an integer) or fabricate a Fabry-Perot filter by separating two reflectors by a half-wave ($[HL]^x HH[LH]^x$).

It is worth mentioning that single layer dielectric structures (for example, pearl luster or nacreous pigments) benefiting from interference effects have been used for their high luster and brilliance in many applications such as plastics, cosmetics, paints, etc. [32] ; one such example is TiO_2-covered mica flakes. However, the fact that these pigments offer practically no color change as a function of the observation angle limits their use for security applications.

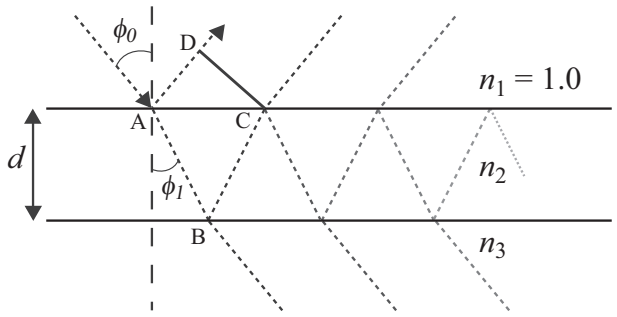

Figure 3.1 Multiple reflections in a thin film of index n_2 and thickness d. The incident medium is air and therefore $n_1 = 1$.

There exist two main categories of optical filters, those based on all-dielectric materials and those based on metallic and dielectric materials (metal-dielectric filters). Using dielectric materials with negligible absorption in the visible offers the possibility of a device which can be used both in reflection and/or in transmission (e.g., through the use of a window or when placed over printed information). On the other hand, a high number of layers is often required in order to obtain a sufficiently high color saturation which inevitably will increase fabrication costs. The addition of metallic layers offers the opportunity of rapidly increasing the reflectance and thus decrease the amount of required layers as well as the total cost. On the other hand, the high absorption of metallic films drastically decreases the transmission as well as the maximum attainable reflection and can thus limit their use in particular applications. Although more expensive, it has also been shown that all-dielectric filters possess a much higher chemical and mechanical stability over time when compared to metallic layers which have a tendency to age in an unpredictable manner [33, 34]. As a result, metal-dielectric structures must typically be laminated for protection. Note that lamination decreases the saturation of colors due to the added surface reflection and, considering Snell's refraction law, can also limit the maximum incidence angle and thus the color shift [33].

3.3.1 All-dielectric filters

Over the years, there have been a multitude of proposed devices. In his paper published in 1973 [3], Dobrowolski proposed numerous all-dielectric filters with interesting properties. Mainly, a red to blue color shifting filter, a broad-band reflector which would hide underlying information at normal incidence and become transparent at higher angles as well as a transparent to red filter (reflection peak in the near-IR would shift into the visible). Note that the last two effects cannot be obtained with metal-dielectric filters.

As previously mentioned, for physical reasons one typically observes color changes towards shorter wavelengths. In this regard, there exists another interesting filter design known for its reverse color shift from blue to red. This effect is obtained by carefully positioning two reflectance bands, one in the blue wavelength region and one in the near-IR. Thus, when the filter is tilted, the blue band shifts into the UV whereas the band in the near-IR falls into the visible (red).

One example of an all-dielectric filter applied for security is the gold to green color shifting filter present on the 1986 Birds of Canada banknote series. More precisely, this filter was based on five layers of SiO_2 and ZrO_2 (HL^3HL^3H @ 585 nm) (see Figure 3.2 for simulated spectra of the gold to green color shift of this particular device) [35]. The filter was transferred from a polyethylene terephthalate (PET) substrate covered by a release layer of organic or synthetic wax [36] using a UV curable black adhesive developed by 3M [33]. Indeed, when using all-dielectric filters, the background onto which the filter is apposed is very important. When using a white background, the light which is transmitted through the filter will be reflected back towards the observer, thus adding itself to the reflected beam and resulting in a decreased saturation. Also, since the colors perceived in reflection and in transmission are complementary, the resulting color can actually be almost completely desaturated. Obviously, the amount of light which is reflected back specularly will greatly depend on the background's surface roughness. As a result, a black background is often used to eliminate the transmitted component of the light. Since optical filters reflect light specularly, it can be difficult to observe the color shift when using a single light source ; artificially roughening the surface has been shown to help. This is not the case for filters used in transmission, since authentication is much simpler.

Placing a filter over sensitive information can also limit forgery while still allowing the information to be read. In fact, tamper evident filters have been developed which exhibit an irreversible color change when tampered with. This effect can be obtained by modifying the adherence between two layers of a thin-film stack [37, 38, 39].

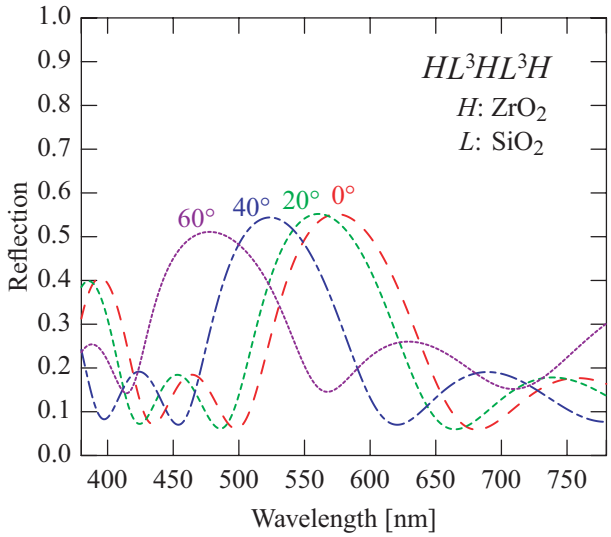

Figure 3.2 Reflection spectra at various angles (unpolarized light) of an all-dielectric interference filter simulating the five-layer optical security device initially developed for the Bank of Canada. The high index of refraction material is ZrO_2 ($n_{550\,\mathrm{nm}} = 1.88$ - taken from the J.A. Woollam material library) and the low index material SiO_2 ($n_{550\,\mathrm{nm}} = 1.46$ [40]). The structure of the device is indicated in the upper right corner.

3.3.2 Metal-dielectric filters

The most popular metal-dielectric structure currently in use is generally based on the following three-layer system : a thin partially absorbing film followed by a dielectric spacer and completed by a metallic reflector. Often described as Fabry-Perot-like, this structure allows the obtention of a very high color saturation with a minimum of layers due to a combination of interference and of selective absorption (at specific wavelengths the electric field reaches a maximum at the absorber) [41]. This absorption also results in a lower brightness when compared with absorption-free all-dielectric filters.

The choice of material for each of the individual layers as well as their thickness is made in order to increase performance and obtain the desired color shifting properties. Modifying the thickness of the spacer allows one to adjust the position of the reflection peaks (see Figure 3.3). In the example presented in Figure 3.3a, the reflection of a Fabry-Perot-like structure based on Cr|MgF_2|Al is shown for various thicknesses of MgF_2 : two quarter-waves (QWs), four QWs and six QWs at 575 nm (knowing that one QW = $\lambda/4n$ and two QW is one half-wave). One can see how the width of the main peak decreases as the thickness is increased ; this correspondingly increases the saturation in color (curve shown is further from the origin in the $L^\star a^\star b^\star$ color space in Figure 3.3a). Thicknesses are therefore typically chosen between 2 to 8 QWs. On the other hand, too many QWs results in multiple peaks in the visible and

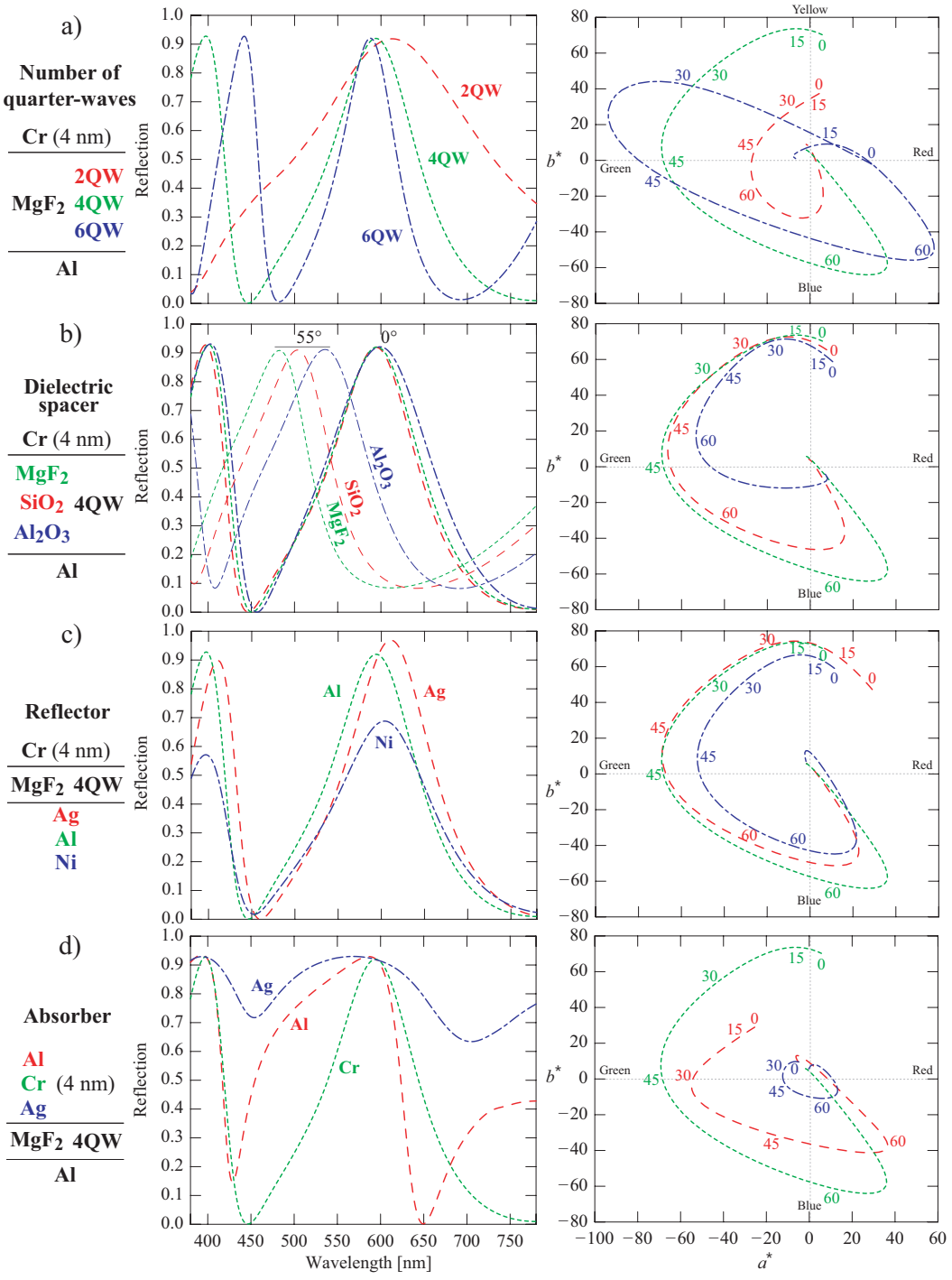

Figure 3.3 Various configurations of Fabry-Perot-like metal-dielectric filters and their effect on the reflectance and the color variation performance in the $L^\star a^\star b^\star$ color space (calculated under illuminant D65). From top to bottom, we present the effect of changing : a) the thickness in quarter-waves of the dielectric spacer (@ 575 nm), b) the dielectric spacer's material, c) the metallic reflector's material, d) the absorber's material.

can thus result in desaturated colors [42]. One can also see, in the present example, that the color varies from gold to green to eventually blue. To obtain a simplified two color shift, considered more obvious for lay viewers [43], it has been shown that an overlying colored dye can filter colors at high angles of incidence (e.g., yellow dye to block blue) [44].

As for the spacer's material, it can be shown that choosing a low index of refraction dielectric material increases the color variation (from Snell's law $n_1 \sin\phi_0 = n_2 \sin\phi_1$; ϕ_1 will be larger for lower values of n_2) so that SiO_2 or MgF_2 are most often the materials of choice. This is clearly demonstrated in Figure 3.3b for three spacer materials of a thickness of 4 QWs : Al_2O_3 with a refractive index n equal to 1.77 at 550 nm [40], SiO_2 ($n_{550\text{ nm}} = 1.49$) and MgF_2 ($n_{550\text{ nm}} = 1.38$) [40].

In order to increase the general brightness of the filter, metals possessing a high reflectance and neutral color such as Ag and Al are typically chosen as the bottom reflector. Figure 3.3c shows the effect of different metals when choosing from Ag, Al and Ni ($R_{\text{Ag}} = 96\%$, $R_{\text{Al}} = 92\%, \text{and } R_{\text{Ni}} = 61\%$ @ 550 nm). As predicted, the only significant effect one notices is the decrease in the maximum amplitude of the reflectance peaks as the reflectance of the mirror decreases. In terms of color variation, Ag and Al offer a very similar performance. Although most devices are reflection based, some transmission based metal-dielectric structures have also been proposed [41, 45]. An effect, which to the best of our knowledge, has not yet been exploited is possible when using a semi-transparent mirror. Indeed, fabricating an asymmetric stack allows one to obtain a device whose color in reflection is dependent on the side of observation, as well as being semi-transparent (triple-color-shift) [46]. Figure 3.4 shows an example of such a filter which presents a purple to black color shift in transmission, a red to yellow shift in reflection and a green to blue shift in reverse reflection.

Finally, it has also been demonstrated that the top semi-absorbing film must present a ratio of $n/k \approx 1$ [47]. We show three examples in Figure 3.3d where the absorber is either Al ($n/k = 0.14$), Cr ($n/k = 0.70$) or Ag ($n/k = 0.04$) all with a thickness of 4 nm ; note that all these metals possess a fairly neutral color. Clearly, the closer the n/k ratio is to one, in this case Cr, the higher the color saturation obtained at normal incidence and the higher the color travel. Despite this finding, simple structures based purely on the use of aluminium ($Al|Al_2O_3|Al$) have recently been proposed as potential candidates for security and decorative purposes [48]. Obviously, the thickness of the absorber must also be optimized.

The fact that metal-dielectric filters require fewer layers have made them the structure of choice to protect most banknotes. Indeed, the sheer number of banknotes which are required to be protected, often reaching the billions, makes cost of fabrication a critical parameter. For example, the Bank of Canada converted its five-layer all-dielectric filter to a three-layer metal-dielectric filter with a similar performance. Cost is also the reason why fabrication of

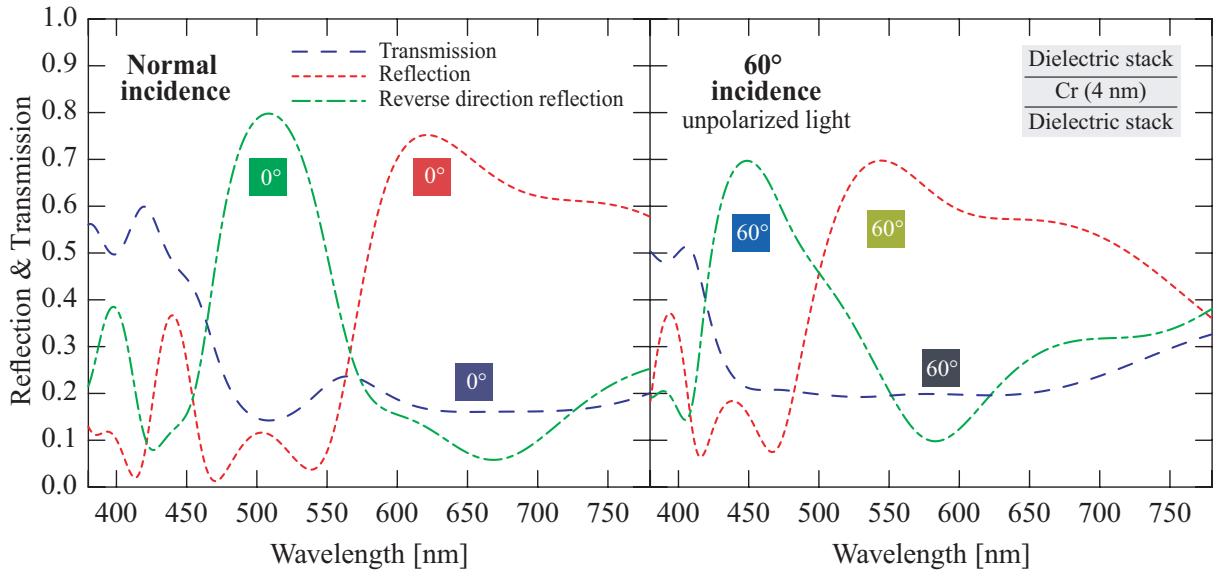

Figure 3.4 Reflection and transmission spectra at normal incidence of a filter with three different color shifts, one in transmission (purple to black) and two in reflection (forward direction from red to yellow and reverse direction from green to blue). Note that the structure of the filter is shown in the upper right corner. The individual colors for each observation condition are also shown at normal and at 60° incidence under illuminant D65.

OVDs is mostly done by roll-to-roll coating using e-beam evaporation, known for its high deposition rate. Systems must also be equipped with an optical monitoring system to control the thickness of the layers *in situ* and consequently the resulting color [49]. A precision as high as 1.5% on thickness is typical and can be required to maintain color consistency [50]. Very often this monitoring system is linked to the deposition parameters in order to immediately re-adjust the deposition rate. Very high uniformity is required in order to ensure a steadfast color across the whole web. Due to the porous nature of e-beam evaporated films, the design may need to be adjusted to account for the absorption of water once exposed to the ambient environment [51].

More recently, it has been proposed to replace the top semi-absorbing film by a metal film presenting nanoclusters [52, 53] (Brandsealing®). By carefully controlling the size and shape of the clusters, the plasmon resonance excitation can be finely tuned and serve as an optical code which is machine readable [54]. Others have also integrated an anisotropically scattering layer over the dielectric spacer which is then coated with a semi-absorbing metal film (anisotropically scattering Fabry-Perot). Although these structures show little change in color when tilted due to their highly diffuse nature, they still retain good color saturation. Their anistropic nature also procures them with rotation-dependent optical properties and therefore they also possess a positive/negative image flip when rotated [55].

3.3.3 Optically variable pigments

Patterning an interference filter into a specific shape is not a simple task. Although it has been done by using masking during deposition, laser etching [56], hot stamping, using soluble materials [57], embossing [58], etc., one method which allows highly complex images to be created is based on using optically variable pigments (OVPs). In this particular case, the desired filter is first deposited onto a release coated web, it is then delaminated, milled into a powder and incorporated into a printing vehicle, thus forming what is known as optically variable ink (OVI) [47, 59] (OVP is produced by Flex Products and OVI by SICPA [60, 61, 62]). These pigments are based on Fabry-Perot-like structures, but consist of five layers (absorber|spacer|mirror|spacer|absorber) since they are symmetric around the opaque mirror. This symmetry is essential since during the printing process, one cannot control on which side the pigment will fall. To ensure the pigments lay flat, the aspect ratio of the thickness versus size of the pigments is kept at approximately $10:1$ [42]. Obviously, the pigments do not all lie perfectly flat ($\approx 10^\circ$ angle on average) so that the diffuse reflection is increased (10% specular and 90% diffuse) and thus results in a decrease in color saturation (average of colors from slightly different angles) [50, 63].

Another advantage procured by the incorporation of OVPs into an ink is that the whole structure is essentially laminated and as a result, oxidation and damaging of the sensitive metallic layers are no longer an issue. Additionally, OVI is more flexible when compared to a foil-type device where the mechanical properties can be limiting once apposed onto a flexible substrate [47].

Lately, in an effort to increase the covert security offered by OVPs, it has been demonstrated that the pigments can be made into various shapes (diamonds, squares, etc.) by using an embossed foil as the substrate during deposition [64] (see Figure 3.5). Each individual pigment can also be marked with a specific symbol or image by patterning one or more of the layers (laser ablation, flexographic printed oil which vaporizes during deposition [64, 65], chemical etching, etc.). When viewed under a microscope, one can easily observe these shaped pigments and therefore rapidly validate the authenticity of the device.

Lastly, note that there are commercial products which display iridescent effects currently on the market (wrapping paper based on co-extruded polymer films, ChromaFlaire by Flex Products [67], etc.). Although the color shifts offered by such products may not be of the same quality as current security devices, the issue of them being used for counterfeiting must be seriously considered.

Figure 3.5 Example of a micro-structured square shaped magenta to green optically variable pigment displaying a Euro symbol. Image taken from [66].

3.4 Additional effects

Realizing that a simple color shift may not be sufficient to protect against future counterfeiters, most of the present research has focused on implementing additional features to the classic ISIS. The main goal is to increase fabrication complexity while still maintaining or even simplifying the authenticity validation phase for the general public. The following is thus a survey of these augmented interference-based devices.

3.4.1 Metamerism

As mentioned in the previous chapter (see section 2.8), metamerism is a phenomenon where two objects with different reflection or transmission spectra appear to possess the same color under a specific light source. Juxtaposing two such elements therefore allows for the creation of a hidden image effect. For example, the 1985 Dutch 250 guilder sported a metameric feature based on green metameric inks. Under normal lighting the feature was fairly uniform in color, but when observed through a red filter, a rabbit would appear (see Figure 3.6). This effect was possible since the inks had almost identical spectra in the green-wavelength region whereas they differed in the red [8]. Hence, the use of a red filter accentuated these differences. In 1999, the polymer Romanian 2000 Lei, went one step further by incorporating a magenta filter onto the banknote itself hence resulting in a self-authenticating banknote.

In the previous examples, the metameric devices were based on classic non-iridescent inks. However, there have also been some examples of interference-based metameric features. To our knowledge, the first metameric feature to be proposed [3] consisted of two filters with identical colors, which when superposed would transmit no light. Perhaps due to its complexity and potential cost, this feature was never implemented but nonetheless it proposed an innovative

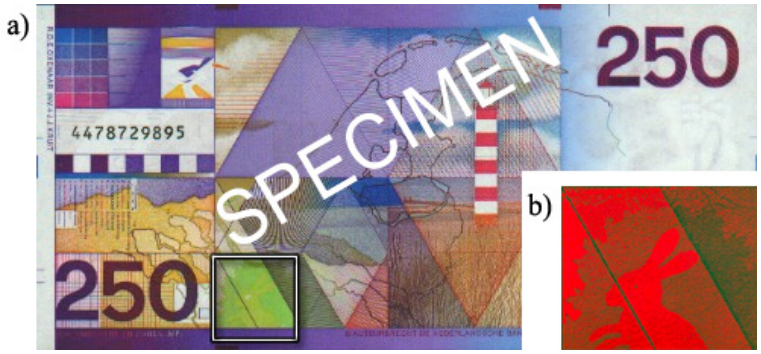

Figure 3.6 The 1985 Dutch 250 guilder sporting a feature based on metameric inks [inside white square in a)]. Notice that the rabbit is still slightly visible on the image even under normal lighting. In b) the inks are viewed through a red filter (image taken from [8]).

concept.

About two decades later, metamerism was once again suggested after having noticed that Fabry-Perot-like metal-dielectric filters with different spacer thicknesses resulted in similar colors [63]. Figure 3.7a presents the variation of color in the $L^\star a^\star b^\star$ color space as a function of increasing MgF_2 thickness for a Al|MgF_2|Cr structure (from 0 to 800 nm). As can be seen, there are multiple points where the color trajectories intersect. These points correspond to different MgF_2 thicknesses which generate identical $a^\star$ and $b^\star$ coordinates. Keep in mind that in order to ensure an adequate color match, one must also consider the luminance value $L^\star$ of both configurations (presented in Figure 3.7b).

In Figure 3.7b we present the difference in color $\Delta E^\star_{\text{ab, D65}}$ between all possible thickness combinations of MgF_2 between 0 and 800 nm. We first notice that this figure is symmetric (line of symmetry $x = y$). We also notice that the lowest $\Delta E^\star_{\text{ab, D65}}$ is obtained along the diagonal since this region corresponds to two samples with identical MgF_2 thicknesses. In total, there are 13 regions with a fairly low $\Delta E^\star_{\text{ab, D65}}$. Let us now choose one of these intersections (see red circle in Figure 3.7a and hexagon in Figure 3.7b) ; the lowest color difference in this particular case is obtained when comparing samples with thicknesses of MgF_2 equal to 383 and 589 nm. The resulting reflection spectra of both these samples are shown in Figure 3.7c. It is fairly straightforward to understand why these two samples are metameric. Indeed, the spectra match fairly well in the region of the human eye's maximum photopic sensitivity (around 550 nm ; see $\bar{y}$ in Figure 2.4 in the previous chapter) whereas they differ in regions where the eye is less sensitive (near-UV and near-IR). The fact that both filters possess different spectra results in their having different color trajectories as a function of the observation angle (see Figure 3.7d). Therefore, at normal incidence both samples are green and at an angle of 45° the 383 nm MgF_2 filter displays a bluish tint whereas the 589 nm MgF_2 filter is more purplish. As

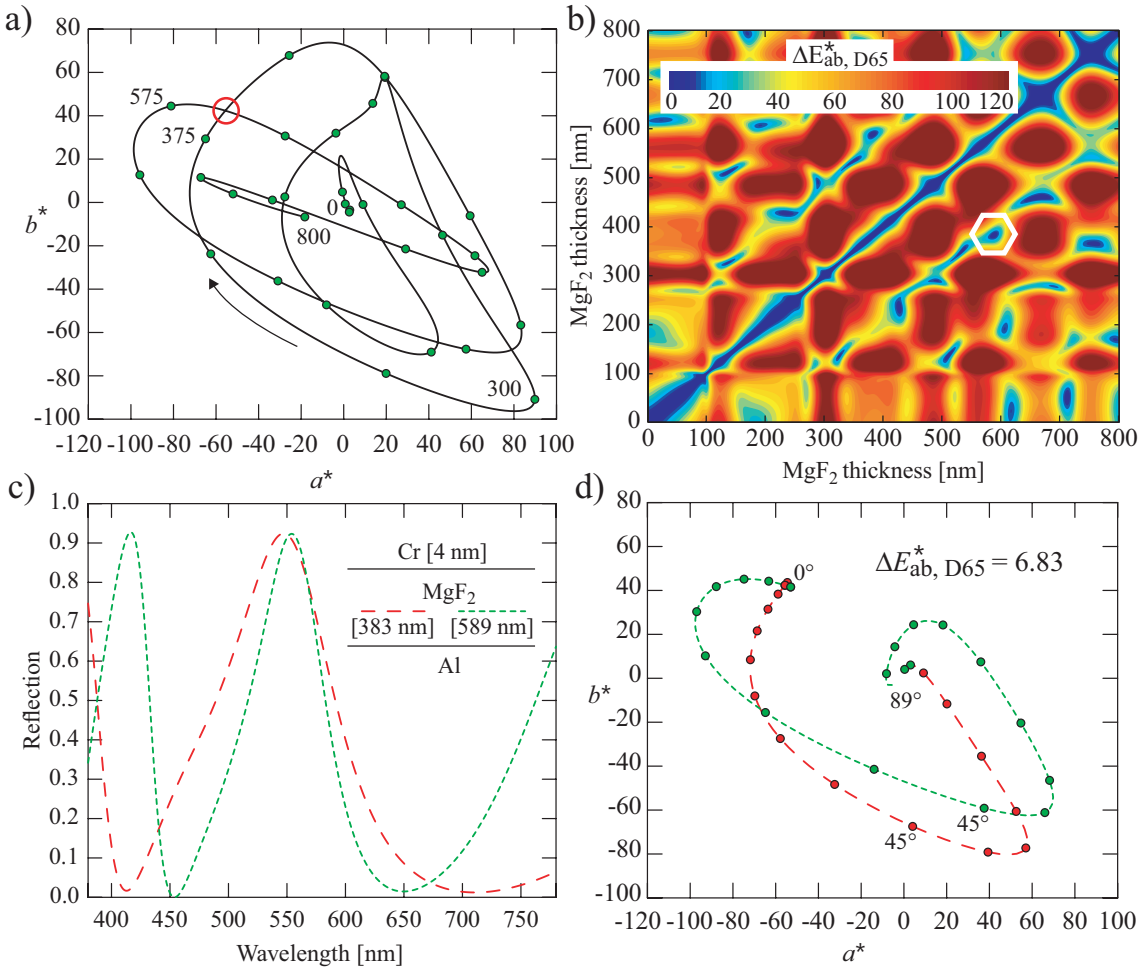

Figure 3.7 Metameric pairs based on metal-dielectric Fabry-Perot-like filters. Part a) shows the variation in color in the $L^\star a^\star b^\star$ color space when the thickness of the MgF_2 layer is varied between 0 and 800 nm. Each green dot represents a 25 nm increment in thickness. Interestingly, the outer boundary formed by the present curve represents the gamut of all possible colors attainable by the present structure. Part b) presents the $\Delta E^\star_{\text{ab, D65}}$ for all thickness combinations. This figure is symmetric (line of symmetry $x = y$) and shows that there are 13 combinations resulting in a low color difference. In part c) we show the reflection spectra of the chosen metameric pair [red circle in a) and white hexagon in b)]. Note that the structure of the simulated filters is also shown in the upper right corner. Finally, d) shows the color variation of both filters as a function of the observation angle. Notice how at 0° the colors coincide (the color difference is also indicated). Each dot represents a 5° increment in angle. This data generated using a combination of OpenFilters [68] and my own *Matlab* program.

a result, printing both these filters side-by-side allows the creation of hidden images. In fact, a product has been developed using exactly this principle and adopted by the pharmaceutical industry (MetaSwitch)[64, 69]. In addition, a similar effect is also possible by replacing one of the variable inks with a non-iridescent material (NIM) (e.g. metallic inks).

In the example just presented, $\Delta E^{\star}_{\mathrm{ab,\ D65}} = 6.83$, a value which is fairly high and which may result in a slightly different color appearance even at normal incidence. When changing the illuminant to incandescent or fluorescent lighting, the color differences are even higher ($\Delta E^{\star}_{\mathrm{ab,\ A}} = 11.79$ and $\Delta E^{\star}_{\mathrm{ab,\ F1}} = 9.40$). As a result, the present device is highly sensitive to changes in light sources and therefore to changes in observer. Consequently, these metameric features are often optimized for specific lighting conditions (usually fluorescent lighting due to its popularity). Other variations of more complex metal-dielectric metameric structures have also been proposed, such as a 9 layer design (additional absorber|dielectric pair) which allows the fabrication of a filter that presents the same color at normal incidence as well as the same color shift as a typical five-layer OVP but with the absence of reflection peaks in the near-UV and near-infrared [47, 70]. As a result, this type of feature could only be identified via a machine.

In Chapter 6 we will show how, by using a slightly higher number of layers, we were able to surpass these shortcomings ; i.e. designed and fabricated metameric pairs with a good performance (lower $\Delta E^{\star}_{\mathrm{ab}}$) and less sensitivity to changes in light sources and observers which can also be used in a transmission mode.

3.4.2 Magnetic films

The presence of magnetic materials (Fe_2O_3, Fe_3O_4, barium or strontium ferrite, soft iron or nickel particles, etc.) in security has typically been used to include covert information in documents [71] ; obviously a high coercivity (resistance to demagnetization) is necessary to ensure protection against erasure. They are also commonly used for anti-theft security labels [72]. It follows that by combining regular inks with magnetic inks with identical colors one can encrypt information readable using various types of detectors and sensors (see the Canadian 5 dollar bird series banknote from [71], for an example).

More recently, optically variable pigments combining both interference effects and a magnetic signature have been demonstrated. Although mixing color shifting pigments with magnetic inks may seem as the simplest solution, the colorless nature of the latter renders these mixtures unattractive. A better solution can be obtained by integrating the magnetic material in the structure of the interference filter. For example, one can replace the metallic reflector or absorber by a specific magnetic material (e.g. Co-Ni alloy reflector|MgF_2 spacer|Cr absorber [73]). Although a slightly more expensive solution, incorporating the magnetic film below the

reflector allows the preservation of the optimized optical performance of the filter.

The presence of a magnetic material also allows for another interesting possibility. Indeed, when in the presence of a magnetic field, each individual pigment will align itself with the magnetic field (see Figure 3.8). As a result, when an ink comprising these pigments is cured in the presence of a magnet, interesting optical effects can be created [74]. In the present case, the reflection will be at its lowest in region 1 since light is essentially lost due to multiple reflections between pigments and absorbed by the substrate whereas it will be at its highest in region 2. The pigments in region 3 having a fairly acute angle will also present a fairly low reflectivity. Finally, the magnetic field's intensity decreasing as a function of distance, pigments in region 4 will only be subjected to low magnetic forces and will naturally lay flat (as non-magnetic pigments). For a complete survey of the optical effects which can be generated using this technology, consult the article by Raksha *et al.* [75]. Commercial applications of this concept have been proposed [76, 77] and implemented in high-speed printing [78].

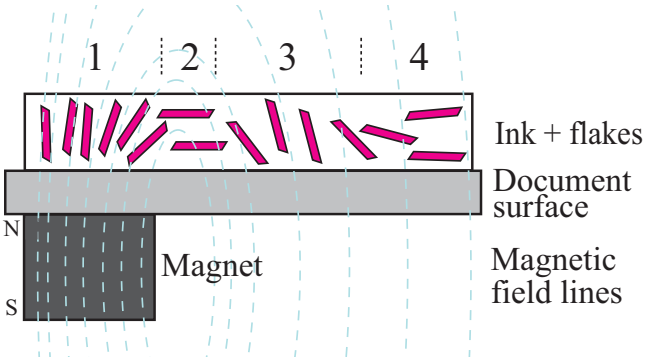

Figure 3.8 Magnetic color shifting pigments exposed to a cylindrical magnet's magnetic field. Notice how the pigments align with the magnetic field lines. This alignment allows for the creation of interesting optical effects. Figure inspired from [74].

3.4.3 Combining interference and diffraction

Although DOVIDs are outside the scope of the present thesis, it is important to note that there are significant efforts to combine them with ISISs in the hopes of generating stronger features benefiting from the advantages of both technologies. Indeed, holograms do present interesting optical effects, but the security they procure has lately been questioned due to the relative ease with which they can be counterfeited [1]. Another key feature resides in the fact that interference-based devices can still be viewed under diffused lighting whereas diffractive devices perform best under direct lighting. Their combination therefore results in an increased versatility making authentication possible under various types of lighting situations [74]. For

a complete review of diffraction-based devices see [8].

As is well known, diffraction arises when light arrives upon a surface possessing a periodic structure whose period is near the wavelength of the incident light. Following the Huygens-Fresnel principle, each point on the diffractive grating becomes a secondary source of spherical light emission. These spherical waves then interfere constructively and destructively and result in each wavelength being diffracted at a specific angle. The following equation allows for the calculation of these angles :

$$m\lambda = l(\sin\phi_0 + \sin\beta), \tag{3.2}$$

where m is the diffraction order, λ is the wavelength, l is the distance between two grooves, and ϕ_0 and β are the incident and diffracted angles respectively (relative to the normal of the surface) [64]. When light arrives at normal incidence ($m\lambda = l\sin\beta$), equation 3.2 dictates that higher wavelengths will be diffracted at higher angles (see Figure 3.9a). Also note that, in the present case of a grating with 1400 lines/mm as presented in Figure 3.9, only the first order is visible.

When light arrives obliquely, for example at 45 degrees (see Figure 3.9b), the zero order ($m = 0$) will be specularly reflected at the same opposite equivalent angle. We can also see that the -1 order has been rotated clockwise, so that contrary to ISIS the observed color change as a function of the observation angle is from shorter to higher wavelengths when observing a diffraction grating. Also note that higher orders are now also visible. Changing the shape (triangular, sinusoidal, etc.), depth and orientation (blazed) of the grooves of a grating allows one to modify the relative intensities of the various orders [79]. Interesting color effects can also be obtained by using combination gratings ; the superposition of two diffractive grating profiles or more [80].

Recently, the concept of printable holograms through the use of diffractive pigments has been demonstrated [81, 82]. The fact that these pigments contain ferromagnetic materials allows for their alignment using electromagnetic fields and thus the creation of interesting three dimensional (3D) effects but also rotation-dependent color effects by printing flakes with a 90 degree difference in orientation [66]. Indeed, in order to observe diffraction the grooves must be perpendicular to the observation direction. Finally, metameric diffractive pigments have also been proposed [83, 84].

Depositing an interference filter on an embossed substrate results in a highly complex interaction of diffraction and interference [64, 85, 86]. Generally speaking, the effect of the interference filter is to block specific wavelengths so that the rainbow effect of diffraction is attenuated and only specific colors are enforced. Various configurations of these two effects are presented in [87]. Once again, using an all-dielectric filter allows for transmission based devices to be created [88]. The simplest configuration being the use of a high refractive index (e.g.,

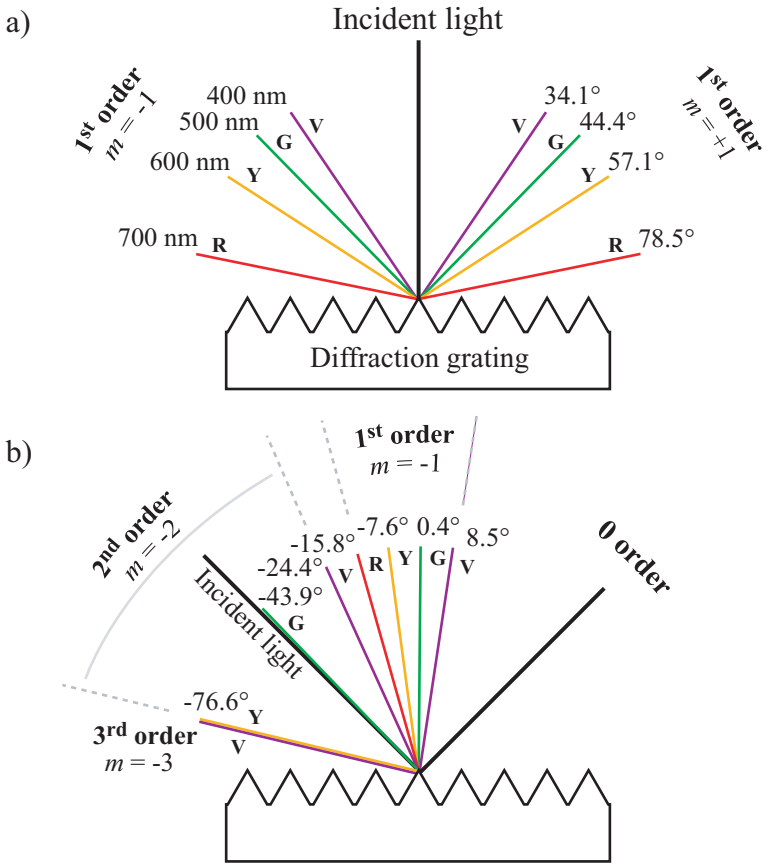

Figure 3.9 Diffraction of light at a) normal and b) 45° of incidence for four different wavelengths on a 1400 lines per mm grating. Letters indicating the color of the wavelength are indicated next to each beam of light (R = red, Y = yellow, G = green and V = violet). Notice that the -2nd order yellow coincides with the -3rd order violet which can result in a decrease in saturation. This figure was inspired by [64].

ZnS) on an embossed polymer substrate for see-through holograms [89]). Another possibility is to simply laminate a hologram with an interference filter [90, 91].

From equation 3.2, it can be seen that when the grating spacing is equivalent to half the wavelength of light (200 nm for a 400 nm violet light ; more than 5000 lines/mm), no order other than the zero order will be present ($2m - \sin\phi_0 = \sin\beta$). Note that, for spacings between 200 and 400 nm, diffraction will occur, but at very high angles of incidence. These structures are known as zero-order diffraction (ZOD) gratings [92]. Although ZODs do not present any diffraction they do present a surprising in plane color variation (rotation induced color shift) if viewed parallel or perpendicular to the grooves, typically from red to green [93]. For obvious reasons ZODs are harder to replicate since they require very high embossing precision [8].

3.4.4 Other color shifting technologies

There are other technologies displaying color shifting properties. This is the case of co-extruded polymer films first developed by Dow Chemical in the late 1960's [94]. Essentially used for decorative and packaging purposes, due to a fairly low color uniformity, the technology has matured and coextruded polymer films have now made their way into the optical security field. Indeed, 3M has recently proposed filters based on PET and acrylic polymer layers (poly(methyl methacrylate) (PMMA)) as well as polyethylene naphtalate (PEN) and coPEN. The low index contrast (1.67 vs 1.50 in the case of PET and PMMA, respectively) requires a very high number of layers. For example, an orange to yellow color shifting film consisting of 275 layers of PEN and coPEN has been demonstrated with a total thickness of 33 μm. Interestingly, due to the stretching which occurs during extrusion, both the PET and PEN layers display birefringence. This birefringence allows for the creation of interesting polarization effects (different colors when viewed in s and p polarization as well as in plane rotation dependent color shifts when viewed under polarized light parallel or perpendicular to the stretch direction) [94].

There are obviously other technologies which display angle-dependant color variations, which for reasons of conciseness, have not been covered in the present chapter ; mainly liquid crystals [95, 96, 97], Lippmann photography, volume-reflection holography and even nano-crystalline cellulose [98]. For those interested, a detailed coverage of these technologies in the context of security is given in the book by van Renesse [8].

3.4.5 Active devices

Lately, it has become clear that an ongoing trend in security is the integration of active features in future anticounterfeiting devices [99]. For example, De La Rue, in one of their

2010 patents [100] clearly mentions that inks may contain "functional components that react to an external stimulus" such as "fluorescent, phosphorescent, infrared absorbing, thermochromic, photochromic, magnetic, electrochromic, conductive and piezochromic" materials. In the present section we will concentrate our attention on structures which not only present an active optical change, but which also endeavour to preserve the passive optical change of ISISs.

One such example is Fabry-Perot-like structures incorporating a luminescent material which offer an overt color shift as well as a covert feature, in the present case, the emission of light under the influence of an external stimulus (ultraviolet, visible or infrared radiation, electric [101] or magnetic fields, chemicals or even pressure) [102]. Incorporating the luminescent material inside an interference filter also renders the light emission angle dependent ; this feature can thus provide an added level of security [103, 104]. Others have replaced the dielectric spacer (see section 3.3.2) by a piezoelectric material which, under the application of fairly high voltages (100-1000 V), sees its thickness change and as a result changes the color of the device [105]. Such high voltages would obviously require extreme caution when authenticating the device and could potentially limit their applicability.

Recently, photonic crystals have been proposed as possible innovative structures for optical security devices [106]. By using colloidal self-assembly, low-cost 3D photonic crystals were fabricated. In this particular case, self-organized monodisperse silica microspheres were deposited onto a periodic lattice. The space in between the spheres was then filled with the desired material. The spheres were then dissolved resulting in what is typically called an inverse opal structure displaying an angle-dependent color variation. If the matrix material is elastomeric, devices which show a color change under an applied pressure are possible. This change in color due to compression results from a decrease in the distance between the spherical cavities and therefore in the total optical thickness. A similar effect has been demonstrated in Fabry-Perot-like structures using a pressure-deformable space layer [107]. In addition, using an electrically active matrix results in a structure whose color can be changed by applying an electric field [108]. Similarly, an electrochromic WO_3 based inversed opal structure has been proposed as a tunable photonic band gap [109]. Such a structure possessing iridescence as well as a change in color following the application of a voltage (to allow ion intercalation) could be of interest for security as a two level authentication device.

The rapid evolution of printed electronics has also led to various proposed optical security devices where the features are optically variable when a voltage is applied. Here too, electrochromic materials are very often the materials of choice due to the low potential required to switch them as well as their memory effect (colored state is maintained once voltage is removed). For example, Hewlett-Packard has recently suggested an electrochromic device for

security tags [110]. Another example based on electrochromics has been suggested for security documents such as passports and smart cards [111]. In this particular case, the electronic components of the passport (radio frequency identification (RFID) technology) can also be used to power the feature via a radio frequency (RF) signal. Based on a five to seven layer structure the total thickness is approximately 30 μm. Such a high thickness may limit their use for banknotes (a pile of 1000 banknotes would result in 3 cm of added thickness). This technology is based on an electrochromic viologen containing TiO_2 matrix apposed onto a white reflector (reflection based device) [112]. Others have also suggested the use of electrochromic paper as a potential candidate for vouchers, tokens and banknotes [113]. Although all of these examples offer an innovative means of authentication, they are mostly aimed as a second level authentication feature for experienced personnel and not for the general public. In Chapter 7, I will present how, through the use of metamerism, we have developed an innovative means of uniting both an ISIS and an electrochromic device. In the following two Chapters (8 and 9) we have gone even further by combining both an angle depended color shift and a voltage-driven color change into a single structure.

3.5 General functionality considerations

Other than the optical performance of an ISIS, it is important to add that other characteristics are required in order for a device to be commercially viable [36, 47]. First and foremost, the device must offer a good protection against counterfeiters (hard to duplicate, simulate and originate). To increase the ease of use, the color shift must be easy to detect. This implies choosing the right color shift and a minimum device size to view it adequately ($\sim$1 cm^2). For example, choosing a red to green color shift might not be ideal considering that most colorblind individuals (between 7 to 10% of the male population) have difficulty distinguishing red from green. The color of the filter must also be stable as a function of time when exposed to the every day wear and tear of the protected product but must also be stable from one production series to another to ensure color consistency (thickness control during deposition). Calculating the effect of deposition errors on the color of a filter is possible and color tolerances can be defined, however, the best method of testing this issue is always to proceed with real life testing. For obvious reasons, the used materials must also meet environmental, safety and health regulations. In the particular case of banknotes, all OVDs must resist very stringent durability tests such as crumpling, abrasion, laundering in washing machines, immersion in chemical solvents, etc. so as not to shorten the banknotes lifetime [35]. Finally, generally speaking, the fabrication costs must be kept low although some higher-end products such as passports may allow for more expenditure.

Lastly, although we have covered, to the best of our knowledge, the main concepts and innovations in the present field, the reader who would like to learn more can also read the excellent chapter written by J.A. Dobrowolski [51], the inventor of the first ISIS as well as the complementary chapter on the same subject written by R.L. van Renesse [8]. For the latest developments, the biennial conference Optical Document Security is highly recommended. The next chapter will present an in-depth view of active materials, with special emphasis put on electrochromism, the main physical effect behind the proposed devices of the current thesis.

CHAPTER 4

ELECTROCHROMIC MATERIALS

4.1 Foreword

In the previous chapter, I presented some examples of active security devices. Since the present thesis pertains mostly to electrochromic (EC) materials, the present chapter will therefore focus on this particular type of chromogenic material. The literature on the subject is abundant and the reader interested in obtaining more information may read the book by Monk *et al.* [114] which covers inorganic as well as organic EC materials in much detail. For an in depth description of inorganic EC materials, in particular WO_3, the book by Granqvist, although published in 1995, is still a great starting point [115]. There are also multiple reviews which are readily available [116, 117, 118, 119, 120].

In this chapter, following a brief introduction on chromogenic materials, I introduce the basic characteristics of EC WO_3 films. This will be followed by an overview of the most accepted models for the coloration and bleaching processes. Typical device structures will then be presented with an emphasis on "Deb-type" devices. In addition, I then present the main characteristics of electrochromic devices (ECDs) required to quantify their performance. Finally, various examples of current and future applications of EC materials will be presented.

4.2 Introduction

Electrochromic materials are part of a larger family of materials termed chromogenic, that is whose optical properties can be changed by the application of an external source of energy. When this change occurs in the visible spectrum a color change ensues. In the case of EC materials, this change of color occurs upon the application of a voltage ; we will soon see that, in the case of WO_3, the color change requires the double-insertion of electrons and ions. It therefore goes without saying, that in order to implement such a process, EC materials must be part of a multilayer device. Typical device structures will be covered in Section 4.4.

There are obviously other examples of chromogenic materials (see Table 4.1 [128]). Each of them possess their pros and cons in respect to their potential use in optical security devices. For example, photochromic materials are well known for their use in self-opacifying glasses when exposed to UV light. On the other hand, the user has no control over the process and, as a result, this may limit their applicability. For obvious reasons, gasochromic materials would simply be unpractical. Thermochromic materials have been proposed and implemented in

Table 4.1 Examples of chromogenic materials

Type	**Energy source**	**Examples of materials**
Electrochromic	Electric potential	Hexacyanoferrates $Fe_4^{3+}[Fe^{2+}(CN)_6]_3$ (Prussian blue),transition metal oxides, viologens, etc.
Gasochromic	Gas	WO_3
Photochromic	Light	Ag_3VO_4, AgCl-CuCl, a-WO_3, spirooxazines, ZnS [121, 122, 123]
Piezochromic	Pressure	EuSe, EuTe, SmS, polymer blends [124, 125]
Thermochromic	Heat	V_2O_3, VO_2, Fe_3O_4, Ti_2O_3 [126, 127]

security devices, but their high sensitivity to changes in temperature has limited their use. Indeed, devices activated by, for example, applying a finger on them, have been shown to be unreliable since the temperature of the said finger can vary between users [i]. Also note that these materials are fairly easily available and have found their way in many commercial products : so called "mood rings", toys, battery life indicators, child fever indicators, etc. Finally, piezochromic materials are often based on fairly expensive elements and also typically require large pressures to change their color (e.g. under 2.7 GPa CdS changes from yellow to deep red [124]). Thus, we are left with EC materials as our main potential candidate. Let us now see what makes this category of materials so special.

As previously mentioned, EC materials see their color change upon the application of a voltage. Most importantly, this color change is reversible simply by applying an inversed potential. Essentially, an electrochromic device (ECD) behaves like a battery whose charge manifests itself by a change in optical properties. There are obviously other characteristics which make EC materials good candidates for optical security devices. To name a few :

- Low voltages are sufficient to change their appearance (1-2 V).
- Devices can be switched between their colored and bleached states thousands of times without significant degradation.
- ECDs present a memory effect, that is they maintain their coloration after removing the potential. Depending on the device, this effect can persist for a few minutes up to many hours. Also note that simply short-circuiting the device will result in bleaching (no-power consumption).
- Power therefore need only be applied when switching is required.
- In some materials, the color change can be quite striking.
- The coloration can be controlled and thus the device can be stopped at various stages

i. Source : Discussions with the Optical Security Material (OSM) team of the Bank of Canada.

of coloration (gray scale).

Among the EC materials, there exist two main families, the inorganics and the organics. Table 4.2 presents a resumé of the principal differences between these two categories [120]. In general, organic EC materials offer a wider variety of color changes [129, 130] as well as much faster coloration and bleaching dynamics. Indeed, in terms of color change, inorganic EC materials are fairly limited and typically show a variation between a transparent state and a colored and absorbing state whereas, organic EC materials often show transitions between two colored states. On the other hand, organic materials are more susceptible to degradation following UV irradiation [131] and as a result of secondary reactions during switching (although much progress has been made) [122] ; these limitations obviously affect the device lifetime. For these reasons, and considering that the main expertise of the laboratory in which this research was performed is inorganic thin films, my attention was mainly focused on inorganic EC materials. Also note that using inorganic materials results in the use of complex fabrication methods (mostly vacuum-based) which is beneficial from a security standpoint.

Table 4.2 Comparison between inorganic and organic electrochromic materials.

Property	**Inorganic**	**Organic**
Preparation method	Sophisticated (sputtering, evaporation, etc.)	Simpler techniques (dip coating, spin coating, etc.)
Total cost	Elevated	Small
Variety of colors	Limited	Vast
Contrast	Moderate	High
Response time	Slow	Fast
Chemical stability	High	Low
Mechanical properties	Brittle	Flexible

From the wide range of available inorganic materials, I chose the most popular and most studied of the transition metal oxides, that is WO_3 [116, 115]. Indeed, this particular material possesses the highest coloration efficiency (CE), that is the highest transmission variation, due to absorption, as a function of inserted charge. Although bulk WO_3 possesses a yellowish color (e.g. magnetron's target), in thin film form, it is for all practical purposes colorless. In its colored state on the other hand, it is dark and opaque blue (so-called "bronze" state).

There are other inorganic transition metal oxides exhibiting EC properties (see Figure 4.1 for a complete list). These oxides can be separated into two categories, those that color upon the insertion of ions and electrons in which case they are termed cathodic and those that color upon extraction of ions and electrons in which case they are termed anodic. Therefore, WO_3, which colors upon the application of a negative potential on its adjoining electrode,

is a cathodic EC material. Other than WO_3, other electrochromes are also popular for their intense color change, e.g. MoO_3 (cathodic : colorless to blue), IrO_2 (anodic : brown to colorless) and NiO (anodic : dark-brown to colorless) [132]. A complete list of all metal-oxide electrochromes and their color changes is available in the book by Monk [114]. One may have noted that vanadium oxide is both anodic and cathodic. Indeed V_2O_5 exhibits anodic and cathodic behaviour at different wavelengths while VO_2 is purely anodic [115].

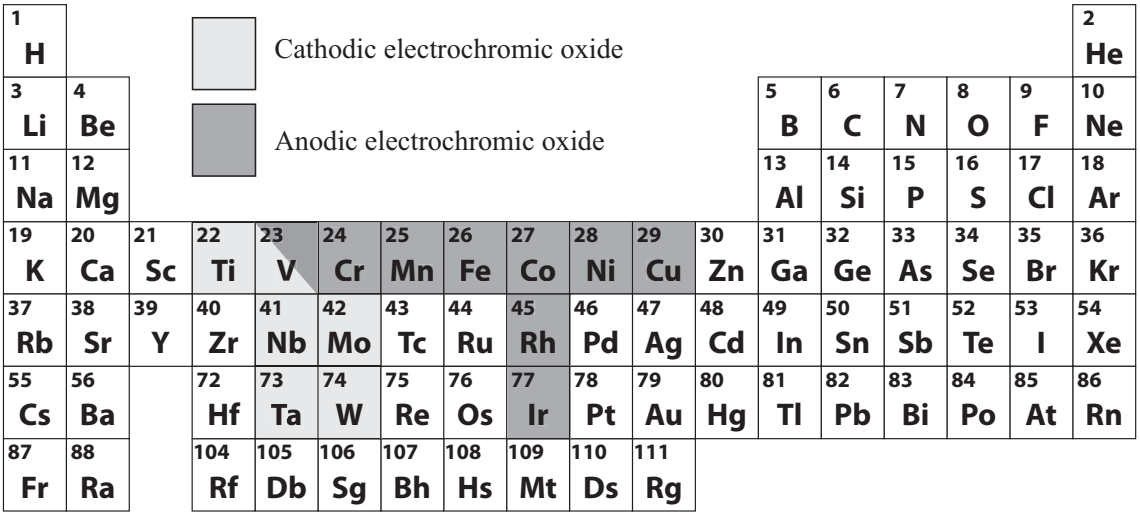

Figure 4.1 Periodic table indicating which transition metals possess electrochromic properties when oxidized. Light gray areas indicate cathodically coloring materials whereas, dark gray areas, indicate anodic EC materials. This figure was highly inspired by [115].

4.3 Tungsten oxide thin films

4.3.1 Discovery of electrochromism in WO_3

The first observation of a chromogenic material dates back to 1704 when Diesbach discovers the chemical coloration of Prussian Blue [122]. In 1815, Berzelius observes that heated WO_3 under a hydrogen flow changes color. In 1930, Kobosew and Nekrasson demonstrate the electrochemical reaction of WO_3 in acid. Twelve years later, in 1942, Talmay prints WO_3 and MoO_3 into paper to create what he termed “electrolytic writing paper”. About a decade later, in 1953, Kraus shows that WO_3 can be colored and bleached in H_2SO_4. Finally, Deb fabricates the first ECD based on WO_3 in 1969 ; for this reason, Deb is typically cited as the father of EC technology. Following the experiments by Deb, research on fabricating ECDs based on WO_3 seriously began. Note that the term electrochromism was actually termed by J.R. Platt in 1961.

4.3.2 Coloration mechanisms

As previously mentioned, coloration is based on the dual-insertion of an electron and ion. Due to their much bigger size, ions are usually the rate limiting species. For obvious reasons, the smaller the ion, the easier it will be to insert into the film. This explains why hydrogen and lithium are the two most popular choices of ions, the former having an approximately ten times faster diffusion coefficient [115]. It is important to add that the ion intercalation and deintercalation are facilitated by the structure of the transition metal oxides which is typically MeO_6 octahedra which are arranged in corner-sharing and edge-sharing configurations, where Me is a transition metal (the crystal structure is often termed as perovskite-like, defect perovskite, or simply the rhenium oxide structure) [133]. As mentioned by Niklasson in [134], "we may safely assume that the basic building blocks are similar in the amorphous structure, although bond lengths and bond angles exhibit some disorder". Now, since the space between the interconnected octahedra is sufficient for ion insertion and diffusion (inside the close-packed oxygen array [135]), ions can therefore be inserted with minimal bond making and breaking [136].

In the case of tungsten oxide, a simplified representation of the uptake of ions and electrons is given by the following reaction :

$$WO_3 + xM^+ + xe^- \leftrightarrow M_xWO_3,$$

where e^- is an electron, M^+ is a cation such as H^+, Li^+, Na^+, etc. and x is the intercalation level. This is certainly a simplified representation since it doesn't take into account for the presence of hydroxyl groups, incorporated water (which enhances diffusion but can lead to the formation of soluble tungstate ions (dissolution), and hydration), sub-stoichiometry, etc., all of which will impact the EC performance of a film. In the case of amorphous films, coloration is perceived due to the creation of an absorption band centered around 1 µm. Figure 4.2 shows the variation in optical properties (n and k[ii]) of an amorphous WO_3 film deposited by thermal evaporation. One can clearly distinguish the increasing extinction coefficient in the near infrared during ion intercalation.

In 1972, Deb associated the coloration mechanism in amorphous WO_3 to the formation of color centers between the inserted electron and a positive structural defect such as an oxygen ion vacancy [138]. Since then, this view has slightly changed, and although the coloration mechanisms in amorphous WO_3 are still the subject of much discussion, the general mechanisms are now fairly well understood.

Let us consider what happens to WO_3 during intercalation. Being a semiconductor, WO_3 in its bleached state will have a Fermi level situated in the bandgap since it possesses no

ii. The absorption coefficient α is given by $\alpha = 4\pi k/\lambda$, with λ the wavelength of light.

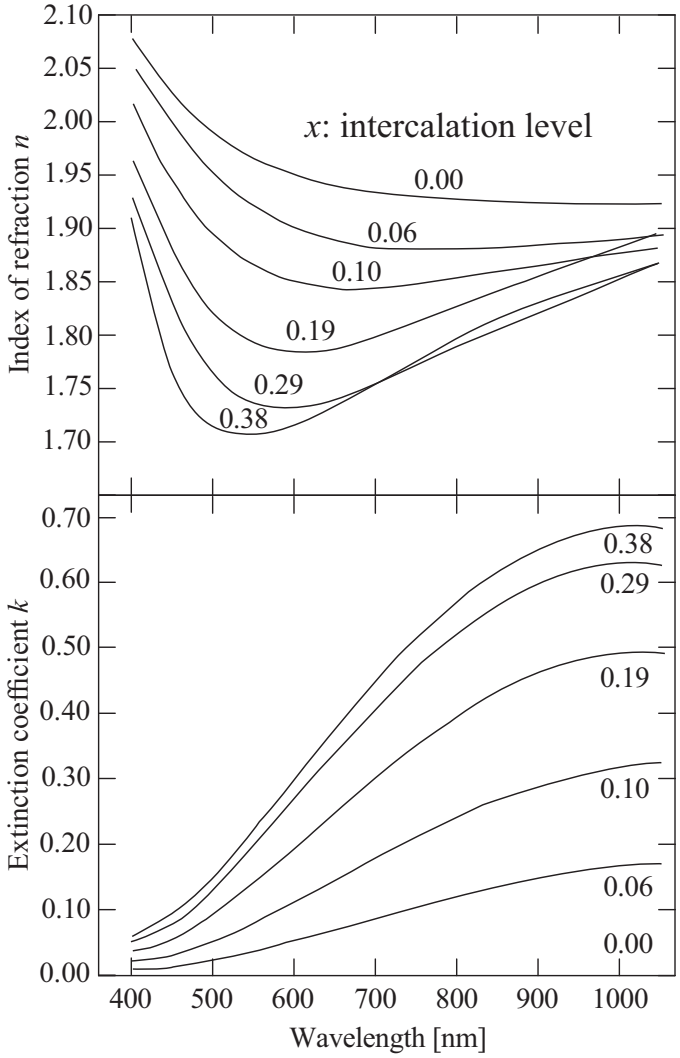

Figure 4.2 Optical properties of an amorphous WO_3 film deposited by thermal evaporation at different intercalation levels. The optical properties were obtained through fitting the reflectance and transmittance curves of the samples obtained during coloration. Data taken from [137].

free electrons. Upon coloration, the Fermi level will be raised into the conduction band, more precisely in the 5d orbitals of the tungsten atoms [139] (see the following article for a schematic band structure explanation [140]). Once inserted, the electrons are considered localized and occupy the lower part of the conduction band [141]. The mechanism responsible for the appearance of absorption is termed either small polaron absorption [142] (electron which polarizes its surroundings and causes a lattice distortion) or intervalence (same element) charge transfer [143] ; note that both models are in principal very similar.

More precisely, the general consensus is that electron transitions between W^{5+} and W^{6+} valence states are responsible for the observed absorption. As we will soon see, it has also been proposed that W^{4+} valence states may play a role at higher intercalation levels [144]. Also note, that if the intercalation level goes over $\sim$0.32, the films take on a more metallic character in conjunction with an increased conductivity.

As for the inserted ions, although they do not contribute to the optical properties of the film, they do maintain neutrality and are responsible for the coloration and bleaching dynamics (rate limiting species). In the case of hydrogen, the ions are located near an oxygen atom and can thus form a hydroxide unit. If a second ion is introduced nearby, it has been shown that it is more energetically favourable to form another hydroxide bond than to form a water molecule [116]. A review of the aforementioned mechanisms is given by Granqvist in [133]. Another review of these models is made by Deb where he also discusses some of their shortcomings [145].

4.3.3 Coloration and bleaching dynamics

Now that we've covered the main mechanisms behind the EC properties of WO_3 films, it is interesting to look at what is actually happening with the electrons and the ions during the intercalation/deintercalation processes.

Coloration phase

Let us start with the coloration process. In this particular case, four mechanisms can impact the coloration :

- The transport of the ions and electrons inside the film.
- The presence of a Helmholtz double layer at the film-electrolyte interface which acts as a capacity (created by an excess of ions at the insertion sites).
- The presence of a second barrier at the electrode-film interface (electron insertion site).
- The transport of charges (ions) in the electrolyte.

Item one can be neglected since the electron and proton diffusion coefficients are considered sufficiently high (the diffusion time can be approximated by $t_D = d^2/4D_\mathrm{i}$ which gives 0.02 s for a 250 nm thick film with a hydrogen diffusion coefficient D_i of 10^{-8} cm^2/s) [146]. The third item is considered an ohmic contact and therefore also will not affect the coloration process. The final item will also be limited at low voltages. Therefore, in most cases, it is the second item which limits the coloration process. Figure 4.3a) shows the basic coloration process based on Crandall's model where the electron is seen to meet-up with an ion near the film/electrolyte interface. Note that migration, the movement of a charge under an electric field, is very often neglected since the electron mobility is sufficiently high to eliminate the presence of a potential gradient [147].

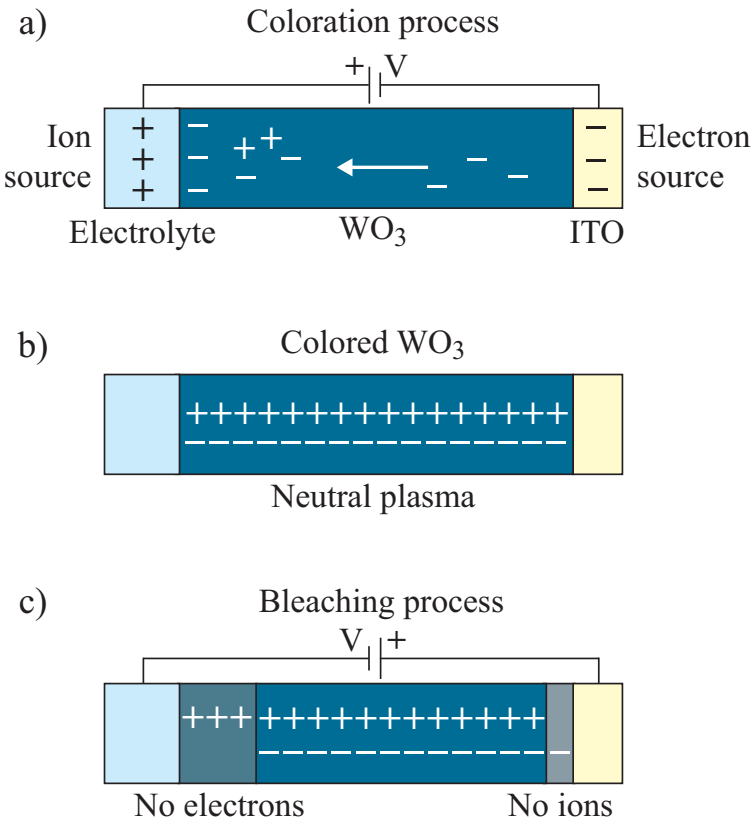

Figure 4.3 Coloration and bleaching processes based on the model by Crandall and Faughnan : a) coloration phase, b) colored and stable state and c), the bleaching phase.

It is also important to note, that as more charges are inserted, the chemical potential of the WO_3 film increases (Fermi level increases as previously mentioned), which makes it harder and harder to insert ions (increasingly energetically disfavoured). This increase in chemical potential results in a back electromotive force which slows down the coloration process. Coloration stops when the chemical potential is sufficient to screen the applied

voltage. Crandall *et al.* have developed an empirical equation which dictates the evolution of this chemical potential [146] :

$$\mu_{\mathrm{H}} = A + 2Bx + nRTln\frac{x}{1-x}, \tag{4.1}$$

where A and B are fitting parameters and R and T represent the gas constant and temperature respectively. Interestingly, n will be equal to 1 if the W^{5+} sites and protons are associated, or 2 if they are not. Term A takes into account the contributions to the free energy of the H_xWO_3 film (reduction of W^{6+} to W^{5+}, changes in interaction between W and O neighbours, H^+ bonding, etc.), while term B takes into account interactions between various entities (W^{5+}-OH^-, OH^--OH^-, etc.). The third and final term is attributed to changes in entropy. As the intercalation increases, μ_{H} increases and consequently the back electromotive force (see equation 4.2). The real effective voltage is thus given by $V_{\mathrm{eff}} = V_{\mathrm{a}} - V_{\mathrm{emf}}$, where V_{a} corresponds to the applied voltage and V_{emf} is given by :

$$V_{\mathrm{emf}} = a + bx - \frac{nRT}{F}ln\frac{x}{1-x}, \tag{4.2}$$

with a and b fitting parameters and F the Faraday constant. Crandall *et al.*'s results showed that $a = 0.16$ V, $b = -0.53$ V, demonstrated that $n = 2$ and, consequently, that the W^{5+} site and hydrogen ion are not associated or, using their terms, "do not have close spatial correlation". Thus once again, it is assumed that the proton is bonded to an oxygen and that the electron is localized at a W atom [146].

Following the previously mentioned considerations [iii] one can derive the coloration current which can be expressed by the following equation [114] :

$$i_c = i_0\Big(\frac{\tau_0}{t}\Big)^{1/2} exp\Big(\frac{eV_a}{4RT}\Big), \tag{4.3}$$

with $\tau_0 = \rho_W de/2i_0$. i_0 represents the exchange current (itself a function of the amount of protons within the film just before the application of the voltage and the current immediately on applying it), ρ_W is the density of W atoms in the film, d is the thickness of the film, e the electronic charge and V_a the applied voltage. The $t^{-0.5}$ and e^{Va} dependence of the current have been experimentally measured and confirmed for low voltages and for a specific range of intercalation levels ($x > 0.03$). Indeed, Ingram, Duffy and Monk showed that the model by Faughnan and Crandall did not work for values of $x < 0.03$, in which case the electrons are rate limiting. Monk actually gives a simple geometrical explanation for this 0.03 value [118]. Finally, note that most models assume that ions are uniformly distributed throughout the

iii. A complete development of the color model can be found in the annexe of Faughnan and Crandall's article on EC displays [148] ; which incidentally is an excellent review on the EC properties of WO_3.

film. On the other hand, other models such as Green's, which make analogies with heat flow, suppose the presence of gradients. Nevertheless, the presented model is generally accepted.

Bleaching phase

In order to bleach a colored sample, one needs only apply an inversed potential. In this case, the back electromotive force actually helps in the bleaching process. In order to bleach, the electrons will need to leave the WO_3 from the electrode side whereas the ions will have to leave from the electrolyte side. Figure 4.3c) shows a simplified image of the bleaching process. As the electrons are removed, a region free of electrons will appear on the electrolyte side and correspondingly a region free of protons on the electrode side (the electron free region will be larger due to the higher mobility of electrons). According to Faughnan and Crandall, a space charge limited current will thus form on both sides, once again the proton side being the rate limiting factor in the bleaching process. The region containing no ions being fairly small and the middle region having a low resistivity, most of the potential will be applied on the region with no electrons. Based on these assumptions, Crandall and Faughnan showed that the bleaching current could be expressed by the following equation [149] :

$$i_b = \frac{(p_H^3 \epsilon \mu_{H^+})^{1/4} V_a^{1/2}}{(4t)^{3/4}}, \tag{4.4}$$

where p_H is the volume charge density of protons in the initial colored state, ϵ the dielectric permittivity ($\sim 50\epsilon_0$ [149]) and $\mu_H{}^+$ the ionic mobility ($D_i = \mu_H{}^+ k_B T/e$). Thus, in this case, we obtain a $t^{-3/4}$ time dependence for the current variation, which incidentally is faster than during the coloration process. The time to completely bleach a WO_3 film is given by :

$$t_b = \frac{ex\rho_W d^4}{4\mu_{H^+} V_a^2 \epsilon}. \tag{4.5}$$

We can clearly see that for a thicker film, the bleaching time will be longer, that for a higher ionic mobility the time will be shorter (higher diffusion coefficient) and that increasing the voltage can also increase the bleaching speed. On the other hand, a higher voltage can induce high concentrations of ions near the surface of the sample and cause irreversible structural changes (degradation) [150] [iv].

iv. Also note that how the potential is applied can have a large impact on a film's durability. For example, applying a constant potential can lead to charge built-up at the film/electrolyte interface which can then lead to locally higher intercalation levels and thus charge trapping (see the article by Kim *et al.* for a discussion on hydrogen injection sites and trapping [151]). Pulsing the voltage can help by allowing the higher concentration "layer" to dissipate. This also allows to decrease the occurrence of undesirable electrolytic side reactions (e.g., formation of gases) [114].

4.3.4 Site-saturation model

When coloring a WO_3 film, although one initially observes a fairly linear increase in optical density [v], at higher intercalation levels, this increase tapers off. An interesting explanation of this effect has been given by Denesuk through the use of a site-saturation model which predicts a maximum total absorption at $x = 0.5$. Indeed, if x is the number of W^{5+} sites and 1-x the amount of remaining W^{6+} sites, than the number of possible W^{6+} to W^{5+} transitions is given by $x(1-x) = x - x^2$. This function reaches a maximum value at $x = 0.5$, the value for which the highest amount of transitions are available. At higher intercalation levels the amount of available transitions goes down and, consequently, the increase in optical density tapers off and can eventually go down.

This model has been refined by considering the formation of W^{4+} sites at higher intercalation levels [144]. In this case, the relative number of W^{4+} sites is given by $x^2/4$ (when $x = 0$, no W^{4+} sites exist whereas when $x = 2$, that is 2 electrons per tungsten atom are available, 100% of the sites will be W^{4+}). Similarly, the number of W^{6+} sites is given by $(2-x)^2/4$ and the number of W^{5+} sites by $x(2-x)/2$. Thus, the number of possible transitions between these sites are obtained by multiplying the previous relative concentrations :

$$P(W^{6+} \leftrightarrow W^{5+}) = x(2-x)^3/8, \tag{4.6}$$

$$P(W^{5+} \leftrightarrow W^{4+}) = x^3(2-x)/8, \tag{4.7}$$

$$P(W^{6+} \leftrightarrow W^{4+}) = x^2(2-x)^2/16. \tag{4.8}$$

Figure 4.4 shows how the relative number of available transitions evolves as a function of the intercalation level. A fairly good match is obtained between the model and the measured absorption of a $WO_{2.89}$ film as a function of intercalation. Note that the model does not take into account the intensities of the various transitions which can explain the observed differences in relative intensity. From Figure 4.4a), on can clearly see that the W^{6+} to W^{5+} transitions are the strongest. For most applications which limit the intercalation levels to under $x = 0.3 - 0.4$, these transitions will therefore be the ones most responsible for the observed absorption. A similar study was also made by Yamada *et al.* [152].

It has also been observed that sub-stoichiometry in WO_3 leads to films with a bluish color (for WO_{3-x} with x higher than 0.25 [134]). Many authors have actually shown that stoichiometric WO_3 films do not possess as high a coloration efficiency as sub-stoichiometric

v. Note that very often, the change in optical density is defined by $\Delta(\mathrm{OD}) = \log(I_0/I)$ for chemists and $\Delta(\mathrm{OD}) = \ln(I_0/I)$ for physicists (I_0 and I are the intensity of light before and after its passage through a material). I personally prefer the latter since it derives naturally from the Beer-Lambert law $I/I_0 = e^{(-\alpha d)} = e^{(-\mathrm{OD})}$ with α the absorption coefficient and d the thickness of the film.

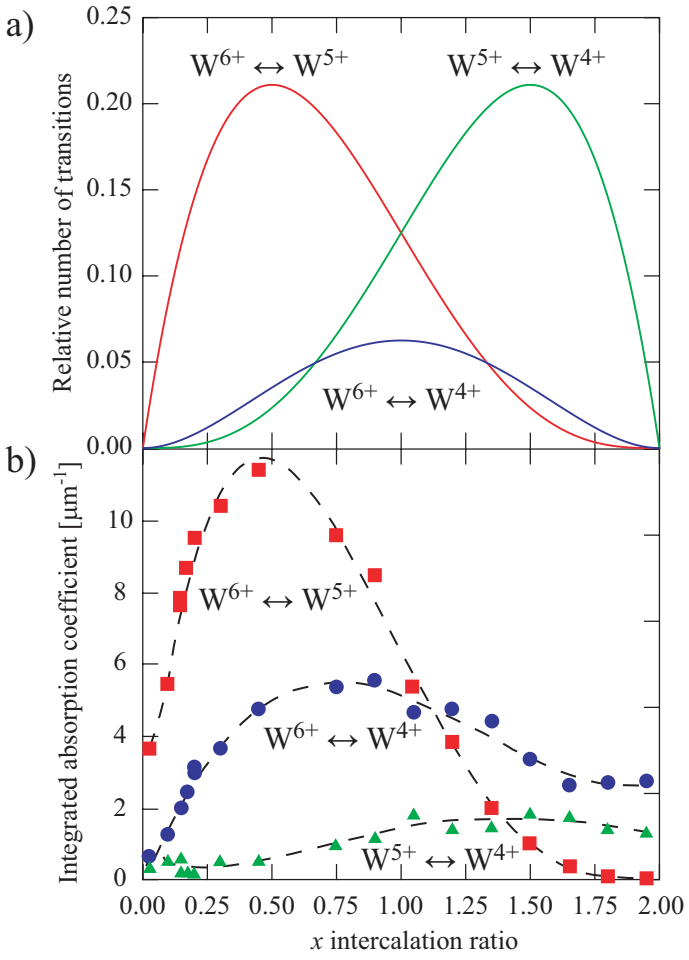

Figure 4.4 a) Relative number of possible transitions between $W^{6+} \leftrightarrow W^{5+}$, $W^{5+} \leftrightarrow W^{4+}$ and $W^{6+} \leftrightarrow W^{4+}$ sites as a function of intercalation and b) comparison with integrated absorption curves obtained during Li^+ intercalation in a $WO_{2.89}$ film. Note that the absorption of the bleached $WO_{2.89}$ was subtracted from the absorption curves and that these curves were then fitted using three Gaussians in order to obtain their relative intensities. This data was taken from the article by Berggren *et al.* [144].

films, to a point where some authors have observed no EC activity in $WO_{2.98}$ films under Li^+ intercalation [153]. Over-stoichiometric films on the other hand ($WO_{3.07}$) have been shown to possess EC properties, but show large irreversibility (do not bleach completely following the first cycle) due to side reactions between the inserted ions (Li^+ in this case) and oxygen interstitials [154]. This has also been observed in the case of crystalline WO_3 films deposited under high oxygen partial pressures [155].

Interestingly, one could conclude from the results of Berggren that sub-stoichiometric films should be avoided to promote $W^{6+} \leftrightarrow W^{5+}$ transitions. One research group has made this hypothesis and published a paper on stoichiometric WO_3 films, deposited by direct current (DC) magnetron sputtering in pure oxygen. Surprisingly, the authors obtained a good performance for their films ($WO_{2.98}$, $WO_{3.01}$ and $WO_{3.05}$) although, in this case, the intercalation was done using protons [156]. Clearly, this is not a simple issue to resolve and many factors come into play which makes the comparison of results quite difficult (deposition technique (microstructure, texture), amount of hydroxylation and hydration ($WO_{3-x-y}OH_x \cdot yH_2O$, with x the level of hydroxylation and y the level of hydration [157]), methodology, etc.).

4.3.5 Crystalline films

Contrary to amorphous WO_3 [vi] where the electrons are localized, in the case of polycrystalline films, the electrons are considered delocalized. Indeed, instead of being absorption modulated during intercalation, these films show a large variation in reflection in the near-IR (reflection can reach 60% at 2.5 microns [158]). This has been explained by considering a free-electron Drude-like behaviour much-like in metals. The variation in reflection is limited by the presence of electron scattering at defects (dislocations, grain boundaries, film surfaces, etc.) and ionized impurities [159] which consequently increase absorption at the expense of reflection [158, 160, 135]. In theory, by minimizing the scattering losses one could obtain an even better performance as modeled by Svensson *et al.* [159]. Figure 4.5 shows an example of the variation in reflectance of a 120 nm polycrystalline WO_3 film deposited at 466°C by RF magnetron sputtering. As the amount of inserted lithium is increased, the reflectance is also seen to increase correspondingly. Furthermore, the reflection band is blue-shifted due to a change in the plasma frequency. Note that in the case of polycrystalline films, which are typically denser, the diffusion rates of the ions are approximately 10 times lower than in amorphous films thus slowing down the coloration and bleaching dynamics. For more details on the structural features and absorption phenomena in amorphous and crystalline WO_x

vi. Although films are often termed amorphous, it has been suggested by Granqvist that they should be viewed more as nanocomposites with grain sizes between 1 and 5 nm (cluster-type microstructure).

films, consult the following review by Niklasson and Granqvist [141].

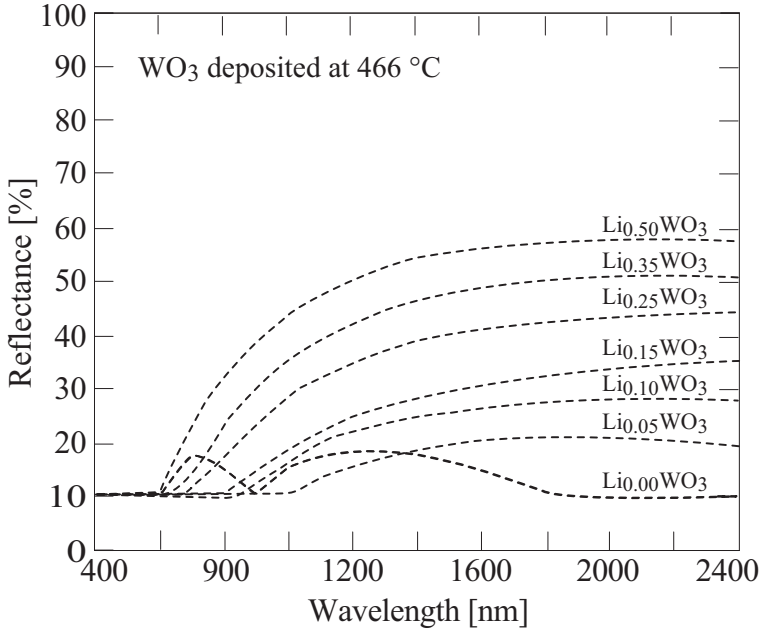

Figure 4.5 Variation in reflection of a crystalline WO_3 film deposited by RF magnetron sputtering at a temperature of 466 °C. Upon Li^+ intercalation, the reflection is seen to increase and the reflection edge is blue-shifted (plasma frequency is increased with the increase of free-electrons). This data was taken from the article by Cogan *et al.* [161].

4.3.6 The effect of the microstructure and surface texture

As we will see in the next chapters, the microstructure of the films is also very important. Indeed, a more porous microstructure is known to enhance the properties of EC films once again by allowing for more space and therefore higher ionic diffusion rates. As a result, glancing angle deposition which engenders highly columnar growth and thus large intercolumnar regions has been shown to increase the speed of ECDs or sensitivity of EC-based gas sensors [162]. For example, a three times faster bleaching was observed for films evaporated at a 50° angle versus a film deposited at normal incidence [163] ; the coloration speed was also shown to linearly increase, although only slightly. These films, which show angular selective properties, could also be interesting from a security point of view since they would be polarization dependent [164].

Lately, in an attempt to increase the performance of WO_3 films, many of the most recent published papers focus on generating fairly extravagant microstructures (e.g. nanowires [165], nanobeads and fibers [166], three-dimensional ordered macropores [167], nanoporous films templated with polystyrene microspheres [168], etc). Many of these structures have shown an

increased performance with the general conclusion that once again, the open nature of the films (higher surface area) results in a better penetration of the electrolyte and as a result facilitates ion insertion. Note however, that although an open microstructure is important, the pores must also be interconnected in order for the films to benefit from the increased surface area.

The surface texture of WO_3 also plays an important role in the performance of the films. A clear demonstration was given by Papaefthimiou *et al.* where they compared a uniform "flat" 300 nm WO_3 thick film with a 150 nm WO_3 covered with 150 nm thick stripes spaced at approximately every 200 μm [169]. Although the effective surface area increased by only 1% and the textured films contained 25% less material, the authors noted a 30% larger current density during cyclic voltammetry measurements as well as a doubling of the Li^+ diffusion coefficient. These results were explained by the higher surface area but also, from the fact that the ions could diffuse sideways from the trenches into the thicker parts of the film. Note finally, that the thinner parts of the film displayed a lighter shade of blue than the thicker parts (less total absorption).

4.4 Devices

As previously mentioned, the insertion of ions and electrons into an EC film requires a particular device architecture. A typical ECD structure is shown in Figure 4.6. In the following, I describe the role of each of the individual components of this structure and then describe in more detail a simplified device structure, often termed Deb-type, due to its inventor.

First of all, the first critical components of an ECD are the electrodes which are obviously required in order to apply a potential. If the WO_3-adjoining electrode is made negative, the film will color since electrons will be inserted from the electrode side while ions will be inserted from the electrolyte side. Inverting the potential will result in the extraction of both charges. Note that the presence of the electrolyte prohibits electrons from reaching the WO_3 during the bleaching phase. For obvious reasons, at least one of the electrodes must be kept transparent ; hence the material of choice is usually indium tin oxide (ITO) which is hard, presents a good adherence and is relatively chemically inert. Recently, speculation on indium reserves has driven prices upwards and promoted the development of other transparent conductive oxides (TCOs) such as SnO_2 doped with F, ZnO doped with Al, etc. Unfortunately, none of these materials has demonstrated a performance on par with ITO. This is particularly important in the case of large area electrochromics where a high resistivity can slow down the coloration dynamics [170] and result in a non-uniform color change across the device. Thin

metallic films can also be used as electrodes, but generally present a lower transmission due to a high reflectance and the presence of absorption. They are also soft in nature and therefore fragile, offer a poor adherence (e.g. gold) and may be highly reactive (e.g. silver which is also used in low-emissivity coatings for its high reflectivity in the IR). One way to increase the transmittance, is to incorporate the metal film between two dielectric layers thus allowing to decrease the reflectivity of the air|metal and metal|underlying film interfaces [171, 172]. For example, one can use TiO_2|Au|TiO_2 [173] as an electrode or even TiO_2|TiN|TiO_2 (which has the added advantage of being made of the same material and can be deposited using a single Ti target [174]). Lately, there has also been some interesting work resulting from the combination of TCOs with metal films (e.g. AZO|Ag|AZO [175] and ZnS|Ag|ZnS [176]). Finally, one of the electrodes can be made opaque if transparency is not important such as in display applications.

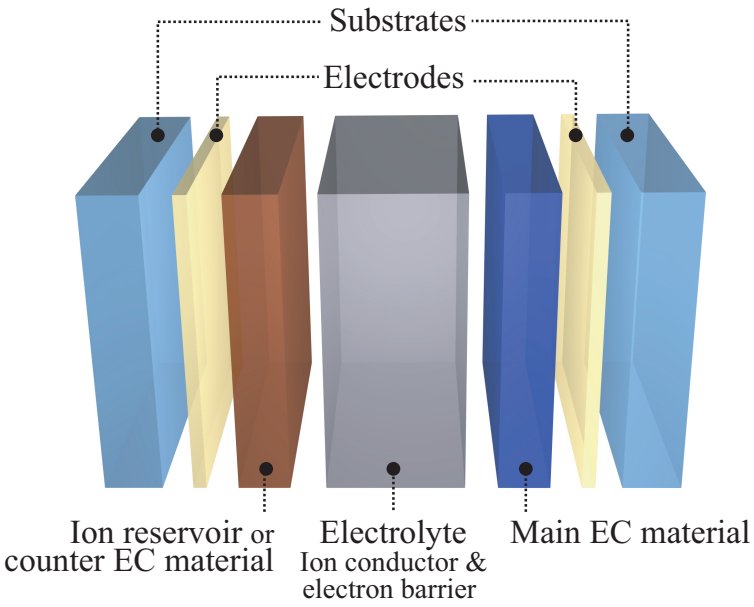

Figure 4.6 Typical electrochromic device structure.

In the case of the counter EC layer and/or ion reservoir, it can be electrochemically active by using an anodic EC material such as IrO_2, V_2O_5 or NiO [177] or inactive, in which case it only serves as a reservoir (e.g., crystalline WO_3 which is less active [178]). Using an anodic material is beneficial since it will color simultaneously with the cathodic EC material, WO_3 in most cases, and thus add to the total coloration efficiency of the device. This film may also serve to neutralize the bluish color of the WO_3 film as is the case when combining it with NiO for smart windows.

The electrolyte, which must be a good electron barrier and a good ion conductor, can

be in a liquid state. This is the case when performing a cyclic voltammetry test in a H_2SO_4 solution for example. The same tests can be made in non-aqueous propylene carbonate with a $LiClO_4$ salt in order to insert Li^+ ions [115]. Although lithium intercalation results in slower dynamics, this type of electrolyte is often chosen to increase a device's durability since the use of aqueous electrolytes has been linked with the dissolution of WO_3 films [114]. In the case of an application, liquid electrolytes are not always the best solution for the simple reason that they can result in leaking. Most devices are thus based on solid electrolytes such as Ta_2O_5, Sb_2O_5, LiF or viscoelastic organic polymers with the addition of a salt (e.g., gelatin + $LiClO_4$ [179]). Examples of devices including polymer electrolytes are given in [178]. An advantage of using polymer electrolytes is procured by the fact that both the cathodic and anodic EC materials can be deposited onto their respective substrate/electrode and then "glued" together ; this is not possible with a solid electrolyte such as Ta_2O_5.

From a fabrication point of view, one may ask how the charges are inserted into the device. A simple solution for hydrogen is its pre-insertion during deposition of a WO_3 film by adding hydrogen gas into the chamber. I have personally done this and observed the coloration of the films which increases with an increase in the hydrogen gas versus total gas ratio. As discussed by Granqvist in his book [115], we have also observed a twofold increase in the deposition rate upon the addition of hydrogen, even in low concentrations. Films deposited at low H_2 concentrations showed essentially no absorption which is interesting from a deposition time saving perspective. This change in the deposition rate could be explained by the hydrogen ions limiting target oxidation [115]. Another method of inserting hydrogen without using electrochemical methods is dry lithiation (heating $LiNbO_3$ powder under vacuum [180]). The coloration of the anodic EC material can also be made prior to device assembly, as in the case with NiO which is colored by treating it with ozone (films are exposed to UV light in the presence of gaseous oxygen [114]).

Interestingly, very few studies on the variation in color of ECDs have been done, even though they can provide interesting information (exact color coordinates, perceived color difference, stability, etc.) [181]. For example, in the context of a security device one could calculate the minimum thickness of WO_3 which is required to obtain a specific color difference (contrast) in a specific amount of time ; indeed, thicker films have been shown to reach larger color differences in a shorter amount of time (for the same applied voltage) but would obviously cost more to deposit [182].

4.4.1 Deb devices

It is during a visit to our laboratories in 2007, that professor Granqvist suggested that I should study a specific device structure which would be highly appropriate for security

applications due to its lower fabrication cost, but also simpler to fabricate. This particular device is often termed Deb-type due to the fact that it was Deb who first introduced it in the mid 1970s [183]. Contrary to the typical structure discussed in the previous section, in a Deb device, both the ion reservoir and electrolyte are combined into a single film. A nice overview of the initial work done by Deb can be found in [131]. Deb actually demonstrated a very interesting concept based on a coupled EC WO_3 film and photoconductive CdS film as a photographic system with a very high resolution [vii]. In the following, we will go through the main characteristics of these devices. Most of the work on these structures having been made for display applications in the 1970s and 80s, they are covered in much detail in the book by Granqvist [115].

The basic structure of a Deb device is the following :

Electrode|EC material|Electrolyte|Electrode.

This type of system is also known as an "open system", since in most cases, interaction with the surrounding atmosphere is necessary for the device to function. Indeed, it has been shown that it is water absorbed in the electrolyte which supplies the required hydrogen ions for coloration ; there therefore exists a threshold voltage for coloration which is due to the required electric field in the insulating layer for the dissociation of water (water electrolysis resulting in H^+ and OH^-). This is the reason why the ion storage layer is not required since one can rely on replenishment from ambient water molecules. More precisely, dissociation of water has been shown to happen at the electrolyte-counter electrode interface [185]. Interestingly, Yoshimura *et al.* [186] determined that the highest performance was obtained for water adsorbed at the interface of WO_3 and their MgF_2 electrolyte. Additionally, half the hydrogen required for the coloration of the WO_3 was observed to come from the ambient while the rest from absorbed water in the MgF_2 [185] (determined by a simple experiment where the order of the WO_3 and MgF_2 were switched to isolate the MgF_2 film from the ambient). Finally, depositing the electrolyte with ambient air or exposing the film to ambient air before adding the top electrode has also been shown to help.

In order for replenishment of the electrolyte to be possible, the top electrode must be permeable to water. The most popular electrode is gold, which can be deposited in very thin layers (typically around 10 nm) while still possessing a good electrical conductivity and permeability to ambient water. Thin gold electrodes have also been shown to create a mixed layer with the underlying electrolyte (in this particular research case MgF_2 [187] in ITO|WO_3|MgF_2|Au). Indeed, while we have not directly observed this during our own studies on Deb devices (see Chapter 7), we have noted that if the top gold electrode is made too

vii. An updated optical memory device based on a similar structure was proposed by Shizukuishi *et al.* [184].

thick, short circuits most often ensue. Another consequence of making the top electrode too thick is that it will inhibit coloration as well as be more prone to breaking, perhaps due to the accumulation of gases [188]. This has been clearly demonstrated by the observation of bubbles at the top Au electrode in the case of a glass|ITO|WO_3|MgF_2|Au Deb-type device. The authors have suggested that the bubbles during coloration are O_2 which are due to the dissociation of water ($4OH^- \rightarrow 2H_2O + O_2$) and insertion of H^+ ions into the MgF_2. During bleaching, H_2 bubbles were also observed at the Au electrode. This exhaust of gases can obviously lead to the delamination of the top electrode and should thus be limited ; this can be done by limiting the voltage intensity [189, 188]. A complete analysis of the effect of the Au counter electrode on the properties of Deb-type devices can be found in the work by Lusis *et al.* [190].

From a practical point of view, also note that Au electrodes are prone to generating short circuits (as I have also personally observed and struggled with). Benson *et al.* [191] mention that very often, a device would simply not color under an applied voltage. Most importantly, by identifying the regions with the highest heat emission (Joule heating) they were then able to isolate these short circuits by engraving a circle around them through the Au electrode and thus operate the device successfully. The authors also mention that substrate cleaning was critical in minimizing this problem.

ITO has also been used as a top electrode, but thicker films are required to obtain a low resistivity which can then limit coloration. We have observed this in our laboratory where the device was shown to color only in very small regions most probably due to the presence of pinholes in the ITO film. One way of solving this problem is by sacrificing the performance in transmission of the ITO thus allowing for a thinner ITO film with a good conductivity.

The role of the electrolyte is obviously to inhibit electrons from reaching the WO_3 during the bleaching process. Many electrolytes have been tested such as Ta_2O_5 [192] in the following device structure : ITO|WO_3|Ta_2O_5|ITO [193]. The use of solid electrolytes such as p-toluenesulfonic acid and urea for display applications have also been proposed (these powders presented a white and diffuse background) [194] as well as LiF (Au|WO_3|LiF|Au) [195]. The performance of the device has been shown to depend on the thickness of electrolyte and, as can be deduced from the previous discussion, ambient humidity. Tests under different levels of humidity have shown that the coloration efficiency increases with an increased humidity, whereas the EC properties disappear completely when in a pure nitrogen environment [196].

To limit the dependence to the ambient humidity, some authors have tested devices under vacuum conditions. In the case of a Cr_2O_3 electrolyte, devices were shown to function even under vacuum due to the high absorptive power of this film for water [189, 197]. A demonstration of this is shown in Figure 4.7 where the mass of SiO and Cr_2O_3 films are measured

at various ambient pressures. One can clearly see that the Cr_2O_3 sample's mass stabilizes once the pressure reaches approximately 10^{-5} Torr in comparison to the SiO sample which stabilizes at 10^{-2} Torr. Also, no deterioration of devices based on Cr_2O_3 was observed up to 5 x 10^6 cycles. This high number of cycles was explained by the absence of gas evolution due to the anodic EC behavior of the Cr_2O_3 which also reacts during coloration with the OH^{-1} anions.

On the other hand, the authors also observed a very quick decrease of the coloration efficiency during coloration due to rapid spontaneous bleaching. The same authors have explored mixed oxides of Cr_2O_3 with Al_2O_3, B_2O_3, CeO_2, GeO_2, MgO, MnO_2, NiO, SiO, TiO_2 and, V_2O_5 in order to increase the memory effect [198]. From their results, a mixed oxide of Cr_2O_3-V_2O_5 (50 % weight) demonstrated an appreciable gain in memory effect (tens of minutes versus seconds) as well as a quick bleaching behavior under a reversed voltage. On the other hand, a drop in optical density was noted as the devices were cycled which thus required a higher applied potential to maintain a constant optical density. The addition of an electron blocking layer (SiO_2 or Nb_2O_5) between the WO_3 and Cr_2O_3 also resulted in an increased open-circuit memory. This effect was explained by the fact that the isolating layer inhibits the direct charge transfer between W^{5+} and Cr^{4+} ions. A complete analysis of the current behavior of such a device during coloration has been done by the same group (initial charging of the dielectrics before the onset of coloration followed by a decrease in current related to the formation of the back electromotive force) [199].

More recently, a device (PET|ITO|WO_3|SiO_2|Ta_2O_5|Au) on a flexible PET substrate (125 μm thick) based on a similar concept was presented [200]. The same authors have also demonstrated that insertion of a 7 nm thick SiO_2 layer accelerates the device's coloration mainly by blocking electrons from reaching the Ta_2O_5 as well as accumulating at the interface and accelerating the intercalation of the H^+ ions (70% drop in transmission in 100 ms at 3 V instead of 300 ms) [201].

Interestingly, Ashrit *et al.* developed a model for their Deb-type device [195]. Figure 4.8 shows the various elements of this model. As can be seen, N_{H_2O} and N_H are both the concentration of water and protons in the electrolyte, while N_0 is the concentration of water in the ambient. g and h are thus the exchange rates of water between the ambient and electrolyte. The amount of water entering and exiting the film is therefore given by hN_0 and gN_{H_2O}. Once water is absorbed into the film, it will be dissociated into H^+ and OH^-, the amount of created protons given by eN_{H_2O}. Recombination of protons with OH^- inside the film is given by fN_H and those leaving the film by iN_H. Once the protons become available they will enter the WO_3 at a rate d (c represents protons exiting the WO_3 film,N_W being the concentration of protons in the WO_3). These protons will then contribute to the formation of

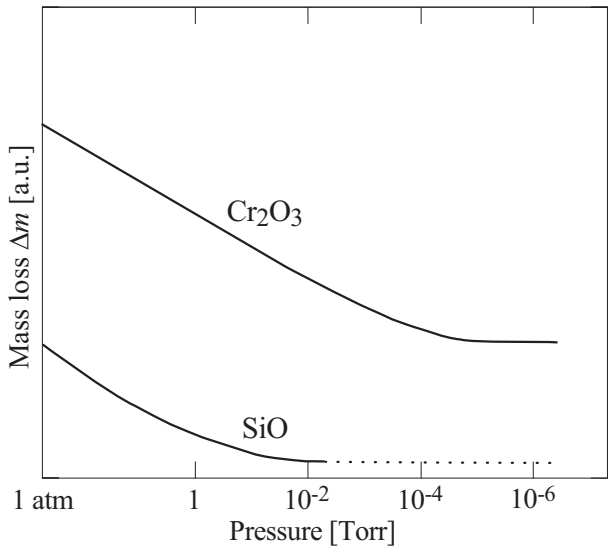

Figure 4.7 Mass loss due to desorption of water in SiO and Cr_2O_3 films under different pressures measured using a quartz balance. Data taken from [197].

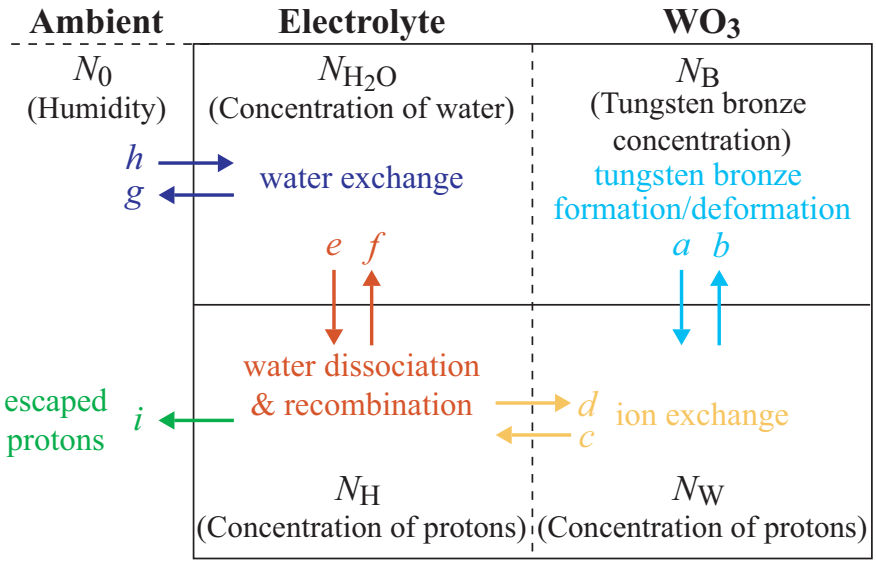

Figure 4.8 Theoretical model developed by Ashrit *et al.* for Deb-type devices. [195]

a tungsten bronze (N_{B} represents their concentration) at a rate b (a represents deformation of tungsten bronze).

Having defined all the variables of the model, it is possible to write the following differential equations describing the variations in concentrations of water, protons, inserted protons and tungsten bronze :

$$\frac{\mathrm{d}N_{\mathrm{H_2O}}}{\mathrm{d}t} = hN_0 + fN_{\mathrm{H}} - (g+e)N_{\mathrm{H_2O}}, \tag{4.9}$$

$$\frac{\mathrm{d}N_{\mathrm{H}}}{\mathrm{d}t} = eN_{\mathrm{H_2O}} + cN_{\mathrm{W}} - (d+f+i)N_{\mathrm{H}}, \tag{4.10}$$

$$\frac{\mathrm{d}N_{\mathrm{W}}}{\mathrm{d}t} = dN_{\mathrm{H}} + aN_{\mathrm{B}} - (b+c)N_{\mathrm{W}} \quad \text{and,} \tag{4.11}$$

$$\frac{\mathrm{d}N_{\mathrm{B}}}{\mathrm{d}t} = bN_{\mathrm{W}} - aN_{\mathrm{B}}. \tag{4.12}$$

Before solving these equations, there are some simplifications that can be made. Indeed, the positive potential of the top electrode will limit the amount of protons exiting the electrolyte so that i can be considered negligible ($i \simeq 0$). Ashrit *et al.* have also noted that the formation of gas bubbles through $4\mathrm{OH}^- \rightarrow 2\mathrm{H_2O} + \mathrm{O_2}$ would limit the formation of water inside the film so that we can set $f \simeq 0$. Finally, we can also pose that the amount of protons exiting the $\mathrm{WO_3}$ film is much lower than those entering the film during coloration (which is also related to the amount of ions created ($eN_{\mathrm{H_2O}} >> cN_W$). As a result, the first two equations simplify to the following :

$$\frac{\mathrm{d}N_{\mathrm{H_2O}}}{\mathrm{d}t} = hN_0 + -(g+e)N_{\mathrm{H_2O}} \quad \text{and,} \tag{4.13}$$

$$\frac{\mathrm{d}N_{\mathrm{H}}}{\mathrm{d}t} = eN_{\mathrm{H_2O}} - dN_{\mathrm{H}}. \tag{4.14}$$

Having presented the model, I will not go through the steps required for solving these differential equations, but will simply present the final solution as determined by Ashrit *et al.*. For one, the concentration in tungsten bronze (protons participating to coloration) can be expressed by :

$$N_{\mathrm{B}}(t) = Ae^{-\lambda_1 t} + Be^{-\lambda_2 t} + \frac{b}{ac}\tau_0, \tag{4.15}$$

with λ_1, λ_2 and τ_0 given by :

$$\lambda_1 = \frac{(a+b+c) - \sqrt{(a+b+c)^2 - 4ac}}{2}, \tag{4.16}$$

$$\lambda_2 = \frac{(a+b+c) + \sqrt{(a+b+c)^2 - 4ac}}{2} \quad \text{and,} \tag{4.17}$$

$$\tau_0 = \frac{ehN_0}{(g+e)}. \tag{4.18}$$

We can also write that :

$$\frac{N_{\mathrm{B}}(\infty) - N_{\mathrm{B}}(t)}{N_{\mathrm{B}}(\infty) - N_{\mathrm{B}}(0)} = \frac{A}{A+B}e^{-\lambda_1 t} + \frac{B}{A+B}e^{-\lambda_2 t}. \tag{4.19}$$

As we previously mentioned, the optical density (OD) is proportional to the amount of tungsten bronze for reasonable levels of intercalation. Thus, by posing that the OD is proportional to N_{B}, equation 4.19 can be rewritten as follows :

$$\frac{OD(\infty) - OD(t)}{OD(\infty) - OD(0)} = \frac{OD(\infty) - OD(t)}{OD(\infty)} = \frac{A}{A+B}e^{-\lambda_1 t} + \frac{B}{A+B}e^{-\lambda_2 t}. \tag{4.20}$$

Hence,

$$\frac{OD(t)}{OD(\infty)} = 1 - Ke^{-\lambda_1 t} - (1-K)e^{-\lambda_2 t}, \tag{4.21}$$

with $K = A/(A+B)$. Now, although the individual rates are essentially impossible to determine, equation 4.21 was shown to model the performance of a Deb device very well. Both exponentials were shown to be essential in order to model the initial fast coloration followed by a slower coloration. It has been suggested that such a behaviour could be explained by a change in the diffusion coefficient during intercalation due to "jamming" of fast diffusion channels [202]. The same authors have also suggested that this phenomenon may be due to a difference between bulk and grain boundary diffusion. Finally, I have presented this work here, since I believe that in the context of comparing the performance of various Deb-type devices, equation 4.21 could become very handy. Indeed, with only three empirical parameters, one could compare the variation in OD, a very important characteristic of any ECD.

4.4.2 Main characteristics of electrochromic devices

Having just shown typical device structures, it is important to know that there are some critical parameters which allow one to quantify the performance of an EC material or ECD and, as a result, compare it with others. This section covers these main parameters.

Contrast ratio

The contrast ratio (CR), is a measure of the intensity of change in color of an EC material. It is simply defined by the following equation :

$$\mathrm{CR}(\lambda) = \frac{R_\mathrm{b}(\lambda)}{R_\mathrm{c}(\lambda)}, \tag{4.22}$$

where R_b is the diffuse reflection in the bleached state and R_c the diffuse reflection in the colored state. Note that the measurements are made on a white diffuse background. As a result, the CR is typically used for display applications.

Coloration efficiency

The CE is an indicator of the change in optical density as a function of the inserted charge. It is given by the following equation :

$$\mathrm{CE}(\lambda) = \frac{\Delta OD(\lambda)}{q} \approx \frac{ln[T_\mathrm{b}(\lambda)/T_\mathrm{c}(\lambda)]}{q} \quad [\mathrm{cm}^2/\mathrm{C}], \tag{4.23}$$

where T_b and T_c represent the transmission in the bleached and colored states, respectively, and q is the density of inserted charge (charge per surface area). As a result of this definition, cathodic EC materials possess a positive CE and anodic EC materials a negative CE. Also, note that this approximation is valid only if the reflectivity does not change much between the colored and bleached states ; this is about the case for amorphous WO_3 films. More details on this particular subject will be given in Chapter 5. As previously mentioned, I've personally chosen to use the natural logarithm, but be aware that many authors use the base ten logarithm to calculate the CE.

Response time

The response time of an ECD is defined as the time required for a device to change between its bleached and colored states and vice versa. There has yet to be formulated a precise definition of the response time which makes it difficult to compare the results of different authors. The response time is usually described by defining a threshold transmission or reflection value, e.g. the time for a device to reach 10% of its initial transmission. Response times for windows are generally in the minutes range while smaller devices with sub-second response times have been demonstrated. In the case of a security device, a response time in the few seconds range would be amply sufficient.

Lifetime

A device's lifetime is obviously very important and is application dependent. In the case of a window which will be installed for more than a decade, a high number of cycles (tens of thousands) is desired without observing significant degradation which incidentally, results from chemical side reactions and changes in the physical properties of the films (changes in crystallinity, cracks due to stress during insertion/extraction, etc.) [203]. Also note, that soliciting a higher variation in transmittance from a device (more inserted charge) will lower its lifetime. One of the simplest methods of quantifying a devices lifetime is by using electrochemical techniques such as cyclic voltammetry combined with optical measurements (see Chapter 5).

In an application such as security, the requirements on a device's lifetime with respect to the number of cycles will be decreased. Indeed, let us suppose that a device is apposed onto a low currency banknote and that this bill is exchanged five times per day for five years, the total of cycles reaches approximately 9000 ; a number which is readily achievable. On the other hand, the durability requirements of security devices on banknotes are extremely stringent (see section 3.5) and may limit the lifetime of an ECD. Initial applications should therefore target less demanding markets such as passports, identity cards, etc.

Appearance

This last property may be qualitative, but it is extremely important for many applications. Indeed, not only does this pertain to the color uniformity, especially in the case of large area electrochromics, but also the color itself both in the bleached and colored states. For example, in the case of EC windows which are typically in the m^2 range, high conductivity electrodes must be used to ensure a uniform coloration (mainly for aesthetic purposes). In this same context, neutral colors are often desired in the opaque state in order to preserve indoor color rendition. In the case of security devices which are more in the cm^2 range, uniformity issues should not be a problem. On the other hand, we will also see that in terms of color, WO_3 in its pure form offers limited possibilities. We discuss possible solutions for this issue in Chapter 10.

4.5 Applications

As previously mentioned, it is following the experiments by Deb in 1969 on WO_3 [204] that research on ECDs seriously began. The initial applications of WO_3 were envisaged for displays. For those interested in this particular subject, a 1975 paper by Chang *et al.* from IBM presents a general discussion of EC systems for displays [205] and a review is also given

by Dautremont-Smith [206]. Unfortunately, the fairly slow switching speeds of these devices, the problem of spreading (material colors in zones where it should not), short lifetimes and the advent of much faster liquid crystal displays limited their applicability and compelled scientists to explore other possible avenues for EC materials. Still, there was some very interesting work done on displays for wrist watches based on liquid electrolytes as well as on organic electrochromics [207]. Nowadays, the progress which has been made since the 1980s in EC materials has resulted once again to their potential integration into displays (see Table 4.3).

Presently, EC materials are part of two main applications. The first popular application consists in variable reflectivity mirrors. These mirrors which, by decreasing their reflectivity reduce the risks of a driver being blinded by a car's headlights during nighttime driving (anti-dazzling), have found their place in many luxury cars (the main supplier is *Gentex*) [208]. Note, that in this particular case, the EC materials are in a liquid state.

The second application pertains to the use of EC materials in the fabrication of smart windows ; that is a window whose transmittance can be modulated. Although often taken for granted, windows are an essential part a building's design for the obvious reason that they allow a visual contact with the outside world and are thus good for moral (man spends 90% of his time indoors [209]). By letting in natural sunlight, they also contribute to indoor lighting which reduces the need for artificial lighting and incidentally also allows for better color rendition. The problem is that windows are also a major point of energy exchange (gain of heat in summer and loss of heat in winter). Coupled with the current architectural trends which promote increased window sizes, these energy fluxes are a cause of additional energy consumption (cooling and heating) [210].

To solve these issues, present day static windows are equipped with low-emissivity coatings (often silver-based) which allow one to reflect the infrared, that is the main region of blackbody emission of an object at typical Earth temperatures (by Wien's law, at 0°C, a body's maximum emission is around 10 μm - see Equation 2.10). Note that the blackbody emission curves for temperatures between -50 and 100° C are shown in Figure 4.9a. One can clearly see that the emission is mostly concentrated between 3 and 50 μm. Now, in particularly warm countries, one may also want to reflect the near-IR part of the spectrum (0.78 to 3 μm) in order to limit the transmission of the heat arriving from the sun (whose main emission lies between 0.25 nm and 3 μm - see Figure 4.9b) ; this can be done by adjusting the reflection edge of the low-emissivity coating.

On the other hand, in countries such as Canada, where the winters are cold and the summers are warm, one may wish to allow the near-IR part of the spectrum (0.78 to 3 μm) to enter during the cold months of winter in order to benefit from this additional source of

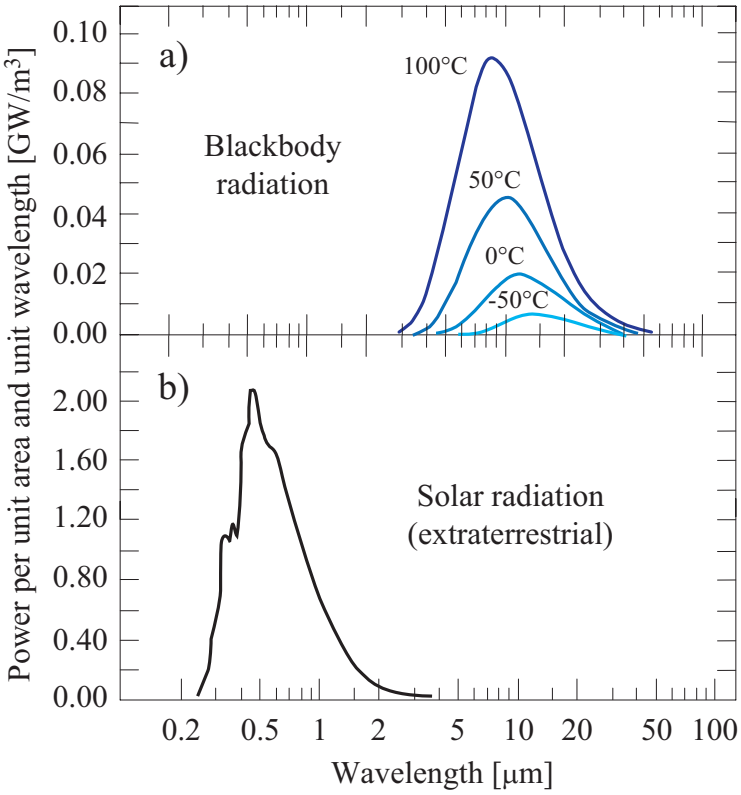

Figure 4.9 a) Blackbody emission curves for bodies at typical Earth temperatures between -50 and 100°C and b) solar radiation beyond the Earth's atmosphere (extraterrestrial). Note that this curve is simply given as an indicator of the range of wavelengths which are of interest for smart windows since the energy which reaches the Earth is affected by the atmosphere's absorption. Also note that ∼50% of the energy from the sun is in the IR. The data for this figure was taken from [172].

heating, while rejecting it during the summer. These two requirements cannot be met with a passive window design and therefore require the use of a dynamic window. For example, these two opposite conditions can be fulfilled by using WO_3. Indeed, in its bleached state, the visible and near-IR will be transmitted, whereas in its colored state, part of the visible and most of the near-IR will be "blocked". Note that since the energy is "blocked" by absorption and thus re-emitted as blackbody radiation, amorphous WO_3-based windows must be combined with a low-emissivity coating which reflects the infrared for wavelengths over approximately 3 μm. Another alternative is to use WO_3 in its polycrystalline form (see section 4.3.5) [161]. Additionally, not only do these windows allow to control the amount of heat which enters a building, they also permit to lower the visible transmittance allowing to benefit from a luminosity control for optimum user comfort (instead of using blinds or curtains). When compared with potentially thermochromic- or photochromic-based window designs, EC windows offer more flexibility for optimizing daylight and solar gain transmission [191]. For an interesting overview of these other potential chromogenic materials in the context of smart windows see [136]. It has also been lately suggested that combining thermochromic films with ECDs may lead to an increased modulation and performance [211].

A simple evaluation of the energy savings offered by EC windows has shown that as much energy could be saved as the energy which would be produced if the window was replaced by a solar cell (assuming a 1000 kWh/m^2yr solar energy density and a 17% efficiency solar cell) [212]. Additionally, in moderately warm climates, the use of smart windows could completely alleviate the need for air conditioning. It has been evaluated that 0.9 years of operation (for a prototype ECD window) is sufficient to compensate the production and operating energy requirements of such a window [213]. Interestingly, the most energy consuming element in a window is actually the aluminum frame which represents approximately 90% of the total primary energy [214]. For a precise evaluation of the energetic performance of an EC smart window, see the article by Papaefthimiou *et al.* [214]. The possibility to dynamically control a window also brings up the issue of control. Indeed, much work is being done in this particular context in order to maximize user comfort while also minimizing annual energy consumption [215].

Since powering an EC window is also an issue (buildings are not equipped with all the required electric circuitry), some researchers have even proposed to combine solar cells with smart windows in a tandem configuration in order to power them ; although interesting such configurations suffer from a relatively low transmission in the bleached state (approximately 30%) [145]. A side-by-side configuration may be a more plausible alternative [216].

Finally, commercial EC windows must fulfill many requirements : durability (more than 15 000 cycles), UV stability, neutral color to preserve interior color rendition, low leakage

current for good memory effect (due to edge shorts and defects in the films such as pinholes - mostly the ion conductor), cost effective and resist temperatures from -40 to 120°C [217]. Most requirements have nowadays been fulfilled although the cost of such windows is still very high. While many predict a drop in price following high production volumes, others have suggested using less expensive deposition methods such as atmospheric spray pyrolysis [218] ; although to date, performance is not up to par. Roll-to-roll coating is another solution which is being explored and which is known to decrease production costs. By depositing the ECD on a polymer web, one can then transfer it onto any desired substrate [219]. Also, polymer substrates are lighter and therefore important for applications in eyewear and aircraft windows [220]. For more details on the current state-of-the-art fenestration technologies and all associated companies with future challenges see [221, 222]. Granqvist also gives a good overview of the current situation in ECDs in one of his latest papers [223].

Finally, there are obviously many other applications which have been suggested for EC materials. Figure 4.10 shows how different configurations of an ECD can lead to very different applications. Indeed, these four examples cover all the ways in which an EC materials can be used : transmission modulation as in smart windows, reflectivity modulation as in anti-dazzling mirrors, diffused reflection modulation for displays and, finally, emissivity modulation for thermal control. Table 4.3 presents other applications of interest [viii].

viii. Although I have focused my attention on the EC properties of WO_3, it is important to note that this material has also been shown to color under seven other modes of excitation such as : electrocoloration (shown by Deb), UV irradiation (allowing for the photocatalytic decomposition of water), thermocoloration, exposure to atomic hydrogen, gasochromic when exposed to H_2 gas, ion beam irradiation and, electron irradiation [127, 115]. All of these other modes can obviously lead to other innovative uses of WO_3.

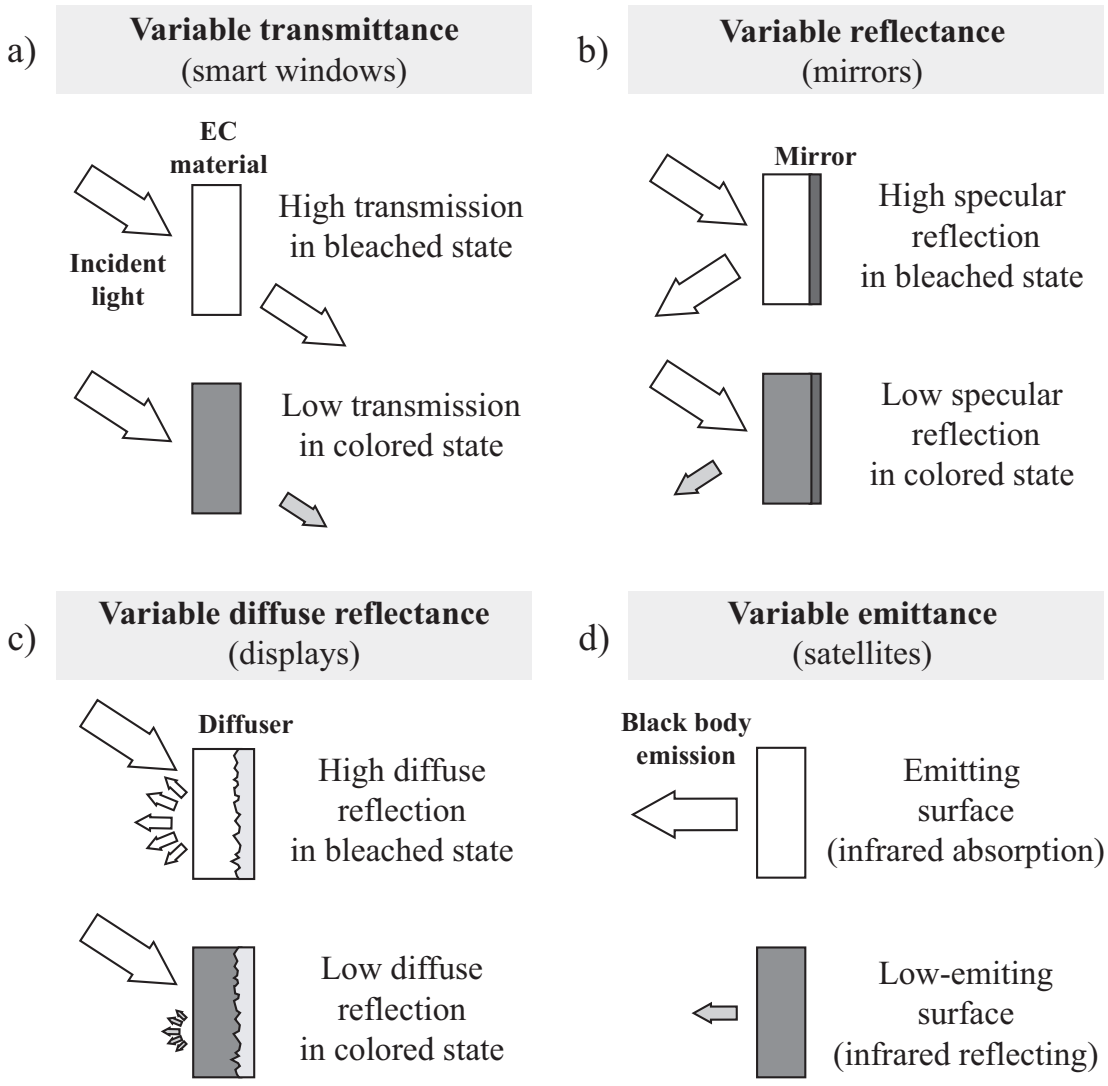

Figure 4.10 Four configurations in which EC materials can be used. When used as in configuration a), the EC material can modulate the amount of light being transmitted (e.g. smart windows). Using a reflective material (e.g. aluminum) as one of the electrodes such as in configuration b), results in variable reflectivity devices (e.g. automobile rear-view mirror). Displays are possible if using a diffuser as in c) (e.g. paper, TiO_2 nanoparticles, etc.). d) Finally, variable emittance devices in the infrared are also possible (based on polycrystalline WO_3). This figure was highly inspired by Granqvist [177].

Table 4.3 Possible applications of electrochromic materials

Application	**Description**	**References**
Airplane windows	Switchable passenger windows planned for future aircraft.	[224, 122]
Cathodic television with variable transmittance	Although this technology will probably never be implemented, EC materials were proposed in order to enhance a television's performance in various lighting conditions.	[225]
Data storage	Based on organic electrochromes, the authors propose high density storage devices.	[226, 227, 228]
EC display	Organic EC materials possessing faster response times, they are often proposed for display applications. Note that slower EC materials are of interest for displays such as billboards where the switching time is not important. Flexible displays based on inkjet printed WO_3 nanoparticles have also been recently proposed.	[229, 230]
EC glasses	EC materials allow the user to control the opacity of his glasses. This same concept is proposed for visors on motorcycle helmets. Note that in this particular case, switching speeds are critical for security reasons.	[231]
EC nanocrystal quantum dots	For future electronics and optoelectronics where charge-injection will allow control over the optical properties of colloidal semiconductor nanoctrystals.	[232]
Electronic paper	As previously mentioned, the incorporation of EC materials in a paper's fibers procures it interesting properties.	[113]
Gas sensors	Au-WO_3 and Al-WO_3 nanocomposites demonstrate a variation in their conductance when exposed to different gases. Another popular alternative is WO_3 covered by a catalyst such as platinum.	[233, 122]
Optical iris	Electrochromic iris for camera lenses.	[234]
Photolithography	Different etching characteristics for the colored and the uncolored material.	[235]
Smart clothing	Incorporation of EC materials in textiles for displays, camouflage, fashion, etc.	[236, 237]
Sunroof	Sunroof for Ferrari car by Saint-Gobain.	[123]
Temperature sensor	Device which allows one to know if frozen foods have been exposed to higher temperatures during transport. At a certain temperature, ionic conductivity through the electrolyte is activated.	[238]
Tunable photonic crystals	A WO_3 photonic crystal matrix is rendered adjustable by the characteristic change in index of refraction of WO_3 under lithium insertion. Idem for TiO_2.	[109, 239]
Variable emissivity	Variable emittance of WO_3 for satellite temperature control. In the case of Franke *et al.* the device is based on the use of amorphous WO_3 as the ion reservoir and crystalline WO_3 as the EC layer.	[240, 241, 242]

CHAPTER 5

EXPERIMENTAL METHODOLOGY

This section presents the main experimental methodology applied in the context of this thesis. In the first part, details on the deposition technique of the films will be given, while the second part will focus on the main optical, physical and electrochemical characterization techniques.

5.1 Sputtering

5.1.1 Electrochromic samples

In general, simply by looking at the literature, one can clearly see that WO_3 has been deposited by essentially every deposition technique known to man. Nevertheless, two of the most popular deposition processes have been evaporation and sputtering, the latter one being of interest for its fairly simple implementation on large scales. This is one of the reasons why all of the EC samples deposited during my thesis were made by radio frequency (RF) magnetron sputtering.

Sputtering, a physical vapor deposition (PVD) technique, is based on the momentum transfer from impinging ions to a target's atoms. If sufficient energy is transferred, this leads to an ejection of the target's atoms and their condensation on a substrate. The simplest form of sputtering, direct current (DC) sputtering, uses a target held at a negative potential (cathode) relative to the anode onto which are positioned the substrates where the films will grow. Electrons, naturally present in the deposition chamber, will first be accelerated from the cathode towards the anode, resulting in the ionization of the inserted gas (usually argon) and creation of a plasma. These generated ions will then be accelerated towards the cathode and impact the target thus generating secondary electrons which are necessary to maintain the discharge. If the energy of the ions is sufficiently high (higher than the threshold energy, that is the binding energy of the target's surface atoms), sputtering will ensue. Note, that only conducting targets may be used in DC sputtering since, if the resistivity of the target is too high, it becomes impossible to sustain the discharge. Depositing in reactive environments (in the presence of oxygen, nitrogen, etc.) is also more complex due to target poisoning (hysteresis effect) [243].

To circumvent these problems, RF sputtering was introduced. In such a case, a 13.56 MHz signal is applied to the target which, by increasing the plasma frequency, allows the

application of a current through a dielectric target [244]. In this case, the anode and the cathode constantly exchange roles but, due to the higher mobility of the electrons, both electrodes will acquire a negative potential (with respect to the plasma). If the substrates and chamber are grounded, the large size difference between the target and the substrate/chamber surfaces results in the creation of a significant negative potential on the target which leads to its sputtering.

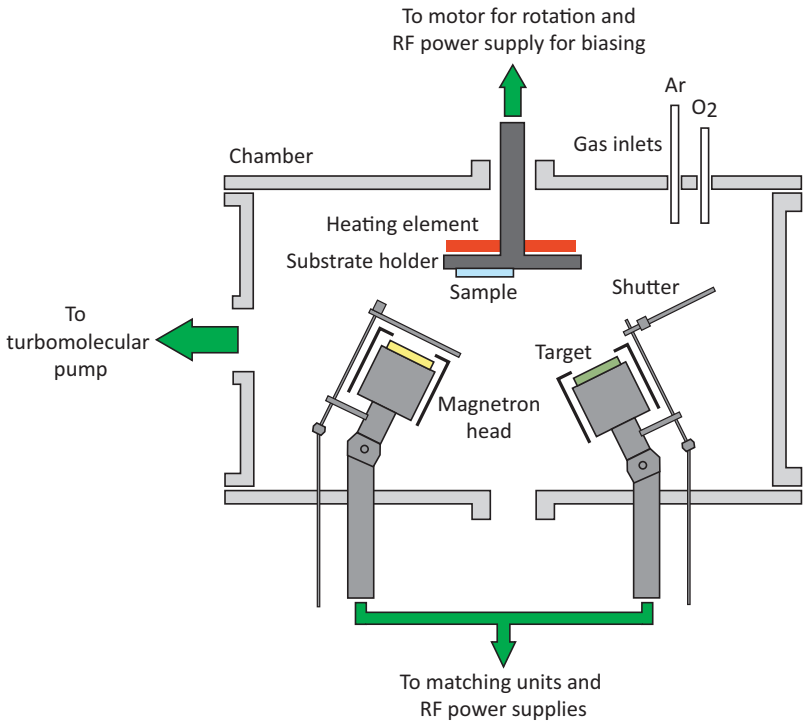

Figure 5.1 Schematic representation of the deposition chamber used for radio-frequency magnetron sputtering. Although only two magnetrons are shown, this chamber was equipped with four magnetrons. Three of them were used in the context of this project when fabricating Deb-type EC devices in order to deposit all the required films without breaking vacuum (see Chapter 7). Two magnetrons were used simultaneously when depositing composite films (see Chapter 9). Also note, that this chamber can be heated up to temperatures of approximately 350°C.

In order to increase the plasma density, and therefore sputtering and deposition rates, the cathode is generally formed of a magnetron. In such a configuration, permanent magnets are placed under the target resulting in the plasma's confinement (one to two orders of magnitude gain in current when compared to simple DC sputtering). Indeed, the confined electrons increase the ionization probability thus increasing the plasma density. A schematic representation of the RF magnetron sputtering deposition system used in the context of this

thesis is shown in Figure 5.1.

It is also important to note that of all the adjustable deposition parameters (gas ratios, gas flows, pressure, temperature, etc.), it is the deposition pressure and temperature as well as the energy and flux of impinging ions which have the highest impact on the microstructure of a growing film. The effect of these first two parameters on the microstructure of sputtered thin films has been studied and is schematically represented in the well known structure zone model developed by Thornton (see Figure 5.2) [245]. As can be seen, a higher deposition temperature, leads to denser films (zone T - transition from zone 1 to zone 2) and eventually to polycrystalline films at elevated temperatures (zone 2 resulting from the surface diffusion of adatoms and zone 3 from additional lattice and grain-boundary diffusion). Increasing the pressure delays the onset of zone T and promotes the creation of a more columnar and porous microstructure resulting from shadowing effects (zone 1). As mentioned in Chapter 4, porosity is a prerequisite in order to obtain "good" EC films and therefore the great majority of the samples in this thesis have been deposited at low temperatures and relatively high pressures (the deposition conditions for all samples will be given in their respective chapters). As a result, ion bombardment, which can lead to densification, without needing to be completely eliminated, was not required in the present context. Therefore, no biasing was used during the deposition of my EC films.

5.1.2 Passive metameric interference filters

Finally, the all-dielectric non-electrochromic metameric filters were deposited using dual ion beam sputtering (DIBS) in a *Spector II* system from Veeco-Ion Tech. One of three 35 cm diameter targets (Nb, SiO_2 or Ta) was sputtered using a 16 cm ion beam generated by a Kaufman gridded ion source. A second 12 cm ion source was also used simultaneously in order to increase the density of the deposited layers [246]. By adding oxygen and argon into the chamber as well as in the ion beams, Nb_2O_5, SiO_2 and Ta_2O_5 were deposited. The substrates were rotated at 600 rpm for improved homogeneity. For more details on the DIBS process as well as on the deposition parameters, please refer to [247].

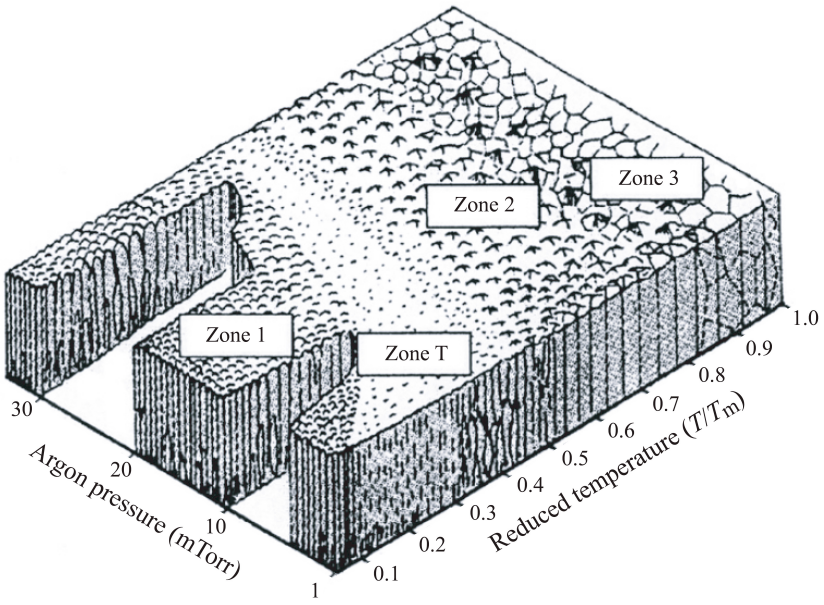

Figure 5.2 Structure zone model indicating the effect of the deposition pressure and temperature on the microstructure of a thin film. Note that T_{m} is the melting point temperature of the coating material. This figure was taken from [223] which was originally published in [245].

5.2 Optical characterization techniques

5.2.1 Spectrophotometry

Spectrophotometry is the most popular characterization technique when it comes to measuring the transmission, reflection or absorption spectrum of a sample. In the present context a Perkin Elmer *Lambda 19* was used to measure the optical spectra of samples deposited on B270 glass substrates or on ITO. This particular spectrophotometer is based on a double-beam configuration which allows one to remove the effect of fluctuations of the light source and detector during each measurement. Equipped with halogen and deuterium light sources it allows measurements between 175 and 3200 nm. Typical measurements in the present context were made between 250 and 2000 nm at every nanometer. When reflection measurements are required, two modules may be installed, one allowing for specular reflection measurements using a VW configuration (at a 7.5° angle of incidence), the other allowing for the total reflection to be measured using an integrating sphere from Labsphere (at a 8° angle of incidence). The use of an integrating sphere is particularly useful in the case of diffusive samples (rarely the case in the present context).

Note, that while one can obtain the optical properties (n and k) from transmission and reflection measurements using the method developed my Manifacier [248], the FCSEL possessing several ellipsometers, the measured spectra were combined with the ellipsometric data during the analysis process thus reinforcing the obtained results. Also note, that the *Lambda 19* is based on the use of two monochromators which results in very refined wavelength measurements but at the cost of speed. It is therefore impossible to make wideband (multiple wavelengths) *in situ* measurements such as required during the coloration of an EC sample. On the other hand, it is possible to make *in situ* measurements by choosing a single specific wavelength (single-wavelength measurements).

In the case where wideband *in situ* measurements are needed, one can use a charge-coupled device (CCD)-array-based spectrophotometer such as the Ocean Optics *USB2000* used in the context of this work. This type of spectrophotometer is equipped with a diffraction grating which splits the incoming light as a function of its wavelength. The diffracted light is then sent onto a CCD thus allowing for a complete spectrum to be measured simultaneously. Although in this case a significant gain in speed is obtained (several spectra per second), one must typically choose between the desired spectral range and resolution (the resolution is lower than what is obtained from using a monochromator-based spectrophotometer). For a given CCD, these characteristics are chosen by selecting an appropriate diffraction grating spacing; generally, a higher groove density will lead to a higher optical resolution but, will also reduce the spectral range.

5.2.2 Spectroscopic ellipsometry

Spectroscopic ellipsometry is a powerful nondestructive contactless technique when it comes to the characterization of the optical properties of materials ($N = n - ik$ with N the complex index of refraction containing n the index of refraction and k the extinction coefficient). When measuring the properties of a thin film, ellipsometry also allows one to obtain the thickness of the film, but can also supply information on its surface roughness, spatial thickness uniformity, the uniformity of its optical properties as a function of thickness, the presence of anisotropy, etc. Contrary to popular belief, all of these properties are not directly obtained, but indirectly determined through the use of a theoretical optical model.

The basic principle

The basic principle behind ellipsometry is the study of the change in polarization state upon reflection (or transmission) on a sample. Indeed, when polarized, light's electric field can be expressed by using two polarization states: s et p. The s polarization is perpendicular to the incident plane of propagation (the "s" comes from the German word for perpendicular "*senkrecht*") while the p polarization if parallel to this same plane. When both polarizations are in phase, their addition leads to linear polarization, when of same amplitude but out of phase by 90° their addition leads to circular polarization while any other amplitude/phase configuration leads to an elliptic polarization. This is from where ellipsometry derives its name. Thus, when light arrives upon a surface at oblique incidence, the reflected light (or transmitted) will generally be elliptically polarized. The basic ellipsometric parameters, Ψ and Δ, which are related to the Fresnel reflection coefficients, can be obtained from the following equation:

$$\rho = -\frac{r_p}{r_s} = tan\Psi e^{i\Delta}, \tag{5.1}$$

where Ψ is related to the ratio in amplitude of r_p and r_s while Δ, is related to their difference in phase. The Fresnel coefficients r_s and r_p are given by:

$$r_s = \frac{N_0 cos\phi_0 - N_1 cos\phi_1}{N_0 cos\phi_0 + N_1 cos\phi_1} \quad \text{and} \quad r_p = \frac{N_1 cos\phi_0 - N_0 cos\phi_1}{N_1 cos\phi_0 + N_0 cos\phi_1}, \tag{5.2}$$

where N_0 is the index of refraction of the incident medium and N_1 the index of refraction of the second medium (film or substrate). ϕ_0 is the angle of incidence of the incident beam, while ϕ_1 is the angle of refraction in the second medium obtained from the Snell-Descartes relation. The fact that ellipsometry is based on a ratio of two components also results in the additional advantage that it is insensitive to light source fluctuations and does not require any reference measurement.

It can be shown quite readily that ellipsometry is a highly sensitive technique (down to the ångström), by comparing the results of a reflection measurement performed using spectrophotometry and ellipsometry on a TiO_2 covered glass substrate (see Figure 5.3). One can clearly see, that although the spectrophotometric data essentially does not change for films under 1 nm, the ellipsometric data is seen to change significantly even in the presence of a 1 ångström thick film (most notably Δ).

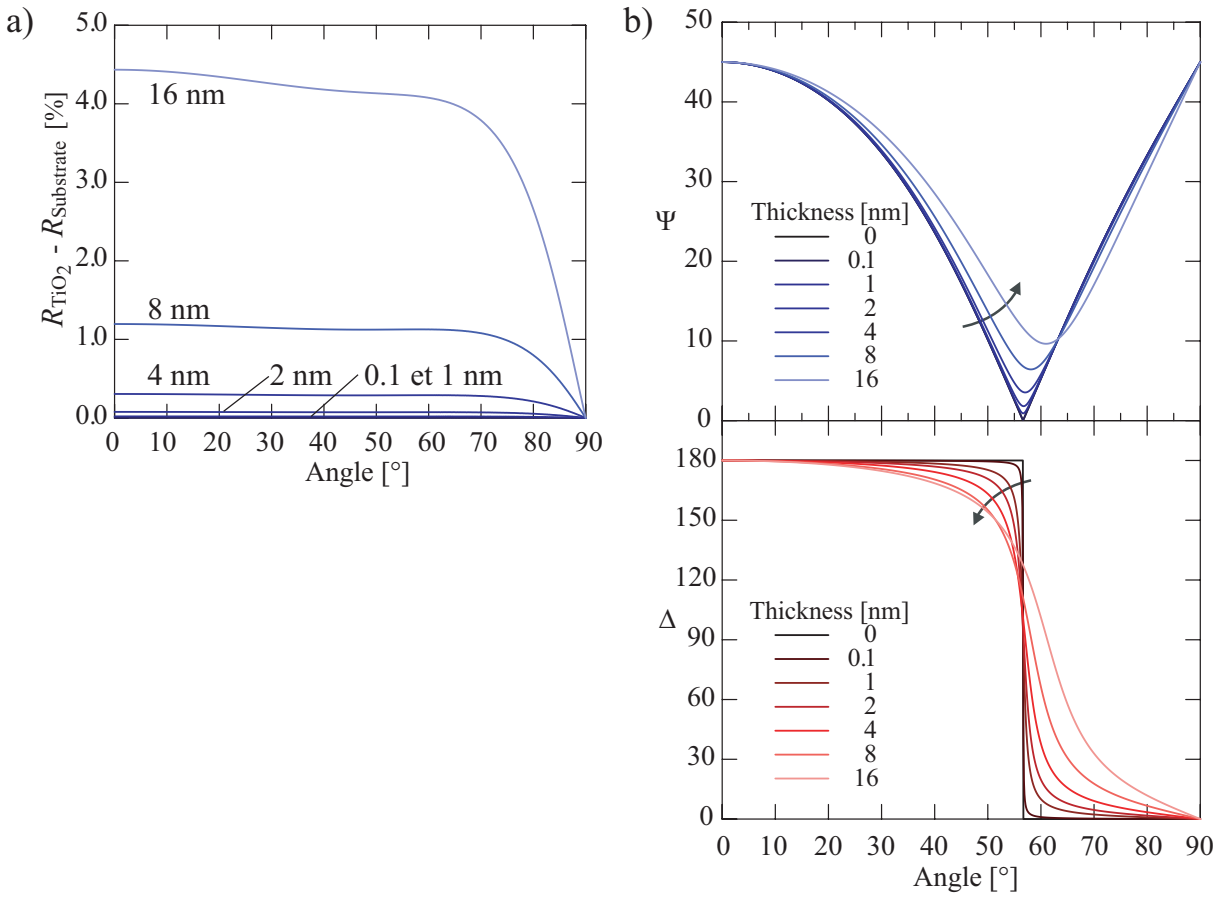

Figure 5.3 Comparison between the sensitivity of spectrophotometry and ellipsometry to the addition of a TiO_2 ($n = 2.2$ at 550 nm) thin film on a glass substrate ($n = 1.52$ at 550 nm). a) Difference in unpolarized reflection between a TiO_2 covered glass substrate and a bare substrate. b) Variation in Ψ et Δ for a TiO_2 covered glass substrate. Thicknesses of TiO_2 are varied between 0 and 16 nm.

Main components

In order to determine the change in polarization state upon reflection/transmission on a sample, one needs to know the polarization of the incident and reflected/transmitted light.

The basic components of an ellipsometer required to perform this analysis are shown in Table 5.1 following the path of a light beam from source to detector.

During the course of my Ph.D., I had the chance of working with three different ellipsometers, all from J.A. Woollam Co., Inc.:

- A monochromator-based rotating analyzer ellipsometer (RAE) allowing measurements at multiple angles of incidence (variable angle spectroscopic ellipsometry (VASE)) with a 280 to 1600 nm wavelength range.
- A CCD-array-based fixed-angle rotating compensator ellipsometer (RCE) (*M-2000*) with a 245 to 1650 nm wavelength range.
- A CCD-array-based variable angle dual-rotating compensator ellipsometer (*RC2*) with a 200 to 1700 nm wavelength range.

Most of the results which have been presented in this thesis were measured on the *M-2000*, although recently, I have begun using the *RC2*. This particular ellipsometer has the added advantage of performing rapid measurements at multiple angles as well as allowing the measurement of the transmission and reflection spectra of a sample. Multiple-angle measurements allow for a higher amount of collected data thus increasing the accuracy of the theoretical optical model as well as being essential in the case of the analysis of samples consisting of multiple films. This particular ellipsometer can also be outfitted with additional modules, mainly: a heating cell allowing *in situ* annealing measurements, an electrochemical cell, a microprobe and a moveable stage allowing for the mapping of a sample's whole surface.

Data analysis

As previously mentioned, once the data is acquired, an optical model (based on the use of oscillators such a Tauc-Lorentz, Gaussian, Cauchy approximation, etc.) must be built in order to derive the optical properties and thickness of the film(s). The parameters of the model are then adjusted in order to reproduce the experimentally determined Ψ and Δ values. An optimization algorithm (Levenberg-Marquardt) is then used to optimize the values of these parameters by minimizing the difference between the experimental and theoretical data (minimize the mean square error). It is important to add that one must always start the optimization process with the most accurate initial parameters (approximate thickness, optical properties, etc.); failing to do so can result in an inappropriate solution (local minimum solution versus absolute minimum solution). In the case of my WO_3 films, a typical model included a Tauc-Lorentz oscillator to take into account the absorption in the UV, an offset to take into account the absorption outside the measured spectral region, as well as a surface roughness layer (modeled using the Bruggeman effective medium approximation (EMA) - see Chapter 9). More details on ellipsometry can be found in the book by Tompkins and Irene

Table 5.1 Main components present in an ellipsometer.

Component	Description
Light source	The choice of the light source will dictate the spectral wavelength range in which a measurement is possible. For example, the M-2000 is equipped with a xenon lamp allowing measurements between 245 and 1650 nm.
Monochromator	As in the case of spectrophotometry, this is one of the means used in order to perform a measurement at a specific wavelength.
Polarizer	Linearly polarizes the light incoming from the light source. Polarizers are essentially wavelength independent in the region of interest and relatively inexpensive making them an almost ideal component.
Compensator	Based on a birefringent material, a compensator will retard one polarization more than the other thus resulting in a phase shift. In the case of a quarter-wave plate, introducing a 90° shift to one polarization transforms linearly polarized light into circularly polarized light. The use of a compensator in an ellipsometer allows the definition of Ψ between 0 and 90° and Δ between 0 à 360° with a higher accuracy. Indeed, using only polarizers limits the range of Δ between 0 and 180° since a polarizer possesses two identical positions (0 and 180°). Sensitivity is also reduced near 0 and 180° due to low intensity variations in the signal near these angles. Using a compensator also allows to measure depolarization resulting from non-uniformity, backside reflections, etc.
Analyzer	Based on a polarizer, this component is positioned after the sample in order to analyze the beam after its reflection from the sample's surface.
Diffraction grating	When not using a monochromator, gratings allow to diffract the incoming beam onto a CCD-array detector. This offers the possibility of making extremely fast wideband acquisitions (under 1 s) such as required during *in situ* measurements. On the other hand, the spectral resolution is limited as well as fixed when compared to monochromator-based ellipsometers.
Detector	Transforms the incoming light into an electrical signal. It is through a Fourier transform analysis of the signal that the Ψ and Δ parameters are obtained. Note that the detector is a CCD when using a diffraction grating.

[249].

5.3 Physical characterization techniques

5.3.1 Atomic force microscopy

Atomic force microscopy (AFM), was used in order to observe the surface topography, determine the surface roughness as well as the surface area difference (SAD) (ratio between the area of the surface topography and the total measured area) of my samples. AFM is based on a very sharp tip at the end of a cantilever which is raster scanned over the surface of a sample. The tip-sample interactions result in the tip's deflection which is measured using a laser beam reflected off the back of the cantilever. Sub-nanometer resolution is possible using AFM and therefore makes this quite inexpensive characterization technique a valuable tool. A *Dimension 3100* atomic force microscope from Digital Instruments was used for all measurements presented in this thesis.

5.3.2 Rutherford backscattering spectroscopy

Rutherford backscattering spectroscopy (RBS) allows one to determine a quantitative composition profile as a function of depth using a beam of high energy particles (2.042 MeV He^+ ions in the present case). This information is obtained by measuring and analyzing the energy and number of backscattered ions resulting from elastic collisions with atomic nuclei in the sample. It can be shown that the energy of a backscattered ion is a function of the mass of the nucleus it originated from (impacted) and will thus result in a detected peak positioned at a specific energy. Note that the energy of the backscattered particle is also affected by the distance it travels inside the film through interactions with electrons and glancing collisions with nuclei, so that the observed peaks will possess a width proportional to the thickness of the film (ions backscattered from the surface (independent on the thickness of the film) will have a high energy while ions backscattered from the film|substrate interface will have a lower energy proportional to the thickness of the film). The relative concentration of the various elements may also be determined from the relative peak intensities.

In order to detect the presence of hydrogen atoms, which due to their lighter mass cannot be measured using RBS, elastic recoil detection (ERD) measurements were performed. By using the same setup previously described, the lighter hydrogen atoms will be recoiled (expelled) from the film and collected at a second appropriately positioned detector. Figure 5.4 shows the setup which was used in the present case. In order to stop all atoms other than hydrogen ions (mostly the scattered helium ions), a 6 μm-thick mylar foil was placed in front of the detector [250].

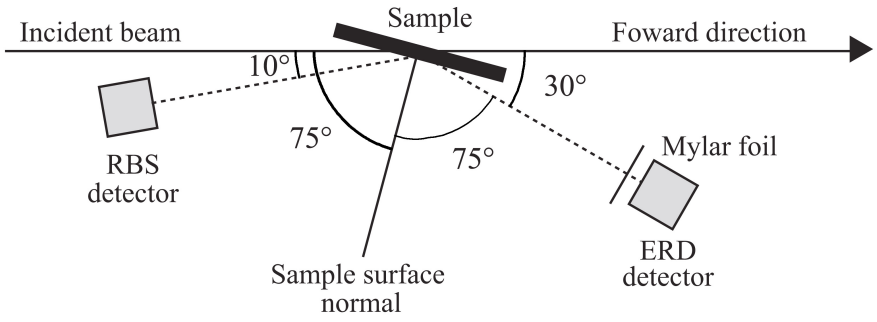

Figure 5.4 Setup used in the context of the RBS and ERD measurements performed on the samples presented in the present thesis.

5.3.3 Scanning electron microscopy

Scanning electron microscopy (SEM) was used in order to observe the microstructure of some of my samples. Based on an electron beam which is raster scanned on the surface of a sample, SEM allows a highly magnified view of a sample to be obtained in a quick and nondestructive matter. The interaction of the beam of electrons with the sample results in the creation of electrons as well as high energy photons (X-rays). Mainly two types of electrons are emitted: secondary electrons which result from inelastic collisions (scattering) with atomic electrons and backscattered electrons which result from elastic collisions with atomic nuclei. The energy of secondary electrons is rather low (< 50 eV) and as a result they are mostly emitted from within the first few nanometers of the surface. Since the angle at which the incident beam hits a surface affects the number of secondary electrons emitted (higher surface angle increases the number of electrons), detecting these electrons results in a variation in brightness as a function of the surface topography.

In the case of backscattered electrons, the fact that higher atomic number elements increase backscattering, results in a signal which is element sensitive. Thus, detecting these electrons allows for a chemical contrast image to be generated. Finally, one can also analyze the elemental composition of a sample using the generated X-rays through the use of energy-dispersive X-ray spectroscopy (EDX) or wavelength-dispersive X-ray spectroscopy (WDX).

The SEM used in the present work (JEOL *JSM-7600F* at 5 kV) was equipped with a field emission gun (FEG) electron source allowing for a high resolution as well as measurements at low voltages (high emission current is possible even at low acceleration voltages). As a result, non-conductive samples may be measured without the addition of a conductive coating.

5.3.4 X-ray diffraction

X-ray diffraction is typically used to characterize the crystalline phases, as well as their orientation (texture), present in a material. Indeed, according to the Bragg equation ($\lambda = 2dsin\theta$ where λ is the wavelength of the incoming X-ray, d the spacing between two atomic planes and θ the angle of diffraction), a different atomic spacing between planes will result in a different angle of diffraction. In the case of a thin-film, the incident beam's angle of incidence must be as high as possible (grazing-incidence; typically at a 1° angle above the surface) in order to obtain a sufficient signal arriving from the thin film (versus the substrate). The detector is then moved between two prescribed angles in order to observe the diffraction peaks. The pattern which is obtained then allows one to identify a sample's various crystalline phases. Also note that from a diffraction peak's width and by using the Scherrer equation one can also determine the average size of the crystallites. A Philips *X'pert* diffractometer using Cu Ka radiation ($\lambda = 1.5406$ Å; 50 kV acceleration voltage and 40 mA filament current) was used to confirm that all my samples were amorphous in nature (absence of diffraction peaks).

5.4 Electrochemical characterization techniques

In order to characterize the electrochromic properties of the WO_3-based films deposited during this thesis, I conceived and developed an experimental setup allowing electrochemical measurements in combination with *in situ* transmission measurements. Of all the electrochemical techniques, the principal one that was used was cyclic voltammetry. In the following, I present the main characteristics of this technique as well as the information it can provide on a given WO_3 thin film.

5.4.1 Cyclic voltammetry

Cyclic voltammetry (CV) is part of a large family of electrochemical analysis techniques which study the chemical response of a given system following an electrical stimulation; other techniques include chronoamperometry (constant voltage), chronopotentiometry (constant current), electrochemical impedance spectroscopy [i], etc. The basic principal of CV consists in applying a potential ramp at a determined rate v (scan rate) back and forth between two set values using a potentiostat (in this case an *Autolab PGSTAT302N* from Metrohm Autolab); this results in a triangular shaped voltage profile. At the same time, the generated current is monitored.

i. Electrochemical impedance spectroscopy could be a very useful method to implement since it can give information on diffusion, porosity and the effect of interfaces [115]. Note that, just like in ellipsometry, impedance measurements must be modeled using an equivalent electrical circuit (so called Randles circuits).

Just like in infrared spectroscopy, where a measurement can provide information on the presence of specific chemical bonds (noted by the presence of absorption bands at specific energies), in a similar fashion cyclic voltammetry gives a "fingerprint" of the electrochemical processes occurring at the sample by scanning through a range of potentials (activation energies). It also allows one to quickly determine the appropriate voltage levels for best operation (too high voltages can lead to gas evolution and a sudden increase in current), measure charge insertion/extraction ratios and observe if the process is reversible. Figure 5.5 shows the characteristic shape, often termed "duck-shaped", obtained for an amorphous WO_3 film deposited by RF magnetron sputtering measured in a 1 M H_2SO_4-distilled water solution at 100 mV/s. The fact that the curve is smooth is indicative that no phase changes have occurred [115]. The appearance of peaks is seen in crystalline films and can indicate different diffusion paths.

The potential is initially started at 0.6 V and decreased at a rate of 100 mV/s down to -0.6 V. The bottom region where the current is negative corresponds to the coloration phase of the WO_3 films (cathodic current). The top region therefore corresponds to the bleaching phase (anodic current). One can note the presence of a maximum current during this particular phase (peak anodic current, i_p). Provided the electrochemical reaction is reversible [ii], one can use the Randles-Sevčik equation to calculate the diffusion coefficient of the ions:

$$i_p = 0.4463 n_e F A c_s \sqrt{\frac{n_e F v D_i}{RT}}, \tag{5.3}$$

where n_e is the number of electrons taking part in the reaction, F is the Faraday constant (C/mol), A the working electrode area (cm^2), c_s the solution concentration (mol/cm^3), v the scan rate (V/s), R the universal gas constant ($J/mol \cdot K$) and T the ambient temperature (K). It is also important to note that no peak cathodic current is observed. Indeed, maximum oxidation/reduction peaks are the result of a rapid increase in current which rapidly reduces the concentration of available reactant and thus subsequently decreases the current. Since the back electromotive force limits the coloration speed, no reduction peak is observed in Figure 5.5. On the other hand, extremely slow cycling (1 mV/s) has led to the appearance of a reduction peak [230].

Knowing the scan rate, one can convert the increments in potential ΔV into increments of time Δt. By multiplying the current by the Δt value, one obtains the inserted or extracted charge. Multiplying all negative current values by Δt and adding them up gives the total inserted charge, while the positive currents provide the extracted charge. The ratio of the

ii. One can plot the anodic peak current versus the square root of the scan rate to confirm this; a linear behaviour is indicative of a reversible process. Note that an increased scan rate will generate a higher anodic peak current.

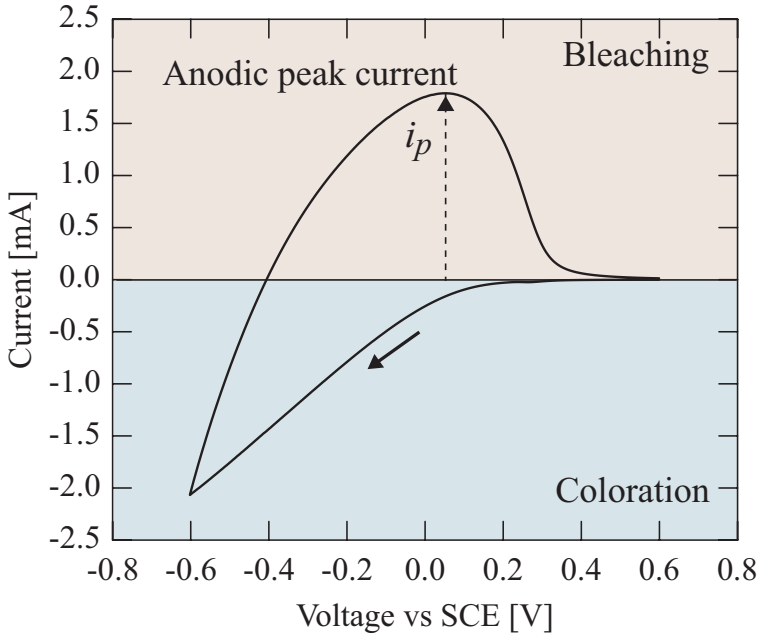

Figure 5.5 Characteristic voltammogram for an amorphous WO_3 film. The data corresponds to the 100 mV/s voltammogram presented in Figure 7.4 of Chapter 7.

inserted versus extracted charge is a good indicator of either charge trapping or the presence of secondary reactions resulting in a non-reversible process. By studying the evolution of the inserted and/or extracted charge as a function of the number of cycles, one can also gain information on the long term durability of a coating (degradation). Multiple cycles also allow one to observe how many cycles are required to reach a steady state (I typically made 10 activation cycles). Finally, knowing the amount of inserted charge also permits one to calculate the intercalation ratio x by using:

$$x = \frac{QM}{eAd\rho_M N_A}, \tag{5.4}$$

where Q is the inserted charge, e the elementary charge, N_A the Avogadro constant, and d, M, and ρ_M are the thickness, molar mass, and density of the studied film respectively.

Experimental setup

The experimental setup used in the context of this thesis is shown in Figure 5.6. It consisted of three electrodes immersed in a 0.1 or 1 M H_2SO_4-distilled water solution. Specifically, a WO_3 covered ITO|glass substrate was used as the working electrode, a platinum foil as the counter electrode and a saturated calomel electrode as the reference electrode (note that 0.244 V must be added to convert a potential measured using a saturated calomel

electrode to obtain the voltage using a standard hydrogen electrode). The potentiostat thus applies the desired voltage by using the reference electrode as its reference point (the potential being measured between the reference electrode and the working electrode), while the current was measured between the working and counter electrodes. The cell can be sealed to

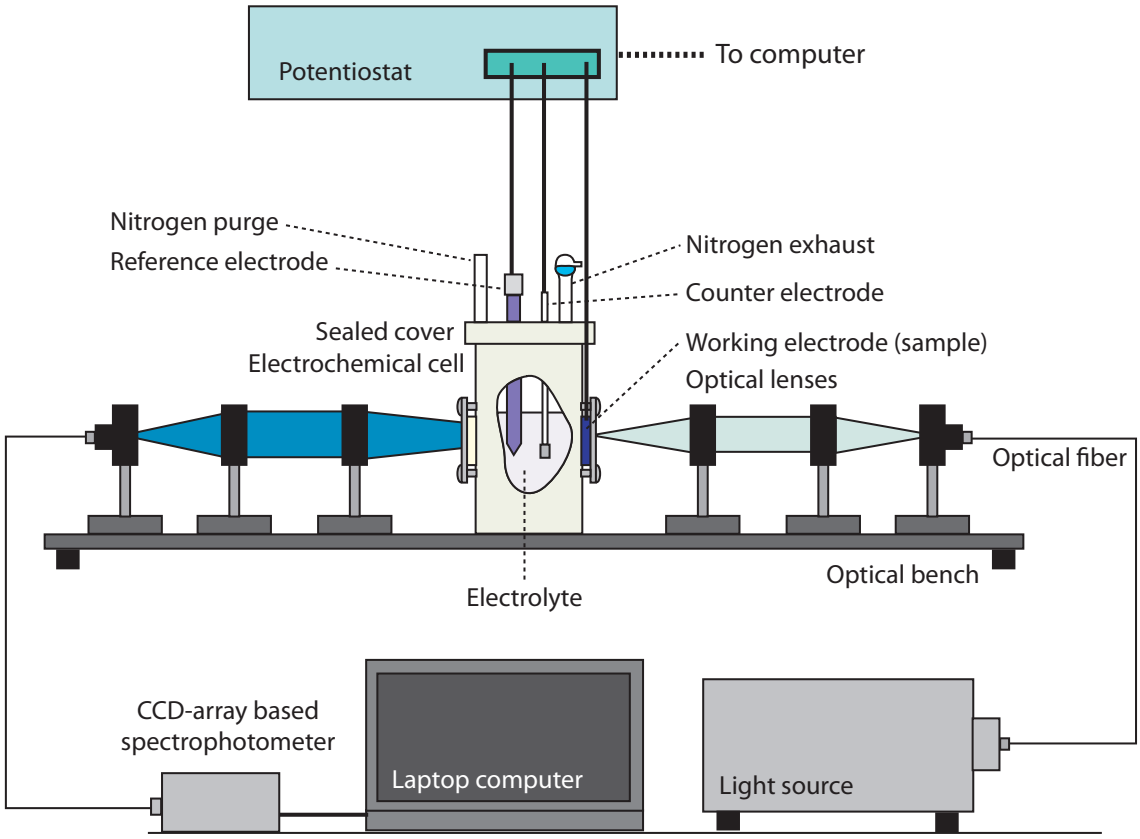

Figure 5.6 Electrochemical measurement setup with combined *in situ* transmission measurements.

avoid air from entering (a nitrogen purge can be applied to remove the presence of oxygen which can generate unwanted currents through reduction of O_2). Note, that the working electrode also constituted one of the windows of the electrochemical cell. This methodology allowed me to preserve the same surface area for every studied sample. This was important when calculating the density of inserted and extracted charges (calculation of the coloration efficiency). Since the cell was equipped with two windows, a beam of white light could pass through it, thus permitting *in situ* transmission measurements. The complete setup, consisting of a stabilized light source (*DH-2000* from Ocean Optics), fiber optics, lenses and spectrophotometer (*USB2000* also from Ocean Optics) is shown in Figure 5.6.

By using the transmission measurement, one can calculate the coloration efficiency (CE)

using the following formula:

$$\mathrm{CE} = \frac{ln[T_b/T_c]}{[Q/A]}, \tag{5.5}$$

where T_b and T_c are the transmission in the bleached and colored states respectively. Note that this formula does not take into account the reflectivity of the sample. Indeed, some light will be lost due to reflections at the first electrolyte|film and film|ITO interfaces. The assumption which is made here is that the change in reflectivity between the bleached and colored states is negligible, which in the case of amorphous WO_3 is not unreasonable.

A more accurate calculation of the change in optical density can be obtained by considering the reflectivity of the sample in conjunction with its transmission [$\Delta(OD) = ln((T_b/(1 - R_b))/(T_c/(1 - R_c)))$ [251]. Once again, R_b and R_c are the reflection in the bleached and colored states respectively]. This approximation, which is valid in the case of very absorbing media was obtained from [252]. One can also see that the numerator which takes into account the bleached state is also valid, since when absorption is negligible, $T_b + R_b = 100\%$ and as a result, the numerator will be equal to 1. Finally, all these approximations do not take into account the multiple reflections present in the case of thin film interference and consequently, using optical modeling and/or *in situ* ellipsometry could be a very useful tool in order to obtain a more accurate evaluation of the CE (more will be said on the subject of *in situ* ellipsometry in Chapter 10).

CHAPTER 6

METAMERIC INTERFERENCE SECURITY IMAGE STRUCTURES

6.1 Foreword

My work on developing new security devices based on ISIS started in summer 2003 during my master's. It is during an optometry course entitled "the science of vision" (autumn 2003) that the concept of developing a metameric device came to me. I initially started by designing pairs of filters with identical colors yet very different transmission spectra. Using such pairs of filters one could create a device uniform in color at normal incidence (or any other angle) and having a specific image which would appear at higher angles of incidence (hidden image effect). Indeed, the fact that the metameric filters possessed different spectra resulted in contrasting angle-dependent color shifts. Unfortunately, their metameric nature also made them very sensitive to changes in light sources and observers as well as to deposition errors. Consequently, a color match was extremely difficult to achieve. An example of such a pair of metameric filters is presented in the present article.

Having noted these issues, we decided to replace one of the interference filters by a non-iridescent material (NIM) (e.g., transparent colored polymer). By doing so, we decreased the cost of the metameric device, made fabrication simpler and also allowed for more stable devices to be designed and fabricated. By designing filters which matched the transmission or reflection spectrum of the NIM, we were able de decrease the sensitivity to changes in illuminants (decrease metamerism) and incidentally to changes in observers (e.g., color blind individuals). The devices presented here were fabricated during the beginning of my Ph.D. and in the context of an *Idea to Innovation* grant from NSERC.

Although not shown in the present paper, we have also demonstrated the possibility of creating a hidden image effect by patterning the filter and NIM into a series of pixels as shown in Figure 6.1 [253].

Finally, we have also tested the optical and mechanical stability of our metameric filters under various environments meant to simulate the everyday wear and tear of a banknote. This work, which was also published in context of the *Idea to Innovation* grant [34], demonstrated that all-dielectric filters showed very little variation following exposure to temperature cycling, humidity, chemical agents, and tribomechanical intrusion. On the other hand, metal-dielectric filters were shown to be more sensitive and thus would require encapsulation in order to maintain their metameric properties.

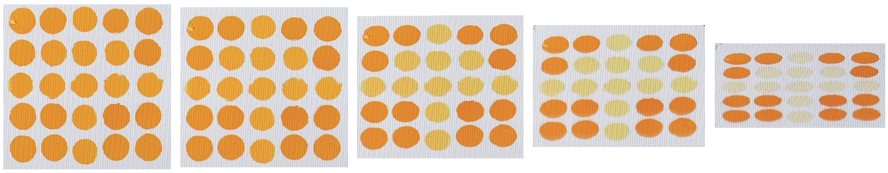

Figure 6.1 Transmission based metameric device presenting a hidden image combining a transparent coloured paint and an interference filter presented at different (approximate) angles of incidence. Notice that at high angles of incidence an arrow appears.

6.1.1 $\Delta E^{\star}_{\mathbf{ab}}$ vs $\Delta E^{\star}_{\mathbf{00}}$

In the context of the design of metameric filters, the issue of calculating color differences has come up a few times during the referee process. In fact, some have argued that the $\Delta E^{\star}_{\mathrm{ab}}$ color difference formula is out-of-date when compared with the new $\Delta E^{\star}_{00}$ formula [18]. In all my color calculations, I have continued to use the $\Delta E^{\star}_{\mathrm{ab}}$ formula for two simple reasons : one for its simplicity and two, because from my practical experience with metameric devices [254], my defined thresholds seemed sufficient to ensure a good color match. Although, the color difference offered by the $\Delta E^{\star}_{00}$ formula is more perceptually uniform, in most of my work I was simply analyzing a single set of metameric samples. Thus, a lower $\Delta E^{\star}_{\mathrm{ab}}$ value still ensures a better color matching pair under specific lighting conditions and is simply used to ensure a sufficient color match.

Also, since the $\Delta E^{\star}_{00}$ formula is relatively new, it still has not been clearly adopted by the industry (e.g., International Organization for Standardization (ISO) norms). As mentioned in the book by Schanda [6] :

"*a further testing phase with other data is welcome to receive independent information on the validity of the formula* [referring to the $\Delta E^{\star}_{00}$ formula]". He has also noted that the $\Delta E^{\star}_{00}$ formula :

"*was developed from data sets nearly under reference conditions and is thus thought to be exactly valid only under these conditions. If other conditions are chosen, parametric factors should be estimated from previous experiments or should be newly elaborated*".

We mention this information since the evaluation of the color difference of a metameric security device is usually not done in "reference conditions". In fact, the most effective way to define a precise color matching threshold is to proceed to real-life testing under specific lighting conditions and with a variety of different observers. This has also been noted by J.A. Dobrowolski, the inventor of ISIS, in his paper published in 1989 [33]. On the issue of color tolerances of anticounterfeiting coatings he mentions :

"*This is clearly a very complex matter, and only approximate answers are possible*".

Indeed, there are many phenomena which can affect color perception that calculations can only take you so far. Here are some elements which can affect how we perceive a colored surface :

- The size, shape, hue, saturation and luminance of the object as well as the surrounding environment.
- Variations in color perception among the normal color vision population. Also, 8% of the male population suffers from color-defective vision (0.5% of the female population).
- Old age leads to yellowing of the eye's lens due to UV light.
- An object's color is affected by the colors surrounding it. This effect is called simultaneous contrast and results from the interaction between cones.
- The ability of the human eye to adapt as previously mentioned (color constancy).
- Previous exposure of the eye.
- Etc.

Therefore, although the newer color difference formulas are more perceptually linear, they simply are not adapted to be used in the present context. It is consequently for all of the above mentioned reasons that I chose to continue using the $\Delta E^{\star}_{\mathrm{ab}}$ color difference formula.

ARTICLE 1 : METAMERIC INTERFERENCE SECURITY IMAGE STRUCTURES

Bill Baloukas and Ludvik Martinu

Department of Engineering Physics, École Polytechnique de Montréal,
P.O. Box 6079, succursale Centre-ville, Montréal, Québec H3C 3A7, Canada

Applied Optics, vol. 47, no. 10, 2008, p. 1585-1593.

Abstract

In the present work, we study innovative interference security image structures based on metamerism. We have designed, fabricated and evaluated different structures which can be used in transmission or in reflection. These metameric structures are either a combination of two different interference filters or of an interference filter and a non-iridescent colored material. In the latter case, by closely matching the spectra, the sensitivity of the device to changes in light sources and observers is minimized. Due to the intrinsic color shift of interference filters, one can create a hidden image which appears at a specific observation angle. The presence of the hidden image, as well as in some cases of the non-iridescent material, which serves as a color reference, increases the complexity of such devices, while facilitating the user's authentication process as well as automatized detection by using a laser at a specific angle. We present the design approach, analyze the filters' sensitivity to deposition errors, and evaluate the performance of prototype devices prepared by dual ion beam sputtering.

6.2 Introduction

We presently live in an age where technology's affordability and accessibility make counterfeiting relatively easy and thus frequently tempting. This causes considerable problems in many spheres of activity such as banknotes, valuable documents (passports, identification (ID) cards, credit cards, cheques, etc.) and others. The advent of inexpensive high-resolution printers has also made it simple for practically anyone to print out fake money.

In general, counterfeiting not only affects banks and governments but also the general public. In fact, according to the Canadian Bankers Association, in 2006, debit card skimming reached $94.6 million, an increase of 34% compared to 2005, while credit card fraud totalled $185.45 million, an increase of 10% [255]. Even more alarming, estimates from the World Health Organization show that probably more than 10% of prescription drugs on the world market are counterfeit [21]. This percentage is even higher in developing countries. Counterfeit products can range from a bottle of shampoo to aircraft parts. The resulting problem is therefore not only related to the country's economy, but also the impact on public security due to the fact that most counterfeit products fail to meet safety standards. Consequently, including the use of security devices on such products and maintaining the public's awareness about them are critical in the fight against counterfeiting.

In this context, our work focuses on OVDs [256], more precisely, on interference security image structures (ISISs) [51]. These devices are based on thin film interference [10], and they offer an interesting variation of color as a function of the observation angle ; this not only makes them simple to authenticate, but also renders documents immune to photocopiers, photography or reprographic processes. For these reasons, ISISs have been very well accepted in the U.S., in Canada and in other countries, provided they are well positioned on the document and offer an effective color shift [2].

Historically, this type of device was first applied on currency in 1989 on the *Birds of Canada* series banknotes, and was presented as a patch offering a gold to green color shift [33]. The initial design consisted of 13 dielectric layers, but today, it has evolved into a security thread consisting of a three layer metal-dielectric stack, still offering the same color shift. Another version of ISIS is optically variable ink (OVI) [47, 67]. OVI consists of a thin film filter which is first released from the substrate, ground into flakes and then incorporated into a liquid medium permitting printing. More complex OVDs, developed in recent years, combine diffraction [74], which is the basic effect behind holograms, with the color shift due to interference.

Another way to complexify ISISs devices, is to incorporate the concept of metamerism [5], a well known phenomenon in the industry, where color matching and color tolerances

are important. For example, different materials that match under daylight may appear very different under incandescent lighting, potentially leading to serious problems. Metameric inks have also been proposed for their use in self-verifying documents [257] or in printed hidden images which can be revealed under UV lighting [258]. Although interesting, these technologies require the use of a filter or UV light source in order to authenticate them.

The principle of metameric filters was first presented by Dobrowolski [3] in 1973, where two interference filters of the same color could, when superimposed, block all transmitted light. Inspired by the latter idea, we have proposed to explore new opportunities of the concept based on metamerism in innovative security devices [46, 259]. A product based on metamerism, used in reflection and developed by Flex Products ("MetaSwitch") has also been commercialized [260].

In the present work, we investigate a combination of two model interference filters, in a complex system, and we demonstrate the formation of an impressive hidden image effect in such metameric pairs [261]. We further present more simple, yet as performing OVDs based on the same principles, while considering two approaches, namely (i) a filter and a transparent NIM, and (ii) a filter and a reflective NIM pair.

6.3 Theoretical background

The working principle behind the studied devices relies on metamerism. As defined by the Commission Internationale de l'Éclairage (CIE), two objects displaying the same color (identical tristimulus values) under a specific illuminant and for a specific observer, are termed metameric if their spectral distributions differ in the visible spectrum [262]. One way of measuring the stability of metamerism is to evaluate the color difference which is obtained when changing the light source or observer. Intuitively, if two spectral distributions differ widely (see Figure 6.2, for example), one can expect the color match to be highly sensitive to changes in light sources (illuminant metameric failure) or when observed by a color blind individual (observer metameric failure). The only way one can diminish the illuminant and observer sensitivity is to increase the similarity between the two spectra. Two identical spectra (isomeric), would lead to a perfect color match under all conditions. Although the term metamerism defines that two samples have "perfectly" identical tristimulus values, for practical reasons, in the remaining of this paper, we will describe our samples as being metameric if no color distinction can be detected by a human observer under a given light source.

The color difference, $\Delta E^{\star}_{\mathrm{ab,\,I}}$ [262] (where I is added in order to indicate the illuminant), is obtained by calculating the distance between the color coordinates of two objects. In our case, the calculations are performed in the $L^{\star}a^{\star}b^{\star}$ color space, which is considered more

perceptually linear than the xyY color space. The following equations allow to convert the XYZ tristimulus values to the $L^\star a^\star b^\star$ color space [4] :

$$L^\star = 116\left(\frac{Y}{Y_n}\right)^{1/3} - 16 \tag{6.1}$$

$$a^\star = 500\left[\left(\frac{X}{X_n}\right)^{1/3} - \left(\frac{Y}{Y_n}\right)^{1/3}\right] \tag{6.2}$$

$$b^\star = 200\left[\left(\frac{Y}{Y_n}\right)^{1/3} - \left(\frac{Z}{Z_n}\right)^{1/3}\right], \tag{6.3}$$

for $X/X_n, Y/Y_n$ and $Z/Z_n > 0.008856$. X_n, Y_n and Z_n are the reference white tristimulus values. Once the $L^*a^*b^*$ coordinates are calculated for both objects, $\Delta E^\star_{\mathrm{ab,\,I}}$ is obtained by :

$$\Delta E^\star_{\mathrm{ab,\,I}} = \sqrt{(L_2^\star - L_1^\star)^2 + (a_2^\star - a_1^\star)^2 + (b_2^\star - b_1^\star)^2}. \tag{6.4}$$

A just-noticeable color difference is usually obtained for $\Delta E^\star_{\mathrm{ab}} \simeq 1$ [15] in the case of uniform color patches under specific viewing conditions. For $\Delta E^\star_{\mathrm{ab}}$ values lower than 1, no color difference can be observed, and evidently, for $\Delta E^\star_{\mathrm{ab}}$ higher than 1 the color difference increases. In this paper, all color pairs possessing $\Delta E^\star_{\mathrm{ab}} \leq 2$ will be considered metameric, which is still a very good compromise in order to add more flexibility to the design process and to lower the number of layers. More advanced color difference equations exist (CIE94 [4] and CIE2000 [18]), but their metamerism threshold is still not clearly defined. Also note, that although these equations offer a more uniform color space, the fact that the way we perceive color is also dependent on many other factors (simultaneous contrast, previous exposure to light, surrounding environment, etc.) renders them unnecessarily complicated for the present application. The best way to define a threshold is to develop an on site test using precise observation conditions.

6.4 Experimental methodology

In the first set of experiments, we have optimized the deposition of optical filters using dual ion beam sputtering (DIBS) in a *Spector II* © system manufactured by Veeco-Ion Tech. Two Kaufman gridded ion sources were used during deposition. The first 16 cm ion source was used to sputter one of the two 35 cm diameter targets, either SiO_2 or Ta. The second 12 cm ion source was used simultaneously to increase the density of the deposited layers [246]. By adding O_2 as well as Ar to the chamber and to the ion beams, SiO_2 and Ta_2O_5 were deposited. The parameters of the individual ion beams are given in Table 6.1. The substrates

were rotated at 600 rpm for improved homogeneity. Since only time was used to monitor the thickness of the layers during the deposition process, slight variations are expected.

Table 6.1 Deposition parameters in the DIBS system.

Parameter	SiO_2	Ta_2O_5
Voltage of sputtering beam (V)	1250	1250
Current of sputtering beam (mA)	600	600
Voltage of ion assist beam (V)	400	550
Current of ion assist beam (mA)	75	150
Deposition rate (nm/s)	~ 0.21	~ 0.30

Optical constants as well as thickness and deposition rate of the dielectric optical materials deposited on c-Si were obtained by variable angle spectroscopic ellipsometry (J.A. Woollam Co., Inc.). Analysis of the ellipsometric data was performed by using the *WVASE32* software also from the J.A. Woollam Co., Inc. Finally, the fitting was done using the Cauchy dispersion model [263].

The filters were designed using the *TFCalc 5.1* by Software Spectra, Inc. and *OpenFilters* developed at École Polytechnique de Montréal [68]. Color calculations were performed in the xyY and $L^*a^*b^*$ color spaces using standard illuminants (D65 - average daylight with a correlated colour temperature of 6500 K, A - incandescent lighting and F1 - fluorescent lighting), defined by the CIE [262]. Transmission measurements were obtained using a Perkin-Elmer *Lambda 19* spectrophotometer.

In the second series of experiments, we fabricated metameric devices by integrating a specific image structure composed of a NIM and of an interference filter. Devices used in transmission were fabricated on B270 glass substrates which were cleaned using soap and hot water and then rinsed with acetone and isopropanol. Filters used in reflection were deposited on <111> c-Si.

The NIM used for transmission devices was a water based transparent paint by Pébéo. It is important to note in this case that any NIM can be used as long as it is transparent and non-translucent (absence of scattering) in order for the optical effect to be similar to that of an interference filter. The material was spin coated using a Laurell Technologies Corporation spin coater. The coating was then annealed at 160°C for 40 minutes. In the case of reflective devices, the NIM must be purely specularly reflective.

Creation of patterns was made by masking of specific regions using antistatic high temperature polyimide tape by Wescorp and etched in a capacitively coupled radio-frequency O_2 plasma for 60 minutes. Evidently, if more precise motifs are wanted, one might consider using other microfabrication techniques such as laser ablation or photolithography.

6.5 Results and discussion

6.5.1 Design and performance of metameric filters

In the initial stage of the work on metameric ISISs, we concentrated on designing two metameric all-dielectric filters under illuminant D65 at normal incidence for use in transmission. It is important to note that the same principles also apply in reflection. An example of such a type of metameric pair is shown in Figure 6.2. Although the transmission spectra of filters A and B differ widely, their colors at normal incidence match very closely under illuminant D65 ($\Delta E^{\star}_{\mathrm{ab,\ D65}} = 0.24$). The designs of filters A and B, which consist of 19 and 15 layers, respectively, are given in Table 6.2 ; they consist of a low index material, SiO_2 (index of refraction $n = 1.474$ @ 550 nm) and a high index material, Ta_2O_5 ($n = 2.118$ @ 550 nm), both with negligible absorption in the visible region (380-780 nm).

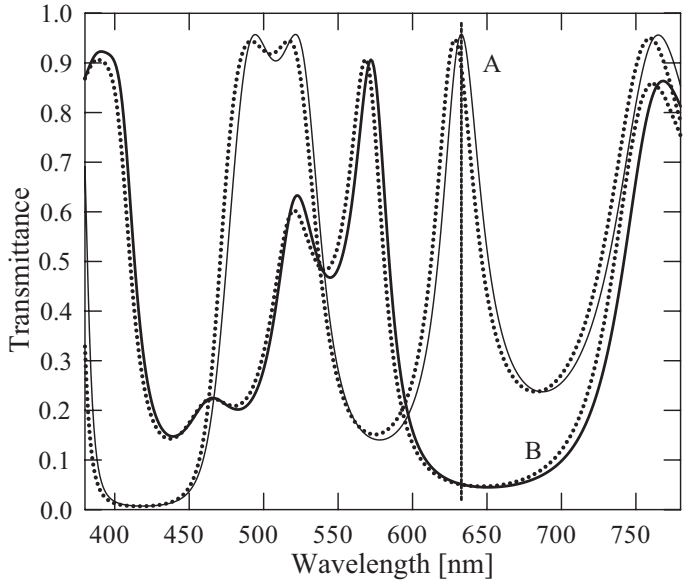

Figure 6.2 Transmission spectra of metameric filters A and B (solid lines) under illuminant D65 at normal incidence. The experimental curves are also shown (dotted lines). Take note of the high difference in transmission at 632.8 nm, the wavelength of a HeNe laser. $\Delta E^{\star}_{\mathrm{ab}}$ between both theoretical filters for several illuminants are : $\Delta E^{\star}_{\mathrm{ab,\ D65}} = 0.24$, $\Delta E^{\star}_{\mathrm{ab,\ A}} = 39.00$ and $\Delta E^{\star}_{\mathrm{ab,\ F1}} = 14.47$.

Another feature was also included in the design procedure of filters A and B, namely the high difference in transmission at 632.8 nm, the wavelength of a helium-neon laser (HeNe) laser. In fact, filter A transmits 95%, while filter B transmits 5%. This high difference in transmission could be beneficial in order to rapidly authenticate the device by using a laser. One can also imagine incorporating information in a way similar to a barcode by judiciously

Table 6.2 Design of filters A, B, C and D.

#	Material	Filter thickness [nm]			
		A	B	C	D
1	Ta_2O_5	65.61	73.74	44.16	15.09
2	SiO_2	151.61	117.61	75.47	131.82
3	Ta_2O_5	63.94	79.55	50.58	78.92
4	SiO_2	81.88	99.90	82.30	94.61
5	Ta_2O_5	56.87	75.09	67.33	72.89
6	SiO_2	63.40	139.43	47.63	119.73
7	Ta_2O_5	38.69	66.14	111.66	71.21
8	SiO_2	54.31	90.95	53.25	93.54
9	Ta_2O_5	50.52	61.30	58.03	66.92
10	SiO_2	66.54	76.34	145.25	99.76
11	Ta_2O_5	50.65	19.62	9.15	35.15
12	SiO_2	72.93	75.86	139.97	92.10
13	Ta_2O_5	56.34	61.16	41.05	84.58
14	SiO_2	81.03	90.70	199.33	-
15	Ta_2O_5	62.02	63.80	78.83	-
16	SiO_2	39.33	-	85.28	-
17	Ta_2O_5	24.65	-	76.02	-
18	SiO_2	84.07	-	118.01	-
19	Ta_2O_5	63.30	-	51.78	-
20	SiO_2	-	-	52.98	-
21	Ta_2O_5	-	-	5.20	-
	Total	1227.69	1191.19	1513.26	992.32

patterning both filters.

In order to choose an appropriate hidden image effect, one needs to perform a detailed color analysis. Once the filters are designed, their theoretical color variation can be calculated as a function of the observation angle : Figure 6.3 presents the color variation in the xy color space for both filters. Visibly, they start off at the same color coordinates, but as the angle of incidence is increased their color paths diverge. This was done expressly in order to maximize the color difference at oblique incidence. Filter A varies from green to purple, while filter B goes from green, to blue to finally purple. This difference in color is what permits the creation of an image that appears only at oblique incidence.

The high difference in transmission at normal incidence leads to a mismatch in color under other illuminants which differ from D65, such as illuminant A ($\Delta E^{\star}_{\mathrm{ab,\ A}} = 39.00$). Consequently, the hidden image effect would be lost in many lighting conditions as well as when observed by a color blind individual. This is usually seen as a drawback, however, if a color match is obtained for a highly specific light source, this could be used as a second level of verification by specialized personnel.

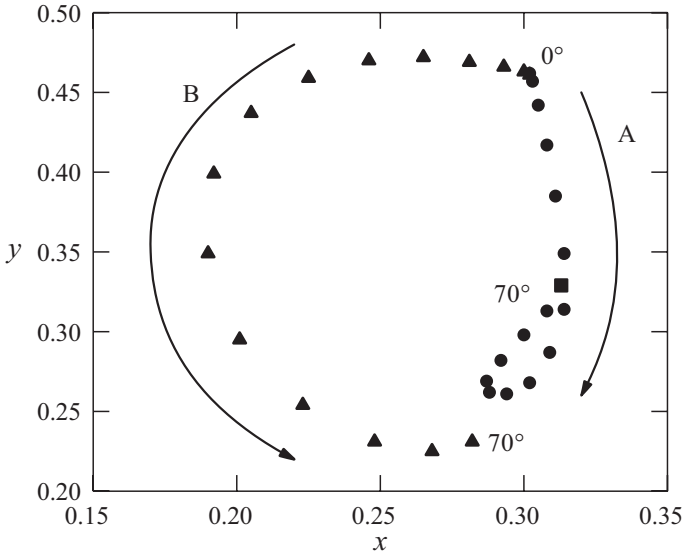

Figure 6.3 Color variation in the CIE xy color space of filters A (circles) and B (triangles) as a function of the observation angle (0° to 70°). The square represents the reference white. Calculations are done for the D65 illuminant.

Also shown in Figure 6.2 are the experimental spectra obtained for both filters A and B, which suffer from a slight shift towards shorter wavelengths due to thinner than desired layers. This has a direct effect on the color difference between these filters which is no longer satisfactory ($\Delta E^{\star}_{\mathrm{ab,\ D65}} = 15.51$). As a consequence, the filters no longer match in color when observed with the naked eye at normal incidence.

Following the previous results, our priority was to minimize the sensitivity to light sources and observers. In such a case, one may consider designing a pair of filters with almost identical spectra but with different color paths. While interesting, this solution would still lead to a very high number of layers and render the device too complex. Another option is the combination of a filter with a NIM. Figure 6.4 presents an all-dielectric filter (Filter C in Table 2) at normal incidence which has been optimized in order to match the transmission spectra of a purple colored paint by Pébéo. As can be seen, both spectra are very similar, which results in a color difference close to 1 under three very different illuminants (see Figure 6.4). As a consequence, both the filter and the NIM are indistinguishable in transmission at normal incidence. It must be added that many different NIMs were tested. Many were rejected simply because it was impossible to reproduce their color with a reasonable amount of layers or because the color variation shown by the interference filter was disappointing (for example, from yellow to white).

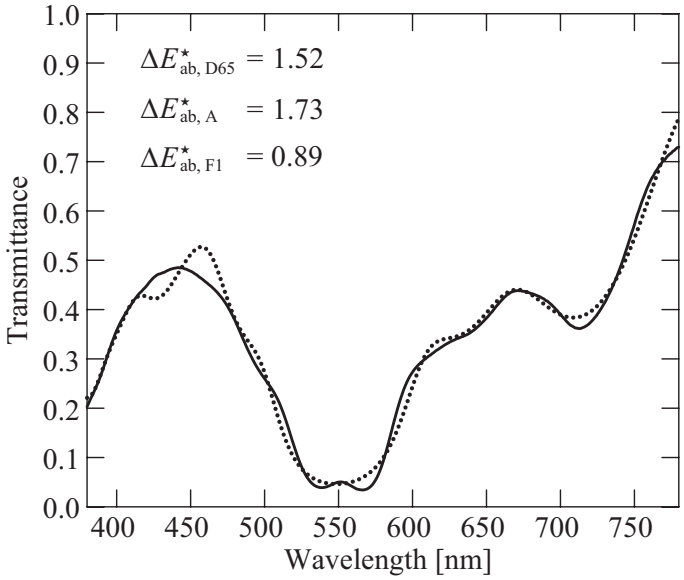

Figure 6.4 Comparison between the transmission spectra of a NIM (solid line) and interference filter C (dotted line). $\Delta E^{\star}_{ab}$ is also shown under different illuminants.

The number of layers may seem large, but in this case it was necessary in order to obtain a sufficiently low $\Delta E^{\star}_{ab}$ under the studied illuminants. A lower number of layers could be obtained by either diminishing the constraints on the $\Delta E^{\star}_{ab}$ threshold or by using a more simple NIM with less spectral features. One might even consider adjusting the NIM to a specific filter. More research and development is needed in this case.

Figure 6.5 presents the variation of color at 5 degree intervals in transmission and reflection for filter C. In transmission, the filter varies from purple to yellow. As is always the case for

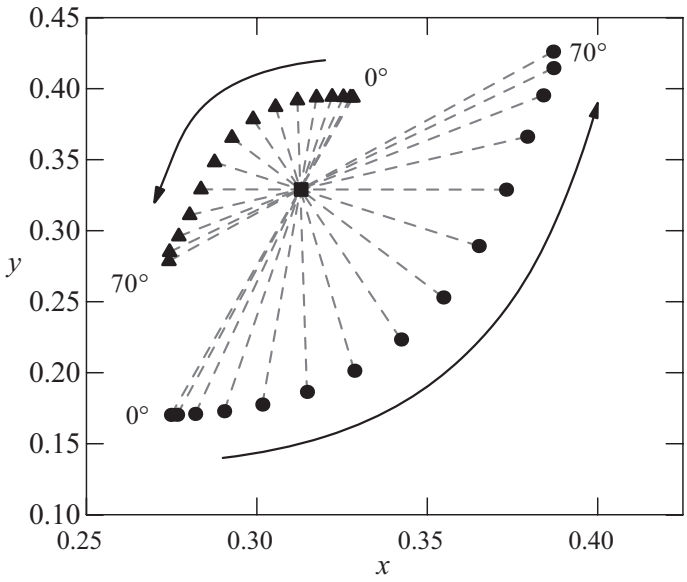

Figure 6.5 Color variation in the CIE xy color space of filter C as a function of the observation angle (0° to 70°). Circles represent transmission, triangles reflection, and the square is the reference white. Calculations are done for the D65 illuminant. The dashed lines connect complementary colors.

all-dielectric filters where absorption is negligible, the color obtained in reflection corresponds to the complementary color of that obtained in transmission. This is demonstrated by the fact that all line connections between a reflection and transmission color at a specific angle pass through the reference white (see Figure 6.5). Filter C consequently varies from a greenish yellow to a light violet color in reflection.

Finally, at non-normal incidence the filter's spectrum is shifted towards shorter wavelengths and large spectral variations are obtained at specific wavelengths. This feature can therefore possibly be used to automate the authenticity verification by scanning the device with a laser.

The devices described above were designed to be used in transmission. Although this makes the verification of its authenticity very simple, many applications do not offer a transparent medium onto which the device can be affixed. We now present a metameric pair between a filter and a specularly reflective NIM which can be used in reflection. In this case, the filter's reflectance spectrum was tailored in order to match that of gold. The optical properties of gold were obtained from ref. [40]. Figure 6.6 shows the reflectance of designed filter D on c-Si, and Table 2 also presents the individual layer thicknesses. A very large difference between the reflection spectra of gold and of the filter is observed at wavelengths higher than 650 nm. This has little effect on $\Delta E^{\star}_{\mathrm{ab}}$ since the sensitivity of the human eye is very low

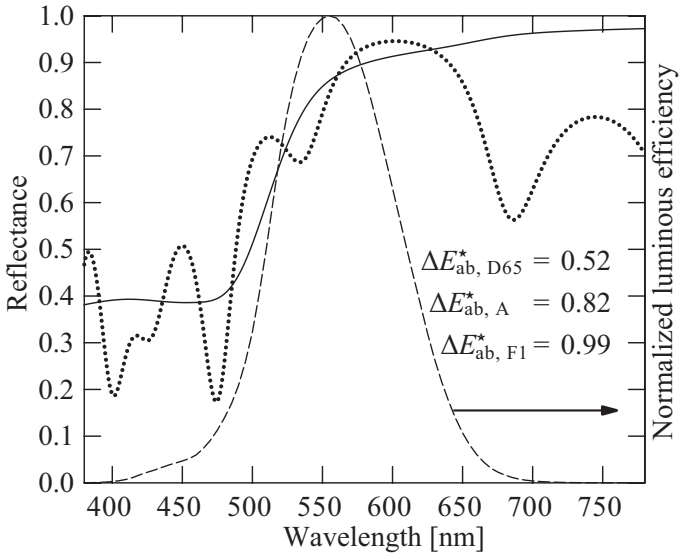

Figure 6.6 Comparison of the reflection spectra between gold (solid line) and filter D (dotted line). The dashed line represents the photopic luminous efficiency curve of the average human eye. $\Delta E^{\star}_{ab}$ is also shown under different illuminants.

in that region, especially for values over 700 nm (see photopic luminous efficiency in Figure 6.6). When designing filters, it is important to keep this fact in mind in order to eventually diminish the total number of layers necessary to obtain a good color match, while still not compromising the effect for observers with a defective color vision.

The color of filter D varies from gold to green, much like the variation of color seen on the Canadian banknote ISIS. Once again, a hidden image effect can be obtained if both the filter and NIM are patterned.

6.5.2 Analysis of the effect of deposition errors

The shift as a function of wavelength observed in the deposited filters brings up the issue of the sensitivity of the designs to deposition errors. Indeed, if one wants to obtain a color match at normal incidence, a more precise control on the layer thickness is needed, such as by using broadband optical monitoring. This consequently makes fabrication of the device more complex. We have therefore studied the effect of deposition errors on the color of our filters. Using the *OpenFilters* software, we varied the thickness of the SiO_2 and Ta_2O_5 layers between 99% and 101% of their nominal values, and generated 441 transmission spectra. We suppose that our process is stable for a reasonable amount of time and that the deposition errors on every layer of the same material are correlated and simply due to inaccuracy of the deposition rate. Multiple filters deposited under the same conditions and with the same

design showed nearly identical spectra. The different filters that are presented in this article were deposited over a long period of time over which the deposition rates changed which explains why the spectra are not always shifted in the same direction. Figure 6.7 shows the results of our calculations for filters A and B (part a) and also for filter C (part b). As can be seen, there is a central region for which $\Delta E^{\star}_{\text{ab, D65}} \leq 2$ is obtained. The width of this region depends on the sensitivity of the designed filter or device.

Since both filters A and B suffer from slight deposition errors, this results in a very small region for which a color match could be obtained. Only 25 (5.7%) out of the 441 generated filters have a value of $\Delta E^{\star}_{\text{ab, D65}} \leq 1$ and 61 (13.8%) a $\Delta E^{\star}_{\text{ab, D65}} \leq 2$. For filter C, these values are, respectively, 31.1% and 59.6% which is a significantly increased yield compared to the previous results ; hence, this type of device is less sensitive to deposition errors.

Using the $\Delta E^{\star}_{\text{ab, D65}}$ value obtained between filters A and B ($\Delta E^{\star}_{\text{ab, D65}} = 15.51$), we can conclude from Figure 6.7, that the error on each of the layers is around 0.6%. For filter C, $\Delta E^{\star}_{\text{ab, D65}}$ being equal to 8.08, we obtain a more than 1% error on each of the layers of the filter indicating that our calibration of the deposition rates was less accurate. It should be noted, on both figures, that there is a clear sign of a compensation phenomenon taking place ; in fact, thicker layers of SiO_2 can be compensated by thinner layers of Ta_2O_5 in order to obtain an appropriate color and vice versa. One could imagine exploiting this observation if monitoring was used during deposition.

This brings up the issue of the fabrication feasibility of such devices in large quantities. The combination of filters A and B exhibiting a very high sensitivity to deposition errors would consequently be costly to fabricate. This is another reason why we developed the metameric filter-NIM pair devices. Indeed, due to the presence of a reference color, which should be almost invariable, one only needs to control the color of the filter very precisely. In fact, when comparing present devices on the market, small variations of color can be observed from one to another. Since there is no reference color, only the color shift is important. This is not the case for the present devices. One way to facilitate fabrication would be "off-angle" metamerism. If the metameric pair is designed to match at an angle of 45°, a slight shift of the spectral properties would not cause much of a difference since metamerism would still occur near that angle. On the other hand, the device would be rendered less attractive. We now present our results on the filter-NIM pairs.

6.5.3 Fabrication of non-iridescent material devices

As we have now demonstrated, lower sensitivity to deposition errors of the filter-NIM pair makes this type of device highly interesting. In the following, we describe two approaches.

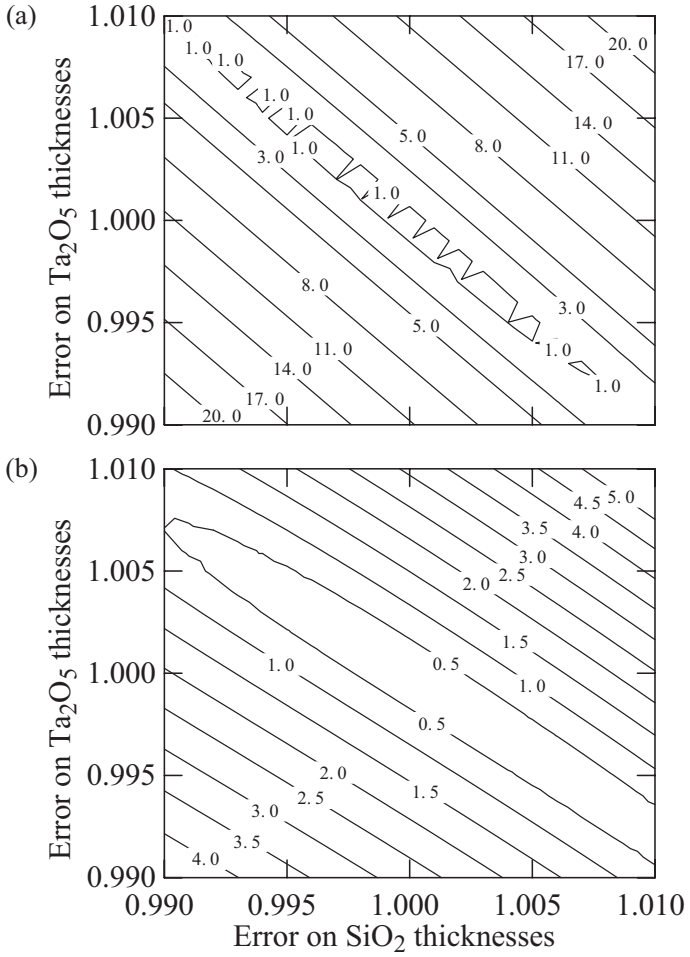

Figure 6.7 $\Delta E^{\star}_{\text{ab, D65}}$ as a function of deposition error between (a) simulated filters A and B and (b) filter C and its initial design. The (1.000, 1.000) coordinates correspond to the original filters.

Device based on transmission

The present device is based on the combination of filter C with a transparent NIM. Once the NIM is spin coated, we proceed to the creation of a specific image using a mask during plasma etching. This is done in order to add visual impact and make the device more aesthetically pleasing. It must be added, that the complementary color also makes the filter appear metallic-like, while the NIM remains matt and of the same color when seen in reflection. This creates a surprising effect when the device is seen in transmission due to the fact that it is uniform in color at normal incidence in transmission.

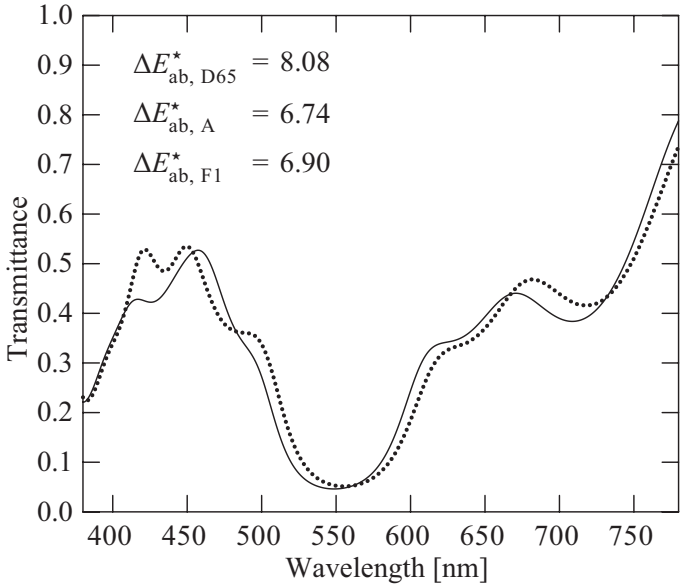

Figure 6.8 Comparison between the transmission spectra of filter design C (solid line) and the deposited interference filter (dotted line). $\Delta E^{\star}_{\text{ab}}$ is also shown under different illuminants.

As shown in Figure 6.8, the experimental transmission spectrum is shifted towards the red part of the spectrum, indicating that the layers are slightly thicker than predicted. As a result, the filter and the NIM do not match in color at normal incidence ($\Delta E^{\star}_{\text{ab, D65}} = 7.79$), but become so at close-to-normal incidence due to the characteristic shift towards the blue part of the spectrum of the ISIS. It is important to note that the filter and the NIM would never be metameric if the layers were thinner than predicted.

Figure 6.9 presents photographs of the final model device taken at different angles. As can be seen at near normal incidence, the NIM (circle) matches in color with the interference filter. As the angle is increased, the filter begins to shift from purple to yellow as was predicted by the initial design. Another interesting element was added in this case : The device, which represents the logo of Polytechnique's technology transfer firm Univalor, matches not only

in shape but is also very close in color to the original logo at non-normal incidence. This color resemblance also helps the user to identify the authenticity of the device by recalling a familiar image. Finally, one can imagine creating a high resolution image consisting of small

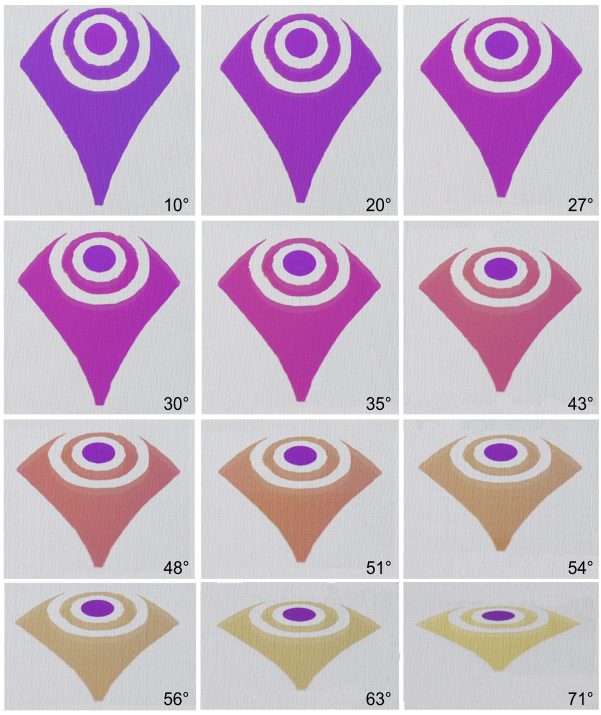

Figure 6.9 (Color online) Transmission device observed at different angles of incidence (approximate). Notice that due to the initial spectral mismatch, the color match occurs around 20°. Colors may vary due to display and printing limitations.

pixels of NIM and of an interference filter. In this case, the device would be uniform in color at normal incidence and a hidden image would appear at oblique incidence.

Device based on reflection

Finally, Figure 6.10 presents the transmission spectra at normal incidence of the deposited filter and of the designed filter D on B270 glass which was prepared simultaneously with the c-Si sample. Since a transmission measurement is simpler than a reflection measurement (reflection measurement is limited to an angle of 8°), and assuming that the filters on B270 glass and Si are identical, we can obtain reliable information on the accuracy of the deposited filter. Very good agreement is obtained between both curves and, consequently, a very low $\Delta E^{\star}_{\mathrm{ab}}$ is obtained for all illuminants as illustrated in Figure 6.10. When visually compared to a gold sample, the color match is highly convincing.

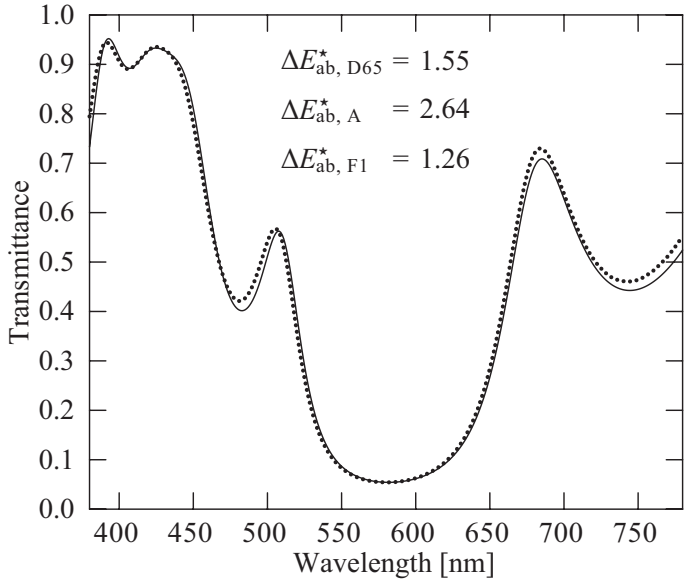

Figure 6.10 Comparison of the transmission spectra between filter design D (solid line) and the deposited filter (dotted line). $\Delta E^{\star}_{ab}$ is also shown under different illuminants.

6.6 Conclusion

We have demonstrated new ISIS devices based on metamerism that can be used in transmission or in reflection and that offer augmented security protection due to an increased fabrication complexity and ease of authentication. The use of a pair of metameric filters providing two distinct color shifts as well as a hidden image at normal incidence under a specific light source is interesting for use on high value documents and products. For a more affordable device, one of the filters may be replaced by a non-iridescent material. This material having a predefined color in reflection or transmission serves as a reference ; the user therefore knows what color to expect. The fabrication is consequently more complex due to a more stringent process control. Also, the spectral color match assures a higher color stability under different light sources and observers. Finally, creating a pattern of a known image adds to the complexity and visual appearance of the device. Ongoing work now focuses on developing devices containing metallic layers, depositing onto polymer substrates, as well as optimizing the mechanical properties in order to increase their durability.

6.7 Acknowledgments

Bill Baloukas wishes to acknowledge the FQRNT and NSERC for their financial support. We also thank Mr. F. Turcot for his expert technical assistance and Dr. O. Zabeida for valuable comments. The authors also acknowledge Dr. J.A. Dobrowolski, NRC-Ottawa, for

very stimulating discussions. This work was supported by the NSERC Canada Strategic grant as well as the Université de Montréal Valorisation de l'innovation et du capital intellectuel (VINCI) program.

CHAPTER 7

ACTIVE METAMERIC SECURITY DEVICES USING AN ELECTROCHROMIC MATERIAL

7.1 Foreword

In the previous paper, I presented examples of transmission or reflection based metameric devices. The anticounterfeiting properties of theses devices were provided by the presence of a color reference for the interference filter and by their angle-dependent color variation. The possibility of creating a hidden image effect was also mentioned as an additional level of complexity. Following the development of these devices and having discussed with the Bank of Canada, we decided to explore a new avenue : active materials. The goal of this research was therefore to develop a new category of devices which would possess two levels of authentication : one passive and the other active. Having gained considerable experience with ISIS devices, we thus decided to preserve the angle-dependent color shift as the passive authentication component.

As for the active component, we had to choose an appropriate category of materials. Indeed, there exists a wide variety of active materials (see Chapter 4) each of them responsive to a different type of external source of energy (heat, light, voltage, pressure, etc.). Looking closely at the available options, we realized that electrochromic materials had the highest potential of being used in future security devices for many reasons[i]. Firstly, by applying a fairly low voltage, the user would have complete control over the change in color of the device. Secondly, the device structure's complexity would protect from reorigination. Last but not least, from the point of view of feasibility, we new that inorganic electrochromic materials such as WO_3 had been extensively studied and their use demonstrated in other applications such as smart windows [212]. It is for these main reasons, that we decided to explore electrochromic-based optical security devices.

Having chosen EC devices (ECDs), our attention was immediately drawn to WO_3, the most popular inorganic EC material. My initial work was therefore focused on depositing and characterizing WO_3 films. Following the optimization of these films, I then spent a significant amount of time in incorporating them into a functional ECD.

Although in itself, an ECD represents a potentially interesting second-level authentication

i. The other energy sources possessed disadvantages which, from our point of view, disqualified them for potential security devices (see Chapter 4 for more details).

feature, in the present paper we propose an innovative pairing between an ECD and an ISIS through metamerism. This pairing ties in both features into a single device and also increases its complexity. In fact, the result is a security feature that presents an angle dependent color shift, a voltage-driven color shift as well as a disappearing image effect.

7.1.1 Absence of photos of our device

The following addresses the fact that no pictures of an actual device were included in the present article. While I do agree that a picture of the combined ISIS and EC device would have been valuable, no pictures were presented simply due to the fact that both elements (ISIS and EC) were not on the same substrate. It was consequently very hard to compare them.

Although we did not show a picture of the ECD, both elements were characterized and designed in such a fashion that a metameric match is possible and was clearly demonstrated. Therefore, the concept of an active metameric device was established. It is following these encouraging results that we decided to propose a structure such as the one presented in Figure 7.2. We are able to make these assertions, since we applied the same design methodology presented in Chapter 6 which resulted in a functional metameric device.

Incidentally, we did try filming the ECD and ISIS devices side-by-side but the obtained color match was not to our satisfaction. We explain this slight color difference by the following considerations :

- The fact that the camera “sees” differently than the human eye (transmission versus reflection of the interference filter, white balance, lighting issues, etc.).
- The size of both objects (large visual angles have an effect on color perception).
- The fact that, although our ECD is clearly functioning and on the right track, we noted a faster than desired degradation (mainly due to the fragility of the top Au electrode) which inevitably affected the color matching properties of our final device.

The following figure shows a picture extracted from a video taken during the coloration of the ECD. One can see that although the color match is not perfect, it is still fairly close.

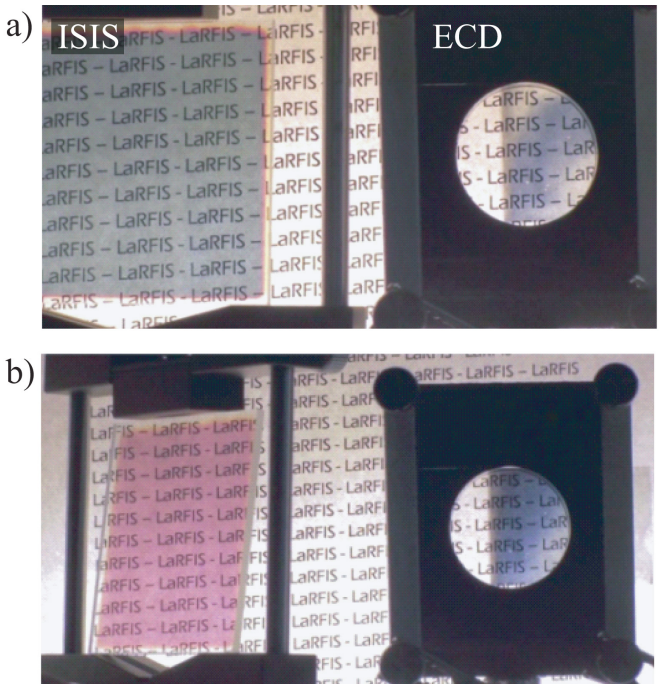

Figure 7.1 Picture of the metameric filter and ECD extracted from a video taken during the coloration phase. In a) one can see the color match between both elements and in b) the angle-dependent color variation of the ISIS. Note that the uncolored region of the ECD corresponds to the ITO electrode.

ARTICLE 2 : ACTIVE METAMERIC SECURITY DEVICES USING AN ELECTROCHROMIC MATERIAL

Bill Baloukas, Jean-Michel Lamarre and Ludvik Martinu

Department of Engineering Physics, École Polytechnique de Montréal,
P.O. Box 6079, succursale Centre-ville, Montréal, Québec H3C 3A7, Canada

Applied Optics, vol. 50, no. 9, 2011, p. C41-C49.

Abstract

In order to increase the anti-counterfeiting performance of interference security image structures, we propose to implement an active component using an electrochromic material. This novel device, based on metamerism, offers the possibility of creating various surprising optical effects, it is more challenging to duplicate due to its complexity, and it adds a second level of authentification. By designing optical filters that match the bleached and the colored states of the electrochromic device, one can obtain two hidden images, one appearing when the device is tilted, and the other one disappearing when the device is colored under an applied potential. Specifically, we present an example of a filter which is metameric with the colored state of the electrochromic device, demonstrate how the dynamic nature of the device offers more fabrication flexibility, and discuss its performance. We also describe a design methodology for metameric filters based on the luminous efficiency curve of the human eye : this approach results in filters with a lower number of layers and hence lower fabrication costs, and with a lower color difference sensitivity under various illuminants and for non standard observers.

7.2 Introduction

Counterfeiting costs the G20 countries more than 100 billion euros per year [20]. In the never-ending race against counterfeiters, governments and institutions have, until now, maintained a suitable lead by wielding technology to their advantage ; in this respect, the currency industry is an excellent example. For instance, various optical security features [43] such as holograms, interference security image structures (ISISs) [33], watermarks and micro printing [256] have been in circulation for many years. As a result, one of the most important efforts has been to "educate" the general public to detect false bills and/or documents.

Holograms and ISISs are part of a specific category of devices termed iridescent, meaning that their appearance is dependent on the angle under which they are observed. This color change as a function of the observation angle inhibits reproduction by most reprographic techniques such as printing, scanning, etc. This optical effect has also proven to be a highly efficient means of detection by the general public [2]. Unfortunately, iridescent consumer products are now also readily available, and may render basic interference-based devices obsolete. For this reason, various solutions have been proposed, such as combining ISIS devices with holographic elements [74], magnetic elements [73], etc. Another solution has been presented in our previous paper, in terms of metameric ISISs [254].

As defined by the Commission Internationale de l'Éclairage (CIE) [262], two objects which display the same color under a specific illuminant and for a specific observer are termed metameric if their reflection or transmission spectra differ in the visible spectrum. Devices based on metamerism offer a higher performance and an extra level of security which can hence prolong the life cycle of ISISs. In fact, by matching the color at normal incidence of an interference filter with the color of a non-iridescent material (NIM), a hidden image, which only appears as the angle of observation is increased, can be fashioned [254]. The NIM also offers the advantage of serving as a color reference making detection much easier including for observers with color vision deficiencies.

In the present work, we propose to go one step further by combining an EC device [114], whose color can be changed by applying a potential, with a metameric ISIS. Contrary to most present-day passive devices, this novel combination will lead to the addition of an active mode of authentification, i.e. an external source of energy is required in order to change the appearance of the device.

The most popular inorganic material [115] is tungsten oxide, WO_3. First developed for electrochromic (EC) applications by Deb in 1969 [204], WO_3 has been the material of choice for most current and future applications due to its high coloration efficiency. A simplified representation of the EC reaction in WO_3 is given by :

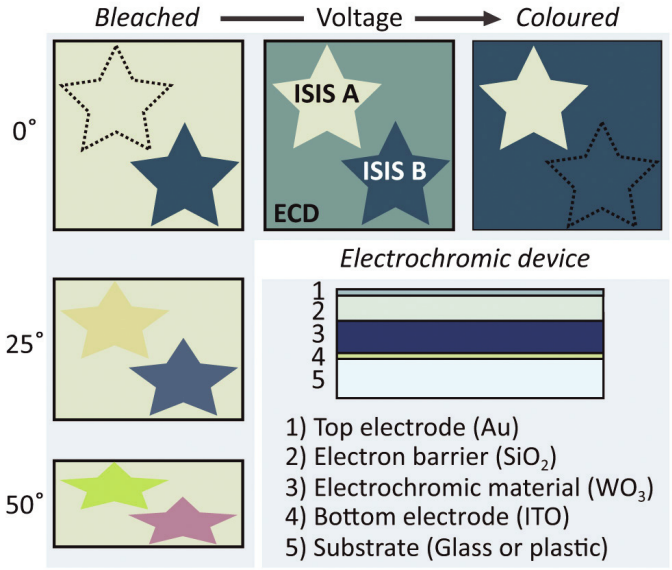

Figure 7.2 (Color online) Conceptual example combining ISISs with an ECD. ISIS A is metameric with the bleached state of the active device and is therefore invisible at normal incidence (dashed star). ISIS B is metameric with the colored state of the electrochromic device (ECD) and consequently becomes invisible during coloration. When the whole device is tilted, both ISISs change color while the rest of the device essentially remains the same. The layered structure of our ECD is also shown.

$$WO_3 + xM^+ + xe^- \leftrightarrow M_xWO_3,$$

where e^- is an electron, and M^+ is a cation such as H^+, Li^+, etc. In the as deposited state, WO_3 is a high index of refraction transparent material; however, following insertion of ion-electron pairs, it develops a dark blue and opaque color. This coloration is due to a very wide absorption band, centered at approximately 1000 nm in amorphous WO_3 [264], which essentially absorbs most of the light of the visible spectrum except for the blue region.

An interesting property of EC materials is that their color is maintained after the removal of the applied potential (memory effect). The material can then be bleached and brought back to its initial state by applying an inverted voltage. These specific properties have made EC materials likely candidates in a multitude of applications such as variable reflectivity mirrors [265], smart windows [266], variable emissivity coatings [240], electronic ink [267], etc. For these reasons, we believe that EC materials are favorable candidates for future active security devices.

In the present work, we study the combination of a metameric interference filter with the colored state of an electrochromic device (ISIS B in Fig. 7.2) based on a structure proposed by Deb *et al.* (see Fig. 7.2) [183]. We present the design, fabrication and characterization of the EC device and of the metameric filter. Finally, our methodology for designing metameric filters, crucial to ensure device performance and minimal fabrication costs, will be presented.

7.3 Concept of the EC/ISIS device

An active device offers the opportunity of having two levels of inspection [256]. In this case, ISIS A (see Fig. 7.2) is matched in color with the bleached state of the EC device and thus invisible at normal incidence, while ISIS B (see Fig. 7.2) matches the colored state. Consequently, simply by changing the observation angle, ISIS A can be made to appear, while the EC stack serves as a color reference at normal incidence. This surprising hidden image effect was presented in our previous paper [254]. ISIS B also offers a color shift as a function of the observation angle, but disappears when the EC material is colored. The latter effect would be especially useful for cashiers, bank tellers or anyone having to deal with money on an everyday basis.

7.4 Experimental methodology

7.4.1 Film and device fabrication

The ECD (see Fig. 7.2) were deposited on 2.5 cm by 5 cm ITO coated glass substrates with an average sheet resistance of 50 $\Omega/\square$. Part of the substrate was masked during deposition to

allow access to the ITO electrode for cyclic voltammetry measurements and device testing. All ITO substrates were first cleaned with soap and washed with de-ionized water, and then immersed in isopropanol for 15 min. in an ultrasonic bath. For optical characterization, individual coatings were deposited on B270 glass and Si substrates.

The complete devices were deposited by radio frequency magnetron sputtering in a custom made vacuum chamber equipped with three magnetrons fitted with WO_3, Si and Au targets. The base pressure was approximately $2.5x10^{-6}$ Torr. The deposition conditions as well as the thicknesses of each of the coatings are given in Table 7.1.

Table 7.1 Deposition parameters and thicknesses of the individual electrochromic device layers.

Coating	**Pressure**	**Ar**	**O_2**	**Power**	**Thickness**
-	[mTorr]	[sccm]	[sccm]	[W]	[nm]
WO_3	40	20	5	150	$\simeq$250
SiO_2	7	25	10	200	$\simeq$150
Au	15	20	-	75	$\simeq$8

The interference filters (SiO_2 and Nb_2O_5 layers), designed using the *OpenFilters* software [68], were deposited using a *Spector II* dual ion beam sputtering system (manufactured by Veeco-Ion Tech) equipped with two Kaufman gridded ion sources. The primary 16 cm ion source was used to sputter from one of the two 35 cm diameter targets respectively made of SiO_2 and Nb. The secondary 12 cm ion source was used to simultaneously bombard the growing films to increase the density of the deposited layers [246]. For more details on the deposition conditions, see our previous papers [254, 268].

7.4.2 Electrochromic characterization

In order to characterize the EC properties of the WO_3 coatings, cyclic voltammetry measurements were performed using an *Autolab PGSTAT302N* potentiostat/galvanostat with a 1 M H_2SO_4-distilled water solution. An ITO substrate coated with WO_3 and with an exposed surface of 0.75 cm^2, a Pt foil, and a saturated Calomel Electrode (SCE) were used as the working, counter and reference electrodes, respectively. The measurement cell containing the acid solution was equipped with two windows allowing one to monitor the optical transmission spectra. The first window consists of the sample under evaluation, while the second window is made out of glass. The cyclic voltammetry measurements were preceded by 10 activation cycles done at a 50 mV/s scan rate between -0.6 V and 0.6 V. Following these cycles, 5 measurement cycles at varying scan rates (100 mV/s, 50 mV/s, 25 mV/s, 10

mV/s and 5 mV/s) were performed. In the case of the ECDs, the cycling was done using a programmable voltage source (*Keithley SourceMeter Model 2410*). A -3 V potential was applied for 30 seconds in order to color the device, and a 30 second +3 V potential in order to bleach it.

In situ transmission measurements were performed during cyclic voltammetry and device testing in order to calculate the coloration efficiency. The setup consists of a stabilized deuterium tungsten halogen light source from Ocean Optics (*DH-2000*) equipped with an optical fiber outlet. A series of lenses were used in order to focus the beam onto the device and collect the transmitted beam into a second optical fiber connected to an Ocean Optics spectrophotometer (*USB2000*). This setup allowed us to measure a complete spectrum from 380 nm to 850 nm approximately every 500 ms (30 averaged measurements of 3 ms plus signal treatment time).

7.4.3 Optical characterization

Variable angle spectroscopic ellipsometry (*VASE*, J.A Woollam Inc.) combined with transmission measurements using a Perkin Elmer *Lambda 19* spectrophotometer were used to obtain the optical properties (refractive index and extinction coefficient), as well as the thickness of all deposited materials. The data were analyzed with the *WVASE 32* software (J.A Woollam Inc.). Figure 7.3 presents the optical properties of the deposited SiO_2 ($n_{550\,nm} = 1.45$) and WO_3 coatings ($n_{550\,nm} = 2.04$). The extinction coefficient of SiO_2 is negligible for the presented wavelengths. This is also the case for the WO_3 coatings for wavelengths above 380 nm.

Quantifying the color of the ECDs and interference filters is very important in the case of security devices. Color calculations are performed in the xyY color space and in the case of color differences in the $L^\star a^\star b^\star$ color space. The color difference between object 1 and object 2 is given by :

$$\Delta E^\star_{\mathrm{ab,\,I}} = \left[(L^\star_2 - L^\star_1)^2 + (a^\star_2 - a^\star_1)^2 + (b^\star_2 - b^\star_1)^2\right]^{1/2}, \tag{7.1}$$

where $L^\star_{\mathrm{i}}$, $a^\star_{\mathrm{i}}$, $b^\star_{\mathrm{i}}$ are, respectively, the lightness, and color-opponent dimensions of object i. I indicates the illuminant under which the color difference is calculated. It is accepted that no color difference between two objects is discernable for values of $\Delta E^\star_{\mathrm{ab}} \leq 1$ [15]. In practice higher $\Delta E^\star_{\mathrm{ab}}$ values will occur. For this reason, although very slight color differences can be observed for values of $\Delta E^\star_{\mathrm{ab}} \geq 2$, we will consider $\Delta E^\star_{\mathrm{ab}} \leq 4$ as acceptable. In fact, the most effective way to define a precise color matching threshold is to proceed to real-life testing under specific lighting conditions and with a variety of different observers.

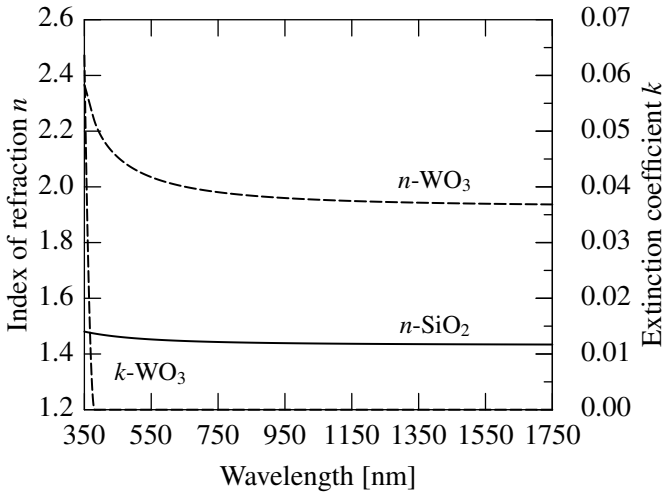

Figure 7.3 Dispersion curves of the as-deposited SiO_2 (solid curve) and WO_3 (dashed curve) coatings.

Colors will be defined under the following CIE standard illuminants which represent possible environments under which a device may be inspected : D65 (average daylight with a correlated color temperature of 6504 K), A (incandescent lighting) and F1 (fluorescent lighting).

7.5 Results and discussion

7.5.1 Cyclic voltammetry and *in situ* transmission

The results of the WO_3 coating characterization by cyclic voltammetry are presented in Figure 7.4 ; the characteristic "duck" shape obtained for WO_3 films can be clearly seen.

From the peak current (i_{p}) during the bleaching phase, one can calculate the diffusion coefficient D_i (cm^2/s) using the Randles-Sevčik equation [114] :

$$i_p = 0.4463 n_e F A c_s \sqrt{\frac{n_e F v D_i}{RT}}, \tag{7.2}$$

where n_e is the number of electrons taking part in the reaction, F is the Faraday constant (C/mol), A the working electrode area (cm^2), c_s the solution concentration ($\mathrm{mol/cm}^3$), v the scan rate (V/s), R the universal gas constant ($\mathrm{J/mol \cdot K}$) and T the ambient temperature (K). Based on the observations of Lefteriotis *et al.* [269], the lowest diffusion coefficient obtained from the 5 mV/s cyclic voltammogram, in our case $D_i = 7.6\mathrm{x}10^{-11}$ cm^2/s, is probably the best estimate. This result is comparable to values obtained by other authors [116].

In order to compare the performance of various coatings, it is useful to calculate the

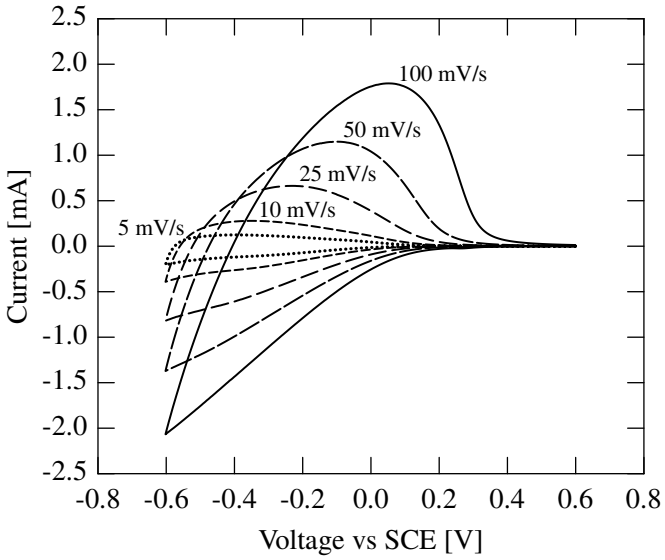

Figure 7.4 Cyclic voltammograms of the WO_3 coating at different scan rates (5 mV/s, 10 mV/s, 25 mV/s, 50 mV/s and 100 mV/s).

coloration efficiency (CE) which is directly related to the microstructure of the deposited material [115]. The CE (cm^2/C) is given by :

$$\mathrm{CE} = \frac{ln[T_b/T_c]}{[Q/A]}, \tag{7.3}$$

where T_b is the optical transmission in the bleached state, T_c the optical transmission in the colored state, and Q (C) the inserted charge. Figure 7.5 presents the optical transmission obtained in the darkest colored state (100% transmission corresponds to the bleached state) during the 50 mV/s cyclic voltammetry measurement, and the resulting CE. The value of CE = 75 cm^2/C at 550 nm is similar to that obtained by Subrahmanyam *et al.* [270].

In the following, these characteristics will be used to assess the performance of the device, while further optimization could be performed in the future.

7.5.2 Electrochromic device

Following characterization of the individual layers, we fabricated the complete ECD. It is composed of an ITO-covered glass substrate, a WO_3 layer, a SiO_2 layer and a final Au layer used as an electrode (see Fig. 7.2 and Table 7.1 for the individual thicknesses of the coatings). All three layers were prepared without breaking the vacuum. This is very important, since the applied voltage necessary to switch the device is highly sensitive to the quality of the top and bottom electrodes. Figure 7.6 shows the variation of the transmission spectrum

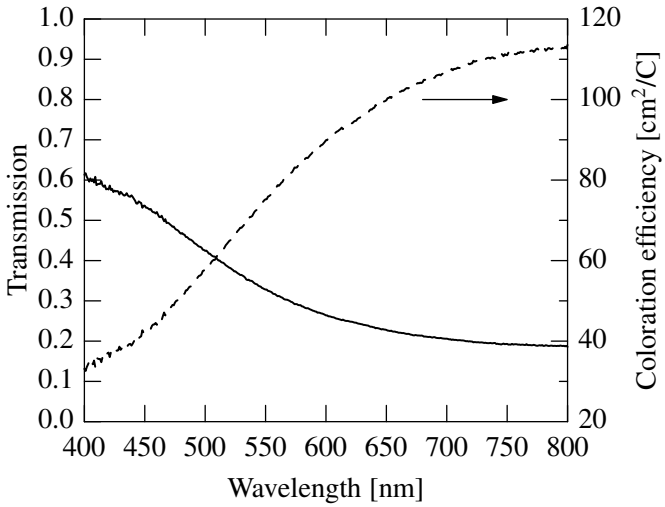

Figure 7.5 Transmission obtained in the darkest colored state for the 50 mV/s cyclic voltammetry measurement and corresponding coloration efficiency (dashed curve).

of the device as a function of time when a -3 V potential is applied for 30 seconds. The characteristic variation of the WO_3 layer can be clearly seen, the maximum absorption being located in the near infrared (outside our spectrophotometer's measuring range). Also note that the interference oscillations present in the bleached state disappear after approximately 10 seconds of coloration due to the high absorption in the WO_3 layer. It is also important to add that contrary to most EC systems, the present device does not contain an ion storage layer. While this simplifies fabrication, it makes the device functionality dependent on the ambient humidity, its ion source being the hydrogen in the water molecules absorbed in the SiO_2 layer [131, 115].

To demonstrate the functionality of the device, Figure 7.7 presents the variation of the luminance (Y_T coordinate in the xyY color space) in transmission for five coloration and bleaching cycles. The results confirm that the bleached state is recovered rapidly and completely. One also notes that the device hasn't reached its maximum coloration after 30 seconds; a lower transmission is consequently attainable.

7.5.3 Metameric filter

First level of authentification

Having characterized the active system, we chose to design a filter which is metameric with the 20 second transmission spectrum presented in Figure 7.6 (as ISIS B in Fig. 7.2). In this specific application where a document may be verified several times a day over a period of

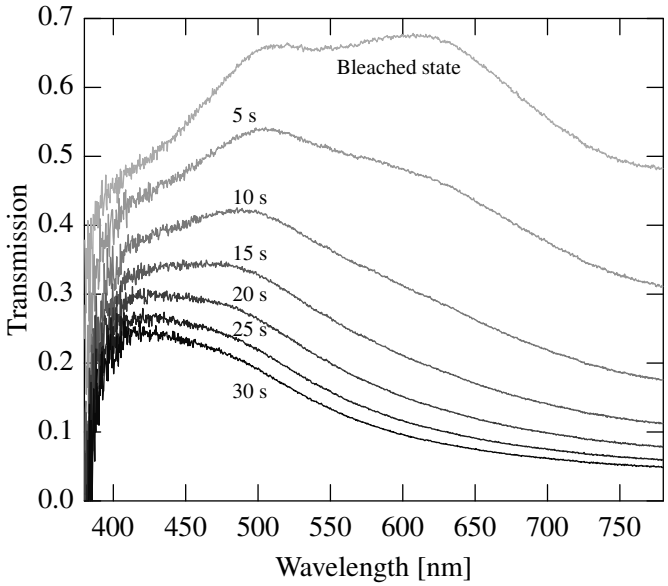

Figure 7.6 Variation of the transmission spectrum of the electrochromic device for an applied voltage of -3 V for up to 30 seconds.

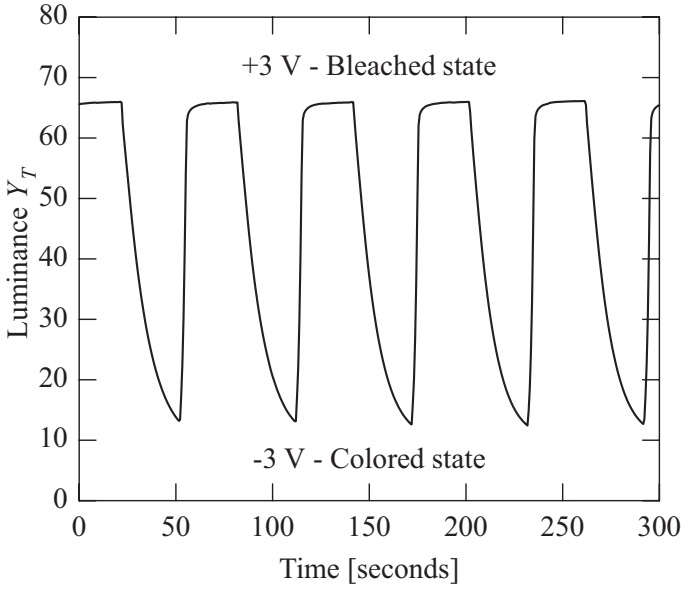

Figure 7.7 Luminance variation in transmission for five coloration and bleaching cycles of the ECD. Higher luminance values correspond to a higher transmission.

several years, thousands of cycles can be expected and consequently the lowest transmission state for a specified coloration time can be affected due to degradation. To increase the potential lifetime of the device, the most colored state wasn't used as a color reference. Also note that a lower coloration time can be selected, but it is important to ensure a sufficiently convincing color variation between the bleached and the colored states.

The resulting metameric filter matching the colored state of the device consists of 13 layers of SiO_2 ($n_{550\,nm} = 1.49$) and Nb_2O_5 ($n_{550\,nm} = 2.28$) whose thicknesses are given in Table 7.2. More details on the design methodology will be given in section 7.5.4. Figure 7.8 presents the transmission spectrum of the designed filter as well as the color difference with respect to the target spectrum. Values of $\Delta E^{\star}_{\text{ab}} \leq 1$ are obtained for illuminants D65, A and F1.

Table 7.2 Design of the metameric filter.

#	**Material**	**Thickness** [nm]	#	**Material**	**Thickness** [nm]
1	Nb_2O_5	19.9	8	SiO_2	97.8
2	SiO_2	88.9	9	Nb_2O_5	66.4
3	Nb_2O_5	48.8	10	SiO_2	104.3
4	SiO_2	46.0	11	Nb_2O_5	60.5
5	Nb_2O_5	45.2	12	SiO_2	88.6
6	SiO_2	89.9	13	Nb_2O_5	97.9
7	Nb_2O_5	58.6			

To visualize the performance of the metameric filter and ECD, Figure 7.9 presents their respective color variations in the xyY color space. At normal incidence both the active component and the filter show the same color at the 20 second coloration mark, but as the observation angle is increased, the filter's color varies from blue to light red. This color variation is the basis of the current passive ISISs.

Finally, the transmission spectrum of the fabricated filter is also presented in Figure 7.8 (dotted curve). Since only time was used to control the thicknesses of the individual layers, slight transmission variations are expected and observed. We will give examples of the filter's performance in the next section.

Second level of authentification

The dynamic nature of the ECD invites one to calculate the variation of the color difference as a function of time during the coloration and the bleaching cycles. Figure 7.10 presents $\Delta E^{\star}_{\text{ab, D65}}$ at four angles of observation of the interference filter (the color variation of the

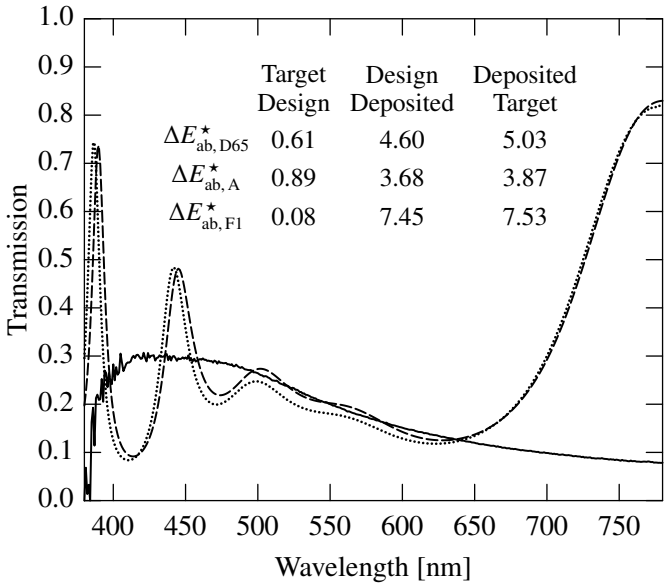

Figure 7.8 Transmission spectra of the targets (solid curve - WO_3 20 seconds coloration state), the designed filter (dashed curve) and the deposited filter (dotted curve). Also included are the $\Delta E^{\star}_{ab}$ values under different illuminants between the target and the design, the design and the deposited filter, and the deposited filter and the target.

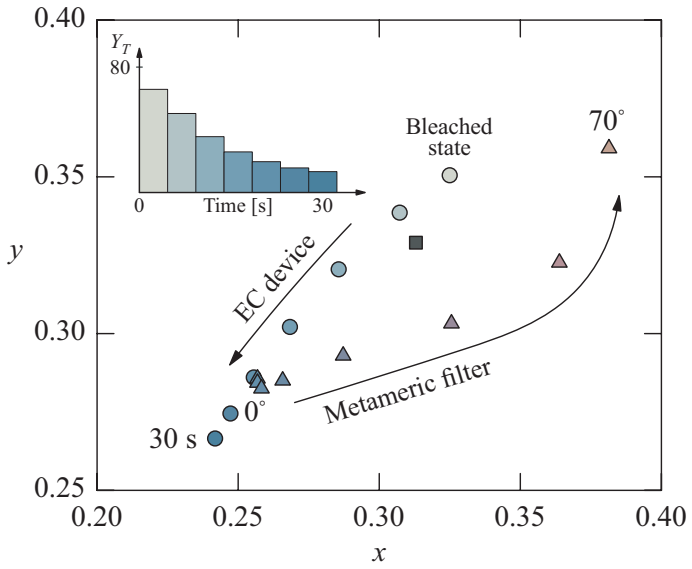

Figure 7.9 (Color online) Color variation of the ECD during coloration (circles) and of the metameric interference filter as a function of the observation angle (triangles). The square represents the reference white. Upper inset shows the luminance (Y_T) variation with time of the ECD. Calculations are done under illuminant D65 in the xyY color space.

EC stack is negligible for these angles especially in its colored state). The color difference is not at its lowest at 20 seconds since the calculations were done for a different coloration and bleaching cycle than the one used to design the filter in order to demonstrate the versatility of the device. It is interesting to note that a color match is obtained for a six second time period at normal incidence (see the gray region in Figure 7.10) ; a feature which appears important in order to ensure that the user has time to observe the color match. This time period diminishes as the angle is increased, but a color match is still possible at an angle of approximately 30°, thus offering some leeway when observing the device. Note that the observed asymmetrical color variation is due to different coloration and bleaching mechanisms of WO_3 [114]. In spite of these different mechanisms, a color match is also obtained during the bleaching phase.

We have also observed that the dynamic nature of the ECD can compensate, to some extent, the transmission fluctuations of the deposited metameric interference filter as well as the slight color fluctuations the EC material may suffer as a function of time. In fact, in the case of our deposited filter, small deviations of the transmission, caused by thickness inaccuracies, are sufficient to increase the color difference over our defined color matching threshold ($\Delta E^{\star}_{\mathrm{ab}} \leq 4$) at the 20 second coloration mark for two out of three of the chosen illuminants (see Fig. 7.8 and Fig. 7.10). Nevertheless, we obtain a minimum value of $\Delta E^{\star}_{\mathrm{ab,\ D65}}$ = 3.15 during the coloration phase at a time of approximately 23 seconds (see Fig. 7.10). This higher time is explained by the lower transmission of our deposited filter. It is also interesting to note that a value of $\Delta E^{\star}_{\mathrm{ab,\ D65}} = 2.83$ is obtained during the bleaching phase. In the previous analysis, we assumed that the interference filter is stable as a function of time. Indeed, we have tested the color stability of a wide variety of optical filters following various environmental tests (to be published).

In the previous example, the presented filter was metameric with the colored state of the active element (ISIS B in Fig. 7.2). One could also choose to create a metameric filter with the bleached state of the device (ISIS A in Fig. 7.2). Note that since the bleached state transmission is known to vary during the initial lifetime of some ECDs, it could be necessary to cycle the devices before designing the metameric filter. Also, in order for this configuration to work in the present context, the color of the bleached state of the ECD at normal incidence would need to be modified, WO_3 being essentially colorless and unattractive in its as deposited state. This could be done either by adding a colored layer on the backside of the substrate, by replacing the WO_3 by an organic EC material, or in a more complex way, by modifying the bleached state of the WO_3 layer. For example, this can be done by doping with various metals such as gold [271].

Finally, the 20 second coloration time of the present device would be too long for real life

applications. Various parameters can decrease the coloration time. For example, increasing the applied voltage can lead to a faster coloration but quicker degradation ; thus a precise range of voltages should be specified to ensure a device's long-term functionality. Higher porosity of the WO_3 layer can also be considered [272, 273] as would a more humid environment [131]. We estimate that times between 2 and 5 seconds should be acceptable ; on the contrary, a more rapid operation wouldn't give enough time to observe the color match and therefore authenticate the protected document. Finally, replacing WO_3 by an organic EC material could also further lower the coloration time.

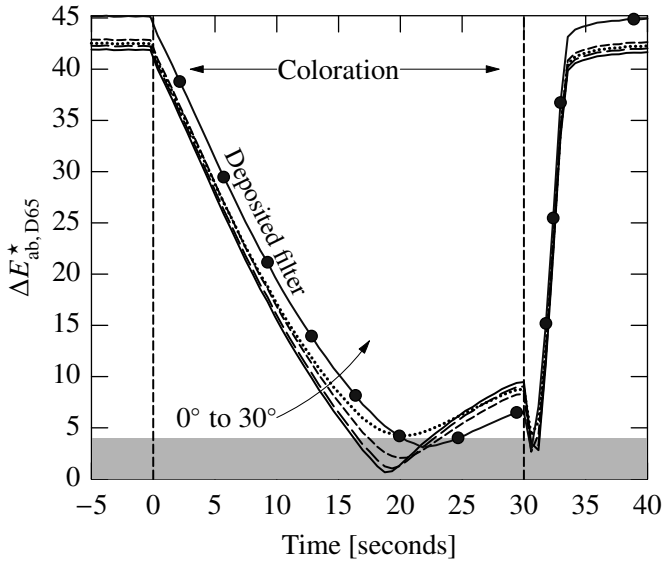

Figure 7.10 Theoretical color difference under illuminant D65 between the ECD and the designed filter for four angles of observation (0° to 30°). The gray area indicates the color matching zone ($\Delta E^{\star}_{ab,\,D65} \leq 4$). The curve with the black dots is the color difference obtained for the deposited filter at normal incidence.

7.5.4 Filter design considerations

In this section, we present a methodology which allows one to diminish the number of layers (lower cost) while maintaining a low color difference between the filter and the NIM, and a high performance under various illuminants.

At first glance, it may seem that designing a metameric filter is simple with today's software ; however, in order to obtain and optimize the most efficient and performing design, it is necessary to use a series of specific steps. As an initial structure for the previously presented metameric filter (see Fig. 7.8), the following quarter-wave "chirped" filter design was used : $(0.6H0.6L)(0.8H0.8L)(HL)^2(1.2H1.2L)^2H$, where H and L represent a high and

a low index of refraction material of quarter-wave thickness (Nb_2O_5 and SiO_2 in our case). These types of "chirped" filters are often used to design broadband reflectors. The following step consists in optimizing the thicknesses of the individual layers of the initial structure as a function of various specific targets such as the spectrum and/or the color to obtain in reflection and/or transmission.

Table 7.3 Color difference for filters designed using different types of targets and methods.

Targets	$\Delta E^{\star}_{\mathbf{ab,\ D65}}$	$\Delta E^{\star}_{\mathbf{ab,\ A}}$	$\Delta E^{\star}_{\mathbf{ab,\ F1}}$
Color D65	0.021	6.144	6.790
Color D65, F1	0.031	4.235	0.002
Color D65, F1, A	0.244	0.019	0.070
Color D65 + $T_{\text{E.T.}}$[a]	2.846	5.351	3.949
Color D65, F1 + $T_{\text{E.T.}}$	3.776	3.692	2.604
Color D65, F1, A + $T_{\text{E.T.}}$	2.063	2.107	4.683
Color D65 + $T_{\text{I.P.T.}}$[b]	0.407	1.833	4.474
Color D65, F1 + $T_{\text{I.P.T.}}$	0.606	0.949	0.077
Color D65, F1, A + $T_{\text{I.P.T.}}$	0.430	0.462	0.784

[a] Equal tolerances.
[b] Inversely proportional tolerances.

Color targets

The simplest method is to use color targets based on the color coordinates of the NIM (in our case the ECD) under a specific illuminant (D65, A and F1 for example). As can be seen in Table 7.3, this method usually leads to excellent color matches, especially when color targets under more than one illuminant are included in the design process. However, the fact that color is defined by only three values results in a multitude of possible solutions (see definition of metamerism in section 7.2), many of which can lead to highly sensitive color differences under various light sources and observers. Interestingly, an increased number of illuminants in the design process leads to a filter which closely matches the target transmission spectrum in the 450 nm to 650 nm region (see Fig. 7.11a).

To explain this effect, let us consider the luminous efficiency curve of the human eye (see Fig. 7.11a). From this curve, one concludes that the human eye has its maximum sensitivity at 555 nm and is practically insensitive for wavelengths below 420 nm and above 680 nm. One can infer that although color calculations are usually performed between 380 nm and 780 nm, it is the region between 420 nm and 680 nm that has the most impact. This weighing process naturally takes place when using only color targets. Note that such studies of color

constancy have been explored [274].

Addition of transmission targets

Since designing a filter by taking into account all possible types of illumination is impossible, addition of transmission or reflection spectrum targets appears be very useful. In fact, this method very often leads to more efficient designs, but is also prone to creating filters with a large number of layers since multiple targets leave very little leeway during optimization. In the case of a fixed number of layers, the performance of the filter is diminished under all illuminants (see Table 7.3) due to large oscillations generated over the whole visual spectrum (see Fig. 7.11b).

Inspired by the previous observations, one way to solve these problems, is to add tolerances to the spectrum targets which are inversely proportional to the luminous efficiency curve of the human eye. Doing so leads to a lower divergence between the spectra of the filter and that of the NIM in the 420 nm to 680 nm region (see Fig. 7.11c), while maintaining low color differences (see Table 7.3). Essentially, this method guides the optimization in the right direction, while the color targets themselves fine-tune the spectrum to minimize the final color differences. Therefore, the risks of obtaining metameric filters which are highly sensitive to changes in illuminants and/or to non standard observers such as colorblind individuals are lowered.

7.6 Conclusion

We have presented the ground work for the first combination of an ISIS with an active component, in this case an electrochromic device. Such a feature could prolong the usability of ISIS devices as well as increase their effectiveness by offering a surprising effect as well as an additional level of security. The angle-dependent color variation of the interference filter provides a quick and easy method of verification similar to present-day security devices while, in the case of the ECD, not only does it serve as a color reference for the ISIS, but it also offers an EC color shift accessible by applying a low voltage. We have shown how the combined use of both these technologies can lead to interesting optical effects. Although the presented example is transmission based, future devices could also be used in reflection. It is important to note that the presented ECD could also be replaced by any other type of EC architecture. We have also shown that the dynamic nature of this type of system allows a certain margin of error for the deposition of the metameric filters and could also alleviate problems, to a certain extent, which may appear due to the degradation of the EC material.

Finally, we have demonstrated that incorporating the luminous efficiency curve of the

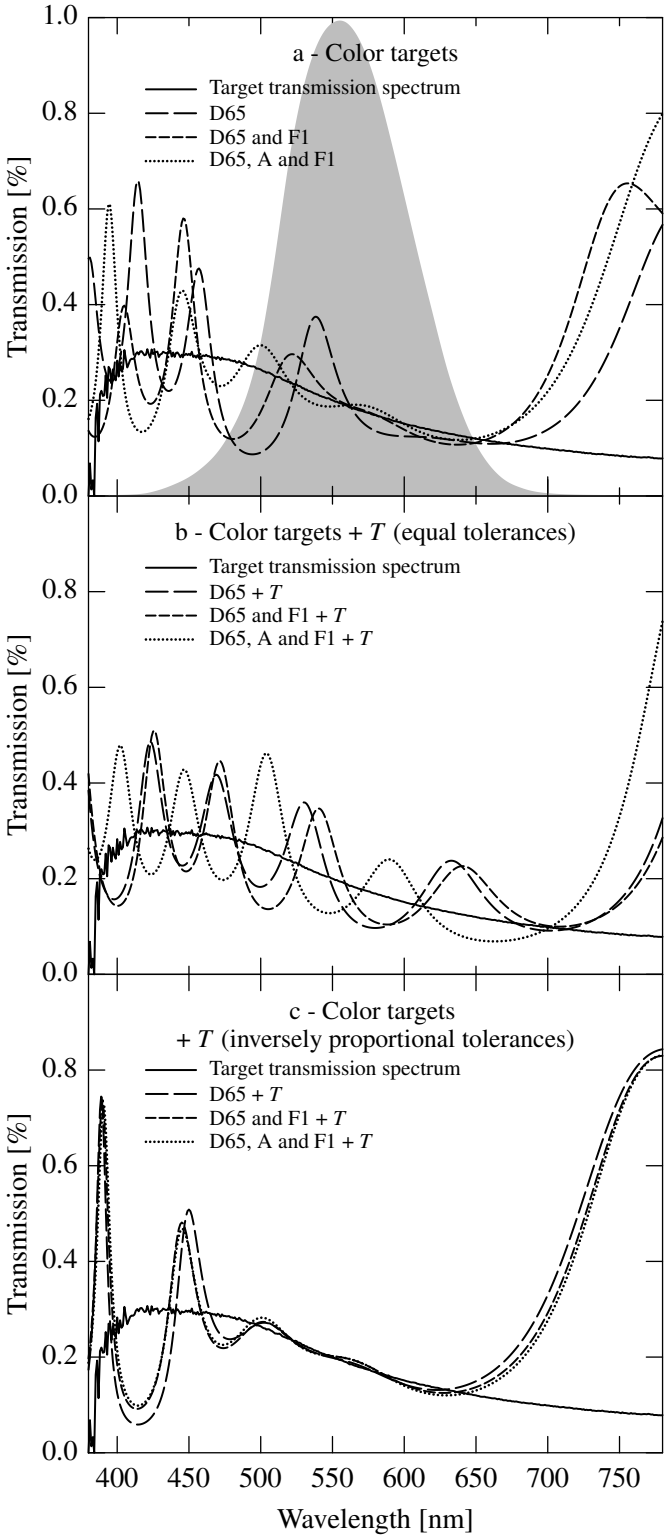

Figure 7.11 Comparison of the transmission spectra of various design strategies of a metameric filter. A specific 13 layer quarter-wave stack was used as a starting point for the refining process. Optimization targets are indicated in the figure : (a) color targets only, (b) color and transmission targets with equal tolerances, (c) color and transmission targets with tolerances that are inversely proportional to the luminous efficiency curve of the human eye (gray area in (a)).

human eye into the design process results in optimal metameric filters whose color difference is stable under most light sources and ultimately for various observers. This method also offers the possibility of reducing the total number of layers of the filters. Further work will focus on modifying the color of the bleached state of the WO_3 coatings in order to increase the attractiveness and complexity of future devices and combining both the ISIS and EC materials into a single device.

7.7 Acknowledgments

Bill Baloukas acknowledges Le Fonds Québécois de la Recherche sur la Nature et les Technologies (FQRNT) and the National Sciences and Engineering Research Council of Canada (NSERC) for their scholarships. We also thank F. Turcot and S. Chénard for their expert technical assistance, A.-P. Lamarche and A. St-Georges-Robillard for their help with some of the experiments, Dr. O. Zabeida for his valuable comments, and Prof. C.G. Granqvist (Uppsala University) for fruitful discussions. This work was supported by NSERC of Canada through its STPGP 350496-07 strategic grant.

CHAPTER 8

ELECTROCHROMIC INTERFERENCE FILTERS FABRICATED FROM DENSE AND POROUS TUNGSTEN OXIDE FILMS

8.1 Foreword

Following the demonstration of a passive/active device based on the combination of an ISIS and ECD, we realized that a simpler and less costly approach was required. It is following the preparation of part of a research proposal that the idea of how to combine both the angle-dependent and voltage-driven color shifts came to me. In fact, it is the work done by Dr. Vernhes, a research associate of the FCSEL, on single material interference filters [275] that inspired the following paper. Also note that similar multilayer concepts have been explored for thermochromic as well as photochromic materials for an enhanced performance [276, 277]

The result of the present work is an interference filter which presents a variation of color as a function of the observation angle but that can also be colored electrochemically. Additionally, this electrochromic interference filter (EIF) could potentially be designed to be metameric with a NIM such as presented in Chapter 6. Although in the present case we did not include the fabricated 27 layer filter in an all-solid state device, the idea is that this type of structure could be included in any type of ECD.

It is also important to note that this paper focuses on the potential use of WO_3-based filters for applications in smart windows. It is our desire to publish in *Solar Energy Materials & Solar Cells*, a journal where work on EC materials is often published, that prompted us to put the emphasis on smart windows. Security applications are nonetheless mentioned as another potential application.

ARTICLE 3 : ELECTROCHROMIC INTERFERENCE FILTERS FRABRICATED FROM DENSE AND POROUS TUNGSTEN OXIDE FILMS

Bill Baloukas, Jean-Michel Lamarre and Ludvik Martinu

Department of Engineering Physics, École Polytechnique de Montréal,
P.O. Box 6079, succursale Centre-ville, Montréal, Québec H3C 3A7, Canada

Solar Energy Materials & Solar Cells, vol. 95, no. 3, 2011, p. 807-815.

Abstract

Smart windows offer an opportunity to reduce energy consumption. However, the use of multiple optical elements, such as low emittance coatings and electrochromic devices, is detrimental to the luminous transmittance of these high performance windows. Although the addition of antireflective coatings has helped to reduce this problem, some elements, such as high index of refraction materials still give rise to loss of light. We show that replacing the single WO_3 active coating, the main component of an electrochromic device, by an appropriately designed electrochromic interference filter can significantly increase the transmittance. This active filter is based on a stack of dense and porous WO_3 layers. We first study the effect of porosity on the physical and electrochromic properties of WO_3 prepared by radio frequency magnetron sputtering. We demonstrate that the overlying dense coating does not inhibit the coloration of the underlying porous coating. The best performing films are combined into a 27 layer quarter-wave interference filter which is shown to cycle between bleached and colored states, while providing attractive transmission. Finally, we discuss various filter designs which can increase the transmission of an electrochromic device in its bleached state, as well as the potential use of active filters for optical security devices possessing two levels of authentication.

8.2 Introduction

Faced with a growing population and increasing energy demands, society is faced with one of two options : produce more energy or find ways to reduce consumption. Very often, the former implies burning more fossil fuels with the adverse affects we all know too well. The latter starts with changing energy consumption habits, but can also be effectively tackled by the use of technology. For example, smart windows have been proposed as such a technology. In fact, the use of smart windows could lead to energy savings in cooling and lighting costs as well as offering adjustable lighting levels for user comfort [278].

High performance smart windows are nowadays very often based on a combination of multiple glass panes, each with its own particular function (low emittance, variable transmittance, etc.). Since the principal function of a window is to offer a clear outside view, ensuring a high optical transmittance is very important. Unfortunately, the high quantity of interfaces diminishes the transmission and, as a result, addition of antireflective (AR) coatings on each of the window components has become crucial [172, 279]. Although this addition has helped, the presence of other elements, such as the high refractive index (n_{H}) materials present in electrochromic devices, results in losses due to their high reflectivity. This is the case with WO_3, the most popular electrochromic EC material. In this work, we propose a way to increase the transmittance by transforming the single WO_3 layer into an electrochromic interference filter (EIF). A similar concept has recently been explored for thermochromic VO_2 films, which intrinsically possess a low transmittance, by alternating TiO_2 and VO_2 layers [276].

In order to design and fabricate an interference filter [10], at least two constituents with different optical properties are necessary. Since the cost of interference filters is very often related to the total number of layers and their thickness, it is important to minimize these parameters by maximizing the difference of index of refraction (optical contrast) between the constituents. In the case of dielectric filters, maximizing the optical contrast results in a higher reflectivity at the interfaces, and thus in a more pronounced interference effect. The easiest method of obtaining two sets of optical properties is to use two different materials. In the present work, we have chosen WO_3 as the n_{H} material. Since there are no low index of refraction (n_{L}) cathodic EC materials, we propose the use of porous WO_3 as the n_{L} material.

One method to change the density of WO_3 deposited by magnetron sputtering is to vary the deposition pressure [245]. In fact, a higher pressure leads to an increased number of collisions between the sputtered atoms and the gas in the vaccum chamber, thus lowering the energy of energetic particles and augmenting their obliqueness. This oblique component is known to enhance the presence of voids in coatings due to atomic shadowing. For example,

in glancing angle deposition, atomic shadowing is used to produce highly porous films [272]. Another approach is to use substrate bias modulation in order to obtain multilayer or graded layer single-material porous-dense optical filters [275].

In the present work, we first study the effect of the deposition pressure on the physical and electrochemical properties of WO_3 films. We then test simple configurations of alternating porous and dense coatings to assess their resulting behavior. Following these tests, a multilayer quarter-wave filter is fabricated and characterized. Finally, we discuss how the use of EIFs can increase the luminous transmittance of smart windows, and can also lead to innovative active optical security devices.

8.3 Experimental methodology

8.3.1 Deposition conditions

Coatings were deposited in a custom made vacuum chamber by radio frequency magnetron sputtering from a 50 mm diameter WO_3 target at a power of 150 W, while using an Ar and O_2 gas mixture (4 :1 Ar to O_2 ratio). The base pressure was approximately $2.5\text{x}10^{-6}$ Torr.

The WO_3 coatings were deposited on 2.5 cm by 5 cm ITO-coated glass substrates with an average sheet resistance of 50 $\Omega/\square$. ITO substrates were cleaned with soap and de-ionized water, and in isopropanol for 15 minutes using an ultrasonic bath. Part of the substrate was masked during the deposition to allow access to the ITO electrode for cyclic voltammetry measurements.

8.3.2 Physical characterization

Samples were deposited on Si and on B270 glass for optical characterization. Variable angle spectroscopic ellipsometry (*VASE*, J.A Woollam Inc.) combined with transmission measurements using a Perkin Elmer *Lambda 19* spectrophotometer, were used to obtain the samples' optical properties (refractive index and extinction coefficient), as well as their physical thickness. The data were analyzed with the *WVASE 32* software (J.A. Woollam Co., Inc.). The interference filters were designed using the *OpenFilters* software [68].

Rutherford back scattering (RBS) measurements were performed in a Tandem linear accelerator with a 2.042 MeV He^+ ion beam at a scattering angle of 170° (between the forward direction of the incident beam and the detector). The same accelerator was used for elastic recoil detection (ERD) measurements with a 1.5 MeV He^+ ion beam. The angle between the beam direction and the sample surface normal was 75° as well as between the detector and the sample surface normal (30° scattering angle). To stop all ions except hydrogen ions, a 6 μm-thick Mylar foil was placed in front of the detector [250].

To verify the crystalline or amorphous structure of the films, grazing incidence (1 degree) X-ray diffraction (XRD) was performed with a Philips *X'pert* diffractometer using Cu Kα (1.5406 Å) radiation. The acceleration voltage was set at 50 kV and the filament current at 40 mA. Finally, scanning electron microscopy images of the cross sections of the samples were taken with a JEOL *JSM-7600F* at 5kV electron beam acceleration voltage.

8.3.3 Electrochromic characterization

Cyclic voltammetry measurements were performed using an *Autolab PGSTAT302N* potentiostat/galvanostat in a 1 M aqueous solution of H_2SO_4. An exposed surface of 0.75 cm^2 of WO_3, a Pt foil, and a SCE were used as the working, counter and reference electrodes, respectively. In order to perform optical transmission measurements, the cell was equipped with two windows : the first window consisting of the sample under evaluation, and the second window being an uncoated glass substrate. The cyclic voltammetry measurements were performed at a 50 mV/s scan rate between -0.6 V and +1.5 V.

In situ transmission measurements were performed during cyclic voltammetry to evaluate the coloration efficiency. The setup consisted of a stabilized deuterium tungsten halogen light source from Ocean Optics (*DH-2000*) equipped with an optical fiber outlet, a series of lenses to focus the beam onto the device and collect the transmitted beam into a second optical fiber connected to an Ocean Optics spectrophotometer (*USB2000*). This setup allows the acquisition of a complete spectrum (380 nm to 850 nm) approximately every 500 ms (30 averaged measurements of 3 ms plus signal treatment time).

8.4 Characterization of the dense and porous WO_3 material

8.4.1 Physical properties

We deposited a series of WO_3 films at different pressures ranging from 5 mTorr to 80 mTorr (see Table 8.1). As expected, the deposition rate decreases with increasing total pressure. For a better comparison, we prepared film thicknesses close to those required in the design of the interference filters.

Following spectroscopic ellipsometry measurements on both Si and B270 glass, we obtained the optical properties of as deposited samples (n and k at 550 nm) as presented in Figure 8.1. To increase the validity of our model, both the ellipsometric data and transmission spectra of the films were combined during the modeling. The absorption coefficient, which is negligible in the visible spectrum, is not shown. In order to fine tune the optical model, a graded top layer was added for the films deposited at all pressures above 5 mTorr. This layer represents a reduction of the index of refraction for the last 5% of the layer thickness.

The need to include such a graded layer increased for coatings deposited at higher pressures, indicating the presence of a higher surface roughness. As can be seen in Figure 8.1, the index of refraction of the films is maximum at low deposition pressures ; it decreases with increasing pressure, and reaches a minimum value for pressures above 40 mTorr.

The 5 mTorr and 80 mTorr films' compositions were analyzed by RBS and ERD ; their composition can be expressed as $H_{0.05}W_{0.21}O_{0.72}$ with 2% Ar, and $H_{0.15}W_{0.18}O_{0.67}$, respectively. The incorporation of 2% of Ar in the dense film is to be expected due to a higher energy of the incident deposition flux. Also important to note is the presence of hydrogen in the films arising from absorbed water. The resulting composition can be expressed as $WO_{3-x-y}OH_x \cdot yH_2O$ where x is the degree of hydroxylation and y the degree of hydration of the WO_3 [157]. The oxygen to tungsten ratio in the films can be calculated from two extreme cases : 100% of the H is part of water, and 100% of the H is part of OH groups. These two cases result in a ratio of 3.3 ± 0.1 and 3.1 ± 0.2 for the dense and porous coatings, respectively. This suggests that the films are slightly overstoichiometric. However, a small error on the evaluation of the hydrogen concentration can significantly affect the O/W ratio. Infrared measurement attempts were inconclusive in obtaining more precise information because the coating thickness was too small.

RBS-ERD measurements allow one to calculate the density of the films : supposing a density of 7.16 g/cm^3 for bulk WO_3 [115], we obtain a packing density of 91% and 76% for the dense and porous films, respectively. These results are also presented in Figure 8.1. Note that the values include hydrogen and oxygen due to the absorbed water. In all cases, XRD measurements indicated that the films are amorphous.

Using the Lorentz-Lorenz EMA, we also calculated the packing density (P) using the refractive indices obtained by ellipsometry (which contain the water contribution) :

Table 8.1 Deposition conditions and thickness of the WO_3 films.

Pressure [mTorr]	Deposition rate [Å/s]	Thickness [nm]
5	1.8	79
10	1.3	82
15	1.1	86
20	0.8	73
40	0.4	93
80	0.2	95

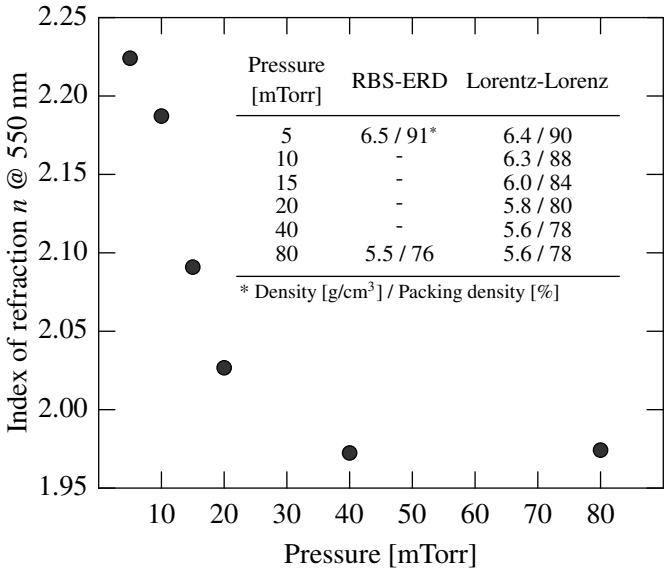

Figure 8.1 Index of refraction at 550 nm as a function of the deposition pressure. The density and packing density of the films obtained by RBS-ERD measurements and calculated using the Lorentz-Lorenz effective medium approximation are also indicated.

$$P = \frac{n_f^2 - 1}{n_f^2 + 2} \frac{n_b^2 + 2}{n_b^2 - 1}, \tag{8.1}$$

where n_f and n_b are the refractive indices of the film and of the bulk WO_3 ($n_{b,\ 550\ \mathrm{nm}} = 2.5$ [280]), respectively. The calculated values are very close to those obtained by RBS-ERD (see Figure 8.1).

To confirm our previous observations, we analyzed cross-section SEM-FEG images of the most dense and the most porous films (see Figure 8.2). It can be seen that the dense film is uniform and featureless. On the other hand, the porous film presents cavities and indications of a columnar type of growth, thus exhibiting a more open structure. This supports our previous assumption pertaining to a higher quantity of absorbed water and to a need to include a graded top layer when refining the ellipsometric model [281].

8.4.2 Electrochemical properties

In order to assess the electrochromic performance of the WO_3 films, we performed cyclic voltammetry measurements (see Figure 8.3). The shape of the voltammograms clearly indicates that the inserted charge is highly dependent on the density of the films (see Table 8.2), an observation also made by other authors [282]. This behavior can be linked to the effective surface area of the films which affects the transfer rates between the electrolyte and

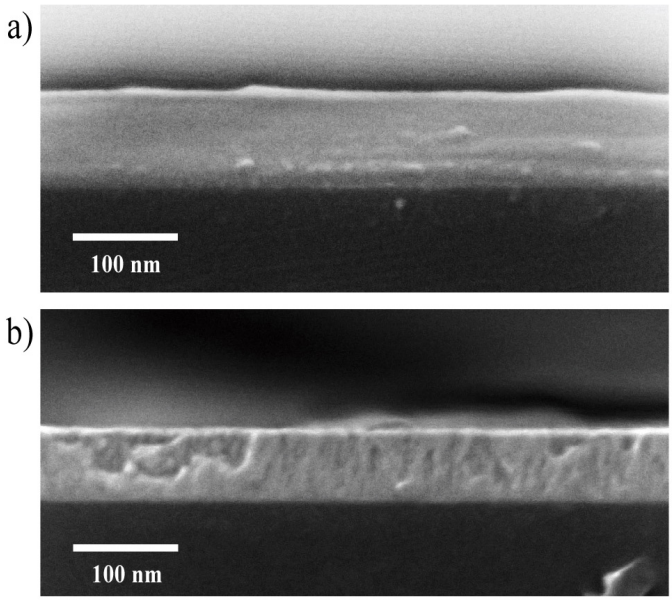

Figure 8.2 SEM-FEG images of the a) dense 5mTorr and b) porous 80 mTorr WO_3 films.

WO_3 [283]. Therefore, the most dense film does, in fact, exhibit the lowest inserted charge and the lowest variation in transmission between the bleached and the colored states (see Table 8.2). Interestingly, the inserted charge decreases for deposition pressures higher than 20 mTorr. We believe that this effect is caused by a rapid degradation of the films through voltage-enhanced dissolution [284] resulting in a decreasing thickness of the films, as we will explain below.

The film density also has an impact on the coloration and bleaching times of the films. For example, as can be seen on the cyclic voltammograms in Figure 8.3, the decrease in anodic current is much slower for the low pressure deposited films, in agreement with others [118, 285]. The fact that the porous layers contain more water has also been shown to lead to faster electro-optic response times [286], since water serves as a source of hydrogen ions as well as an electrolyte for ion transfer inside the film during coloration [287]. Table 8.2 presents a summary of the EC characteristics obtained for all the coatings studied in this work.

From the maximum anodic current obtained during the cyclic voltammetry measurements, we calculated the diffusion coefficients of the films by using the Randles-Sevčik equation [114]. As expected, the diffusion coefficient of the most dense film is significantly lower (2 orders of magnitude) than the other ones; this in part explains its very slow bleaching rate in agreement with other authors [273, 149].

It is also important to assess the durability of the films by performing a higher number of

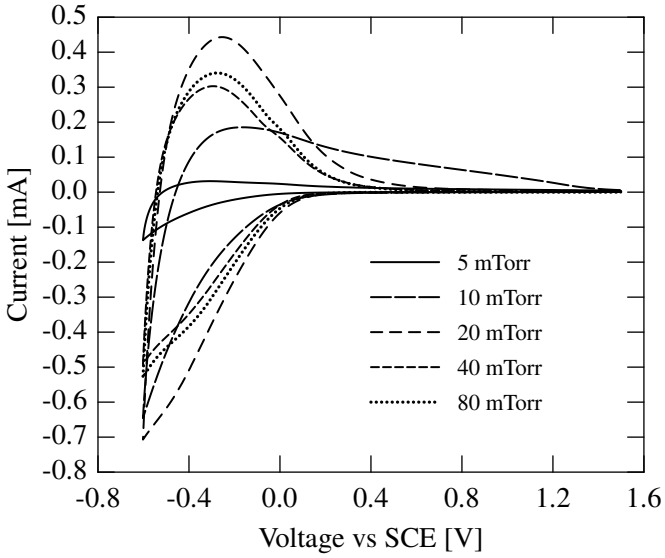

Figure 8.3 Cyclic voltammograms (second cycle) for a scan rate of 50 mV/s of WO_3 films deposited at different pressures.

Table 8.2 Electrochromic properties of the WO_3 films deposited at different pressures obtained for the second voltammetric cycle.

Pressure [mTorr]	Inserted charge [mC]	Diffusion coefficient [cm^2/s]	CE_{550nm} [cm^2/C]	ΔT_{550nm} [%]
5	0.7	4.9E-13	80	6.8
10	3.8	1.7E-11	73	30.8
20	5.1	9.6E-11	48	27.9
40	3.4	4.5E-11	42	17.4
80	3.8	5.7E-11	45	20.5

cyclic voltammetry measurements. The use of a relatively "aggressive" electrolyte, combined with the small thicknesses of the films, results in an accelerated degradation which, in the present case, is already visible after a few cycles. It is important to note that we chose this particular electrolyte and concentration mainly because we could rapidly assess the differences in durability of the individual coatings as well as for practical reasons ; our previous devices being based on hydrogen insertion [288]. Note that testing in an anhydrous $LiClO_4$-propylene carbonate solution could significantly reduce degradation [115]. Figure 8.4 shows the normalized inserted charge (with respect to the first cycle of each film) and normalized ΔT for 10 voltammetry cycles. Both these parameters rapidly decrease for deposition pressures of 20 mTorr, 40 mTorr and 80 mTorr. The corresponding coatings clearly suffer from a fast degradation which is increasingly pronounced as the porosity increases. The degradation of WO_3 films in aqueous H_2SO_4 by dissolution due to polytungstate ion formation, amplified by voltage, is well known [284]. The density of the films, therefore, clearly affects their long-term durability.

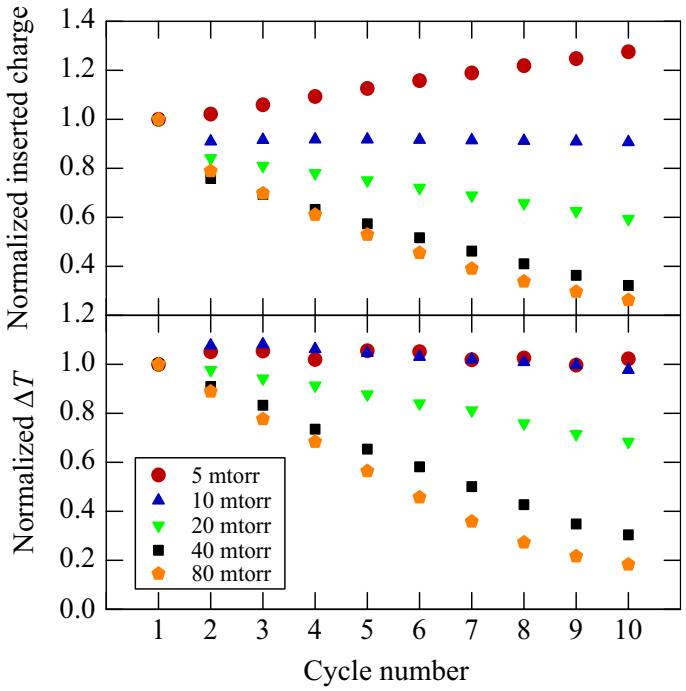

Figure 8.4 Normalized inserted charge and normalized variation in transmission at 550 nm for ten consecutive voltammetric cycles for WO_3 films deposited at different pressures.

From the *in situ* transmission measurements taken during the cyclic voltammetry, it is possible to calculate the CE [114]. Although the CE has been shown to depend on the intercalation level [289] (which in our case is 0.04 and 0.26 for the 5 mTorr and 80 mTorr

films, respectively) and to increase with porosity [290], due to an increased delocalization of the inserted electrons, it is interesting to note that a significantly higher CE is obtained for the two most dense films. Considering the complex kinetic behavior of hydrous/hydroxylated WO_3 films, it is difficult to give a definite explanation at this point ; here we assume that this behavior is once again caused by the degradation of the porous films, whose CE incidentally decreases after every cycle in agreement with others [291, 292].

From the previous observations, we can conclude that porous films do present some advantages : higher coloration and faster electro-optical response. On the down side, too much porosity leads to a poorer long-term durability of the films similar to the observations by others [291]. Although very dense coatings do present an increased stability, they are also prone to very slow coloration and bleaching times, decreasing optical transmission in the bleached state, and very little transmission variations. It is therefore no surprise that the 10 mTorr film possessing intermediate properties offers the overall best performance. In the following sections, we will combine dense and porous films into one system, thus obtaining advantageous properties of both types of layers.

8.5 Characterization of double layer systems

To gain insight into the behavior of the films when stacked and to determine if the use of very dense layers inhibits the coloration of the underlying porous film, we fabricated two sets of samples with the following configurations : Sample A (ITO|95 nm of WO_3 at 80 mTorr|81 nm of WO_3 at 5 mTorr), and sample B (ITO|79 nm of WO_3 at 5 mTorr|98 nm of WO_3 at 80 mTorr). The deposition conditions were the same as for the films presented in Table 8.1. In Figure 8.5, we present the inserted charge as a function of the number of cycles for samples A and B as well as the evolution of the normalized ΔT and CE. Although sample A does perform better for the initial part of the test (higher inserted charge, ΔT and CE), due to the "protection" offered by the top dense coating, it also eventually degrades. This is probably due to the degradation of the underlying porous coating. The initial increase in inserted charge also follows the same trend as the dense 5 mTorr film in Figure 8.4.

In the case of sample B, one notices the initial degradation of the top porous layer at a rate which is comparable with the single 80 mTorr film in Figure 8.4. This initial decrease in inserted charge is followed by a more stable regime offered by the underlying dense coating. In fact, after approximately 60 cycles, the CE reaches a value of 70 cm^2/C which is comparable to the one obtained for the 5 mTorr deposition pressure (not shown here). It is important to note that the initial ΔT for sample A is very high (43%), indicating that the dense film does not inhibit the contribution of the underlying porous film. This behavior of a tandem film

configuration where a thin protective layer of electron-bombarded WO_3 with slow dynamics covers a more rapid yet fragile oxyfluoride WO_3 layer has also been observed by Azens *et al.* [293].

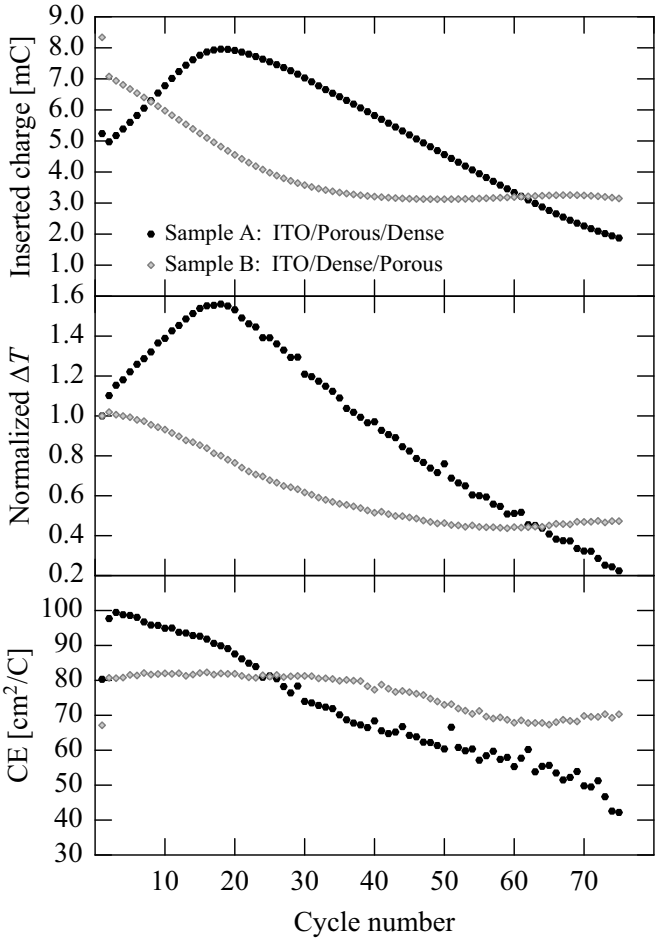

Figure 8.5 Inserted charge, normalized transmission variation at 550 nm and coloration efficiency (CE_{550nm}) for 75 consecutive voltammetric cycles for samples A and B.

8.6 Quarter-wave stack reflection filter

Following the preceding results, we fabricated a 27 layer quarter-wave reflection filter ($(HL)^{13}H$) based on a succession of layers deposited at pressures of 10 mTorr and 40 mTorr. We chose to deposit the dense coatings at 10 mTorr instead of 5 mTorr in order to benefit from its proven better performance. In the case of the low index layers, we chose a pressure of 40 mTorr instead of 80 mTorr due to a faster deposition rate, lower degradation time during cyclic voltammetry, and essentially an identical index of refraction. This configuration leads

to an index difference of approximately 0.22. The resulting filter's cross-section is presented

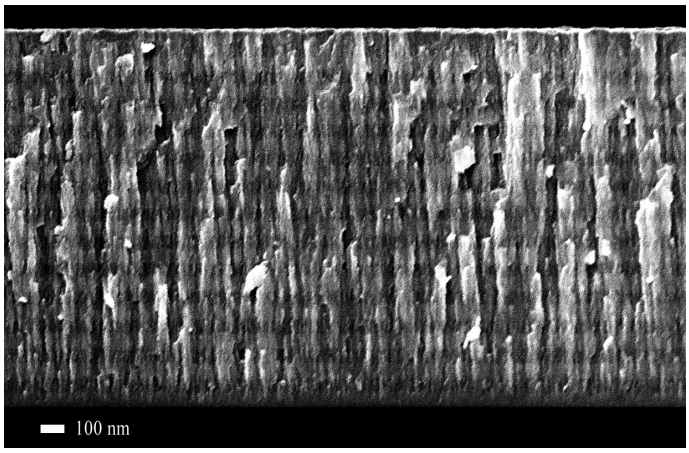

Figure 8.6 27 layer quarter-wave filter consisting of dense and porous WO_3. The variation in contrast between the dense and porous layers is clearly seen.

in Figure 8.6, where the lighter areas represent the dense WO_3 ; the subtle contrast is a result of the low density difference between the dense and the porous WO_3. Also note that the periodicity of the filter is well maintained considering that only time was used to control the thickness of the individual layers.

The resulting transmission spectrum of the deposited quarter-wave filter is presented in Figure 8.7. The reflection band which is obtained at 506 nm is very narrow due to the small index contrast between both materials. Its position is shifted, its intensity lowered and its shape slightly asymmetric, when compared to the "perfect" quarter-wave filter (see Figure 8.7) ; this is due to a slight decrease in the index contrast and thus optical thickness as a function of the number of layers. Such an effect was also observed by Vernhes *et al.* for Si_3N_4 films [281] and was attributed to the propagation of the microstructure of the underlying porous films into the subsequent overlying dense films. One method of correcting this undesirable effect, presented by the same authors, is to plasma treat the porous layer's surface in order to smooth and densify it, and hence to inhibit the microstructure propagation.

Figure 8.7 also presents an example of a simulated 27 layer interference filter based on a progressive decrease in optical thickness :

$$((1\text{-}0.01x)H(1\text{-}0.01x)L)^{13}(0.87H),$$

with H a quarter-wave layer of WO_3 deposited at 10 mTorr, L a quarter-wave layer of WO_3 deposited at 40 mTorr for a reference wavelength of 537 nm, and x an integer which varies from 0 to 12 for every additional quarter-wave layer. This designed filter duplicates the experimentally obtained reflection band quite well. It is important to note that other design

configurations can lead to similar results. Our model is simply used to demonstrate that a decreasing optical thickness results in a displacement of the transmission towards shorter wavelengths, and it also explains the asymmetric shape of the reflection band.

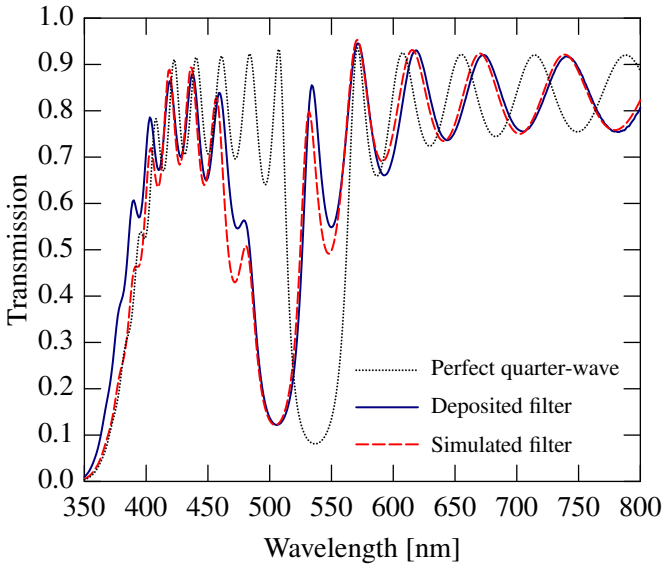

Figure 8.7 Transmission spectrum of the fabricated 27 layer quarter-wave filter based on porous and dense WO_3 on B270 glass. Also shown are a perfect quarter-wave filter with a reference wavelength of 537 nm and a simulated interference filter based on a gradual decrease in optical thickness which simulates the obtained experimental reflection band.

Cyclic voltammetry was also performed on the previous interference filter and its transmission variation was measured *in situ*. Figure 8.8 shows the evolution of the transmission as a function of wavelength during a coloration cycle. The first observation is the dramatic decrease in the reflection band at 506 nm. This effect is due to the incorporation of water into the filter before and during the electrochemical testing : this particularly affects the porous layers by increasing their index of refraction, thus reducing the index contrast between the dense and the porous films. As a result, the transmission in the bleached state of the filter around 500 nm increases as a function of time, as presented in Figure 8.9. Even so, a variation in optical transmission is clearly observed during the coloration cycle, demonstrating that an EIF is feasible. Note that in real life applications, the EIF would possibly be part of an encapsulated all solid-state device, thus limiting the presence and absorption of water.

At wavelengths which are outside the reflection band, for example at 750 nm, the transmission in the bleached state slowly decreases after each cycle (see Figure 8.9) until it stabilizes after approximately 20 cycles. Contrary to the single layer dense films, which reached a lower bleached state transmission after every cycle, in the present case, the transmission still

increases during the bleaching phase and has not reached a saturated state before the subsequent cycle. Consequently, a longer bleaching phase would have permitted the bleached state transmission to increase. One method to accelerate the decoloration of the filter would be to decrease the density of both the dense and the porous films. By doing so, the diffusion coefficient of the dense layers would be increased and the optical contrast maintained.

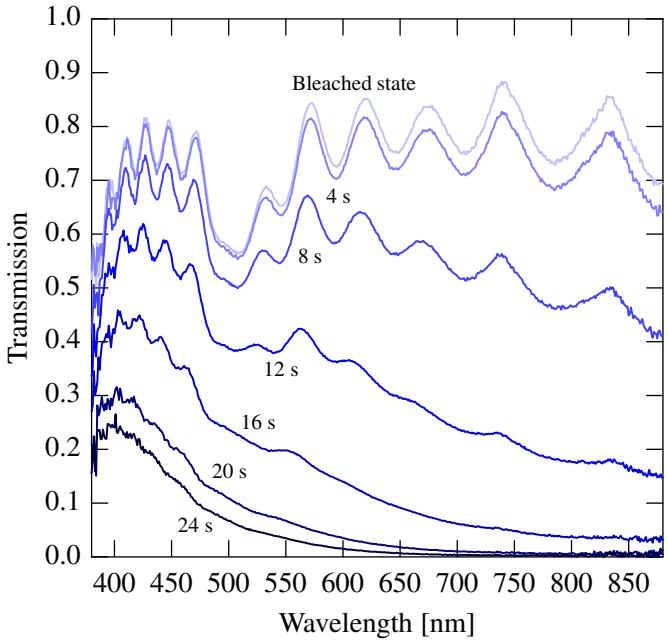

Figure 8.8 Transmission variation during a coloration cycle of the 27 layer porous/dense WO_3 filter. The reference was taken with a microscope glass substrate installed instead of the filter before testing.

8.7 Possible applications of EC interference filters

8.7.1 Smart window with higher luminous transmittance

Having fabricated a relatively complex EIF and demonstrated its functionality, we can assume that many types of interference filters can be created. As a result we can design a filter which increases the optical transmittance of an electrochromic window in its bleached state. To compare various designs, we use the luminous transmittance Y_T obtained from the

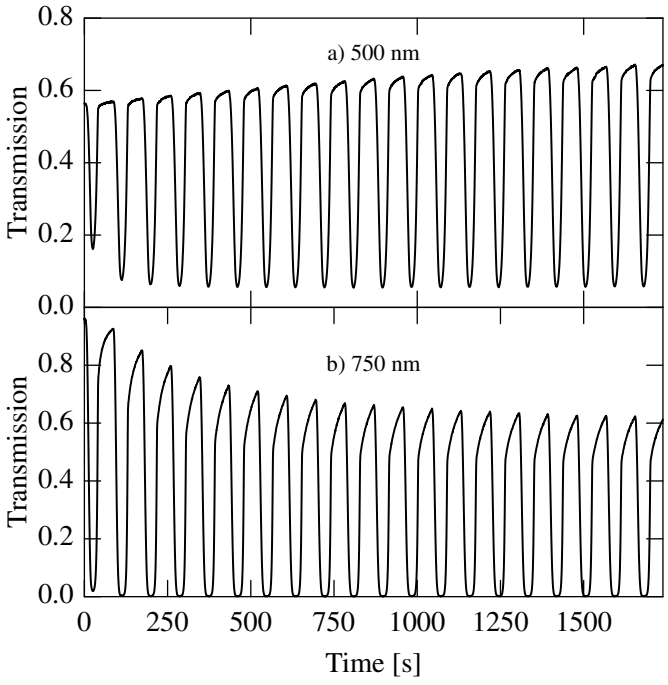

Figure 8.9 Transmission variation for the 20 initial voltammetric cycles of the 27 layer porous/dense WO_3 filter at two positions : a) 500 nm - position of the reflection band, and b) 750 nm.

xyY color space and defined by [4] :

$$Y_T = \frac{100 \sum_{380\text{ nm}}^{780\text{ nm}} S_\lambda T_\lambda \bar{y}_\lambda \Delta\lambda}{\sum_{380\text{ nm}}^{780\text{ nm}} S_\lambda \bar{y}_\lambda \Delta\lambda}, \tag{8.2}$$

where S_λ represents an illuminant defined by the International Commision on Illumination (CIE), T_λ the transmission of the designed filter, $\bar{y}_\lambda$ the 2 degree CIE standard observer color-matching function, and λ is a wavelength in the visible range (380 nm to 780 nm). Y_T is normalized by the Y tristimulus value of the illuminant under which the calculations are done ; in this case the CIE D65 illuminant. The luminance transmittance, which depends on the human eye's sensitivity, therefore gives a better appreciation of the perceived transmittance. For comparison purposes, a single 500 nm WO_3 layer ($n_{550\text{ nm}} = 1.97$) on ITO possesses a Y_T value of 83.2, while a B270 glass substrate without antireflection coatings possesses a Y_T value of 91.2. Consequently, a large amount of light is lost due to the interference and reflection caused by the WO_3 film as well as by the absorption of the ITO layer. While

nothing can be done for the latter, the former can be solved by replacing the WO_3 film by an EIF.

Table 8.3 Designed filters which increase the luminous transmittance by transforming a single WO_3 coating into an EIF. The substrate is B270 glass covered with a 20 nm ITO coating. Take note that the indices lower than 1.97 were simulated and not deposited.

Filter	# of layers	Thickness [nm]	n_H @ 550nm	n_L @ 550nm	Index contrast
A	5	288	2.22	1.97	0.25
B	7	471	2.22	1.97	0.25
C	9	641	2.22	1.97	0.25
D	13	817	2.22	1.97	0.25
E	5	328	2.22	1.88	0.35
F	5	355	2.22	1.78	0.45
G	5	405	2.22	1.68	0.55
H	5	325	1.97	1.78	0.20
I	3	275	1.88	1.68	0.20

Figure 8.10 presents various filters (whose details are shown in Table 8.3) designed using WO_3 coatings with different porosities and the CIE D65 xyY color coordinates as targets (xyY = (0.31, 0.33, 100)). Part (a) of Figure 8.10 presents filters possessing an increasing number of layers. As can be seen, the luminous transmittance is heightened for Filters A to D ($Y_T > 91$), but is not significantly affected by the total thickness of the filters. In this particular case, the low index contrast results in a transmission which is particularly increased in the 500 nm to 600 nm range where the luminous efficiency of the human eye is at its maximum value. This demonstrates that, in the present context, increasing the luminous transmittance is a better design strategy than trying to increase the transmittance for the whole visible spectrum.

Part (b) of the same figure presents the effect of increasing the index contrast between the high and low index materials. A higher index contrast leads to a better performance ($Y_T = 94.15$, a higher value could be obtained by eliminating the backside reflection of the substrate with an antireflective coating), although it also increases the physical thickness of the filters (see Filters E to G in Table 8.3) ; thicker layers of the low index material are required for an equivalent optical thickness. Note that the simulated lowest index film, which has a packing density of approximately 0.6, has been obtained by Beydaghan *et al.* by glancing angle deposition [272]. Finally, part (c) of Figure 8.10 shows that two films possessing the same index contrast, but with different average indices also perform differently. In fact, Filter I, whose average index is lower, performs well even though it is based on a 3 layer design.

Although all the filters are presented at normal incidence, it is important to note that at higher angles of incidence, they are still equal to or outperform a single WO_3 film. Also note that we chose to maintain a neutral color when designing our filters, but one could also design a filter with a specific color in mind. Interestingly, in many of the presented designs, the reflection in the near infrared is increased thus decreasing the transmission of part of the infrared solar spectrum (0.7 μm to 3 μm [172]). Indeed, one could eventually design and fabricate a more efficient dielectric hot mirror (visible light is transmitted, while infrared light is reflected).

8.7.2 Security devices and other applications

In a previous paper [288], we showed how the combination of metameric interference filters [254] with an electrochromic device offers two levels of authentication, as well as an extra level of complexity to overcome. Since a color variation from transparent to dark blue is fairly unattractive, changing the intrinsic color variation of WO_3 is of interest. For instance, some color changes have been demonstrated by mixing WO_3 with other EC oxides such as MoO_3 and V_2O_5 [294]. Different colors have also been noted with the addition of nanoparticles of Au, Ag, Pt, etc. [295, 296]. Finally, in a method similar to ours, but for completely other purposes, some have fabricated tunable photonic crystals [109].

Our proposed methodology, which preserves the EC properties of WO_3, offers a simple and effective way to modify the color of the bleached state of WO_3 by its transformation into a classical interference filter. The fact that EIFs also offer a color shift as a function of the observation angle as well as an electrochromic color variation allows one to combine both these effects (see [288]) into a single security device (see Figure 8.11). For example, the EIF of the previous section varies from green to blue as a function of the observation angle in reflection, as well as from green to an opaque navy blue under an applied voltage. As a result, the incorporation of such an EIF into an all solid-state device is expected to lead to a new category of active optical security devices.

Finally, any application requiring an adjustable transmission or reflection spectrum could also benefit by the use of EIFs.

8.8 Conclusion

We have presented an example of an EIF based on the use of porous and dense WO_3 films. In order to chose the most appropriate densities for the low and high index of refraction WO_3, we studied the physical and electrochemical properties of films deposited by radio frequency magnetron sputtering at various pressures. Dense films showed good durability

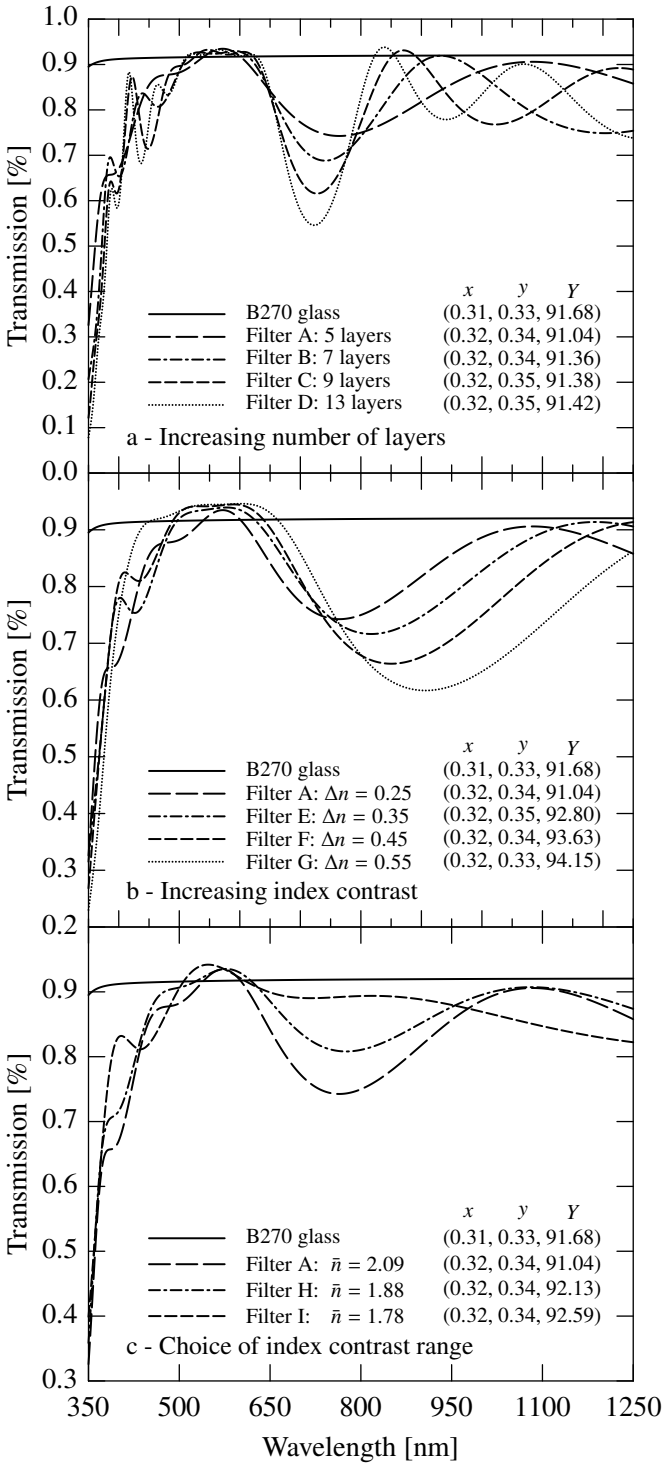

Figure 8.10 Simulated transmission spectra at normal incidence of various filters designed using different strategies and conditions : a) increasing the number of layers, b) increasing the index contrast between the high and low index materials, and c) lowering the average index ($\bar{n}$). All configurations contain an underlying 20 nm ITO coating on B270 glass. The xyY color coordinates of the filters are also presented. All designs have a color which is close to the reference white (CIE D65).

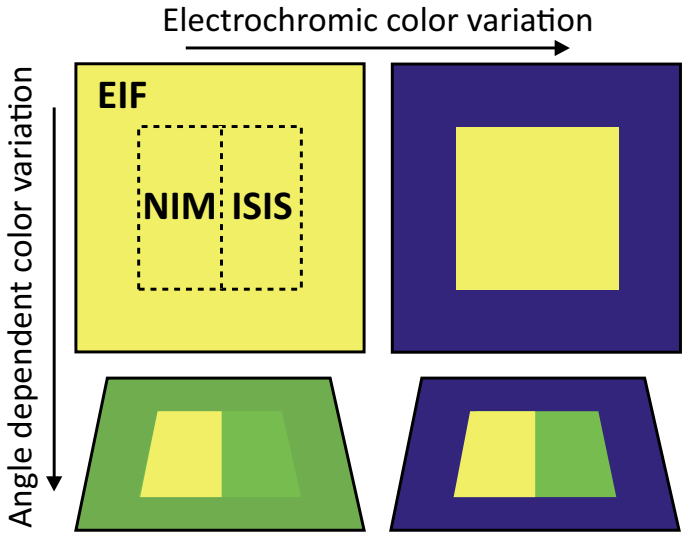

Figure 8.11 Illustration of possible active optical security devices. In the present example, the outer square is the electrochromic interference filter (EIF) while the center square is either a non-iridescent material (NIM) or an interference security image structure (ISIS). At normal incidence both squares form a metameric pair (same color), but under an applied voltage, the EIF colors to a dark blue and the inner square appears. When tilting the device in the uncolored state, both the EIF and ISIS vary to a greenish color which could also potentially be made to match. Finally, another color combination is obtained when the device is tilted in the colored state (bottom right image).

in aqueous H_2SO_4, but little transmission variation, slow electro-optical response times as well as a diminishing bleached state. Porous films presented fast response times and large transmission variations, but degraded fairly quickly. Tandem configurations were then tested to confirm that an overlying dense film can offer some protection to an underlying porous film and does not inhibit its participation to the electrochemical coloration process.

Based on the previous performance assessment, a filter consisting of 27 layers of dense and porous WO_3 was fabricated and tested. The results indicate that it is possible to design and fabricate an EIF with specific spectral characteristics. This filter can then be colored and bleached under an applied voltage.

Following these results, we showed that EIFs offer the opportunity to increase the bleached state transmittance of smart windows. Various filters designed under different conditions were presented in order to demonstrate that a higher luminance transmission is obtainable. From these results, we can also conclude that a relatively low number of layers is required and that, as expected, a higher index contrast is beneficial but not essential. Finally, EIFs could also be useful for future optical security devices with two levels of authentication (angle-dependent color shift and electrochromic color shift), as well as for any application requiring variable transmission/reflection interference filters.

Our future work will focus on increasing the optical contrast between the high and low index of refraction materials, and thus designing and fabricating more complex electrochromic interference filters.

8.9 Acknowledgments

Bill Baloukas acknowledges Le Fonds Québécois de la Recherche sur la Nature et les Technologies (FQRNT) and the National Sciences and Engineering Research Council of Canada (NSERC) for their scholarships. The authors wish to thank Dr. M. Chicoine for the RBS and ERD measurements, and Mr. P. Plamondon for the SEM-FEG images. We also thank F. Turcot and S. Chénard for their expert technical assistance, Dr. O. Zabeida for his valuable comments, and Dr. R. Vernhes whose work on single material filters inspired this paper. This work was supported by NSERC of Canada through its STPGP 350496-07 strategic grant.

CHAPTER 9

WO_3/SiO_2 COMPOSITE OPTICAL FILMS FOR THE FABRICATION OF ELECTROCHROMIC INTERFERENCE FILTERS

9.1 Foreword

In this fourth and final paper, we propose a solution to the low index contrast observed in the case of the porous|dense EIFs. In fact, mixing WO_3 with SiO_2 leads to a much lower refractive index (1.558) and as a result offers the possibility of fabricating filters with a lower amount of layers. Other positive side effects include an increase in the speed of coloration and bleaching as well as an increased chemical stability in comparison with pure porous WO_3 films. Although multilayer filters based on such a configuration have not yet been proposed, Zayim has studied sol-gel deposited WO_3-TiO_2 composite films with a goal to increase their performance while also taking into account the thickness of the film and optical properties to increase transmittance (antireflection) [297]. Note, that in this particular case, the films are extremely porous (e.g., $n = 1.26$ at 688 nm).

Despite the presence of some drawbacks when using high SiO_2 concentrations such as an increase in charge trapping and a decrease of the electron diffusion coefficient, I believe that the filter presented in the following work is highly promising.

ARTICLE 4 : WO_3/SiO_2 COMPOSITE OPTICAL FILMS FOR THE FABRICATION OF ELECTROCHROMIC INTERFERENCE FILTERS

Bill Baloukas and Ludvik Martinu

Department of Engineering Physics, École Polytechnique de Montréal,
P.O. Box 6079, succursale Centre-ville, Montréal, Québec H3C 3A7, Canada

Applied Optics, vol. 51, no. 16, 2012, p. 3346-3356.

Abstract

New security devices based on innovative technologies and ideas are essential in order to limit counterfeiting's profound impact on our economy and society. Interference security image structures have been in circulation for more than twenty years but commercially available iridescent products now represent a potential threat. Therefore, the introduction of active materials, such as electrochromic WO_3, to present day optical security devices offers interesting possibilities. We have previously proposed electrochromic interference filters based on porous and dense WO_3 which possessed an angle-dependent and voltage-driven color shift. However, the low index contrast required filters with a high number of layers. In the present work, we increase the index contrast (0.61) by mixing WO_3 with SiO_2 and study the physical and electrochromic properties of mixtures. We next combine high and low index films in tandem configurations to observe the bleaching/coloration dynamics. To account for the film performance, we propose a simple explanation based on the differences in electron diffusion coefficients. An 11 layer electrochromic interference filter (EIF) based on the alternation of pure WO_3 and $(WO_3)_{0.17}(SiO_2)_{0.83}$ films with a blue to purple angular color shift is then presented. Finally, we discuss possible applications of these EIFs for security.

9.2 Introduction

Optical security devices play an essential role in the fight against counterfeiting [256]. Not only do they represent an obstacle for counterfeiters, but they are also a simple and effective means of authentication for the general public. For example, interference security image structures (ISISs) [33], which have been in circulation on Canadian banknotes since the late 1980s, have clearly demonstrated their effectiveness [2]. Unfortunately, there appears to be an increasing number of iridescent consumer products on the market (e.g. ChromaFlair inks by JDSU [298], co-extruded polymer-based filters [299], etc.) which can potentially be used to mimic present-day ISISs. To protect against these types of future threats, we have recently proposed security features that also benefit from the use of active materials [300], i.e., any material whose properties can be modified by the application of an external source of energy such as heat, light, pressure, current, etc. Specifically, we have studied a combination of a metameric ISIS [254] with an electrochromic (EC) device based on WO_3 [288], the most popular inorganic EC material [115]. This novel combination allows one to fabricate two-level authentication devices : the first level being the simple passive angle-dependent color shift of the ISIS, and the second level being the active electrochromic color variation.

More recently, we have succeeded in combining both previously mentioned authentication features into a single structure [301]. In fact, by simply modifying the density of WO_3 films, we were able to obtain a difference in index of refraction and thus obtain an optical contrast. This contrast is responsible for light reflection at an interface and therefore light interference in the presence of multiple interfaces [10]. More precisely, we presented various designs as well as fabricated a complete electrochromic interference filter (EIF) based on a stack of 27 dense (high index n_{H}) and porous (low index n_{L}) WO_3 layers. Such a high number of layers was required due to a fairly low index contrast (0.22). In the present work, we explore other alternatives to obtain a higher index contrast as well as a higher chemical stability.

While other authors have studied WO_3/SiO_2 mixtures to increase the performance of pure WO_3 [302, 303, 304, 305] (to increase the chemical and long term cycling stability, and quicken the bleaching/coloration dynamics), we propose these mixtures as an alternative method of lowering the index of refraction of WO_3 while still maintaining its electrochemical and mechanical integrity. Since SiO_2 is an effective electron barrier, controlling the amount of SiO_2 is crucial if one wants to lower the average index without completely blocking electron diffusion.

In the present work, we first study the effect of the addition of SiO_2 on the physical and electrochemical properties of WO_3. We analyze simple tandem configurations of pure WO_3 and WO_3/SiO_2 mixtures and evaluate their coloration and bleaching behaviour in anticipation

of more complex structures. We then test the electrochromic performance of an 11 layer blue to purple angle color shifting filter. Finally, we discuss possible solutions to the observed limitations as well as other potential device structures.

9.3 Experimental methodology

9.3.1 Deposition conditions

The pure and composite coatings were deposited by radio frequency dual magnetron sputtering in a custom-made vacuum chamber. The magnetrons were equipped with 50 mm diameter WO_3 and Si targets respectively. To fabricate the mixtures, the power of the WO_3 magnetron was set between 20 and 150 W, while in the case of Si it was maintained at 200 W. The samples were rotated at approximately 10 rpm to ensure thickness uniformity. All depositions were made at a 10 or 20 mTorr working pressure, which was varied by controlling the pumping speed using a throttling valve, in an Ar and O_2 gas mixture (4 :1 Ar to O_2 ratio). The base pressure was approximately 2.5x10^{-6} Torr.

The WO_3 coatings were deposited on 2.5 cm by 5 cm indium tin oxide (ITO) coated glass substrates from Delta Technologies with an average sheet resistance of 12 $\Omega/\square$. ITO substrates were initially cleaned with soap and de-ionized water, and in isopropanol for 15 minutes using an ultrasonic bath. In preparation for cyclic voltammetry measurements, part of the substrate was masked during the deposition to allow access to the ITO electrode.

9.3.2 Physical characterization

Samples were deposited on Si and on B270 glass for optical characterization. Variable angle spectroscopic ellipsometry (*M-2000* and *RC2* from J.A Woollam Inc.) combined with reflection measurements, both provided by the *RC2*, were used to obtain the optical properties (refractive index and extinction coefficient), as well as the physical thickness of all samples. The data were then analyzed with the *CompleteEASE* software (J.A. Woollam Co., Inc.) using a model based on Tauc-Lorentz [306] and gaussian oscillators to account for the UV absorption. The optical properties were then incorporated in the *OpenFilters* software [68] for the filter design.

To obtain the [W]/[Si] + [W] ratio and density of the films, Rutherford back scattering (RBS) measurements were performed in a Tandem linear accelerator with a 2.042 MeV He^+ ion beam at a scattering angle of 170° (between the forward direction of the incident beam and detector). To assess the amount of hydrogen contained in the films, this same accelerator was used for elastic recoil detection (ERD) measurements with a 1.5 MeV He^+ ion beam. The angle between the beam direction and the sample surface normal was 75° as well as between

the detector and the sample surface normal (30° scattering angle). To stop all ions except hydrogen ions, a 6 μm-thick mylar foil was placed in front of the detector [250].

Grazing incidence X-ray diffraction (XRD) was performed with a Philips *X'pert* diffractometer at a 1 degree angle of incidence with respect to the sample surface using Cu Kα (1.5406 Å) radiation. The acceleration voltage was set at 50 kV, and the filament current at 40 mA.

Finally, the surface topography of the films was investigated with a *Dimension 3100* atomic force microscope from Digital Instruments in contact mode.

9.3.3 Electrochromic characterization

Cyclic voltammetry measurements were performed using an *Autolab PGSTAT302N* potentiostat/galvanostat in a 0.1 M aqueous solution of H_2SO_4. A three-electrode configuration was used consisting of an exposed surface of approximately 0.59 cm^2 for the working electrode (WO_3 and WO_3/SiO_2 mixtures), a Pt foil as the counter electrode, and a SCE as the reference. In order to perform optical transmission measurements, the cell was also equipped with two windows : the first window consisting of an uncoated glass substrate, and the second window the sample under evaluation. The cyclic voltammetry measurements were performed at a 50 mV/s scan rate between -0.6 V and +1.5 V.

In situ transmission measurements were performed during cyclic voltammetry to evaluate the coloration efficiency (CE). The setup consisted of a stabilized deuterium tungsten halogen light source from Ocean Optics (*DH-2000*) equipped with an optical fiber outlet, a series of lenses to focus the beam onto the sample and collect the transmitted beam into a second optical fiber, and an Ocean Optics spectrophotometer (*USB2000*). This setup allows the acquisition of a complete spectrum (380 nm to 850 nm) approximately every 0.5 s (30 averaged measurements of 3 ms plus signal treatment time).

To obtain the electron diffusion coefficient (D_e) [307, 308], the samples deposited on B270 glass were placed between two aluminium frames and an O-ring. The cavity formed by the O-ring allowed us to add a 20 v/v % H_2SO_4 aqueous solution. The sample was then placed on an overhead projector and the image projected onto a white surface. A 1 mm indium wire (99.99% purity from Kurt J. Lesker) with a sharpened tip was next put into contact with the sample and a standard digital camera was used to photograph the projected image of the colored region every second. The time evolution of the coloration front was obtained from these pictures.

9.4 Results and discussion

9.4.1 Characterization of the pure WO_3 and WO_3/SiO_2 mixtures

Physical properties

In order to determine the lowest possible concentration of WO_3 which results in the loss of its electrochromic properties, we deposited a series of WO_3/SiO_2 coatings with different concentrations of SiO_2. The applied power on the WO_3 magnetron was set at a value varying between 20 and 150 W, while the SiO_2 magnetron's power was maintained at 200 W. All depositions were made at 10 mTorr, but in order to increase the porosity for reasons which will be explained in section 9.4.1 *Electrochemical properties*, four samples were also deposited at 20 mTorr (see Table 9.1). As expected, the deposition rate decreased with increasing total pressure [245] as well as for a decreasing WO_3 concentration (higher deposition rate of WO_3). As a result, for a better comparison of the samples, the deposition time was adjusted to maintain the thickness of the tungsten containing samples around 250 nm (average thickness is 280 $\pm$ 60 nm).

Following spectroscopic ellipsometry measurements on Si, we obtained the optical properties (n and k) of as deposited samples as presented in Figure 9.1. As can be seen in Figure 9.1, the index of refraction of the films decreases from 2.25 (pure WO_3) to 1.43 (pure SiO_2). Also note, that the absorption coefficient is negligible in the visible spectrum and that the absorption band is seen to move towards higher energies as the SiO_2 concentration increases [309]. This is to be expected due to the low energy bandgap of WO_3 (approximately 3.1 $\pm$ 0.1 eV in the case of our pure WO_3, typical for sputtered films, obtained from the Tauc relation [310] $h\nu\alpha$ vs $(h\nu - E_g)^2$) when compared to that of silica ($\sim$9 eV [311]).

It is possible to approximate the relative volume fractions of WO_3 and SiO_2 of the composite films by using an effective dielectric function [312, 313]. In the particular case of a heterogeneous medium, consisting of two constituents in comparable concentrations, the Bruggeman effective medium approximation (BEMA) can be used. One can calculate the effective index from the following equation :

$$f_{SiO_2}\frac{n_{SiO_2}^2 - n_{WO_3/SiO_2}^2}{n_{SiO_2}^2 + 2n_{WO_3/SiO_2}^2} + f_{WO_3}\frac{n_{WO_3}^2 - n_{WO_3/SiO_2}^2}{n_{WO_3}^2 + 2n_{WO_3/SiO_2}^2} = 0, \tag{9.1}$$

where f_{SiO_2} and f_{WO_3} are the relative concentrations of SiO_2 and WO_3, n_{SiO_2} and n_{WO_3} the refractive indices of the pure constituents and n_{WO_3/SiO_2} the effective index of the film. The resulting theoretical curve is plotted in Figure 9.2 where the minimal index value corresponds to pure SiO_2 and the highest to pure WO_3.

Table 9.1 Deposition conditions and thickness of the WO_3 and WO_3/SiO_2 mixtures. The concentration of WO_3, estimated from the Bruggeman effective medium approximation (see eq. 9.1), is also given.

Pressure [mTorr]	$\mathbf{P_{WO_3}}$ [W]	$\mathbf{P_{SiO_2}}$ [W]	**Thickness** [nm]	$[\mathbf{WO_3}]$ [%]
10	150	0	255	100
10	150	200	256	78
10	100	200	270	68
10	75	200	284	57
10	50	200	290	29
10	40	200	288	17
10	30	200	311	9
10	28	200	289	7
10	25	200	230	6
10	22	200	298	5
10	20	200	230	5
10	0	200	68	0
20	150	0	226	100
20	75	200	292	40
20	50	200	325	23
20	40	200	288	16

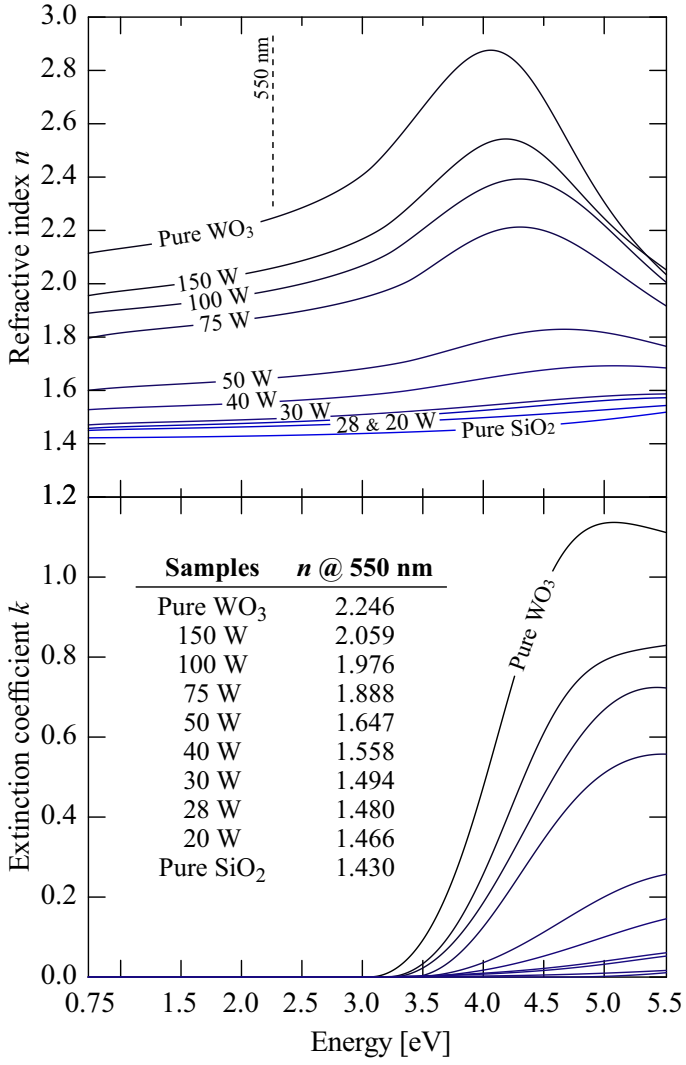

Figure 9.1 Refractive index and extinction coefficient as a function of energy for pure WO_3 and mixed WO_3/SiO_2 films deposited at 10 mTorr. The index of refraction at 550 nm is also shown (2.26 eV). Note that the absorption is negligible in the visible range of the spectrum.

To support the validity of this model, RBS and ERD measurements were performed on four samples. The results are shown in Figure 9.2 as the ratio of [W]/[Si]+[W] as well as the calculated density of the films. The 6.38 g/cm^3 density obtained for pure WO_3 is typical of sputtered films and has been discussed in more detail in [301], whereas the low density obtained for the high SiO_2 concentration films is also typical for porous SiO_2 [314]. As for the [W]/[Si]+[W], the values obtained are fairly close to the BEMA curve (see Figure 9.2). Note that XRD measurements contained a few very wide peaks associated with WO_3. From these peaks, the WO_3 grain size was approximated by the Scherrer equation [315] to be between 1 and 2 nm. Henceforth, we will consider the as-deposited films as forming a composite material, as being essentially amorphous and all samples will be identified using the BEMA model concentration values (see Table 9.1).

It is also interesting to note that the ERD measurements have indicated a concentration of hydrogen which is maximum for the $(WO_3)_{0.17}(SiO_2)_{0.83}$ sample. The detection of hydrogen suggests the presence of absorbed water [157] which is an indicator of the existence of porosity in the films. A similar trend can be observed from the atomic force microscopy images of these same samples (see Figure 9.3). As can be seen, the addition of SiO_2 leads to a higher root mean squared (RMS) roughness, to a higher peak difference in amplitude (between the minimum and maximum values), as well as to a much coarser surface topography. These same samples are also the ones possessing the highest hydrogen content, and therefore, can be considered as having the highest porosity.

Electrochemical properties

In order to assess the electrochromic performance of our films, we performed cyclic voltammetry measurements (see Figure 9.4). Samples were allowed to reach a steady state during the initial ten cycles : the 11$^{\text{th}}$ cyclic voltammogram is thus shown here. The first thing to observe, is the shape of the voltammograms which changes drastically as the concentration in WO_3 decreases. Interestingly, the sample with 29% WO_3 has approximately the same amount of injected charge (2.14 mC) as the pure WO_3 film (2.11 mC) even though it contains three times less WO_3. The variation in transmission, ΔT, for both these samples is also essentially the same ($\Delta T = 19\%$). This can in part be explained by the fact that the high SiO_2 concentration sample possesses a more open microstructure, and therefore a more effective surface area, which in turn affects the transfer rates between the electrolyte and WO_3 [283]. One can also see that the surface area difference (SAD) of the 29% WO_3 is almost twice as large as the SAD of the pure WO_3 sample (see Figure 9.3a and 9.3c) [316].

In the case of lower WO_3 concentrations ($< 29\%$), the voltammograms are seen to decrease in area, even though these films also possess a microstructure which is comparable to the

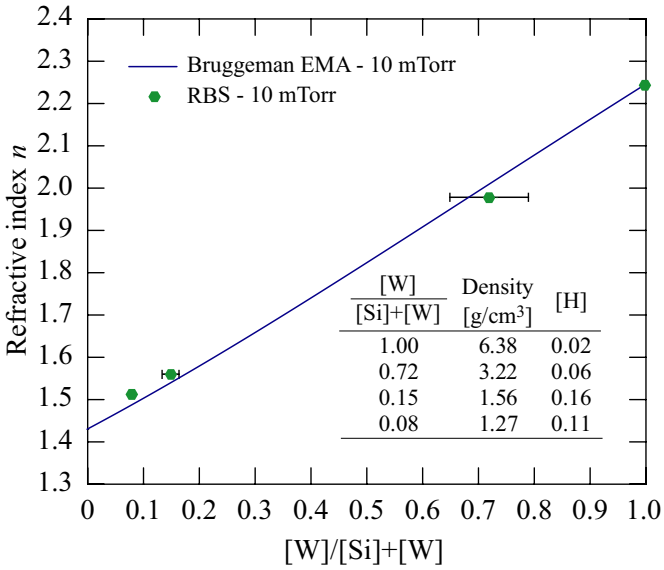

Figure 9.2 Refractive index at 550 nm as a function of the relative WO_3 concentration estimated from the Bruggeman effective medium approximation for films deposited at 10 mTorr. The [W]/[Si]+[W] values obtained from the RBS measurements are also plotted with their corresponding refractive index. The density of the films and their hydrogen content are also shown.

29% WO_3 sample. This is a clear indication that the presence of SiO_2 is beginning to affect the electrochromic performance. For example, in the case of the $(WO_3)_{0.09}(SiO_2)_{0.91}$ sample, the inserted charge is 0.83 mC, and the ΔT value is only 7%. Samples with lower WO_3 concentrations are not shown since they exhibited no EC activity. This disappearance of the EC properties of the films is most probably due to a complete isolation of the WO_3 regions by the SiO_2 material which inhibits any electrons from reaching it analogous to a percolation threshold [302].

To better evaluate the coloration and bleaching performance of the films, it is useful to plot the data of Figure 9.4 in another format ; in this particular case, the inserted charge as a function of time (see Figure 9.5). From Figure 9.5 one can clearly see that the coloration and bleaching speeds are faster for the high SiO_2 concentration films except the 9% WO_3 concentration mixture (although not shown, the transmission variation follows a similar trend). This increase in the response time has also been observed by other authors [303, 305] and was attributed, similarly to our observations, to the presence of an abundant number of diffusion channels and a higher number of phase boundaries available for hydrogen diffusion. Indeed, it has been proposed that space-charge layers can form at the boundaries between both media leading to an enhanced ion conductivity [317, 318].

At this point, one might argue that simply increasing the porosity of WO_3 could also

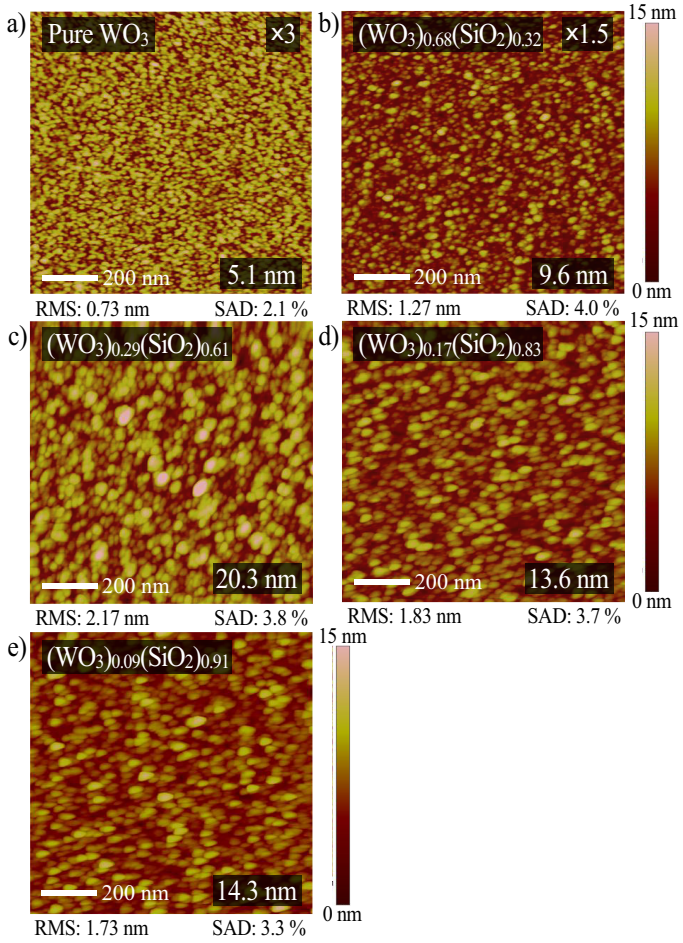

Figure 9.3 Atomic force microscopy images of pure WO_3 and WO_3/SiO_2 mixtures (identified in the upper left corner). The RMS roughness and surface area difference (SAD) are also indicated under each image. The maximum amplitude difference between the minimum and maximum values is shown in the bottom right corner ; we indicate the scaling factor, which was required in order to maintain the same color scale, in the upper right corner for (a) and (b).

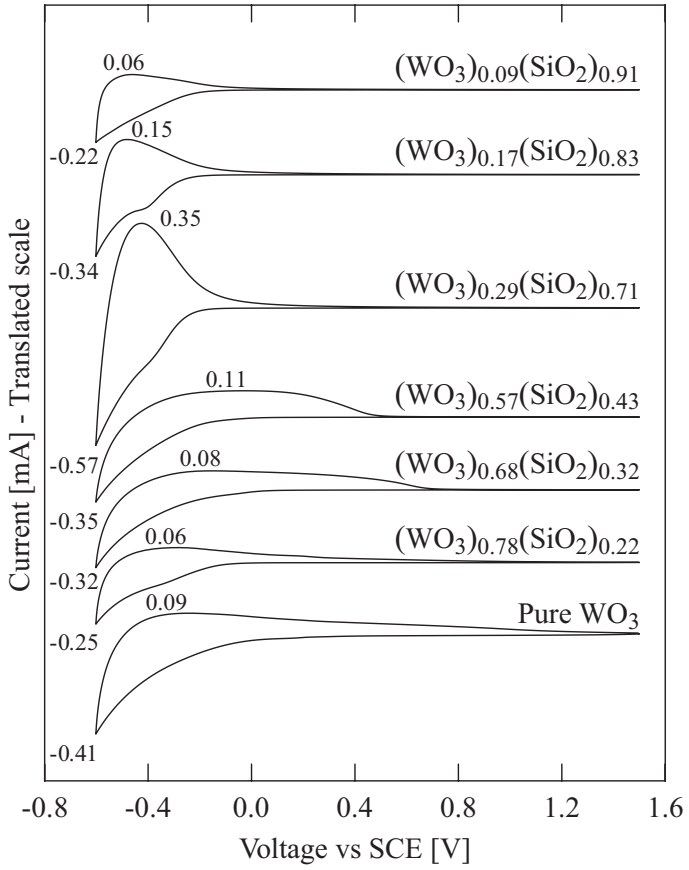

Figure 9.4 11th cyclic voltammogram for films deposited at 10 mTorr with various WO_3 concentrations. The minimum and maximum current values of each cycle are also indicated on the left side of the voltammograms.

result in a similar increase in speed [118, 285]. For this reason, we deposited a higher porosity pure WO_3 film at 20 mTorr (also presented in Figure 9.5). Although the bleaching time is considerably shorter for this sample, when compared with the pure 10 mTorr sample, the insertion/extraction charge peak is still much wider than for the $\leq$ 29% WO_3 composite films. As a result, we believe this is an indicator that porosity and SiO_2 content do not have the same effect on the coloration/bleaching mechanisms. It is also important to note that the WO_3/SiO_2 mixtures start coloring at later times (more negative voltage). This indicates that the barrier for hydrogen transfer across the film-electrolyte interface or the barrier for electron transfer across the ITO-film interface is larger [115] (we will show below that the latter one seems to be the most plausible cause). The fact that these films contain less WO_3 may also result in a faster increase of the insertion coefficient (x in H_xWO_3) and thus faster change in chemical potential. This would then lead to the rapid formation of a large back electromotive force (EMF) [114] which would explain the rapid drop in charge of the composite films during coloration (maximum inserted charge is reached faster). A larger back EMF would also play a beneficial role during the bleaching phase thus resulting in a quicker response [114]. Finally, porous layers are generally assumed to contain more water (e.g., higher hydrogen concentration as confirmed by ERD measurements) ; this can also lead to faster electro-optic response times [286], since water serves as a source of hydrogen ions as well as an electrolyte for ion transfer inside the film during the coloration and bleaching processes [287].

Although the composite films show a faster response, too much SiO_2 leads to charge trapping [319] as is shown in Figure 9.5 (the red dotted line indicates a complete extraction of inserted charges, and the indicated number represents the ratio of extracted vs inserted charge). Furthermore, the fact that these films contain lower quantities of WO_3 can also result in higher ion intercalation levels and thus increase the probability of deep charge trapping [319].

From the maximum anodic current obtained during the cyclic voltammetry measurements, we also calculated the ionic diffusion coefficients (D_i of the films by using the Randles-Sevčik equation [114] (see Figure 9.6a) :

$$i_p = -0.4463 n_e F A c_s \sqrt{\frac{n_e F v D_i}{RT}}, \tag{9.2}$$

where n_e is the number of electrons taking part in the reaction, F is the Faraday constant (C/mol), A is the working electrode area (cm^2), c_s is the solution concentration (mol/cm^3), v is the scan rate (V/s), R is the universal gas constant ($J/mol \cdot K$), and T is the ambient temperature (K). As expected, the densest film (10 mTorr pure WO_3) possesses one of the lowest

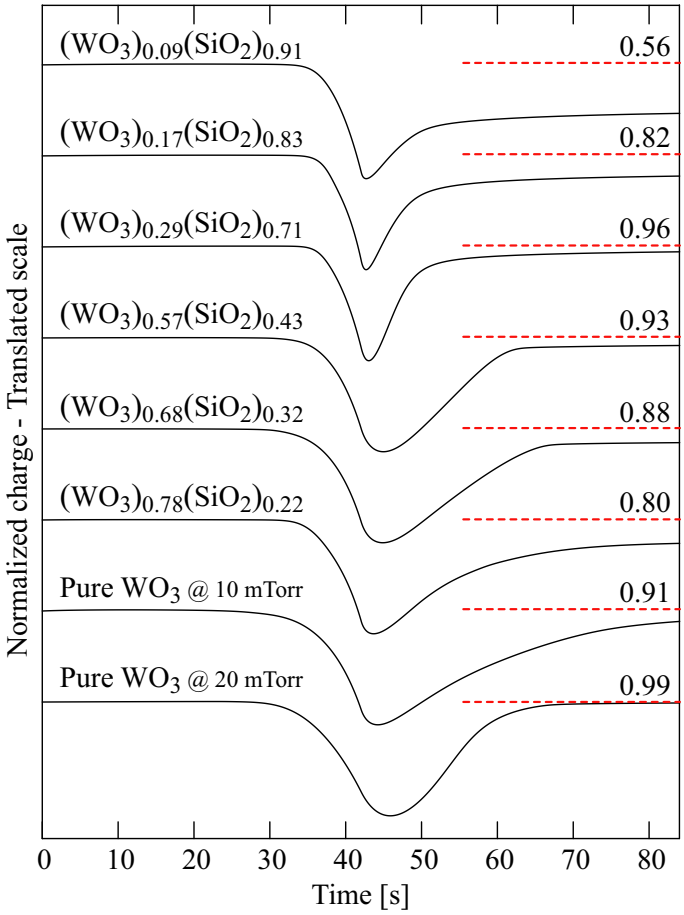

Figure 9.5 Normalized inserted charge evolution as a function of time calculated from the 11th voltammogram presented in the previous figure. The charge was normalized using the maximum inserted charge of each voltammogram. The ratio of extracted vs inserted charge is also indicated on the right side of the figure (dashed line).

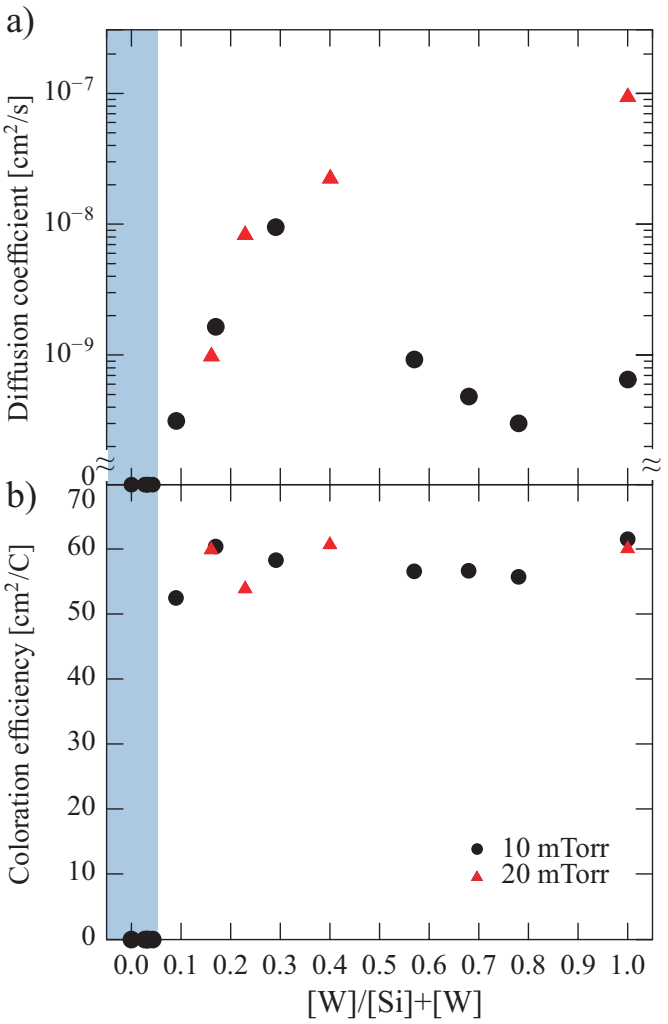

Figure 9.6 (a) Ionic diffusion coefficient and (b) coloration efficiency ($CE_{550\,nm}$) for the 11th cycle of films deposited at 10 and 20 mTorr. The light blue area indicates the region for which the samples indicated no EC activity.

overall D_i ; this in part explains its very slow bleaching rate (see the voltammogram of pure WO_3 in Figure 9.4), a result which is in agreement with what was obtained by other authors [149, 273]. The trend which is observed is also in agreement with our previous observations relating to the films' porosity since the maximum D_i is obtained for the $(WO_3)_{0.29}(SiO_2)_{0.71}$ sample. In the case of the sample deposited at 20 mTorr, the value of D_i of the pure film is significantly higher, but as the amount of WO_3 is lowered the D_i values are seen to match with their 10 mTorr counterparts. This once again indicates that the dynamic behaviour of the composite films is highly affected by the presence of SiO_2. Also note that the samples with the lowest D_i are also the ones with the highest trapping (lowest extracted vs inserted charge ratio) [320].

From the *in situ* transmission measurements taken during the cyclic voltammetry, it is possible to calculate the CE given by [114] (see Figure 9.6b) :

$$\mathrm{CE} = \frac{ln[T_b/T_c]}{[Q/A]}, \tag{9.3}$$

where T_b is the optical transmission in the bleached state, T_c the optical transmission in the colored state, Q (C) the inserted charge, and A the working electrode area (cm^2). Although the CE has been shown to depend on the intercalation level [289] and to increase with porosity [290], due to an increased delocalization of the inserted electrons, it is interesting to note that the CE obtained here is approximately constant for all samples. For the samples that contain less than 9% WO_3, the CE is simply equal to zero due to the absence of transmission variation and hence essentially no EC behaviour. This again suggests that the presence of SiO_2 does not affect the WO_3's electrochromic performance but rather the dynamics of the EC process.

9.4.2 Characterization of double layer systems

We can conclude, from the previous analysis, that the addition of SiO_2 leads to changes in the dynamics of coloration and bleaching. Although higher SiO_2 concentrations lead to a lower index of refraction, they can also result in charge trapping and eventually to the complete disappearance of the EC properties of the film. Before considering the complex case of a complete interference filter, we first explore tandem configurations based on pure WO_3 and composite WO_3/SiO_2 films ; the following double layer stack samples were thus deposited :

A : ITO|72 nm $(WO_3)_{0.17}(SiO_2)_{0.83}$|101 nm WO_3, and
B : ITO|92 nm WO_3|86 nm $(WO_3)_{0.17}(SiO_2)_{0.83}$,

where the WO_3/SiO_2 mixtures were deposited at 10 mTorr and the pure WO_3 films at 20 mTorr. We chose the 83% SiO_2 concentration film for its very low refractive index (1.558) even though the 71% SiO_2 film presented a better EC performance. This configuration thus allowed us to maximize the refractive index contrast, at a value of 0.61, between both films. We also chose the 83% SiO_2 mixture to accentuate the possible adverse effects introduced by the use of high SiO_2 concentrations. The cyclic voltammograms as well as the transmission variation of both these samples are presented in Figure 9.7. For comparison, this same figure also shows the performance of the individual films presented in the previous section.

The results in Figure 9.7 clearly reveal that both tandem configurations behave very differently. In the case of sample A, the onset of coloration occurs at essentially the same time as the single $(WO_3)_{0.17}(SiO_2)_{0.83}$ film. The fact that this film (in Sample A) is not in direct contact with the electrolyte seems to indicate, as previously mentioned, that it is the ITO$|(WO_3)_{0.17}(SiO_2)_{0.83}$ interface region which is responsible for the delayed coloration. More importantly, in the case of sample B, the coloration onset is only slightly affected when compared with the pure film even though the $(WO_3)_{0.17}(SiO_2)_{0.83}$ material is in direct contact with the electrolyte. This once again confirms that the insertion of hydrogen is not hindered by high SiO_2 concentrations.

Let us now look at the coloration and bleaching phases of both samples in more detail. In the case of sample B, although its minimum transmission is not as low as that of the single material WO_3 film (20 mTorr), the shape of its voltammogram and transmission variation curve is practically the same (similar coloration/bleaching mechanism). This suggests that the top $(WO_3)_{0.17}(SiO_2)_{0.83}$ film's only effect is to slightly limit the amount of inserted charge leading to the minimum obtained transmission. This is not the case for sample A, where one can note a very different performance. Although its coloration phase is similar to that of the other samples, it possesses a very slow bleaching phase. This is the reason why the transmission is seen to start at approximately 75%; the sample was simply unable to completely bleach during the previous cycles. In comparison, in spite of a fairly small transmission variation, the single material $(WO_3)_{0.17}(SiO_2)_{0.83}$ film had very little problem bleaching in the allocated time albeit it did show some charge trapping. Hence, since both single films do not present such a slow bleaching phase, the observed behaviour is most probably due to the addition of the $(WO_3)_{0.17}(SiO_2)_{0.83}|WO_3$ interface.

As mentioned above, sample B shows no signs of trapping, and charge transfer dynamics which are very similar to the pure 20 mTorr WO_3 film. As a result, one may assume that the $(WO_3)_{0.17}(SiO_2)_{0.83}$ film is predominantly not participating in the EC effect and that the hydrogen is merely passing through it and not encountering any electrons. To investigate this further, we proceeded with measuring the electron diffusion coefficient D_e using the method

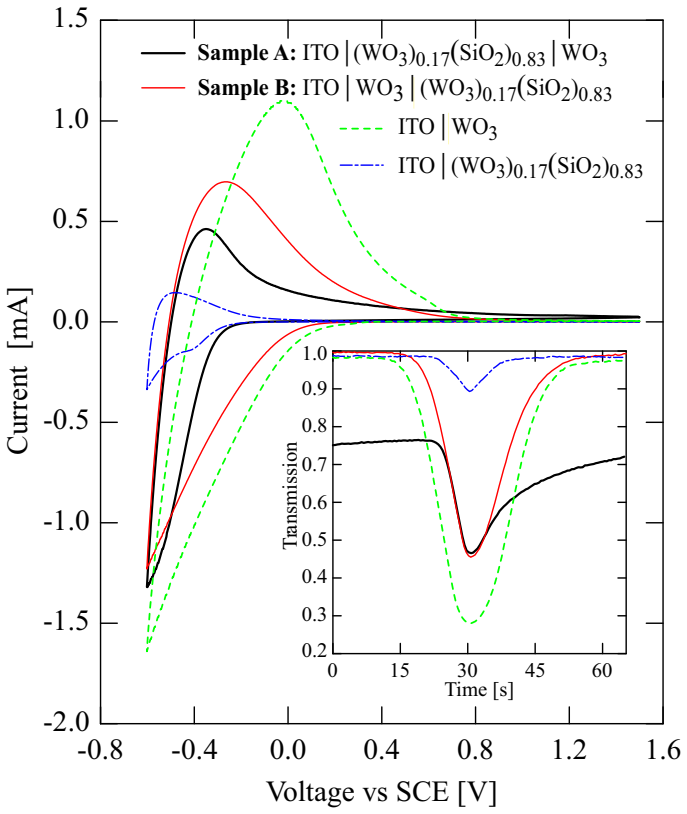

Figure 9.7 11th cyclic voltammograms of two tandem film configurations (A and B) and the individual films they are based on. The transmission variation during this same cycle is also shown in the lower right corner. Note that the transmission reference was made in the bleached state.

developed by Crandall *et al.* [307, 308]. By placing an indium wire in contact with a WO_3 containing film covered by a H_2SO_4 solution one rapidly observes the formation and growth of a blue circle around the point of contact of the indium wire. This coloration is due to the liberation of electrons at the indium tip (dissolution of In in the acid and formation of In^{3+} ions and 3 electrons) and the resulting hydrogen insertion to preserve the sample's neutrality. One can demonstrate from the diffusion equation that in the case of the coloration front (maximum rate of change in concentration area) that :

$$\frac{r_c^2}{2D_e t} = 1, \tag{9.4}$$

where r_c is the radius of the colored circle (cm), D_e the electron diffusion coefficient (cm^2/s) and t the time. Figure 9.8 shows the evolution of the coloration front for a pure WO_3 sample and for two samples containing 68% and 57% of WO_3. We can clearly see that equation 9.4 is valid since we get a correlation coefficient χ^2 close to 1 for all three samples and that the D_e is very much affected by the addition of SiO_2 (the diffusion coefficients are presented in Table 9.2). The value of 0.013 cm^2/s obtained for pure WO_3 is very similar to that obtained by other authors [308] and it should not change much by changing the porosity of the films (e.g., for the 20 mTorr film).

Higher SiO_2 concentration mixtures with even lower diffusion coefficients were not tested for practical reasons, but by extrapolating, one can approximate the value of the D_e for the $(WO_3)_{0.17}(SiO_2)_{0.83}$ sample at $4x10^{-7}$ cm^2/s. Since there is a five orders of magnitude difference between the D_e for the pure and the composite films, we can assume that in the case of samples A and B, electrons will accumulate at the interface when diffusing from a high to a low D_e region. It follows that a space charge limiting effect develops at the interface, and we believe that this explains the observed behaviour of samples A and B. In fact, this could explain why the bleaching phase is slowed down for sample A and why the composite film is essentially not participating in the EC properties of sample B. Although the differences in ion diffusion coefficients are not as large between the pure and composite films, one could also expect a similar ion accumulation at the interface but with minor consequences ; the accumulation would be much slower considering the slow diffusion rates of the ions. That being said, the diffusion coefficient of the electrons is still significantly higher than the ion diffusion coefficient so that the coloration and bleaching mechanisms are still limited by the ion diffusion in the materials themselves.

Table 9.2 Ionic and electron diffusion coefficients for a pure WO_3 film and two composite films all deposited at 10 mTorr. The D_i was calculated using the Randles-Sevčik equation (see eq. 9.2) and the D_e was measured using the method developed by Crandall (see eq. 9.4).

Sample	D_i [cm^2/s]	D_e [cm^2/s]
Pure WO_3	$6.5x10^{-10}$	$(13 \pm 1)x10^{-3}$
$(WO_3)_{0.68}(SiO_2)_{0.32}$	$4.8x10^{-10}$	$(5 \pm 1)x10^{-4}$
$(WO_3)_{0.57}(SiO_2)_{0.43}$	$9.2x10^{-10}$	$(4 \pm 2)x10^{-5}$

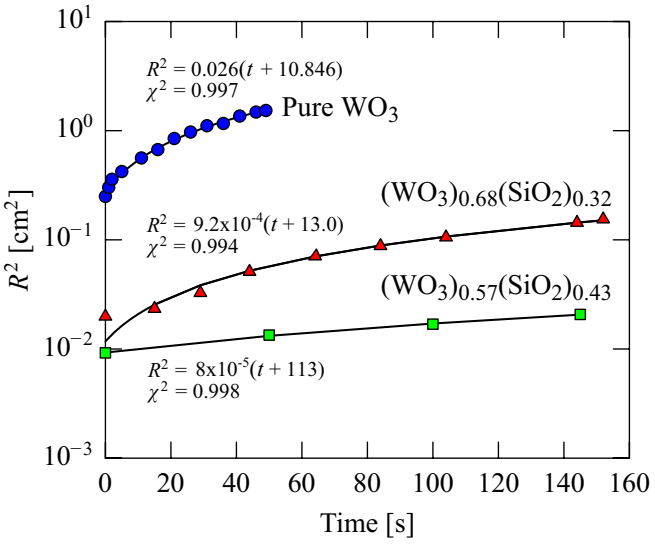

Figure 9.8 Evolution of the coloration front as a function of time for pure WO_3 and two composite films all deposited at 10 mTorr. Note that the initial radius does not start at zero since the image capture was not synchronized with the indium wire contact time and that the indium wire's finite size limits initial measurements.

9.4.3 Electrochromic interference filter

In regard of the preceding results, we fabricated an 11 layer filter based on a succession of pure WO_3 and composite WO_3/SiO_2 layers. We chose the pure WO_3 deposited at 20 mTorr as the high index of refraction material ($n_H = 2.169$) due to its excellent EC properties [large transmission variation ($\Delta T = 70\%$ at 550 nm) and high extracted vs inserted charge ratio (0.99)]. As for the low index material ($n_L = 1.558$), we chose the $(WO_3)_{0.17}(SiO_2)_{0.83}$ for the same reasons mentioned in section 9.4.2. The resulting transmission spectrum of the fabricated filter with its characteristic angle dependent color variation from blue to purple are shown in Figure 9.9.

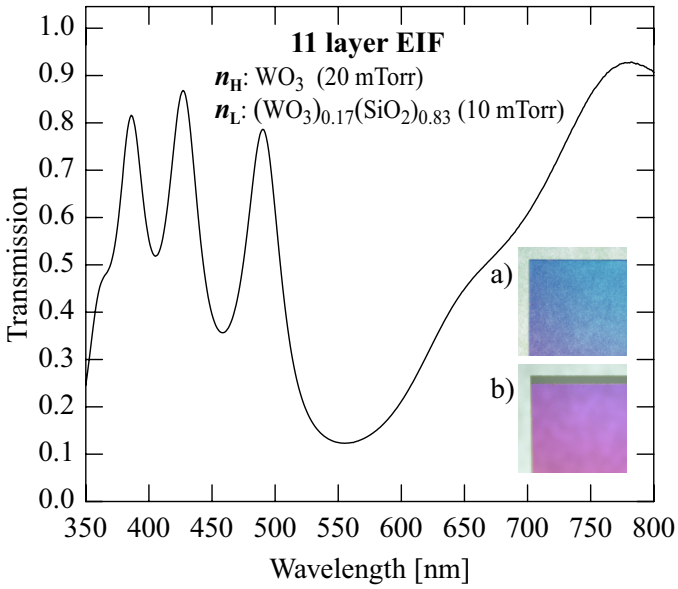

Figure 9.9 (Color online) Transmission spectrum of a fabricated 11 layer interference filter on B270 glass based on pure WO_3 as the high index of refraction and a mixed $(SiO_2)_{0.83}(WO_3)_{0.17}$ film as the low index of refraction material. Pictures of the filter at (a) normal incidence and at (b) a 50° angle show its blue to purple color shift in transmission.

Cyclic voltammetry was performed on the interference filter and its transmission variation was measured *in situ*. Figure 9.10 shows the evolution of the transmission at two different wavelengths (650 nm and 750 nm) for a series of 100 cycles. These wavelengths were chosen since they are outside the maximum reflection band of the filter and closer to the maximum absorption band of amorphous WO_3 (around 1 μm [264]). Note that the transmission at both wavelengths starts off at 100% since the reference spectrum was taken in the bleached state of the filter. The first thing one notices is that the colored state transmission is very low in both cases. Unfortunately, although this low transmission is interesting, the initial five cycles show a very rapid decrease of the bleached state transmission. However, for the subsequent

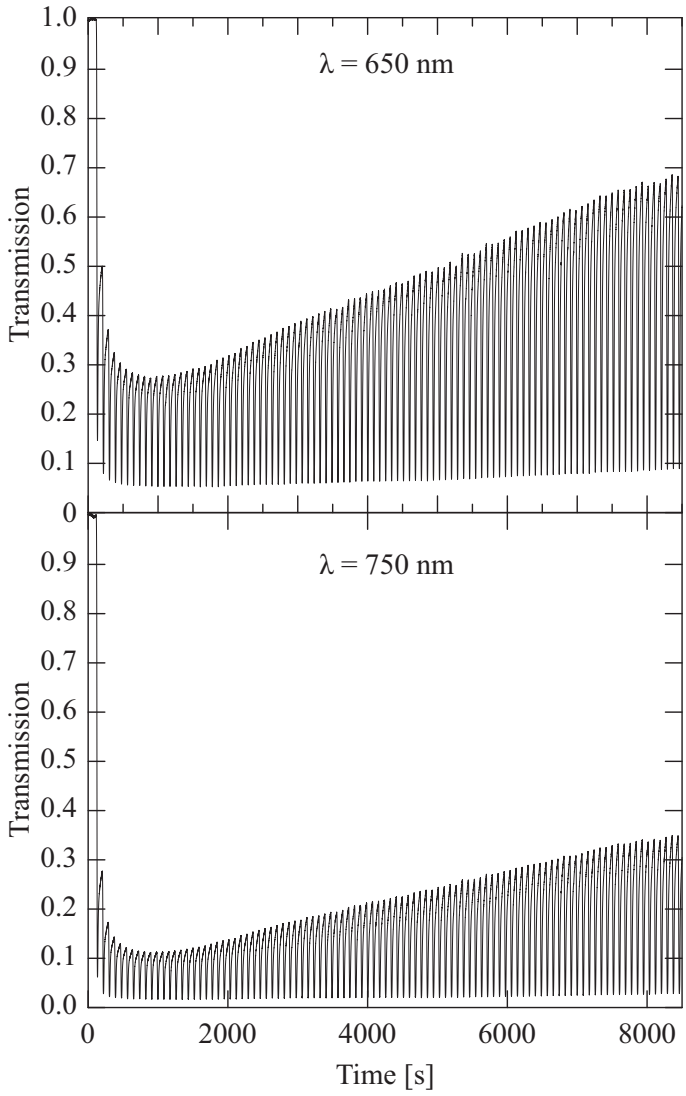

Figure 9.10 Transmission variation as a function of time during 100 cyclic voltammetry cycles for the 11 layer interference filter presented in Figure 9.9. The wavelengths were chosen outside the reflection band of the filter and closer to the maximum absorption band of amorphous WO_3 around 1 μm. Note that the transmission reference was made in the bleached state.

cycles, the ratio of extracted vs inserted charge stabilizes at around 0.95 ; a relatively good value when compared to the 0.82 value obtained for the single $(WO_3)_{0.17}(SiO_2)_{0.83}$ film. On the other hand, as the number of cycles is increased, the ΔT slowly increases so that even after 100 cycles this trend is still ongoing. This could be the result of changes in the optical properties of the filter's individual layers and/or an improvement of the performance of the filter due to the creation of pathways from the repeated insertion and extraction of ions (e.g., the D_i increased as a function of the number of cycles).

Looking closely at the individual cycles, we also notice that the transmission is still increasing and has not yet reached a steady state before the following cycle. This trend is similar to what was observed for the previously presented tandem film configuration A. The fact that the present filter contains five $(WO_3)_{0.17}(SiO_2)_{0.83}|WO_3$ interfaces will only amplify the space charge limitation effect proposed in section 9.4.2. Consequently, the incomplete bleaching of the filter results in a slightly bluish residual color which could have a negative impact on its angle dependant color shifting properties. A longer bleaching time as well as a higher applied voltage could help minimize this problem.

Finally, the presented filter clearly demonstrates that an increased refractive index contrast offers the opportunity of obtaining interesting angle dependent color shifts with a reasonable number of layers. Indeed, a low number of layers is essential if active interference filters are to be used as optical security devices and in other applications. This high index contrast also allows for more design versatility and, therefore, opens the door for more complex designs (e.g., metameric filters [254]). The strong variation in transmission seen during cyclic voltammetry also indicates that the voltage-driven color change between a transparent blue to dark and opaque blue would be significant enough to be clearly observed.

9.4.4 Possible solutions for an improved performance and applications

As we have observed for the previous 11 layer filter, there are two areas of possible improvement of its performance, mainly decreasing the amount of charge trapping and minimizing the effect of the interfaces. For the former, the simplest solution would be to use composite films with higher WO_3 concentrations. This will inevitably decrease the index contrast but should lead to a better performance. To counteract this issue, one could also consider increasing the porosity of the composite films and thus compensate for the higher refractive index [301]. As for the latter, graded index filters could potentially be an attractive solution [312]. By eliminating the presence of interfaces one could rapidly assess their effect on the EC response ; e.g., by comparing with a similar multilayer filter. Also, increasing the electron diffusion coefficient of the WO_3/SiO_2 films in order to decrease the contrast with the pure films could alleviate the space charge limitation effects we have observed. This could be

achieved by doping them with low quantities of a conductive material.

Although the EIF presented in this work was an example of a transmission-based security device, one can also consider a similar reflection-based device. As a matter of fact, we have tested structures using a simple two layer design, such as sample B shown above, on a reflective metallic layer. When covering it with another semi-transparent metallic electrode one can obtain interesting properties similar to the structures forming Deb-type devices [183]. In fact, similar Fabry-Perot-like structures are currently being used in security for their effective angle-dependent color variation, for example, in optically variable inks [47]. The simple addition of a WO_3 film can thus render these structures electrochromic. The second low index film could also be based on pure SiO_2 as we have shown that it induces very little effect on the EC performance of the underlying film. In the case of a Deb device, the overlying film has been shown to serve as a source of hydrogen through the presence of absorbed water [131] ; as a result, a humid environment is required for them to function. Then again, replacing the SiO_2 layer by Cr_2O_3 has also been demonstrated in devices which function even under vacuum [189].

9.5 Conclusion

We have shown that the addition of SiO_2 to WO_3 results in a significant decrease of the index of refraction to a value of approximately 1.5 before the complete disappearance of the EC properties of the film, providing a high index contrast. We have found that the dynamics of the EC effect is very much affected by the SiO_2 ; particularly, for high concentrations of SiO_2, the bleaching and coloration times were significantly shortened. However, WO_3 films with a high concentration of SiO_2 exhibited an increased probability of charge trapping.

We tested tandem configurations of pure WO_3 and mixed WO_3/SiO_2 films and demonstrated that the interface between both films plays an important role in the coloration/bleaching dynamics. We proposed that an accumulation of electrons at the interface, due to large differences in the electron diffusion coefficients of the high and low index films results in a space charge limited effect. As a consequence, we observed a significant increase in the bleaching time for samples based on the ITO|composite|pure WO_3 configuration ; under such conditions, the electrons need to transit from a fast to slow electron diffusion area during bleaching.

Finally, we demonstrated a possibility of fabricating a complete electrochromic interference filter (EIF) based on pure WO_3 and WO_3/SiO_2 mixture layers providing a 0.61 index contrast. This EIF was shown to possess a blue to purple angle-dependent color change as well as a voltage driven color switch. Such effects are particularly suitable for optical security devices with two levels of authentication. On the other hand, there are still several open

issues to resolve. Mainly, the EIF's bleached state transmission initially decreased fairly rapidly although it was slowly regained as the number of cycles increased. This low bleaching resulted in a bleached state with a slightly bluish tint which could affect the angle-dependent color shift.

Our future efforts will, therefore, focus on improving the performance of the EIFs by implementing more porous WO_3/SiO_2 layers with lower SiO_2-concentrations. Such systems appear very promising for all-solid state EC devices.

9.6 Acknowledgments

Bill Baloukas acknowledges Le Fonds Québécois de la Recherche sur la Nature et les Technologies (FQRNT) and the Natural Sciences and Engineering Research Council of Canada (NSERC) for their scholarships. The authors wish to thank Dr. M. Chicoine for the RBS and ERD measurements, F. Turcot and S. Chenard for their expert technical assistance, G. Taillon for the AFM measurements and A.-L. Phaneuf-L'Heureux for her help with some of the experiments. A special thanks goes to Dr. O. Zabeida for his valuable comments, and Dr. J.-M. Lamarre of the National Research Council of Canada for fruitful discussions. This work was supported by NSERC of Canada through its STPGP 350496-07 strategic grant and its RGPIN 105819-05 discovery grant.

CHAPTER 10

GENERAL DISCUSSION, CONCLUSIONS AND PERSPECTIVES

10.1 Foreword

In this final chapter, I will go over the main results presented in the previous four chapters as well as discuss how these results have fulfilled the objectives presented in Chapter 1. I will then present possible interesting avenues to explore at the FCSEL in order to increase our understanding of the presented materials and structures, explore new possibilities, as well as to make the presented concepts a reality.

10.2 Main results

I first demonstrated how it is possible to design ISISs with interesting color shifts but which also present an additional property that is metamerism. By combining two filters with identical colors at a specific angle and different colors at other angles of incidence, interesting optical effects are possible.

On the other hand, the use of two interference filters would be quite expensive in a commercial application notwithstanding the fact that they are also extremely difficult to fabricate due to their high sensitivity to deposition errors (two filters, each varying in color). Indeed, it was demonstrated that it is, for all practical reasons, almost impossible to obtain a good color match between the two presented filters even when considering a $\pm 0.5\%$ error in thickness for each individual layer (a $\pm 1\%$ resolution is most often the maximum value which can be obtained in many optically monitored large-scale deposition systems). The solution to this problem was the replacement of one of the filters by a NIM which is much cheaper to deposit but also more stable in terms of color. By designing filters which match the transmission or reflection spectra of these NIMs, it was shown that universal metameric devices could be fabricated, that is, they can be authenticated under essentially any conventional light source as well as by colorblind individuals (I've actually tested and confirmed this hypothesis on a colorblind colleague of mine). Contrary to a standard ISISs, the metameric devices possess an intrinsic color reference (the NIM) which prohibits the use of other color shifting products. They also offer the additional option of creating an appearing or disappearing image effect as a function of the observation angle.

In an attempt to lower the number of layers of the metameric filters, a design methodology based on the use of the luminous efficiency curve of the human eye was developed. By

using transmission targets with tolerances which are inversely proportional to the luminous efficiency curve (maximum weight in regions of highest sensitivity), I showed how filters with a lower number of layers can be designed without compromising their multi-illuminant and multi-observer performance. Indeed, this methodology allows the filter's spectrum to diverge from the reference NIM's spectrum in the low and high wavelength regions where the eye is less sensitive. Obviously, the luminance efficiency, which also corresponds to the $\bar{y}$ color matching function (see Chapter 2), is only one of three components used in color calculations. Therefore, this design methodology cannot be used by itself, but must be combined with color target coordinates under at least one illuminant. On the other hand, it does guide the optimization process in the right direction by reducing the amount of possible solutions since there exist an infinity of metameric spectra resulting in color matches.

This work on metameric ISISs was then followed by the introduction of a novel concept based on the combined use of an ISIS and ECD. The ECD, which was based on a Deb-type ITO|WO_3|SiO_2|Au architecture, was shown to vary in transmission repeatedly under the application of a ± 3 V potential. By designing a metameric filter matching an intermediate colored state of the ECD, is was possible to create a device displaying a disappearing image effect during coloration. As previously mentioned, such a device possesses two levels of authentication. It was also noted that the dynamic nature of the NIM (the ECD in this case) actually lowers the constraints on the control of the thickness of the layers of the metameric filter.

To combine both the features offered by the previous active device, I then demonstrated that by using porous and dense WO_3 films, it is possible to design and fabricate electrochromic interference filters. But before getting into the complex case of a complete interference filter, I studied the effect of porosity on the physical and electrochemical properties of WO_3 films. It was shown that dense films presented minimal transmission variation, slow response times as well as some charge trapping (resulting in a decreasing bleached state transmission). The porous films on the other hand presented large transmission variations, faster response times and very little charge trapping, but due to the very aggressive nature of the electrolyte, degraded fairly rapidly. Tandem configurations were then tested and confirmed that an overlying dense film did not inhibit the coloration of the underlying porous film and that it also added some protection to the porous film against dissolution. A 27-layer filter was then fabricated and tested, thus demonstrating that the concept of an electrochromic interference filter is possible.

I concluded this part of my work by discussing the possible application of these filters in smart windows. By replacing the single WO_3 film by a filter it becomes possible to increase the transmittance in the bleached state, reflect the near infrared or even give the window

a particular color (e.g., more neutral color). In Chapter 8, we effectively demonstrated an increased luminance transmittance using air as the incident medium. Note, that although in a real window air would not be the incident medium (presence of electrolyte), the methodology still allows one to minimize the losses in reflection at the interface.

Finally, in an effort to increase the index contrast previously obtained using porous|dense WO_3 (0.22), I decided to add SiO_2, a low index of refraction material, to WO_3. The composite films' physical and electrochemical properties were once again studied prior to their integration in a more complex structure. Composite films with refractive indices varying between pure SiO_2 and pure WO_3 were shown to have different coloration and bleaching dynamics. The addition of SiO_2 led to an increase in speed, but too high concentrations increased the probability of charge trapping. Films with concentrations of WO_3 as low as 10% still manifested EC properties thus allowing for very low refractive indices to be obtained. When testing tandem configurations, it was determined that the interface between the pure and composite films played a significant role during the coloration and the bleaching phases. Most surprisingly, the order in which the films were deposited (composite|pure versus pure|composite) had a profound impact during the bleaching phase. The inability of the composite|pure configuration to bleach in the allocated time was attributed to a large difference in the electron diffusion coefficients of the films (1.3 x 10^{-2} cm^2/s for the pure film versus $\sim$4 x 10^{-7} cm^2/s for the 83% SiO_2 containing composite film). It was suggested that this large difference in diffusion coefficients led to the creation of a space-charge-limited effect when electrons travelled from a high to low diffusion coefficient area, as was the case during bleaching in the composite|pure tandem film configuration. I then demonstrated the possibility of fabricating an EC interference filter based on pure WO_3 and WO_3/SiO_2 composite layers with a 0.61 index contrast. This higher index contrast allowed for an interesting blue to purple color-shift to be obtained using only 11 layers.

In summary, the previous four chapters have demonstrated that the concept of an active interference security image structure (ISIS) is possible. This explains the title of the present thesis which mentions : "From passive to active". Indeed, I started my Ph.D. with a good background in passive ISIS devices and the conceptual idea of adding an electrochromic material as a means of increasing their complexity. Following extensive work on WO_3 films and Deb-type devices, I demonstrated that it is possible to combine an interference filter with an electrochromic device in order to create a hybrid device possessing two levels of authentication, but also a synergistic disappearing image effect (Chapter 7). The next two chapters (Chapters 8 and 9) demonstrated that it is possible to combine both the angle-dependent color shift as well as the EC voltage-driven color change in a single structure termed an EC interference filter. It is my belief that these active filters can be designed as to

be metameric with a NIM and thus, result in an active metameric ISIS. This clearly shows that we have gone full-circle by incorporating the features of the passive devices presented in Chapter 6 with an additional active level of authentication.

10.3 General discussion and conclusions

As I mentioned in Chapter 6, although metameric ISISs do already exist, the devices currently on the market are based on OVI and thus present a limited performance when used under light sources other than the one for which they were designed (typically fluorescent lighting). They are also reflection-based and, as a result, cannot be used in transmission. It is these elements which allowed our patent to be awarded in 2011. Through our continued collaboration with Univalor, the firm representing our patent, we have had multiple discussion with various entities (banks, companies, etc.). As a result, we have been able to demonstrate, through a collaborative effort, that transmission-based security devices can be made economically in large quantities. I have also been able to demonstrate metameric devices with a number of dielectric layers as low as 7. One can also imagine designing a transmission-based metameric filter for a single specific light source, as in the case of OVI, consequently reducing the design constraints and lowering the number of dielectric layers. Our collaboration has also led to the concept of a metameric ISIS/DOVID device combining both interference and diffraction.

It would also be possible to decrease the number of layers even more by designing metal/dielectric metameric filters. In particular, since the metallic films will need to be very thin in order for transmission to be non-negligible (typically under 10 nm), one can also imagine combining the triple-color-shift effect with the metameric concept (a prototype device is presently under way). Indeed, most recently, a summer student under my supervision has been able to fabricate a triple-color-shifting filter with only 5 metal-dielectric layers.

In addition, my first paper has been cited by a group in Finland working on parameric (close color match but not undistinguishable as in a metameric pair) security devices based on diffraction gratings [83], and also a group in China working on metal-dielectric gratings [321] ; this clearly shows that the present concept offers a wide range of other possibilities. In addition, considering the fact that the Bank of Canada has recently introduced a new series of polymer banknotes displaying a transparent window, and that paper banknotes with incorporated windows are also being introduced, I sincerely believe that transmission-based metameric interference filters are interesting potential candidates for the future.

With respect to the combination of an ISIS with an ECD, as already mentioned above, this type of device would be fairly expensive. On the other hand, the concept itself is still

of interest, since the active component may not necessarily be an ECD. Indeed, other active materials not requiring complex architectures, which by themselves may have been judged as non-ideal (see Chapter 4), may replace the ECD and result in a cheaper solution. For example, one could combine an ISIS with a thermochromic material. Another possibility, would be to replace the ISIS with a dark blue colored NIM matching the colored state of the ECD and once again decreasing the total cost. Finally, note that although I have used a Deb-type device, any other type of ECD could be used in the present context.

On the other hand, both the porous|dense and $WO_3/SiO_2|WO_3$ EC interference filters are economically feasible. In the case of the former one, I believe that the use of an alternative deposition method such as PECVD could allow for lower refractive indices to be obtained in the case of the porous films without sacrificing the deposition rate (thus increasing the index contrast and decreasing the number of layers). Another option would be to use glancing angle deposition (GLAD) to obtain lower density films. GLAD films being highly anisotropic, filters fabricated using this method would also present interesting polarization dependent properties which are obviously of interest in the context of security applications. Also note, that the rapid dissolution of the porous films would not be a problem in the case of an all-solid state device. Now, in the case of the latter, lowering the amount of SiO_2 and compensating the increase in index of refraction by increasing the porosity could help alleviate the observed issues : essentially, combining the results of Chapters 8 and 9. Since in both cases the presence of interfaces seems to be an issue, application of graded index EC filters may offer interesting possibilities.

Although complex electrochromic interference filters as the ones demonstrated in Chapters 8 and 9 are clearly of interest, there are also simpler structures which could potentially be of interest. In fact, as mentioned at the end of Chapter 9, Deb-type devices have a structure which is very similar to that of OVI. By using an aluminium bottom electrode and optimizing the thicknesses of the EC WO_3 and electrolyte SiO_2 films, it is possible to obtain a device displaying vivid angular color shifts in reflection similar to OVI, but also a dark blue coloration once a voltage is applied to the structure. Once again, work on such structures is currently under way and will be part of a future publication.

Note, that other reflection based EC devices have been already demonstrated, but are typically designed for variable mirror applications and essentially do not present any color variation as a function of the observation angle [322, 323]. An unusual configuration for an electrochromic mirror has been presented by Baucke *et al.*, where the hydrogen ions are shown to diffuse through the metallic reflector into an underlying ion reservoir [324, 325]. This has the added advantage that any type of material can be used for the remaining films of the device since they will be hidden by the reflector. One can actually use another WO_3 film as the ion

reservoir. Obviously, ions must not react with the reflector, therefore Ir, Pt and Rh have been suggested as the most suitable metals [326]. Interestingly, although this is not demonstrated, Baucke also mentions that the mirror can be a dielectric multilayer system [325]. Finally, most recently, others have developed switchable mirrors based on Mg_4Ni hydride films which vary from a reflective state in the intercalated state to a transparent state once hydrogen is removed [327].

Another solution which could lead to a simpler architecture for a device used in transmission, is to use a mutlilayer $WO_3|SiO_2$ filter deposited onto ITO such as suggested by Baucke *et al.* in their mirror application [325]. Even though only the first WO_3 layer in contact with the ITO will be able to color (since electrons cannot reach the other ones), if it is made thick enough, it will be sufficient to display an optically interesting effect. The authors are presently performing tests in order to quantify the effect of the overlying layers on the speed of coloration and bleaching. Finally, another interesting idea for a transmission-based device came to me when reading a paper by Papaefthimiou *et al.* on textured WO_3 surfaces [169]. Indeed, the authors mention that if the ion storage layer is also patterned, this can lead to the creation of different patterns in the colored and bleached states. One could clearly imagine an ECD based on two WO_3 layers separated by an electrolyte. Although the device would always be in a colored state, if the films have different surface patterns, the two colored states could be made to display different images in various shades of blue (an image being composed of different thicknesses of WO_3).

In conclusion, I believe that the first objective of the thesis, which was to develop new thin-film-based security devices has been clearly fulfilled. Although EC materials have recently been suggested for security applications, to my knowledge, this is the first attempt to develop an ISIS device with an EC material. As for the three other objectives, which were in essence "understand, characterize, optimize and integrate", I believe that they have also been fulfilled as described in each of the previous three chapters pertaining to the use of EC materials. In fact, the properties of the films were characterized in order to optimize the final device structure. Note that in some cases, I intentionally did not chose films that would result in the best electrochromic performance, but rather the films which offered the best optical performance (index contrast). This methodology also led to an accentuation of potential EC issues, thus allowing for their clear observation.

10.4 Perspectives and outlook

Obviously, having spent the last six years exploring the possibilities of EC materials, I've had over the years multiple ideas and interests which I simply did not have the time to

explore. Here is a short list of some of these thoughts I believe should be explored at the FCSEL in the near future.

First of all, the recent acquisition of an *RC2* spectroscopic ellipsometer from J.A. Woollam, Inc. which also came equipped with an electrochemical cell, offers a possibility of performing *in situ* optical measurements during coloration and bleaching of EC films. There have obviously been other ellipsometry studies although most often not *in situ* [155, 328, 329, 330, 331, 332]. Indeed, very often, *ex situ* measurements are performed using Li^+ ions which help since decoloration is much slower than when using H^+ ions. Once calibrated, ellipsometry can also serve to determine the amount of inserted ions [333]. Developing this expertise at the FCSEL could become a very useful tool, especially if one wants to take into account the optical properties of the colored films when designing an EC interference filter.

Lately, there has also been a trend of mixing inorganic and organic materials in order to obtain hybrid films with new properties. For example, at the FCSEL, we have explored SiOCH films incorporated into antireflection filters in order to better match the mechanical properties of the filter with those of the polymer substrate. As mentioned by Deb in his 2008 paper [145], I also believe that mixing WO_3 with organic materials can open-up a whole new spectrum of possibilities : faster coloration and bleaching dynamics, access to more color changes, etc. For example, films made with the conducting polymer polyaniline (PANI) and with WO_3 have been shown to vary from royal blue to green, to a pale yellowish-green and finally to a dark blue as the potential is scanned between 0.8 V and -0.5 V. [334]. Other examples include layer-by-layer deposition of tungstenphosphate and poly(hexyl viologen) films [335] and hybrid WO_3 and PEDOT :PSS (poly-(3,4-ethylenedioxythiophene) :poly(styrenesulfonate) films with an increased coloration efficiency [336]. All these examples point towards a new generation of EC materials with potentially interesting properties (e.g., wide range of color changes with good UV resistance),

There has also been some work done on WO_3-carbon nanotube hybrid films in order to obtain a high surface area [337, 338]. We have also explored these types of films through a collaboration with the University of Concordia, where carbon natotubes were used as the bottom electrode. Although our own limited tests were not very successful from an electrochromic point of view (quick degradation) we did observe some very interesting microstructures (see Figure 10.1 for a SEM image of one of our samples imaged after cycling). Bittencourt *et al.* also obtained similar structures and aimed at using these films for gas sensing applications due to their high surface area [339].

Another method of obtaining different color changes for WO_3 which could be easily explored at the FCSEL is to mix WO_3 with other inorganic EC materials (e.g. MoO_3, V_2O_5, etc.) [294, 340]. On can even consider mixing a cathodic and an anodic materials ; e.g., NiO_x

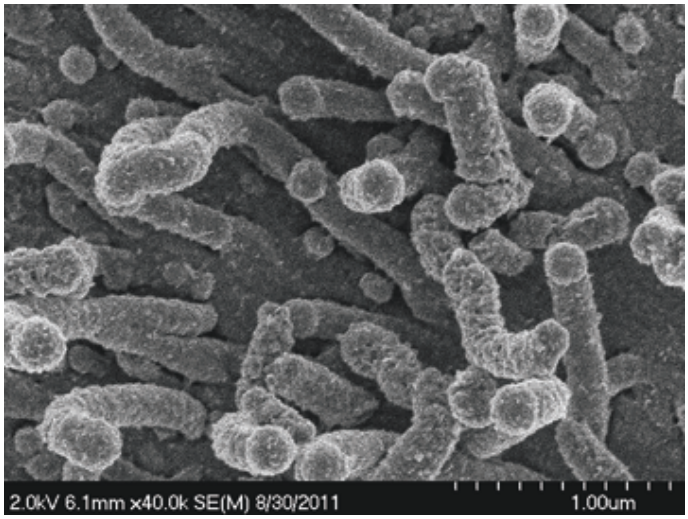

Figure 10.1 WO_3 film grown on top of a carbon nanotube electrode displaying an interesting microstructure with a high surface area.

and WO_3 which leads to a grey/brown to blue color shifting film [341]. Although much research has been done on this particular subject, most of it was motivated by the goal of neutralizing the color in the colored state of WO_3 for smart windows [342]. Finally, metal nanoparticles of Ag, Au and Pt are yet another means of modifying the intrinsic color of WO_3 [295, 343, 344, 345, 346, 347, 348, 349, 350, 271, 351]. I myself have explored co-sputtered Au/WO_3 films at the beginning of my Ph.D., but with only limited interesting results due to the difficulty in generating Au nanoparticles at temperatures below 350°C (to maintain the amorphous nature of the WO_3). A more promising approach (which I only briefly explored) would be multilayer WO_3|Au-nanoparticle films ; the Au nanoparticles obtained by depositing very thin layers, in order to benefit from island growth, in between two WO_3 films. A similar methodology has been proposed for NiO_x films [352].

These are obviously only a few ideas which I believe could be of interest to explore in order to help develop the next generation of active optical security devices. I will be happy to participate in exploring these new and interesting possibilities in the near future.

REFERENCES

[1] S. P. McGrew, "Hologram counterfeiting : Problems and solutions," in *Optical Security and Anticounterfeiting Systems, Los Angeles, California, USA*, vol. 1210. SPIE, 1990, pp. 66–76.

[2] L. Setlakwe and L. A. DiNunzio, "Comparative analysis of public opinion research in the U.S. and Canada," in *Optical Security and Counterfeit Deterrence Techniques V*, vol. 5310. SPIE, 2004, pp. 13–24.

[3] J. A. Dobrowolski, K. M. Baird, P. D. Carman, and A. Waldorf, "Optical interference coatings for inhibiting of counterfeiting," *Optica Acta*, vol. 20, no. 12, pp. 925–937, 1973.

[4] R. S. Berns, *Billmeyer and Saltzman's Principles of color technology*, 3rd ed. John Wiley & Sons Publication, Inc., 2000.

[5] G. Wyszecki, *Color Science - Concepts and Methods, Quantitative Data and Formulae*, 2nd ed. John Wiley & Sons Publication, Inc., 1982.

[6] J. Schanda, *Colorimetry - Understanding the CIE system.* John Wiley & Sons Publication, Inc., 2007.

[7] K. Nassau, *The physics and chemistry of color - The fifteen causes of color*, 2nd ed. John Wiley & Sons Publication, Inc., 2001.

[8] R. L. van Renesse, *Optical Document Security*, 3rd ed. Artech House, 2005.

[9] H. Shi, J. G. Ok, H. W. Baac, and L. J. Guo, "Low density carbon nanotube forest as an index-matched and near perfect absorption coating," *Appl. Phys. Lett.*, vol. 99, no. 21, p. 211103, 2011.

[10] H. A. Macleod, *Thin-Film Optical Filters*, 3rd ed. Institute of Physics Publishing, 2001.

[11] A. Stockman and L. T. Sharpe, "The spectral sensitivities of the middle- and long-wavelength-sensitive cones derived from measurements in observers of known genotype," *Vision Res.*, vol. 40, no. 13, pp. 1711 – 1737, 2000.

[12] G. A. Agoston, *Color theory and its application in art and design.* Springer-Verlag, 1979.

[13] J. M. Overduin, "Eyesight and the solar Wien peak," *Am. J. Phys.*, vol. 71, no. 3, pp. 216–219, 2003.

[14] C. L. Hardin, *Color for philosophers : unweaving the rainbow (expanded edition)*. Hackett Publishing Company, 1988.

[15] B. Hill, Th. Roger, and F. W. Vorhagen, "Comparative analysis of quantization of color spaces on the basis of the CIELAB color-difference formula," *ACM Transactions on Graphics*, vol. 16, no. 2, pp. 109–154, 1997.

[16] G. Sharma, *Digital color imaging Handbook*, 1st ed., G.Sharma, Ed. CRC Press, 2003.

[17] M. Mahy, L. van Eycken, and A. Oosterlinck, "Evaluation of uniform color spaces developed after the adoption of CIELAB and CIELUV," *Color Res. Appl.*, vol. 19, no. 2, pp. 105–121, 1994.

[18] M. R. Luo, G. Cui, and B. Rigg, "The development of the CIE 2000 colour-difference formula : CIEDE2000," *Color Res. Appl.*, vol. 26, no. 5, pp. 340–350, 2001.

[19] "Danger in the repair shop," 2007, [On line]. Available at : http://www.businessweek.com/stories/2007-07-29/danger-in-the-repair-shop [Consulted on 07/10/2012].

[20] *The Impact of Counterfeiting on Governments and Consumers, A REPORT COMMISSIONED BY BASCAP*. Business Action to Stop Counterfeiting and Piracy, 2009.

[21] "Counterfeit Medicines : Some Frequently Asked Questions." *World Health Organization*, [On line]. Available at : http://www.wpro.who.int/mediacentre/factsheets/fs_20050506/en/index.html [Consulted on 07/10/2012].

[22] R. L. van Renesse, *Protection of high security documents*. Renesse Consulting, 2006.

[23] S. E. Church, "The technology and practice of currency printing," in *38th Annual Technical Conference of the Society of Vacuum Coaters, Chicago, Illinois, USA*. Society of Vacuum Coaters, 2001, pp. 425–430.

[24] L. A. DiNunzio and S. E. Church, "Evaluating public awareness of new currency design features," in *Optical Security and Counterfeit Deterrence Techniques IV, San Jose, California, USA*, vol. 4677. SPIE, 2002, pp. 1–14.

[25] H. A. M. de Heij, "A method for measuring the public's appreciation and knowledge of banknotes," in *Optical Security and Counterfeit Deterrence Techniques IV, San Jose, California, USA*, vol. 4677. SPIE, 2002, pp. 15–55.

[26] K. M. Baird, J. A. Dobrowolski, A. J. Waldorf, and P. D. Carman, "Optical interference authenticating means," *U.S. Patent*, no. US 3 858 977, 1975.

[27] M. Davies and J. A. Dobrowolski, "Authenticating system," *U.S. Patent*, no. US 5 568 251, 1996.

[28] P. G. Coombs, S. F. McCaffery, and T. Markantes, "Advanced verification methods for OVI ® security ink," in *Optical Security and Counterfeit Deterrence Techniques VI, San Jose, California, USA*, vol. 6075. SPIE, 2006, pp. I1–I8.

[29] R. M. Klein, S. Gadbois, and J. J. Christie, "Perception and detection of counterfeit currency in Canada : Note quality, training and security features," in *Optical Security and Counterfeit Deterrence Techniques IV, San Jose, California, USA*, vol. 5310. SPIE, 2004, pp. 1–12.

[30] H. H. Weinert, "New developments for the continuous high rate production of physical vapor deposition (PVD) flake pigments without the use of consumable substrates," in *49th Annual Technical Conference of the Society of Vacuum Coaters, San Francisco, California, USA*. Society of Vacuum Coaters, 2006, pp. 642–647.

[31] C.-A. Despland, M. Schmid, and P. Degott, "Creation of novel security features using optically variable magnetic inks," in *Optical Document Security I, San Francisco, California USA*, R. L. van Renesse, Ed. Reconnaissance International, 2008, pp. 1–10.

[32] G. Pfaff, "Optical coatings for special effect pigments," in *47th Annual Technical Conference of the Society of Vacuum Coaters, Dallas, Texas, USA*. Society of Vacuum Coaters, 2004, pp. 79–85.

[33] J. A. Dobrowolski, F. C. Ho, and A. Waldorf, "Research on thin film anticounterfeiting coatings at the National Research Council of Canada," *Appl. Opt.*, vol. 28, no. 14, pp. 2702–2717, 1989.

[34] E. Çetinörgü-Goldenberg, B. Baloukas, O. Zabeida, J. Klemberg-Sapieha, and L. Martinu, "Optical and tribomechanical stability of optically variable interference security devices prepared by dual ion beam sputtering," *Appl. Opt.*, vol. 50, no. 19, pp. 3351–3359, 2011.

[35] J. Rolfe, "Optically variable devices for use on bank notes," in *Optical Security and Anticounterfeiting systems, Los Angeles, California, USA*, vol. 1210. SPIE, 1990, pp. 14–19.

[36] I. Glick, D. F. Grigg, and R. L. Wilkinson, "Manufactoring of optical security devices by sputtering techniques," in *37th Annual Technical Conference of the Society of Vacuum Coaters, Boston, Massachusetts, USA*. Society of Vacuum Coaters, 1994, pp. 85–96.

[37] P. Smits, A. M. Rosenfeld, and H. F. DeFerrari, "Tamper-evident structures," *U.S. Patent*, no. US 4 837 061, 1989.

[38] C. A. Bishop, "The use of vacuum deposited coatings for security applications," in *44th Annual Technical Conference of the Society of Vacuum Coaters, Philadelphia, Pennsylvania, USA*. Society of Vacuum Coaters, 2001, pp. 425–430.

[39] R. W. Phillips, V. C. Spellman, W. L. Gossett, and M. A. Kamerling, "Tamper evident optically variable device and article utilizing the same," *U.S. Patent*, no. US 4 721 217, 1988.

[40] E. D. Palik, *Handbook of Optical Constants of Solids*. Academic Press Inc., 1985.

[41] R. W. Phillips, "Color effects from thin film designs," in *8th International Conference on Vacuum Web Coating, Las Vegas, Nevada, USA*, 1994, pp. 270–284.

[42] R. W. Phillips, "Optically variable films, pigments and inks," in *Optical Thin Films III : New Developments, San Diego, California, USA*, vol. 1323. SPIE, 1990, pp. 98–109.

[43] I. M. Lancaster and A. Mitchell, "The growth of optically variable features on banknotes," in *Optical Security and Counterfeit Deterrence Techniques V, San Jose, California, USA*, vol. 5310. SPIE, 2004, pp. 34–45.

[44] P. H. Berning and R. W. Phillips, "Thin film optically variable article and method having gold to green color shift for currency authentication," *U.S. Patent*, no. US 4 705 300, 1987.

[45] R. W. Phillips and P. G. Coombs, "Transparent optically variable device," *U.S. Patent*, no. US 5 278 590, 1994.

[46] B. Baloukas, S. Larouche, and L. Martinu, "Playing with light - The quest for new optically variable devices," in *48th Annual Technical Conference of the Society of Vacuum Coaters, Denver, Colorado, USA*. Society of Vacuum Coaters, 2005, pp. 381–386.

[47] R. W. Phillips and A. F. Bleikolm, "Optical coatings for document security," *Appl. Opt.*, vol. 35, no. 28, pp. 5529–5534, 1996.

[48] H. G. Lotz and G. Steiniger, "Production of color shift layers with electron beam technology for identification and decorative applications," in *50th Annual Technical Conference of the Society of Vacuum Coaters, Louisville, Kentucky, USA*. Society of Vacuum Coaters, 2007, pp. 742–744.

[49] M. Nofi and J. Matteucci, "On-line evaluation of web coatings for color applications," in *41st Annual Technical Conference of the Society of Vacuum Coaters, Boston, Massachusetts, USA*. Society of Vacuum Coaters, 1998, pp. 392–396.

[50] J. Rolfe, "Vacuum coatings for document security," in *34th Annual Technical Conference of the Society of Vacuum Coaters, Washington, D.C., USA*. Society of Vacuum Coaters, 1991, pp. 20–25.

[51] J. A. Dobrowolski, *Optical Thin-Film Security Devices*, 2nd ed. Artech House, 1998, ch. 13, pp. 289–328.

[52] J. Haglmüller, Y. Alguel, Ch. Mayer, V. Matyushin, G. Bauer, F. Pittner, A. Leitner, F. Aussenegg, and T. Schalkhammer, "Cluster optical coding - from biochips to counterfeit security," in *Photon Processing in Microelectronics and Photonics III*, vol. 5339. SPIE, 2004, pp. 652–663.

[53] M. Bergsmann, F. Kastner, G. Bauer, R. Domnick, and H. Walter, "Novel security feature made by thin film coating technique," in *46th Annual Technical Conference of the Society of Vacuum Coaters, San Francisco, California, USA*. Society of Vacuum Coaters, 2003, pp. 566–569.

[54] G. Bauer, J. Hassmann, H. Walter, J. Haglmüller, C. Mayer, and T. Schalkhammer, "Resonant nanocluster technology - from optical coding and high quality security features to biochips," *Nanotechnology*, vol. 14, no. 12, pp. 1289–1311, 2003.

[55] M. Stalder and F. Seils, "Novel optically variable color devices," in *Optical Security and Counterfeit Deterrence Techniques VI, San Jose, California, USA*, vol. 6075. SPIE, 2006, pp. U1–U10.

[56] J. A. Dobrowolski and A. J. Waldorf, "Method of manufacturing an optical interference authenticating device," *U.S. Patent*, no. US 4 626 445, 1986.

[57] V. P. Raksha, C. J. Delst, P. G. Coombs, C. T. Markantes, and A. Argoitia, "Patterning of a spacer layer in an interference filter," *U.S. Patent*, no. US 2010/0 239 753, 2010.

[58] R. W. Phillips and R. Bie, "Covert security coating," *U.S. Patent*, no. US 7 630 109, 2009.

[59] R. W. Phillips, T. Mayer, and G. S. Ash, "Optically variable thin film flake and collection of the same," *U.S. Patent*, no. US 5 135 812, 1992.

[60] R. W. Phillips, T. Mayer, and G. S. Ash, "Ink incorporating optically variable thin film flakes," *U.S. Patent*, no. US 5 059 245, 1991.

[61] R. W. Phillips, T. Mayer, and G. S. Ash, "Optically variable printing inks," *U.S. Patent*, no. US 5 279 657, 1994.

[62] R. W. Phillips, T. Mayer, and G. S. Ash, "Method of making optical thin flakes and inks incorporating the same," *U.S. Patent*, no. US 5 383 995, 1995.

[63] R. W. Phillips, R. Slusser, and B. Holton, "Angle dependent metamerism in multi-layer thin films," in *Proceedings of the 9th International Conference on Vacuum Web Coating*, 1995, pp. 127–138.

[64] R. W. Phillips and A. Argoitia, "Using vacuum roll coaters to produce anti-counterfeiting devices," in *48th Annual Technical Conference of the Society of Vacuum Coaters, Louisville, Kentucky, USA*. Society of Vacuum Coaters, 2005, pp. 145–152.

[65] M. Schmid, "Optical security in ink : an industry standard that continues to evolve," in *Optical Security and Counterfeit Deterrence Techniques VI, San Jose, California, USA*, vol. 6075. SPIE, 2006, pp. N1–N6.

[66] A. Argoitia and K.-J. Delst, "Micro structured taggants in security pigments and inks," in *Optical Document Security I*, R. L. van Renesse, Ed. Reconnaissance International, 2008, pp. 1–16.

[67] R. W. Phillips and M. Nofi, "Colors by chemistry or by physics ?" in *42nd Annual Technical Conference of the Society of Vacuum Coaters, Chicago, Illinois, USA*. Society of Vacuum Coaters, 1999, pp. 494–499.

[68] S. Larouche and L. Martinu, "OpenFilters : open-source software for the design, optimization, and synthesis of optical filters," *Appl. Opt.*, vol. 47, no. 13, pp. C219–C230, 2008.

[69] R. W. Phillips, C. T. Markantes, S. P. Fisher, R. G. Slusser, P. K. Higgins, and A. F. Bleikom, "Paired optically variable article with paired optical structures and ink, paint and foil incorporating the same and method," *U.S. Patent*, no. US 6 114 018, 2000.

[70] P. G. Coombs and R. W. Phillips, "Optically variable interference device with peak suppresion and method," *U.S. Patent*, no. US 5 214 530, 1993.

[71] T. Jagielinski and F. Chamberlain, "Magnetic imaging of currencies and secure documents," in *Optical Security and Counterfeit Deterrence Techniques IV, San Jose, California, USA*, vol. 4677. SPIE, 2002, pp. 159–168.

[72] H. Lienvens, "Soft magnetic films for security devices," in *38th Annual Technical Conference of the Society of Vacuum Coaters, Chicago, Illinois, USA*. Society of Vacuum Coaters, 1995, pp. 147–151.

[73] P. G. Coombs, V. P. Raksha, and T. Markantes, "Overt and covert verification via magnetic optical security devices," in *Optical Security and Counterfeit Deterrence Techniques IV, San Jose, California, USA*, vol. 4677. SPIE, 2002, pp. 182–193.

[74] P. G. Coombs, A. Argoitia, V. P. Raksha, and R. W. Phillips, "Integration of contrasting technologies into advanced optical security devices," in *Optical Security and Counterfeit Deterrence Techniques V, San Jose, California, USA*, vol. 5310. SPIE, 2004, pp. 299–311.

[75] V. P. Raksha, C. T. Markantes, P. G. Coombs, R. W. Phillips, M. Nofi, and K.-J. Delst, "Printable appearance-changing graphical security devices," in *Optical Document Security I, San Francisco, California, USA*, R. L. van Renesse, Ed. Reconnaissance International, 2008, pp. 1–15.

[76] C.-A. Despland, M. Schmid, and P. Degott, "Creation of novel security features using optically variable magnetic inks," in *Optical Document Security I, San Francisco, California, USA*, R. L. van Renesse, Ed. Reconnaissance International, 2008, pp. 1–10.

[77] V. P. Raksha, C. J. Delst, P. G. Coombs, C. T. Markantes, and A. Argoitia, "Printed magnetic ink overt security image," *U.S. Patent*, no. US 8 025 952, 2011.

[78] V. P. Raksha, J. M. Holman, P. G. Coombs, C. T. Markantes, and R. W. Phillips, "Apparatus for orienting magnetic flakes," *U.S. Patent*, no. US 7 934 451, 2011.

[79] A. Argoitia and M. Whitzman, "Pigments exhibiting diffractive effects," in *45th Annual Technical Conference of the Society of Vacuum Coaters, Lake Buena Vista, Florida, USA*. Society of Vacuum Coaters, 2002, pp. 539–545.

[80] W. R. Tompkin, A. Schilling, and R. Staub, "Color-shifting features for optically variable devices," in *Optical Security and Counterfeit Deterrence Techniques VI, San Jose, California, USA*, vol. 5310. SPIE, 2004, pp. 244–255.

[81] A. Argoitia and S. Chu, "The concept of printable holograms through the alignment of diffractive pigments," in *Optical Security and Counterfeit Deterrence Techniques IV, San Jose, California, USA*, vol. 5310. SPIE, 2004, pp. 275–288.

[82] A. Argoitia and S. Chu, "The concept of printable holograms through the alignment of diffractive pigments," in *47th Annual Technical Conference of the Society of Vacuum Coaters, Dallas, Texas, USA*. Society of Vacuum Coaters, 2004, p. 677.

[83] J. Orava, N. Heikkila, T. Jaaskelainen, and J. Parkkinen, "Diffractive parameric colors," *J. Opt. Soc. Am. A :*, vol. 25, no. 12, pp. 2901–2907, 2008.

[84] A. Argoitia, D. Chu, and N. Teitelbaum, "Security device with metameric features using diffractive pigment flakes," *U.S. Patent*, no. US 7 729 026, 2010.

[85] R. W. Phillips, "Graphic images in optical thin film stacks," in *44th Annual Technical Conference of the Society of Vacuum Coaters, Philadelphia, Pennsylvania, USA*. Society of Vacuum Coaters, 2001, pp. 93–98.

[86] W. C. Kittler Jr., V. P. Raksha, R. W. Phillips, and G. Zambory, "Patterned optical structures with enhanced security feature," *U.S. Patent*, no. US 7 880 943, 2010.

[87] A. Argoitia and R. W. Phillips, "The security enhancement of diffractive optically variable image devices," in *Optical Security and Counterfeit Deterrence Techniques VI, San Jose, California, USA*, vol. 6075. SPIE, 2006, pp. P1–P18.

[88] A. Argoitia, V. P. Raksha, and P. T. Kohlmann, "All-dielectric optical diffractive pigments," *U.S. Patent*, no. US 6 815 065, 2004.

[89] N. A. G. Ahmed and M. Whitnall, "Semi-transparent optical coating for security holograms," in *44th Annual Technical Conference of the Society of Vacuum Coaters, Philadelphia, Pennsylvania, USA*. Society of Vacuum Coaters, 2001, pp. 444–447.

[90] R. W. Phillips and R. Bonkowski, "Security enhancement of holograms with interference coatings," in *Optical Security and Counterfeit Deterrence Techniques III, San Jose, California, USA*, vol. 3973. SPIE, 2000, pp. 304–315.

[91] R. Bonkowski, P. K. Higgins, C. T. Markantes, and R. W. Phillips, "Methods for forming security articles having diffractive surfaces and color shifting backgrounds," *U.S. Patent*, no. US 7 754 112, 2010.

[92] W. R. Tompkin, A. Schilling, and C. Weiteneder, "Zero-order gratings for optically variable devices," in *Optical Security and Counterfeit Deterrence Techniques IV, San Jose, California, USA*, vol. 4677. SPIE, 2002, pp. 227–237.

[93] Y. Chen and W. Liu, "Short period resonant dual-grating structures for applications to anisotropic color change securities," *Opt. Eng.*, vol. 50, no. 4, p. 048001, 2011.

[94] J. M. Jonza and A. D. Dubner, "Multilayer polymeric color-shifting polarizer films," in *Optical Security and Counterfeit Deterrence Techniques IV, San Jose, California, USA*, vol. 5310. SPIE, 2004, pp. 256–263.

[95] F. Moia, "New coloured security elements using Rolic's LPP/LCP technology : devices for 1st to 3rd level inspection," in *Optical Security and Counterfeit Deterrence Techniques IV, San Jose, California, USA*, vol. 4677. SPIE, 2002, pp. 194–202.

[96] F. Moia, "New colour shifting security devices," in *Optical Security and Counterfeit Deterrence Techniques IV, San Jose, California, USA*, vol. 5310. SPIE, 2004, pp. 312–320.

[97] Y. Jiang, B. Wilson, A. Hochbaum, and J. Carter, "Novel pigment approaches in optically variable security inks including polarizing cholesteric liquid crystal (clc) polymers," in *Optical Security and Counterfeit Deterrence Techniques IV, San Jose, California, USA*, vol. 4677. SPIE, 2002, pp. 247–254.

[98] Y. P. Zhang, V. P. Chodavarapu, A. G. Kirk, and M. P. Andrews, "Nanocrystalline cellulose for covert optical encryption," in *Organic Photonic Materials and Devices XIV*, vol. 8258. SPIE, 2012, pp. 825 808–1.

[99] D. J. Trevor, "A path to the next generation of U.S. banknotes," in *Optical Document Security I, San Francisco, California, USA*, R. L. van Renesse, Ed. Reconnaissance International, 2008, pp. 1–8.

[100] A. Jeacock and R. Whiteman, "Security device and method," *U.S. Patent*, no. US 2010/0164219, 2010.

[101] J. A. Dobrowolski, B. T. Sullivan, and R. C. Bajcar, "Optical interference electroluminescent device having low reflectance," *U.S. Patent*, no. US 5 049 780, 1991.

[102] P. G. Coombs, J. Zieba, R. A. Bradley Jr., C. W. Lantman, T. Mayer, R. W. Phillips, and S. A. Yamanaka, "Luminescent pigments and foils with color-shifting properties," *U.S. Patent*, no. US 6 572 784, 2003.

[103] C. D. MacPherson, D. G. Vendette, G. Girouard, and A. O. Stone, "Security device," *World International Property Organization*, no. WO2010096914, 2010.

[104] O. Rozumek and E. Müller, "Pigments having a viewing angle dependent shift of color, method of making, use and coating composition comprising of said pigments and detecting device," *World International Property Organization*, no. WO200160924, 2001.

[105] C. D. MacPherson, "Optically variable devices, their production and use," *World International Property Organization*, no. WO2011130843, 2011.

[106] A. C. Arsenault, U. Kamp, A. Cheng, and G. A. Ozin, "Interactive elastic photonic crystals," in *Optical Document Security I, San Francisco, California, USA*, R. L. van Renesse, Ed. Reconnaissance International, 2008, pp. 1–10.

[107] C. D. MacPherson and B. A. Hardwick, "Optically variable devices, their production and use," *World International Property Organization*, no. WO2011130842, 2010.

[108] A. C. Arsenault, D. P. Puzzo, I. Manners, and G. A. Ozin, "Photonic-crystal full-colour displays," *Nat. Photonics*, vol. 1, pp. 468–472, 2007.

[109] S.-L. Kuai, G. Bader, and P. V. Ashrit, "Tunable electrochromic photonic crystals," *Appl. Phys. Lett.*, vol. 86, p. 221110, 2005.

[110] D. A. Champion and C. S. Betrabet, "Security device," *U.S. Patent*, no. US 7 599 109, 2009.

[111] "Nanochromics printed security solutions," *Advancing Microelectronics*, vol. 38, pp. 14–20, 2011.

[112] D. Corr, U. Bach, D. Fay, M. Kinsella, C. McAtamney, F. O'Reilly, S. N. Rao, and N. Stobie, "Coloured electrochromic "paper-quality" displays based on modified mesoporous electrodes," *Solid State Ionics*, vol. 165, pp. 315–321, 2003.

[113] P. M. S. Monk, F. Delage, and S. M. C. Vieira, "Electrochromic paper : utility of electrochromes incorporated in paper," *Electrochim. Acta*, vol. 46, pp. 2195–2202, 2001.

[114] P. M. S. Monk, R. J. Mortimer, and D. R. Rosseinsky, *Electrochromism and Electrochromic Devices*. Cambridge University Press, 2007.

[115] C. G. Granqvist, *Handbook of inorganic electrochromic materials*. Elsevier, 1995.

[116] C. G. Granqvist, "Electrochromic tungsten oxide films : Review of progress 1993-1998," *Sol. Energ. Mat. Sol. C.*, vol. 60, no. 3, pp. 201–262, 2000.

[117] P. M. S. Monk, *Mechanic and dielectric properties.* Academic Press, 1993, vol. 17, ch. Electrochromic tungsten-oxide-based thin films : Physics, chemistry, and technology, pp. 301–362.

[118] P. M. S. Monk, "Charge movement through electrochromic thin-film tungsten trioxide," *Crit. Rev. Solid State Mater. Sci.*, vol. 24, no. 3, pp. 193–226, 1999.

[119] P. M. S. Monk, *Handbook of advanced electronic and photonic materials and devices.* Academic Press, 2001, vol. 7, ch. Electrochromism and electrochromic materials for displays, pp. 105–159.

[120] P. R. Somani and S. Radhakrishnan, "Electrochromic materials and devices : present and future," *Mat. Chem. Phys.*, vol. 77, no. 1, pp. 117–133, 2003.

[121] A. Samat and R. Guglielmetti, *Kirk-Othmer Encyclopedia of Chemical Technology.* John Wiley & Sons Publication, Inc., 2001, ch. Chromogenic materials, Photochromic.

[122] C. M. Lampert, "Chromogenic smart materials," *Mater. Today*, vol. 7, no. 3, pp. 28–35, 2004.

[123] C. M. Lampert, *50 Years of Vacuum Coating Technology and the Growth of the Society of Vacuum Coaters.* Society of Vacuum Coaters, 2007, ch. Smart materials - Dynamically switchable windows and displays, pp. 70–79.

[124] A. Samat and R. Guglielmetti, *Kirk-Othmer Encyclopedia of Chemical Technology.* John Wiley & Sons Publication, Inc., 2001, ch. Chromogenic materials, Piezochromic.

[125] A. Pucci and G. Ruggeri, "Mechanochromic polymer blends," *J. Mater. Chem.*, vol. 21, no. 23, pp. 8282–8291, 2011.

[126] A. Samat and R. Guglielmetti, *Kirk-Othmer Encyclopedia of Chemical Technology.* John Wiley & Sons Publication, Inc., 2001, ch. Chromogenic materials, Thermochromic.

[127] K. Bange, "Colouration of tungsten oxide films : A model for optically active coatings," *Sol. Energ. Mat. Sol. C.*, vol. 58, no. 1, pp. 1–131, 1999.

[128] C. B. Greenberg, "Optically switchable thin films : a review," *Thin Solid Films*, vol. 251, no. 2, pp. 81–93, 1994.

[129] A. A. Argun, P.-H. Aubert, B. C. Thompson, I. Schwendeman, C. L. Gaupp, J. Hwang, N. J. Pinto, D. B. Tanner, A. G. MacDiarmid, and J. R. Reynolds, "Multicolored electrochromism in polymers : Structures and devices," *Chemistry of Materials*, vol. 16, pp. 4401–4412, 2004.

[130] H. J. Byker, "Electrochromics and polymers," *Electrochim. Acta*, vol. 46, no. 13-14, pp. 2015–2022, 2001.

[131] S. K. Deb, "Reminiscences on the discovery of electrochromic phenomena in transition metal oxides," *Sol. Energ. Mat. Sol. C.*, vol. 39, no. 2-4, pp. 191–201, 1995.

[132] A. Avendaño, A. Azens, G. A. Niklasson, and C. G. Granqvist, "Sputter deposited electrochromic films and devices based on these : Progress on nickel-oxide-based films," *Mater. Sci. Eng., B*, vol. 138, no. 2, pp. 112–117, 2007.

[133] C. G. Granqvist, "Electrochromic materials : Microstructure, electronic bands, and optical properties," *Appl. Phys. A*, vol. 57, pp. 3–12, 1993.

[134] G. A. Niklasson, L. Berggren, and A.-L. Larsson, "Electrochromic tungsten oxide : the role of defects," *Sol. Energ. Mat. Sol. C.*, vol. 84, no. 1-43, pp. 315–328, 2004.

[135] T. E. Haas and R. B. Goldner, "Fundamentals of electrochromism in metal oxide bronzes," in *Large-area chromogenics : materials and devices for transmittance control*, C. M. Lampert and C. G. Granqvsit, Eds., vol. IS4, SPIE. SPIE Opt. Engr. Press, 1990, pp. 170–180.

[136] C. G. Granqvist, "Chromogenic materials for transmittance control of large-area windows," *Crit. Rev. Solid State Mater. Sci.*, vol. 16, no. 5, pp. 291–308, 1990.

[137] C. Ottermann, A. Temmink, and K. Bange, "Correlation of injected charge to optical constants (n, k) of electrochromic films," in *Optical Materials Technology for Energy Efficiency and Solar Energy Conversion IX*, vol. 1272. SPIE, 1990, pp. 111–121.

[138] S. K. Deb, "Optical and photoelectric properties and colour centres in thin films of tungsten oxide," *Philos. Mag.*, vol. 27, no. 4, pp. 801–822, 1973.

[139] L. Berggren, "Optical absorption and electrical conductivity in lithium intercalated amorphous tunsten oxide films," Ph.D. dissertation, Uppsala University, 2004.

[140] C. G. Granqvist, "Electrochromic oxides : A unified view," *Solid State Ionics*, vol. 70-71, no. 1, pp. 678–685, 1994.

[141] G. A. Niklasson and C. G. Granqvist, "Electrochromics for smart windows : thin films of tungsten oxide and nickel oxide, and devices based on these," *J. Mater. Chem.*, vol. 17, no. 2, pp. 127–156, 2007.

[142] L. Berggren, A. Azens, and G. A. Niklasson, "Polaron absorption in amorphous tungsten oxide films," *J. Appl. Phys.*, vol. 90, no. 4, pp. 1860–1863, 2001.

[143] B. W. Faughnan, R. S. Crandall, and P. M. Heyman, "Electrochromism in WO_3 films," *RCA Review*, vol. 36, pp. 177–197, 1975.

[144] L. Berggren and G. A. Niklasson, "Optical charge transfer absorption in lithium-intercalated tungsten oxide thin films," *Appl. Phys. Lett.*, vol. 88, p. 081906, 2006.

[145] S. K. Deb, "Opportunities and challenges in science and technology of WO_3 for electrochromic and related applications," *Sol. Energ. Mat. Sol. C.*, vol. 92, no. 2, pp. 245–258, 2008.

[146] R. S. Crandall, P. J. Wojtiwicz, and B. W. Faughnan, "Theory and measurement of the change in chemical potential of hydrogen in amorphous H_xWO_3 as a function of the stoichiometric parameter x," *Solid State Commun.*, vol. 18, no. 11–12, pp. 1409–1411, 1976.

[147] R. B. Goldner, "Some aspects of charge transport in electrochromic films," in *Proceedings of the International Seminar on Solid State Ionic Devices*, B. V. R. Chowdari and S. Radhakrishna, Eds., vol. 1272. World Publishing Company, 1988, pp. 351–358.

[148] B. Faughnan and R. Crandall, "Electrochromic displays based on WO_3," in *Display Devices*, ser. Topics in Applied Physics, J. Pankove, Ed. Springer Berlin / Heidelberg, 1980, vol. 40, pp. 181–211.

[149] B. W. Faughnan, R. S. Crandall, and M. A. Lampert, "Model for the bleaching of WO_3 electrochromic films by an electric field," *Appl. Phys. Lett.*, vol. 27, no. 5, pp. 275–277, 1975.

[150] J.-G. Zhang, D. K. Benson, C. E. Tracy, and S. K. Deb, "The influence of microstructure on the electrochromic properties of Li_xWO_3 films : Part II. limiting mechanisms in coloring and bleaching processes," *J. Mater. Res.*, vol. 8, no. 10, pp. 2657–2667, 1993.

[151] D.-J. Kim and S.-I. Pyun, "Hydrogen transport through rf-magnetron sputtered amorphous WO_3 film with three kinds of hydrogen injection sites," *Solid State Ionics*, vol. 99, no. 3-4, pp. 185–192, 1997.

[152] Y. Yamada, K. Tajima, S. Bao, M. Okada, and K. Yoshimura, "Optical charge transfer absorption in proton injected tungsten oxide thin films analyzed with spectroscopic ellipsometry," *Solid State Ionics*, vol. 180, no. 6-8, pp. 659–661, 2009.

[153] L. Se-Hee, H. M. Cheong, C. E. Tracy, A. Mascarenhas, A. W. Czanderna, and S. K. Deb, "Electrochromic coloration efficiency of a-WO_{3-y} thin films as a function of oxygen deficiency," *Appl. Phys. Lett.*, vol. 75, no. 11, pp. 1541–1543, 1999.

[154] G. A. Niklasson, A. Norling, G. Possnert, and L. Berggren, "Optical properties of amorphous tungsten oxide films : Effect of stoichiometry." *J. Phys. Conf. Ser.*, vol. 100, p. 082023, 2008.

[155] M. J. DeVries, C. Trimble, T. E. Tiwald, D. W. Thompson, J. A. Woollam, and J. S. Hale, "Optical constants of crystalline WO_3 deposited by magnetron sputtering," *J. Vac. Sci. Technol. A*, vol. 17, no. 5, pp. 2906–2910, 1999.

[156] A. Subrahmanyam, A. Karuppasamy, and C. S. Kumar, "Oxygen-sputtered tungsten oxide thin films for enhanced electrochromic properties," *Electrochem. Solid-State Lett.*, vol. 9, no. 12, pp. H111–H114, 2006.

[157] G. Leftheriotis, S. Papaefthimiou, and P. Yianoulis, "The effect of water on the electrochromic properties of WO_3 films prepared by vacuum and chemical methods," *Sol. Energ. Mat. Sol. C.*, vol. 83, no. 1, pp. 115–124, 2004.

[158] R. B. Goldner, P. Norton, K. Wong, G. Foley, E. L. Goldner, G. Seward, and R. Chapman, "Further evidence for free electrons as dominating the behavior of electrochromic polycrystalline WO_3 films," *Appl. Phys. Lett.*, vol. 47, pp. 536–538, 1985.

[159] J. S. E. M. Svensson and C. G. Granqvist, "Modulated transmittance and reflectance in crystalline electrochromic WO_3 films : Theoretical limits," *Appl. Phys. Lett.*, vol. 45, no. 8, pp. 828–830, 1984.

[160] R. B. Goldner, D. H. Mendelsohn, J. Alexander, W. Henderson, D. Fitzpatrick, T. E. Haas, H. H. Sample, R. D. Rauh, M. A. Parker, and T. L. Rose, "High near-infrared reflectivity modulation with polycrystalline electrochromic WO_3 films," *Appl. Phys. Lett.*, vol. 43, no. 12, pp. 1093–1095, 1983.

[161] S. F. Cogan, T. D. Plante, M. A. Parker, and R. D. Rauh, "Free-electron electrochromic modulation in crystalline Li_xWO_3," *J. Appl. Phys.*, vol. 60, no. 8, pp. 2735–2738, 1986.

[162] D. Deniz, D. J. Frankel, and R. J. Lad, "Nanostructured tungsten and tungsten trioxide films prepared by glancing angle deposition," *Thin Solid Films*, vol. 518, no. 15, pp. 4095–4099, 2010.

[163] T. Miyoshi and K. Iwasa, "Electrochromic displays for watches," in *SID International Symposium*, L. Winner, Ed., vol. 11. Society for Information Display, 1980, pp. 126–127.

[164] D. L. Bellac, A. Azens, and C. Granqvist, "Angular selective transmittance through electrochromic tungsten oxide films made by oblique angle sputtering," *Appl. Phys. Lett.*, vol. 66, no. 14, pp. 1715–1716, 1995.

[165] S. Gubbala, J. Thangala, and M. K. Sunkara, "Nanowire-based electrochromic devices," *Sol. Energ. Mat. Sol. C.*, vol. 91, no. 9, pp. 813–820, 2007.

[166] P. M. Kadam, N. L. Tarwal, P. S. Shinde, R. S. Patil, H. P. Deshmukh, and P. S. Patil, "From beads-to-wires-to-fibers of tungsten oxide : electrochromic response," *Appl. Phys. A*, vol. 97, no. 2, pp. 323–330, 2009.

[167] L. Yang, D. Ge, J. Zhao, Y. Ding, X. Kong, and Y. Li, "Improved electrochromic performance of ordered macroporous tungsten oxide films for IR electrochromic device," *Sol. Energ. Mat. Sol. C.*, vol. 100, no. 0, pp. 251–257, 2012.

[168] V. V. Abramova, A. S. Sinitskii, T. V. Laptinskaya, A. G. Veresov, E. A. Goodilin, and Y. D. Tretyakov, "Nanoporous electrochromic coatings based on tungsten oxide," *Dokl. Chem.*, vol. 407, no. 1, pp. 31–34, 2007.

[169] S. Papaefthimiou, G. Leftheriotis, and P. Yianoulis, "Study of WO_3 films with textured surfaces for improved electrochromic performance," *Solid State Ionics*, vol. 139, no. 1-2, pp. 135–144, 2001.

[170] Y.-M. Lu and C.-P. Hu, "The colored and bleached properties of tungsten oxide electrochromic films with different substrate conductivities," *J. Alloys Compd.*, vol. 449, no. 1-2, pp. 389–392, 2008.

[171] C. G. Granqvist, "Transparent conductive electrodes for electrochromic devices : A review," *Appl. Phys. A*, vol. 57, pp. 19–24, 1993.

[172] C. G. Granqvist, "Transparent conductors as solar energy materials : A panoramic review," *Sol. Energ. Mat. Sol. C.*, vol. 91, no. 17, pp. 1529–1598, 2007.

[173] P. C. Lansåker, J. Backholm, G. A. Niklasson, and C. G. Granqvist, "TiO_2/Au/TiO_2 multilayer thin films : Novel metal-based transparent conductors for electrochromic devices," *Thin Solid Films*, vol. 518, no. 4, pp. 1225–1229, 2009.

[174] C. G. Granqvist, "Window coatings for the future," *Thin Solid Films*, vol. 193-194, no. 2, pp. 730–741, 1990.

[175] C. Guillen and J. Herrero, "Transparent electrodes based on metal and metal oxide stacked layers grown at room temperature on polymer substrate," *Phys. Status Solidi*, vol. 207, no. 7, pp. 1563–1567, 2010.

[176] G. Leftheriotis, S. Papaefthimiou, and P. Yianoulis, "Integrated low-emittance electrochromic devices incorporating ZnS/Ag/ZnS coatings as transparent conductors," *Sol. Energ. Mat. Sol. C.*, vol. 61, no. 2, pp. 107–112, 2000.

[177] C. G. Granqvist, A. Azens, A. Hjelm, L. Kullman, G. A. Niklasson, D. Rönnow, M. Strømne Mattsson, M. Veszelei, and G. Vaivars, "Recent advances in electrochromics for smart window applications," *Sol. Energ.*, vol. 63, no. 4, pp. 199–216, 1998.

[178] C. G. Granqvist, "Electrochromism and smart window design," *Solid State Ionics*, vol. 53-56, no. 1, pp. 479–489, 1992.

[179] C. O. Avellaneda, D. F. Vieira, A. Al-Kahlout, S. Heusing, E. R. Leite, A. Pawlicka, and M. A. Aegerter, "All solid-state electrochromic devices with gelatin-based electrolyte," *Sol. Energ. Mat. Sol. C.*, vol. 92, no. 2, pp. 228–233, 2008.

[180] P. V. Ashrit, "Dry lithiation study of nanocrystalline, polycrystalline and amorphous tungsten trioxide thin-films," *Thin Solid Films*, vol. 385, no. 1-2, pp. 81–88, 2001.

[181] T. Shimomura, T. Furuta, and T. Maki, "Colorimetric evaluation of an ECD for the reflection- and transmission-types," *Jpn. J. Appl. Phys.*, vol. 26, no. 4, pp. L299–L301, 1987.

[182] T. Furuta, T. Shimomura, H. Mada, and S. Kobayashi, "Colorimetric measurement of the WO_3 electrochromic display," *Jpn. J. Appl. Phys.*, vol. 20, no. 11, pp. L768–L770, 1981.

[183] S. K. Deb and H. Witzke, "The solid state electrochromic phenomenon and its applications to display devices," in *IEEE Conference on International Electron Devices Meeting, Washington D.C., USA*, vol. 21. IEEE, 1975, pp. 393–397.

[184] M. Shizukuishi, I. Shimizu, and E. Inoue, "Application of amorphous silicon to WO_3 photoelectrochromic device," *Jpn. J. Appl. Phys.*, vol. 20, no. 12, pp. 2359–2363, 1981.

[185] T. Yoshimura, M. Watanabe, K. Kiyota, and M. Tanaka, "Electrolysis in electrochromic devices consisting of WO_3 and MgF_2 thin films," *Jpn. J. Appl. Phys.*, vol. 21, no. 1, pp. 128–132, 1982.

[186] T. Yoshimura, M. Watanabe, , Y. Koike, K. Kiyota, and M. Tanaka, "Effect of surface states of WO_3 on the operating characteristics of thin film electrochromic devices," *Thin Solid Films*, vol. 101, no. 2, pp. 141–151, 1983.

[187] J. S. E. M. Svensson and C. G. Granqvist, "Electrochromic coatings for "smart windows"," *Sol. Energ. Mat. Sol. C.*, vol. 12, no. 6, pp. 391–402, 1985.

[188] Y. Hajimoto, M. Matsushima, and S. Ogura, "Solid state electrochromism in WO_3," *J. Electron. Mat.*, vol. 8, no. 3, pp. 301–310, 1979.

[189] I. Shimizu, M. Shizukuishi, and E. Inoue, "Solid-state electrochromic device consisting of amorphous WO_3 and Cr_2O_3," *J. Appl. Phys.*, vol. 50, pp. 4027–4032, 1979.

[190] A. R. Lusis, J. J. Kleperis, A. A. Brishka, and E. V. Pentyush, "Electro-optic spectroscopy of electrochromic processes in tungsten trioxide," *Solid State Ionics*, vol. 13, no. 4, pp. 319–324, 1984.

[191] D. K. Benson, C. E. Tracy, and M. R. Ruth, "Solid state electrochromic switchable window glazings," in *Optical materials technology for energy efficiency and solar energy conversion III*, vol. 502. SPIE, 1984, pp. 46–53.

[192] C. Corbella, M. Vives, A. Pinyol, I. Porqueras, C. Person, and E. Bertran, "Influence of the porosity of RF sputtered Ta_2O_5 thin films on their optical properties for electrochromic applications," *Solid State Ionics*, vol. 165, no. 1, pp. 15–22, 2003.

[193] M. Kitao, H. Akram, K. Urabe, and S. Yamada, "Properties of solid-state electrochromic cells using Ta_2O_5 as electrolyte," *J. Electron. Mater.*, vol. 21, no. 4, pp. 419–422, 1992.

[194] M. Shizukuishi, E. Kaga, I. Shimizu, H. Kokado, and E. Inoue, "Electrochromic display device based on amorphous WO_3 and solid proton conductor," *Jpn. J. Appl. Phys.*, vol. 20, no. 3, pp. 581–586, 1981.

[195] P. V. Ashrit, F. E. Girouard, V.-V. Truong, and G. Bader, "LiF as electrolyte for solid state electrochromic structures," in *Optical Materials Technology for Energy Efficiency and Solar Energy Conversion IV*, ser. Proceedings of the SPIE - The International Society for Optical Engineering, vol. 562. SPIE, 1985, pp. 53–60.

[196] H. J. Stocker, S. Singh, L. G. VanUitert, and G. J. Zydzik, "Efficiency and humidity dependence of WO_3-insulator electrochromic display structures," *J. Appl. Phys.*, vol. 50, no. 4, pp. 2993–2994, 1979.

[197] E. Inoue, K. Kawaziri, and A. Izawa, "Deposited Cr_2O_3 as a barrier in a solid state WO_3 electrochromic cell," *Jpn. J. Appl. Phys.*, vol. 16, no. 11, pp. 2065–2066, 1977.

[198] M. Shizukuishi, I. Shimizu, and E. Inoue, "Solid-state electrochromic device consisting of amorphous WO_3 and various thin oxide layers," *Jpn. J. Appl. Phys.*, vol. 19, no. 11, pp. 2121–2126, 1980.

[199] M. Shizukuishi, I. Shimizu, and E. Inoue, "Coloration process in solid-state electrochromic device," *Jpn. J. Appl. Phys.*, vol. 20, no. 3, pp. 575–579, 1981.

[200] H. Yoshimura, T. Sakaguchi, and N. Koshida, "Development of flexible electrochromic device with thin-film configuration," *Jpn. J. Appl. Phys.*, vol. 46, no. 4B, pp. 2458–2461, 2007.

[201] H. Yoshimura and N. Koshida, "Fast electrochromic effect obtained from solid-state inorganic thin-film configuration with a carrier accumulation structure," *Appl. Phys. Lett.*, vol. 88, p. 093509, 2006.

[202] A. Vértes and R. Schiller, "Concentration-dependent diffusitivity : Hydrogen percolation in WO_3," *J. Appl. Phys.*, vol. 54, no. 1, pp. 199–203, 1983.

[203] K. Huang, J. Jia, Q. Pan, F. Yang, and D. He, "Optical, electrochemical and structural properties of long-term cycled tungsten oxide films prepared by sol-gel," *Physica B*, vol. 396, no. 1-2, pp. 164–168, 2007.

[204] S. K. Deb, "A novel electrophotographic system," *Appl. Opt. Suppl.*, vol. 8, no. S1, pp. 192–195, 1969.

[205] I. F. Chang, B. L. Gilbert, and T. I. Sun, "Electrochemichromic systems for display applications," *J. Electrochem. Soc.*, vol. 122, pp. 955–962, 1975.

[206] W. C. Dautremont-Smith, "Transition metal oxide electrochromic materials and displays : a review - Part 1 : oxides with cathodic coloration," *Displays*, vol. 3, no. 1, pp. 3–22, 1982.

[207] D. J. Barclay, C. L. Bird, and D. H. Martin, "Speed considerations for electrochromic displays," *J. Electron. Mat.*, vol. 8, no. 3, pp. 311–331, 1979.

[208] D. R. Rosseinsky and R. J. Mortimer, "Electrochromic systems and the prospects for devices," *Adv. Mater.*, vol. 13, no. 11, pp. 783–793, 2001.

[209] C. G. Granqvist, A. Azens, P. Heszler, L. B. Kish, and L. Österlund, "Nanomaterials for benign indoor environments : Electrochromics for "smart windows", sensors for air quality, and photo-catalysts for air cleaning," *Sol. Energ. Mat. Sol. C.*, vol. 91, no. 4, pp. 355–365, 2007.

[210] J. Svensson and C. Granqvist, "Electrochromic tungsten oxide films for energy efficient windows," *Sol. Energ. Mat. Sol. C.*, vol. 11, no. 1-2, pp. 29–34, 1984.

[211] C. G. Granqvist, P. C. Lansåker, N. R. Mlyuka, G. A. Niklasson, and E. Avendaño, "Progress in chromogenics : New results for electrochromic and thermochromic materials and devices," *Sol. Energ. Mat. Sol. C.*, vol. 93, no. 12, pp. 2032–2039, 2009.

[212] A. Azens and C. G. Granqvist, "Electrochromic smart windows : energy efficiency and device aspects," *Journal of Solid State Electrochemistry*, vol. 7, no. 2, pp. 64–68, 2003.

[213] S. Papaefthimiou, G. Leftheriotis, P. Yianoulis, T. J. Hyde, P. C. Eames, Y. Fang, P.-Y. Pennarun, and P. Jannasch, "Development of electrochromic evacuated advanced glazing," *Energy Build.*, vol. 38, no. 12, pp. 1455–1467, 2006.

[214] S. Papaefthimiou, E. Syrrakou, and P. Yianoulis, "Energy performance assessment of an electrochromic window," *Thin Solid Films*, vol. 502, no. 1-2, pp. 257–264, 2006.

[215] E. S. Lee, D. L. DiBartolomeo, and S. E. Selkowitz, "Daylighting control performance of a thin-film ceramic electrochromic window : Field study results," *Energy Build.*, vol. 38, no. 1, pp. 30–44, 2006.

[216] L.-M. Huang, C.-W. Hub, H.-C. Liu, C.-Y. Hsu, C.-H. Chen, and K.-C. Ho, "Photovoltaic electrochromic device for solar cell module and self-powered smart glass applications," *Sol. Energ. Mat. Sol. C.*, vol. 99, pp. 154–159, 2011.

[217] N. A. O'Brien, J. Gordon, H. Mathew, and B. P. Hichwa, "Electrochromic coatings - applications and manufacturing issues," *Thin Solid Films*, vol. 345, no. 2, pp. 312–318, 1999.

[218] D. T. Gillaspie, R. C. Tenent, and A. C. Dillon, "Metal-oxide films for electrochromic applications : present technology and future directions," *J. Mater. Chem.*, vol. 20, no. 43, pp. 9585–9592, 2010.

[219] A. Azens, E. Avendaño, J. Backholm, L. Berggren, G. Gustavsson, R. Karmhag, G. Niklasson, A. Roos, and C. Granqvist, "Flexible foils with electrochromic coatings : science, technology and applications," *Mat. Sci. Eng. B - Solid*, vol. 119, no. 3, pp. 214–223, 2005.

[220] C. G. Granqvist, "Progress toward roll-to-roll processing of inorganic monolithic electrochromic devices on polymeric substrates," *Sol. Energ. Mat. Sol. C.*, vol. 92, no. 2, pp. 97–100, 2008.

[221] R. Baetens, B. P. Jelle, and A. Gustavsen, "Properties, requirements and possibilities of smart windows for dynamic daylight and solar energy control in buildings : A state-of-the-art review," *Sol. Energ. Mat. Sol. C.*, vol. 94, no. 2, pp. 87–1–5, 2010.

[222] B. P. Jelle, A. Hynd, A. Gustavsen, D. Arasteh, H. Goudey, and R. Hart, "Fenestration of today and tomorrow : A state-of-the-art review and future research opportunities," *Sol. Energ. Mat. Sol. C.*, vol. 96, no. 1, pp. 1–28, 2012.

[223] C. G. Granqvist, "Oxide electrochromics : An introduction to devices and materials," *Sol. Energ. Mat. Sol. C.*, vol. 99, pp. 1–13, 2012.

[224] C. G. Granqvist, "Electrochromics for energy efficiency and indoor comfort," *Pure Appl. Chem.*, vol. 80, no. 11, pp. 2489–2498, 2008.

[225] G. de Vries, "Electrochromic variable transmission glass for picture tubes," *Electrochim. Acta*, vol. 44, no. 18, pp. 3185–3193, 1999.

[226] G. Sonmez and H. B. Sonmez, "Polymeric electrochromics for data storage," *J. Mater. Chem.*, vol. 16, no. 25, pp. 2473–2477, 2006.

[227] S. Möller, C. Perlov, W. Jackson, C. Taussig, and S. R. Forrest, "A polymer/semiconductor write-once read-many-times memory," *Nature*, vol. 426, pp. 166–169, 2003.

[228] R. Sato, N. Kawamura, and H. Tokuaru, "Relaxation mechanism of electrochromism of tungsten-oxide film for ultra-multilayer optical recording depending on sputtering conditions," *Jpn. J. Appl. Phys.*, vol. 46, no. 6B, pp. 3958–3964, 2007.

[229] P. Tehrani, J. Isaksson, W. Mammo, M. R. Andersson, N. D. Robinson, and M. Berggren, "Evaluation of active materials designed for use in printable electrochromic polymer displays," *Thin Solid Films*, vol. 515, no. 4, pp. 2485–2492, 2006.

[230] C. Costa, C. Pinheiro, I. Henriques, and C. A. T. Laia, "Inkjet printing of sol-gel synthesized hydrated tungsten oxide nanoparticles for flexible electrochromic devices," *ACS Appl. Mater. Interfaces*, vol. 4, pp. 1330–1340, 2012.

[231] M. Buyan, P. A. Brühwiler, A. Azens, G. Gustavsson, R. Karmhag, and C. G. Granqvist, "Facial warming and tinted helmet visors," *Int. J. Ind. Ergonom.*, vol. 36, no. 1, pp. 11–16, 2006.

[232] C. Wang, M. Shim, and P. Guyot-Sionnest, "Electrochromic nanocrystal quantum dots," *Science*, vol. 291, no. 5512, pp. 2390–2392, 2001.

[233] L. F. Reyes, A. Hoel, S. Saukko, P. Heszler, V. Lantto, and C. G. Granqvist, "Gas sensor response of pure and activated WO_3 nanoparticle films made by advanced reactive gas deposition," *Sensor. Actuat. B - Chem.*, vol. 117, no. 1, pp. 128–134, 2006.

[234] J.-H. Kang, S.-M. Paek, S.-J. Hwang, and J.-H. Choy, "Optical iris application of electrochromic thin films," *Electrochem. Commun.*, vol. 10, no. 11, pp. 1785–1787, 2008.

[235] S. K. Deb, "Opportunities and challenges of electrochromic phenomena in transition metal oxides," *Sol. Energ. Mat. Sol. C.*, vol. 25, no. 3-4, pp. 327–338, 1992.

[236] P. Talvenmaa, *Intelligent textiles and clothing.* Cambridge, England : Woodhead Publishing Limited, 2006, ch. 11 - Introduction to chromic materials, pp. 193–205.

[237] M. A. Invernale, Y. D., and G. A. Sotzing, "The effects of coloured base fabric on electrochromic textile," *Color. Technol.*, vol. 127, no. 3, pp. 167–172, 2011.

[238] R. A. Colley, P. M. Budd, J. R. Owen, and S. Balderson, "Poly[oxymethylene-oligo(oxyethylene)] for use in subambient temperature electrochromic devices," *Polym. Int.*, vol. 49, no. 4, pp. 371–376, 2000.

[239] L. Liu, S. K. Karuturi, L. T. Su, Q. Wang, and A. I. Y. Tok, "Electrochromic photonic crystal displays with versatile color tunability," *Electrochem. Commun.*, vol. 13, no. 11, pp. 1163–1165, 2011.

[240] E. B. Franke, C. L. Trimble, M. Schubert, J. A. Woollam, and J. S. Hale, "All-solid-state electrochromic reflectance device for emittance modulation in the far-infrared spectral region," *Appl. Phys. Lett.*, vol. 77, pp. 930–932, 2000.

[241] P. Topart and P. Hourquebie, "Infrared switching electroemissive devices based on highly conducting polymers," *Thin Solid Films*, vol. 352, no. 1-2, pp. 243–248, 1999.

[242] J. S. Hale and J. A. Woollam, "Prospects for IR emissivity control using electrochromic structures," *Thin Solid Films*, vol. 339, no. 1-2, pp. 174–180, 1999.

[243] M. M. Waite, S. I. Shah, and D. A. Glocker, *50 Years of Vacuum Coating Technology and the Growth of the Society of Vacuum Coaters.* Society of Vacuum Coaters, 2007, ch. Sputtering sources, pp. 108–119.

[244] M. Ohring, *Materials science of thin films*, 2nd ed. Academic Press, 2002.

[245] J. A. Thornton, "The microstructure of sputter-deposited coatings," *Vac. Sci. Technol. A*, vol. 4, no. 6, pp. 3059–3065, 1986.

[246] D. M. Mattox, "Particle bombardment effects on thin-film deposition : A review," *J. Vac. Sci. Technol. A*, vol. 7, no. 3, pp. 1105–1114, 1989.

[247] B. Baloukas, "Conception et fabrication de dispositifs de sécurité optiques," Master's thesis, École Polytechnique de Montréal, 2006.

[248] J. C. Manifacier, J. Gasiot, and J. P. Fillard, "A simple method for the determination of the optical constants n, k and the thickness of a weakly absorbing thin film," *J. Phys. E : Sci. Instrum.*, vol. 9, no. 11, pp. 1002–1004, 1976.

[249] H. G. Tompkins and E. A. Irene, *Handbook of ellipsometry*. William Andrew Publishing, 2005.

[250] S. C. Gujrathi and S. Bultena, "Depth profiling of hydrogen using the high efficiency ERD-TOF technique," *Nucl. Instrum. Meth. B*, vol. 64, no. 1-4, pp. 789–795, 1992.

[251] S. Green, E. Pehlivan, C.G.Granqvist, and G.A.Niklasson, "Electrochromism in sputter deposited nickel-containing tungsten oxide films," *Sol. Energ. Mat. Sol. C.*, vol. 99, pp. 339–344, 2012.

[252] W. Q. Hong, "Extraction of extinction coefficient of weak absorbing thin films from special absorption," *J. Phys. D : Appl. Phys.*, vol. 22, no. 9, pp. 1384–1385, 1989.

[253] B. Baloukas and L. Martinu, "Advances in metameric security image structures," in *Optical Document Security I, San Franscisco, California, USA*. Reconnaissance International, 2008.

[254] B. Baloukas and L. Martinu, "Metameric interference security image structures," *Appl. Opt.*, vol. 47, no. 10, pp. 1585–1593, 2008.

[255] *2007 Annual Report on Organized crime in Canada*. Criminal Intelligence Service Canada, 2007.

[256] R. L. van Renesse, *Optical Document Security*, 2nd ed. Artech House, 1998.

[257] J. C. Taylor, B. A. Hardwick, W. K. Jackson, P. Zientek, and C. R. Hibbert, "Self-verifying security documents," *U.S. Patent*, US 7 040 664, 2006.

[258] H. Hauser, W. H. Gerber, A. Iqbal, and P. Maurer, "Method of producing forgery-proof colored printed articles," *U.S. Patent*, US 6 013 307 2000.

[259] B. Baloukas, S. Larouche, and L. Martinu, "Use of metameric filters for future interference security image structures," in *Optical Security and Counterfeit Deterrence Techniques VI, San Jose, California, USA*, vol. 6075. SPIE, 2006, pp. T1–T9.

[260] R. W. Phillips and A. Argoitia, "Using vacuum roll coaters to produce anti-counterfeiting devices," in *48th Annual Technical Conference of the Society of Vacuum Coaters, Denver, Colorado, USA*. Society of Vacuum Coaters, 2005, pp. 145–152.

[261] B. Baloukas and L. Martinu, "Interference security image structure," *U.S. Patent*, US 8 064 632 2011.

[262] *Colorimetry*, 3rd ed. International Commission on Illumination, 2004.

[263] *Guide to using WVASE32*. J.A. Woollam Co., Inc., 2001.

[264] O. F. Schirmer, V. Wittwer, G. Baur, and G. Brandt, "Dependence of WO_3 electrochromic absorption on crystallinity," *J. Electrochem. Soc.*, vol. 124, no. 5, pp. 749–753, 1977.

[265] D. R. Rosseinsky and R. J. Mortimer, "Electrochromic systems and the prospects for devices," *Adv. Mater.*, vol. 13, no. 11, pp. 783–793, 2001.

[266] C. G. Granqvist, E. Avendaño, and A. Azens, "Electrochromic coatings and devices : survey of some recent advances," *Thin Solid Films*, vol. 442, no. 1-2, pp. 201–211, 2003.

[267] P. M. S. Monk, C. Turner, and S. P. Akhtar, "Electrochemical behaviour of methyl viologen in a matrix of paper," *Electrochim. Acta*, vol. 44, no. 26, pp. 4817–4826, 1999.

[268] E. Çetinörgü, B. Baloukas, O. Zabeida, J. E. Klemberg-Sapieha, and L. Martinu, "Mechanical and thermoelastic characteristics of optical thin films deposited by dual ion beam sputtering," *Appl. Opt.*, vol. 48, no. 23, pp. 4536–4544, 2009.

[269] G. Leftheriotis, S. Papaefthimiou, and P. Yianoulis, "Dependence of the estimated diffusion coefficient of Li_xWO_3 films on the scan rate of cyclic voltammetry experiments," *Solid State Ionics*, vol. 178, no. 3-4, pp. 259–263, 2007.

[270] A. Subrahmanyam and A. Karuppasamy, "Optical and electrochromic properties of oxygen sputtered tungsten oxide (WO_3) thin films," *Sol. Energ. Mat. Sol. C.*, vol. 91, no. 4, pp. 266–274, 2007.

[271] K.-W. Park, "Electrochromic properties of Au-WO_3 nanocomposite thin-film electrode," *Electrochim. Acta*, vol. 50, no. 24, pp. 4690–4693, 2005.

[272] G. Beydaghyan, G. Bader, and P. V. Ashrit, "Electrochromic and morphological investigation of dry-lithiated nanostructured tungsten trioxide thin films," *Thin Solid Films*, vol. 516, no. 8, pp. 1646–1650, 2008.

[273] C. G. Granqvist, "Progress in electrochromics : tungsten oxide revisited," *Electrochim. Acta*, vol. 44, no. 18, pp. 3005–3015, 1999.

[274] L. T. Maloney and B. A. Wandell, "Color constancy : a method for recovering surface spectral reflectance," *JOSA A*, vol. 3, no. 1, pp. 29–33, 1986.

[275] R. Vernhes, O. Zabeida, J. E. Klemberg-Sapieha, and L. Martinu, "Single-material inhomogeneous optical filters based on microstructural gradients in plasma-deposited silicon nitride," *Appl. Opt.*, vol. 43, no. 1, pp. 97–103, 2004.

[276] N. R. Mlyuka, G. A. Niklasson, and C. G. Granqvist, "Thermochromic VO_2-based multilayer films with enhanced luminous transmittance and solar modulation," *Phys. Stat. Sol. A*, vol. 206, no. 9, pp. 2155–2160, 2009.

[277] T. Ben-Messaoud, J. Riordon, A. Melanson, P. V. Ashrit, and A. Hachéa, "Photoactive periodic media," *Appl. Phys. Lett.*, vol. 94, no. 11, p. 111904, 2009.

[278] E. S. Lee, S. E. Selkowitz, R. D. Clear, D. L. DiBartolomeo, J. H. Klems, L. L. Fernandes, and M. Y. G. J. Ward, V. Inkarojrit, "Advancement of electrochromic windows," California Energy Commission, Tech. Rep. CEC-500-2006-052, 2006.

[279] A. Jonsson, A. Roos, and E. K. Jonson, "The effect on transparency and light scattering of dip coated antireflection coatings on window glass and electrochromic foil," *Sol. Energ. Mat. Sol. C.*, vol. 94, pp. 992–997, 2010.

[280] S. Sawada and G. C. Danielson, "Optical indices of refraction of WO_3," *Phys. Rev.*, vol. 113, no. 4, pp. 1008–1013, 1959.

[281] R. Vernhes, A. Amassian, J. E. Klemberg-Sapieha, and L. Martinu, "Plasma treatment of porous SiN_x: H films for the fabrication of porous-dense multilayer optical filters with tailored interfaces," *J. Appl. Phys.*, vol. 99, no. 11, pp. 114 315–114 315–12, 2006.

[282] K. M. Karuppasamy and A. Subrahmanyam, "Studies on the correlation between electrochromic colouration and the relative density of tungsten trioxide (WO_{3-x}) thin films prepared by electron beam evaporation," *J. Phys. D Appl. Phys.*, vol. 42, no. 9, p. 095301, 2009.

[283] H. Morita and H. Washida, "Electrochromism of atmospheric evaporated tungsten oxide films (AETOF)," *Jpn. J. Appl. Phys.*, vol. 23, no. 1, pp. 754–759, 1984.

[284] T. C. Arnoldussen, "A model for electrochromic tungstic oxide microstructure and degradation," *J. Electrochem. Soc.*, vol. 128, no. 1, pp. 117–123, 1981.

[285] E. Masetti, M. L. Grilli, G. Dautzenberg, G. Macrelli, and M. Adamik, "Analysis of the influence of the gas pressure during the deposition of electrochromic WO_3 films by reactive r.f. sputtering of W and WO_3 target," *Sol. Energ. Mat. Sol. C.*, vol. 56, no. 3-4, pp. 259–269, 1999.

[286] S. A. Agnihotry, K. K. Saini, T. K. Saxena, and S. Chandra, "Electical properties and morphology of obliquely deposited electrochromic wo_3 films," *Thin Solid Films*, vol. 141, no. 2, pp. 183–192, 1986.

[287] A. Lusis, J. Kleperis, and E. Pentjušs, "Model of electrochromic and related phenomena in tungsten oxide thin films," *J. Solid State Electr.*, vol. 7, no. 2, pp. 106–112, 2003.

[288] B. Baloukas, J.-M. Lamarre, and L. Martinu, "Active metameric security devices using an electrochromic material," *Appl. Opt.*, vol. 50, no. 9, pp. C41–C49, 2011.

[289] M. Denesuk and D. R. Uhlmann, "Site-saturation model for the optical efficiency of tungsten oxide-based devices," *J. Electrochem. Soc.*, vol. 143, no. 9, pp. L186–L188, 1996.

[290] J.-G. Zhang, C. E. Tracy, D. K. Benson, and S. K. Deb, "The influence of microstructure on the electrochromic properties of Li_xWO_3 thin films : Part I. Ion diffusion and electrochromic properties," *J. Mater. Res.*, vol. 8, no. 10, pp. 2649–2656, 1993.

[291] B. Reichman and A. J. Bard, "The electrochromic process at WO_3 electrodes prepared by vacuum evaporation and anodic oxidation of W," *J. Electrochem. Soc.*, vol. 126, no. 4, pp. 583–591, 1979.

[292] N. Yoshiike and S. Kondo, "Electrochemical properties of $WO_3 \cdot x(H_2O)$, I. the influences of water adsorption and hydroxilation," *J. Electrochem. Soc.*, vol. 130, no. 11, pp. 2283–2287, 1983.

[293] A. Azens, C. G. Granqvist, E. Pentjuss, J. Gabrusenoks, and J. Barczynska, "Electrochromism of fluorinated electron-bombarded tungsten oxide films," *J. Appl. Phys.*, vol. 78, no. 3, pp. 1968–1974, 1995.

[294] S. Sato and Y. Seino, "Electrochromism in evaporated WO_3-MoO_3-V_2O_5 films," *Electron. Comm. Jpn. 1*, vol. 65, no. 8, pp. 104–111, 1982.

[295] P. V. Ashrit, G. Bader, F. E. Girouard, V.-V. Truong, and T. Yamaguchi, "Optical properties of cermets consisting of metal in a WO_3 matrix," *Physica A*, vol. 157, no. 1, pp. 333–338, 1989.

[296] K.-W. Park, Y.-J. Song, J.-M. Lee, and S.-B. Han, "Influence of Pt and Au nanophases on electrochromism of WO_3 in nanostructure thin-film electrodes," *Electrochem. Commun.*, vol. 9, no. 8, pp. 2111–2115, 2007.

[297] E. O. Zayim, "Optical and electrochromic properties of sol-gel made anti-reflective WO_3-TiO_2 films," *Sol. Energ. Mat. Sol. C.*, vol. 87, no. 1-4, pp. 695–703, 2005.

[298] M. Greissel, "The colors they are a-changin'," *Industrial Paint & Powder*, vol. 77, no. 5, pp. 16–18, 2001.

[299] R. Padiyath, C. Haak, and L. Gilbert, "Spectrally selective window films," in *50th Annual Technical Conference of the Society of Vacuum Coaters, Louisville, Kentycky, USA*. Society of Vacuum Coaters, 2007, pp. 669–673.

[300] M. Schwartz, *Smart Materials*, 1st ed. CRC Press, 2008.

[301] B. Baloukas, J.-M. Lamarre, and L. Martinu, "Electrochromic interference filters fabricated from dense and porous tungsten oxide films," *Sol. Energ. Mat. Sol. C.*, vol. 95, no. 9, pp. 807–815, 2011.

[302] M. Klisch, "12-tungstosilicic acid (12-TSA) as a tungsten precursor in alcoholic solution for deposition of $xWO_3(1\text{-}x)SiO_2$ thin films ($x < 0.7$) exhibiting electrochromic coloration ability," *J. Sol-Gel Sci. Techn.*, vol. 12, no. 1, pp. 21–33, 1998.

[303] D. Li, G. Wu, G. Gao, J. Shen, and F.-Q. Huang, "Ultrafast coloring-bleaching performance of nanoporous WO_3-SiO_2 gasochromic films doped with Pd catalyst," *ACS Appl. Mater. Interfaces*, vol. 3, no. 12, pp. 4573–4579, 2011.

[304] D. Saygin-Hinczewski, M. Hinczewski, I. Sorar, F. Z. Tepehan, and G. G. Tepehan, "Modeling the optical properties of WO_3 and WO_3–SiO_2 thin films," *Sol. Energ. Mat. Sol. C.*, vol. 92, no. 8, pp. 821–829, 2008.

[305] X. Q. Xu, H. Shen, and X. Y. Xiong, "Gasochromic effect of sol-gel WO_3-SiO_2 films with evaporated platinum catalyst," *Thin Solid Films*, vol. 415, no. 1-2, pp. 290–295, 2002.

[306] G. E. Jellison Jr. and F. A. Modine, "Parametrization of the optical functions of amorphous materials in the interband region," *Appl. Phys. Lett.*, vol. 69, no. 3, pp. 371–373, 1996.

[307] R. S. Crandall and B. W. Faughnan, "Measurement of the diffusion coefficient of electrons in WO_3 films," *Appl. Phys. Lett.*, vol. 26, no. 3, pp. 120–121, 1975.

[308] C. W. Peterson, J. Parlett, and R. S. Crandall, "The physics of electrochromism : An advanced laboratory experiment," *Am. J. Phys.*, vol. 47, no. 9, pp. 772–775, 1979.

[309] N. Naseri, R. Azimirad, O. Akhavan, and A. Z. Moshfegh, "The effect of nanocrystalline tungsten oxide concentration on surface properties of dip-coated hydrophilic WO_3-SiO_2 thin films," *J. Phys. D : Appl. Phys.*, vol. 40, pp. 2089–2095, 2007.

[310] J. Tauc, Ed., *Amorphous and Liquid Semiconductors*. Plenum Press, 1974.

[311] F. Messina, M. Cannas, and R. Boscaino, "Generation of defects in amorphous SiO_2 assisted by two-step absorption on impurity sites," *J. Phys. : Condens. Matter*, vol. 20, pp. 275 210–6, 2008.

[312] S. Larouche, H. Szymanowski, J. E. Klemberg-Sapieha, L. Martinu, and S. C. Gujrathi, "Microstructure of plasma-deposited SiO_2/TiO_2 optical films," *J. Vac. Sci. Technol. A*, vol. 22, no. 4, pp. 1200–1207, 2004.

[313] D. E. Aspnes, "Optical properties of thin films," *Thin Solid Films*, vol. 89, no. 3, pp. 249–262, 1982.

[314] M. Jerman, Z. Qiao, and D. Mergel, "Refractive index of thin films of SiO_2, ZrO_2, and HfO_2 as a function of the films′ mass density," *Appl. Opt.*, vol. 44, no. 15, pp. 3006–3012, 2005.

[315] B. D. Cullity, *Elements or X-Ray Diffraction*, 2nd ed. Addisson-Wesley, 1979.

[316] S. Papaefthimiou, G. Leftheriotis, and P. Yianoulis, "Study of WO_3 films with textured surfaces for improved electrochromic performance," *Solid State Ionics*, vol. 139, no. 1-2, pp. 135–144, 2001.

[317] T. Jow and J. B. Wagner Jr., "The effect of dispersed alumina particles on the electrical conductivity of cuprous chloride," *J. Electrochem. Soc.*, vol. 126, no. 11, pp. 1963–1972, 1979.

[318] A. E. Aliev and C. Park, "Development of WO_3 thin films using nanoscale silicon particles," *Jpn. J. Appl. Phys.*, vol. 39, no. 6A, pp. 3572–3578, 2000.

[319] D.-J. Kim and S.-I. Pyun, "Hydrogen transport through rf-magnetron sputtered amorphous WO_3 film with three kinds of hydrogen injection sites," *Solid State Ionics*, vol. 99, no. 3-4, pp. 185–192, 1997.

[320] J. Wang and J. M. Bell, "The kinetic behaviour of ion injection in WO_3 based films produced by sputter and sol-gel deposition : Part II. Diffusion coefficients," *Sol. Energ. Mat. Sol. C.*, vol. 58, no. 4, pp. 411–429, 1999.

[321] Y. Chen and W. Liu, "Design and analysis of multilayered structures with metal-dielectric gratings for reflection resonance and color generation," *Opt. Lett.*, vol. 37, no. 1, pp. 4–6, 2012.

[322] M. P. Cantão, A. Lourenço, A. Gorenstein, S. I. C. de Torresi, and R. M. Torresi, "Inorganic oxide solid state electrochromic devices," *Mater. Sci. Eng., B*, vol. 26, no. 2-3, pp. 157–161, 1994.

[323] T. Niwaa and O. Takai, "All-solid-state reflectance-type electrochromic devices using iridium tin oxide film as counter electrode," *Thin Solid Films*, vol. 518, no. 18, pp. 5340–5344, 2010.

[324] F. G. K. Baucke, "Electrochromic mirrors with variable reflectance," *Sol. Energ. Mat.*, vol. 16, no. 1-3, pp. 67–77, 1987.

[325] F. G. K. Baucke and T. Gambke, "Reflecting electrochromic devices," *Displays*, vol. 9, no. 4, pp. 179–187, 1988.

[326] F. Bange and T. Gambke, "Electrochromic materials for optical switching devices," *Adv. Mater.*, vol. 2, no. 1, pp. 10–16, 1990.

[327] K. Tajima, Y. Yamada, and K. Yoshimura, "Effective density of tantalum oxide thin film by reactive DC magnetron sputtering for all-solid-state switchable mirror," *J. Electrochem. Soc.*, vol. 154, no. 9, pp. J267–J271, 2007.

[328] M. F. Saenger, T. Höing, B. W. Robertson, R. B. Billa, T. Hofmann, E. Schubert, and M. Schubert, "Polaron and phonon properties in proton intercalated amorphous tungsten oxide thin films," *Phys. Rev. B*, vol. 78, no. 24, p. 245205, 2008.

[329] K. von Rottkay, M. Rubin, and S.-J. Wen, "Optical indices of electrochromic tungsten oxide," *Thin Solid Films*, vol. 306, no. 1, pp. 10–16, 1997.

[330] E. Pascual, J. Martí, E. Garcia, A. Canillas, and E. Bertran, "Infrared and UV-visible ellipsometric study of WO_3 electrochromic thin films," *Thin Solid Films*, vol. 313-314, no. 1-2, pp. 682–686, 1998.

[331] Y. Yamada, K. Tajima, S. Bao, M. Okada, K. Yoshimura, and A. Roos, "Optical properties of tungsten oxide thin films with protons intercalated during sputtering," *J. Appl. Phys.*, vol. 103, no. 6, p. 063508, 2008.

[332] I. Valyukh, S. Green, H. Arwin, G. A. Niklasson, E. Wäckelgård, and C. G. Granqvist, "Spectroscopic ellipsometry characterization of electrochromic tungsten oxide and nickel oxide thin films made by sputter deposition," *Sol. Energ. Mat. Sol. C.*, vol. 94, no. 5, pp. 724–732, 2010.

[333] Y. Yamada, S. Kawaji, S. Bao, M. Okada, M. Tazawa, K. Yoshimura, and A. Roos, "Estimation of the amount of the proton injected into tungsten oxide thin films during deposition using spectroscopic ellipsometry," *Thin Solid Films*, vol. 515, no. 7-8, pp. 3825–3829, 2007.

[334] J. Zhang, J.-P. Tu, D. Zhang, Y.-Q. Qiao, X.-H. Xia, X.-L. Wang, and C.-D. Gu, "Multicolor electrochromic polyaniline-WO_3 hybrid thin films : One-pot molecular assembling synthesis," *J. Mater. Chem.*, vol. 21, no. 43, pp. 17 316–17 324, 2011.

[335] W. Caseri, "Color switching in nanocomposites comprising inorganic nanoparticles dispersed in a polymer matrix," *J. Mater. Chem.*, vol. 20, no. 27, pp. 5582–5592, 2010.

[336] M. Deepa, A. K. Srivastava, K. N. Sood, and A. V. Murugan, "Nanostructured tungsten oxide-poly(3,4-ethylenedioxythiophene) :poly(styrenesulfonate) hybrid films : Synthesis, electrochromic response, and durability characteristics," *J. Electrochem. Soc.*, vol. 155, no. 11, pp. D703–D710, 2008.

[337] P. M. Kadam, N. L. Tarwal, S. S. Mali, H. P. Deshmukh, and P. S. Patil, "Enhanced electrochromic performance of f-MWCNT-WO_3 composite," *Electrochim. Acta*, vol. 58, pp. 556–561, 2011.

[338] A. E. Aliev and H. W. Shin, "Nanostructured materials for electrochromic devices," *Solid State Ionics*, vol. 154-155, pp. 425–431, 2002.

[339] C. Bittencourt, A. Felten, E. H. Espinisa, R. Ionescu, N. Moreau, P. Heszler, C. G. Granqvist, J.-J. Pireaux, and E. Llobet, "Evaporation of WO_3 on carbon nanotube films : a new hybrid film," *Smart Mater. Struct.*, vol. 15, no. 6, pp. 1555–1560, 2006.

[340] S. Sato and Y. Seino, "Electrochromism in evaporated WO_3-MoO_3-V_2O_5 films," *Trans. Inst. Electronic Commun. Engr. Japan*, vol. 65, pp. 629–636, 1982.

[341] P. M. S. Monk and S. L. Chester, "Electro-deposition of films of electrochromic tungsten oxide containing additional metal oxides," *Electrochim. Acta*, vol. 38, no. 11, pp. 1521–1526, 1993.

[342] A. Rougier, A. Blyr, J. Garcia, Q. Zhang, and S. A. Impey, "Electrochromic W-M-O (M = V, Nb) sol-gel thin films : a way to neutral colour," *Sol. Energ. Mat. Sol. C.*, vol. 71, no. 3, pp. 343–357, 2002.

[343] P. V. Ashrit, G. Bader, F. E. Girouard, and V.-V. Truong, "Anomalous electrochromic behavior of Ag-WO_3 and Au-WO_3 cermets," in *Optical Materials Technology for Energy Efficiency and Solar Energy Conversion VIII*, ser. Proceedings of the SPIE - The International Society for Optical Engineering, vol. 1149. SPIE, 1989, pp. 7–19.

[344] H. Denga, D. Yanga, B. Chena, and C.-W. Linb, "Simulation of surface plasmon resonance of Au-WO_{3-x} and Ag-WO_{3-x} nanocomposite films," *Sens. Actuators, B*, vol. 134, no. 2, pp. 502–509, 2008.

[345] P. M. Kadam, N. L. Tarwal, P. S. Shinde, S. S. Mali, R. S. Patil, A. K. Bhosale, H. P. Deshmukh, and P. S. Patil, "Enhanced optical modulation due to SPR in gold nanoparticles embedded WO_3 thin films," *J. Alloys Compd.*, vol. 509, no. 5, pp. 1729–1733, 2011.

[346] N. Naseri, R. Azimirad, O. Akhavan, and A. Z. Moshfegh, "Improved electrochromical properties of sol-gel WO_3 thin films by doping gold nanocrystals," *Thin Solid Films*, vol. 518, no. 8, pp. 2250–2257, 2010.

[347] Y. Pang, Q. Chen, X. Shen, L. Tang, and H. Qian, "Size-controlled Ag nanoparticle modified WO_3 composite films for adjustment of electrochromic properties," *Thin Solid Films*, vol. 518, no. 8, pp. 1920–1924, 2010.

[348] E. K. Sichel and J. I. Gittleman, "Characteristics of electrochromic materias Au-WO_3 and Pt-WO_3," *J. Electron. Mat.*, vol. 8, no. 1, pp. 1–9, 1979.

[349] E. K. Sichel and J. I. Gittleman, "Electrochromism in the composite material Au-WO_3," *Appl. Phys. Lett.*, vol. 31, no. 2, pp. 109–111, 1977.

[350] E. K. Sichel and J. I. Gittleman, "Transport and optical properties of electrochromic Au-WO_3 cermets," *Appl. Phys. Lett.*, vol. 33, no. 7, pp. 564–566, 1978.

[351] K.-W. Park, "Modified electrochromism of tungsten oxide via platinum nanophases," *Appl. Phys. Lett.*, vol. 88, p. 211107, 2006.

[352] F. F. Ferreira and M. C. A. Fantini, "Multilayered composite Au-NiO_x electrochromic films," *Solid State Ionics*, vol. 175, no. 1–4, pp. 517–520, 2004.